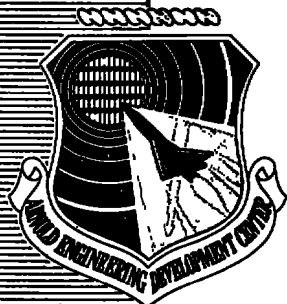


**AEDC-TR-77-55**

cy.3

JUN 10 1977  
DEC 1 1977  
JAN 23 1980  
MAR 24 1981



# **TURBINE ENGINE LOADS SIMULATOR (TELS) RADIOGRAPHIC SYSTEMS REQUIREMENTS STUDY**

**UNITED TECHNOLOGIES CORPORATION  
PRATT & WHITNEY AIRCRAFT GROUP  
COMMERICAL PRODUCTS DIVISION  
EAST HARTFORD, CONNECTICUT 06108**

**June 1977**

**Final Report for Period 1 March 1976 - 28 February 1977**

Approved for public release; distribution unlimited.

Property of U. S. Air Force  
AEDC LIBRARY  
F40600-75-C-0001

**Prepared for**

**DIRECTORATE OF TECHNOLOGY  
ARNOLD ENGINEERING DEVELOPMENT CENTER  
AIR FORCE SYSTEMS COMMAND  
ARNOLD AIR FORCE STATION, TENNESSEE 37389**

## NOTICES

When U. S. Government drawings specifications, or other data are used for any purpose other than a definitely related Government procurement operation, the Government thereby incurs no responsibility nor any obligation whatsoever, and the fact that the Government may have formulated, furnished, or in any way supplied the said drawings, specifications, or other data, is not to be regarded by implication or otherwise, or in any manner licensing the holder or any other person or corporation, or conveying any rights or permission to manufacture, use, or sell any patented invention that may in any way be related thereto.

Qualified users may obtain copies of this report from the Defense Documentation Center.

References to named commercial products in this report are not to be considered in any sense as an endorsement of the product by the United States Air Force or the Government.

This final report was submitted by United Technologies Corporation, Pratt & Whitney Aircraft Group, Commercial Products Division, East Hartford, Connecticut 06108, under contract F40600-76-C-0008, with the Arnold Engineering Development Center, Arnold Air Force Station, Tennessee 37389. Captain Gerald M. Mulenburg and Mr. Forrest B. Smith were the AEDC program monitors.

This report has been reviewed by the Information Office (OI) and is releasable to the National Technical Information Service (NTIS). At NTIS, it will be available to the general public, including foreign nations.

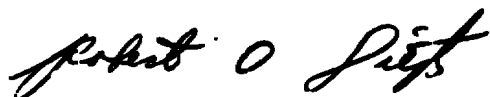
## APPROVAL STATEMENT

This technical report has been reviewed and is approved for publication.

FOR THE COMMANDER



FORREST B. SMITH  
Requirements Planning Division  
Directorate of Technology



ROBERT O. DIETZ  
Director of Technology



# UNCLASSIFIED

REPORT DOCUMENTATION PAGE		READ INSTRUCTIONS BEFORE COMPLETING FORM
1. REPORT NUMBER <b>AEDC-TR-77-55</b>	2. GOVT ACCESSION NO.	3. RECIPIENT'S CATALOG NUMBER
4. TITLE (and Subtitle) <b>TURBINE ENGINE LOADS SIMULATOR (TELS) RADIOGRAPHIC SYSTEMS REQUIREMENTS STUDY</b>		5. TYPE OF REPORT & PERIOD COVERED <b>Final Report - March 1976 - February 1977</b>
		6. PERFORMING ORG. REPORT NUMBER <b>FR 8496</b>
7. AUTHOR(s) <b>B. E. Kinchen</b>		8. CONTRACT OR GRANT NUMBER(s) <b>F40600-76-C-0008</b>
9. PERFORMING ORGANIZATION NAME AND ADDRESS <b>United Technologies Corporation, Pratt &amp; Whitney Aircraft Group, Commercial Products Division, East Hartford, Connecticut 06108</b>		10. PROGRAM ELEMENT, PROJECT, TASK AREA & WORK UNIT NUMBERS <b>Program Elements 65807F and 63723F</b>
11. CONTROLLING OFFICE NAME AND ADDRESS <b>Arnold Engineering Development Center (DYFS) Air Force Systems Command Arnold Air Force Station, Tennessee 37389</b>		12. REPORT DATE <b>June 1977</b>
14. MONITORING AGENCY NAME & ADDRESS (if different from Controlling Office)		13. NUMBER OF PAGES <b>202</b>
		15. SECURITY CLASS. (of this report) <b>UNCLASSIFIED</b>
		15a. DECLASSIFICATION/DOWNGRADING SCHEDULE <b>N/A</b>
16. DISTRIBUTION STATEMENT (of this Report)  <b>Approved for public release; distribution unlimited.</b>		
17. DISTRIBUTION STATEMENT (of the abstract entered in Block 20, if different from Report)		
18. SUPPLEMENTARY NOTES  <b>Available in DDC</b>		
19. KEY WORDS (Continue on reverse side if necessary and identify by block number) <div style="display: flex; justify-content: space-between;"> <div> <b>X-ray</b> <b>radiographic</b> <b>RF transport</b> <b>electron beam</b> </div> <div> <b>linear accelerator</b> <b>radiographic clearance measurements</b> <b>engine testing</b> <b>simulated engine flight loads</b> </div> <div> <b>flight loads</b> <b>clearance measurement</b> </div> </div>		
20. ABSTRACT (Continue on reverse side if necessary and identify by block number) <p>An analytical program was conducted to define the radiographic requirements necessary for the implementation of a radiographic system in a Turbine Engine Loads Simulator (TELS) facility. Data from the TELS studies provided the flight conditions which were used to determine the rotor case deflections of the engine under load. Source positioning and areas to be radiographed were located by analyzing the gyroscopic moments acting on the engine during centrifuge operation. An X-radiation source to measure internal</p>		

# UNCLASSIFIED

# UNCLASSIFIED

## 20. ABSTRACT (Continued)

clearances was selected after relationships between radiographic requirements and source parameters were established. Two-radiographic system concepts, on-centrifuge and off-centrifuge, were evaluated for integration into the TELS system. The on-centrifuge concept was selected because of its potential in offering more flexibility in source positioning. This concept locates as many of the critical components as possible near the center of rotation of the centrifuge and utilizes a linear accelerator with RF power. To implement the on-centrifuge concept in the TELS facility, preliminary design requirements were identified and recommendations for further study made.

## PREFACE

This final report describes the work conducted during the period 1 March 1976 through 28 February 1977 by Pratt & Whitney Aircraft, East Hartford, Connecticut, under contract No. F40600-76-C-0008 for the USAF, Arnold Engineering Development Center. This report presents results obtained from investigation of radiographic requirements, systems and technical problems associated with implementing a radiographic system in a Turbine Engine Loads Simulator (TELS) facility.

Mr. Bruce E. Kinchen served as program manager and author of the report and provided technical direction throughout the program. Acknowledgement is given to Alan J. Zukor for his contribution during the mechanical component studies. Air Force program monitors for this work were Capt. Gerald M. Mulenburg and Mr. Forrest B. Smith, Directorate of Technology, Arnold Engineering Development Center.

This report submitted on 1 March 1977 is in compliance with the requirements of Task V of the Statement of Work, and was prepared under the Contractor's reference No. PWA FR-8496. The Program Elements were 65807F and 63723F.

The reproducibles used in the reproduction of this report were supplied by the authors.

## TABLE OF CONTENTS

<u>SECTION</u>	<u>PAGE</u>
INTRODUCTION	11
SUMMARY	12
RECOMMENDATIONS FOR RESEARCH AND DEVELOPMENT	14
RADIOGRAPHIC REQUIREMENTS	16
GENERAL	16
MATERIAL TYPES AND THICKNESS	18
THICKNESS SENSITIVITY	21
TIME RESOLUTION OF THE RADIOGRAPHIC SYSTEM	32
SPATIAL RESOLUTION REQUIREMENTS	33
DETECTOR INFLUENCE ON CHOICE OF SOURCE	41
GEOMETRY	46
SOURCE PARAMETERS	48
RADIATION SPECTRUM	48
RADIATION PULSE LENGTH	49
RADIATION OUTPUT	50
TIMING ACCURACIES FOR OFF-CENTRIFUGE SYSTEM	52
TARGET SIZE	53
TARGET MATERIAL SELECTION	53
TARGET THICKNESS	53
IMPLEMENTATION OF X-RAY SOURCE	60
SELECTION OF CONCEPT	60
ELECTRON BEAM TRANSPORT (Variation A)	64
Electrostatic Deflection of Electrons	64
Magnetostatic Deflection of Electrons	67
R-F TRANSPORT (Variation B)	68
ALIGNMENT OF X-RAY SOURCE UTILIZING WAVE GUIDE TRANSMISSION	73
EXPERIMENTAL PROCEDURES FOR ENGINE TESTING	75
POSITIONING SYSTEM – CONCEPTUAL MECHANICAL DESIGN	75
Modifications to Existing Design	76
Motorized X-Ray Support Frame	78
SYSTEM REQUIREMENTS	84
GENERAL REQUIREMENTS	84
X-RADIATION SOURCE REQUIREMENTS	84
DETECTOR SYSTEM REQUIREMENTS	85
CONTROL SYSTEM REQUIREMENTS	86
FILM TRANSPORT AND VIDEO FLUOROSCOPY	87
FILM PROCESSING AND DATA ANALYSIS	87
Processing of Magnetically Stored Images	87
Computer Image Processing	88
TELS SHIELDING REQUIREMENTS	90

## TABLE OF CONTENTS (Cont'd)

SECTION	PAGE
REFERENCES	95
APPENDIX A – ON/OFF CENTRIFUGE CONCEPTS	96
APPENDIX B – DEFLECTION ANALYSIS OF MAGNETRON CATHODE	103
APPENDIX C – ON CENTRIFUGE SOURCE POSITIONING	107
APPENDIX D – OFF-CENTRIFUGE SOURCE POSITIONING	155
APPENDIX E – RADIATION SHIELDING CALCULATIONS	161
APPENDIX F – TELS LOADS ON THE LINEAR ACCELERATOR	188
LIST OF SYMBOLS	195

## LIST OF ILLUSTRATIONS

FIGURE		PAGE
1	Typical Exposure Curves for Tungsten (w), Cold Rolled Steel (Fe), Natural Uranium (u), and Lead (Pb)	17
2	X-ray Source Selection Procedure	18
3	Path Length and Radiation Intensity Through a Cylindrical Section of an Engine	21
4	Two Mean Free Path Lengths for Various Materials vs Photon Energy	25
5	$(1 + \frac{I_S}{I_D})$ for Various Electron Energies vs Steel Thickness	28
6	$(1 + \frac{I_S}{I_D})$ vs Energy for Steel	29
7	Minimum Detectable Thickness Through 7.62 cm of Specific Materials vs Photon Energy	30
8	Measurement of Unsharpness	35
9	Modulation Transfer Function for Fine Grain Radiographic Film with Lead Intensifying Screens at 2.15 MeV	36
10	Minimum Visually Observable Clearance Based on Film MTF	37
11	Output of Detector is Proportional to the Area of the Source Not Blocked From View by the Edge	37
12	Modular Transfer Function for Uniform Emitting Circular Source	38
13	Modulation Transfer Function for Uniformly Emitting Circular Source	39
14	Modulation Transfer Function for Uniformity Emitting Circular Source and Radiographic Film	40
15	Minimum Visual Observable Clearance Based on Film/Source MTF	40
16	Speeds of Various X-ray Film	42
17	Modulation Transfer Function for Various Speed X-ray Film	43

## LIST OF ILLUSTRATIONS (Cont.)

FIGURE		PAGE
18	Silicon Photodiode Output vs Exposure	44
19	Spectral Sensitivity of X-ray Film	45
20	Variation of Geometric Unsharpness, Exposure Time, and Radiation Intensity With Target to Object Distance	47
21	Intensity Spectrum for Tungsten at Various Electron Energies	49
22	Radiation Required to Expose Kodak Film Through 7.62 cm of Steel	51
23	Energy Loss of Electrons in Various Target Materials	54
24	Critical Energy vs Atomic Number	54
25	Incident Electron Range Through a Tungsten Target	55
26	Relative On-Axis Radiation vs Target Thickness for 20 MeV Bremsstrahlung	56
27	Intensity Angle Distribution @ 20 MeV After Passing Through 10 cm of Uranium	57
28	Intensity Angle Distribution @ 20 MeV	57
29	Half Angle to Half Intensity for Various Energies at 1 Meter from Target	58
30	Typical Electrical Circuit Structure of a Magnetron	61
31	Schematic View of a Klystron Tube	62
32	X-ray Support to Provide Axial and Radial Repositioning	77
33	Modification to Original TELS Design Allowing Axial Positioning	79
34	Frame Design for Reducing Size of X-ray Unit Support Structure	80
35	Schematic of X-ray Support Frame Allowing Movement of the Channel Support	82

## LIST OF ILLUSTRATIONS (Cont'd)

FIGURE		PAGE
36	Block Diagram of Computer Image Processing System	89
37	Layout of TELS Facility Without Earthen Revetment	91
38	Inner Fencing and Location of Control Room	92
39	Shield Construction Composed of Lead and Steel	94
A	RF Power Transmission Scheme	97
B-1	Magnetron Cathode Cross Section	103
C-1	Alignment of X-ray Beam at the Engine Axial Station	107
C-2	Lightweight Fighter Turbofan Engine Rotor Case Pinch Point Locations, Case F1	117
C-3	High Bypass Ratio Turbofan Engine Rotor-Case Pinch Point Location, Case F7	118
C-4	Lightweight Fighter Turbofan Engine Rotor-Case Pinch Point Locations, Case F1	121
C-5	Lightweight Fighter Turbofan Engine Rotor Case Pinch Point Locations, Case F2	123
C-6	Lightweight Fighter Turbofan Engine Rotor Case Pinch Point Locations, Case F2	125
C-7	Lightweight Fighter Turbofan Engine Rotor Case Pinch Point Locations, Case F3	127
C-8	Lightweight Fighter Turbofan Engine Rotor Case Pinch Point Locations, Case F4	129



## LIST OF ILLUSTRATIONS (Cont'd)

FIGURE		PAGE
C-9	Lightweight Fighter Turbofan Engine Rotor Case Pinch Point Locations, Case F5	131
C-10	Lightweight Fighter Turbofan Engine Rotor Case Pinch Point Locations, Case F6	133
C-11	Lightweight Fighter Turbofan Engine Rotor Case Pinch Point Locations, Case F7	135
C-12	Lightweight Fighter Turbofan Engine Rotor Case Pinch Point Locations, Case F8	138
C-13	Lightweight Fighter Turbofan Engine Rotor Case Pinch Point Locations, Case F9	139
C-14	Lightweight Fighter Turbofan Engine Rotor Case Pinch Point Locations, Case L1	141
C-15	Lightweight Fighter Turbofan Engine Rotor Case Pinch Point Locations, Case L1	143
C-16	Lightweight Fighter Turbofan Engine Rotor Case Pinch Point Locations, Case L2	155
C-17	Lightweight Fighter Turbofan Engine Rotor Case Pinch Point Locations, Case L2	157
C-18	Lightweight Fighter Turbofan Engine Rotor Case Pinch Point Locations, Case C1	159
C-19	Lightweight Fighter Turbofan Engine Rotor Case Pinch Point Locations, Case C1	161
E-1	Attenuation of Primary Beam by a Series of Shields	177
E-2	Relationship of Control Room to X-ray Source	184

## LIST OF TABLES

TABLE		PAGE
I	X-Ray Absorption Coefficient, $\text{cm}^{-1}$	19
II	Concepts for Implementation of X-ray Source	61
III	Weight Estimate for X-ray Positioner	83
IV	Service Requirements for X-Radiation Source	90
C-I	High Bypass Ratio Turbofan Static Deflections with Nacelle Installed	113
C-II	Lightweight Fighter Engine Static Deflections	114
C-III	Test Requirements and TELS Operating Parameters	119
E-1	Primary Radiation Workload	168
E-2	Leakage Radiation Workload	169
E-3	Scattered Radiation Workload	171
E-4	Scattered Radiation Workload	174
E-5	Primary, Leakage, Scatter Radiation	176
E-6	Total Dose at Outer Fence	177
E-7	Workload at Various Distances	178

## INTRODUCTION

Current technological advances in turbine engine design and materials have provided the capability for designing and building lightweight, more powerful aircraft engines. One characteristic of these engines is that their structures tend to be more flexible and therefore, more vulnerable to maneuver loads. At larger operating and flight loads, the engine case and internal components are subjected to increased distortion.

To date, there have been few engine problems traceable to maneuver loads. However, the effects of such loads on rotor bowing and case ovalization are not currently well understood, and there is evidence that case ovalization in some high bypass ratio commercial engines has resulted in short term performance deterioration. The case deflections and the quantity of turbine blades being repaired for tip damage as well as the clearances observed in high pressure compressors suggest that these deflections may be already adversely affecting life cycle costs.

To evaluate distortion effects on engine structure and operation, the Air Force is sponsoring development of a Turbine Engine Loads Simulator (TELS) centrifuge facility that would impose simulated flight loads in an operating engine, and provide the capability to obtain high quality radiographs showing internal clearances and changes in clearances in the engine under load. A part of this program addressed the requirements, systems, and technical problems associated with implementing a radiographic system in a TELS facility. The areas of investigation consisted of: 1) identification of the radiographic requirements for obtaining the quality of radiographs needed for the measurement of internal engine clearances during the testing of gas turbine engines on the proposed TELS, 2) identification of radiographic systems that offer the potential of meeting the TELS requirements, 3) identification of significant technical problems that require resolution before a practical radiographic system that meets AEDC's requirements can be built, and 4) radiation shielding to ensure personnel safety.

## SUMMARY

A radiographic system is an attractive approach toward understanding the effects of different loadings on internal clearances and component distortion of a gas turbine engine. A major problem is obtaining high quality radiographs showing these clearances and changes in clearances.

Under Air Force Contract F40600-76-C-0008, an analytical program was conducted to investigate radiographic requirements for a Turbine Engine Loads Simulator (TELS) centrifuge facility which will have the capability of simulating flight loads on an operating engine. The program addressed: 1) radiographic requirements for obtaining the quality of radiographs needed for the measurements of internal engine clearances during testing of gas turbine engines on the proposed TELS, 2) radiographic systems that offer the potential of meeting the TELS requirements, and for the more promising systems, identify the preliminary facility requirements, 3) significant technical problems that require resolution before a practical radiographic system meeting AEDC's requirements could be built, and 4) shielding requirements to ensure personnel safety.

Two different radiographic concepts were evaluated for integration into the TELS facility. One system mounted the radiographic equipment on the centrifuge arm, while the other mounted the equipment off the centrifuge arm. In the off-centrifuge concept, the large size and weight of the machines presented enormous problems for positioning flexibility required by the hinge-gimbal engine positioner. The most practical off-centrifuge mounted scheme appears to be multiple "off-the-shelf" X-ray sources uniformly distributed around the circumference of the centrifuge. In this case, timing and centrifuge motion limit the usefulness of such a design.

The on-centrifuge was therefore selected as the most viable concept to meet the TELS requirements. This concept locates as many components as possible near the center of rotation of the centrifuge and utilizes a linear accelerator as an X-radiation source. To implement this type of apparatus, several concepts were studied of which the following appear most feasible:

- 1) The R-F power is generated at the center of rotation of the centrifuge and transmitted via a system of rigid and flexible waveguides and couplings to an accelerator structure mounted at the gas turbine location.
- 2) The most attractive concept from an operational viewpoint is to have the modulator and pulse transformers located at the center of rotation of the centrifuge and the accelerator structure, R-F oscillator, and other necessary components at the gas turbine location. The high voltage pulses to the electron gun, control grid, and R-F power supply would be supplied with flexible conductors.

Selection of the X-ray source was made by first establishing the relationship between the various radiographic parameters important in engine radiography and the X-ray spectrum.

The specific items addressed were engine materials and material thickness, thickness sensitivity, spatial resolution and time resolution. These relationships were utilized to describe the required spectrum for engine radiographs. The relationship between X-ray spectrum and electron energy was then developed. An electron energy of approximately 10 MeV appeared to be suitably rich in the X-ray spectral components required for engine radiography.

Data from the TELS studies were used to calculate the flight loads that would be imposed on the engine operating in actual flight conditions. Important parameters necessary to calculate engine rotor deflections due to the action of gyroscopic moments and linear accelerations were identified. The most important of these were the rotor polar moments of inertia, the rotor speed, and the components of the centrifuge angular rate and centripetal acceleration perpendicular to the rotor centerline. The rotor case pinch points and the clearances of interest were identified once the horizontal and vertical components of the rotor displacement were determined.

Preliminary design requirements were identified to accommodate the on-centrifuge concept utilizing R.F. transport. These requirements were associated with the accelerator supports, detector, film processing, data analysis, and personnel safety. The areas that require further investigation involve: 1) the X-radiation source, which consists of the linear accelerator and its associated components, 2) the image processing system, 3) interface devices to accommodate the required interaction between the engine, detectors, positioner, and X-ray source, and 4) alternative techniques to measure internal clearances in the engine.

## **RECOMMENDATIONS FOR RESEARCH AND DEVELOPMENT TO PROVIDE AN OPERATIONAL SYSTEM**

1. No commercially available linear accelerator has been qualified in excess of 1-g. Conversations with manufacturers indicate that existing R-F oscillators capable of the power outputs required for the TELS application, as well as the electron gun, will definitely not accept 15-g loads. In order to provide a system for utilization above 1-g normal, a three phase approach is recommended.
  - a) Design and construct the 15-g compatible electron gun and accelerator structure, and mount the available R-F power supply at the center of rotation. Utilize waveguide to transport power to the accelerator at the engine location.
  - b) Concurrently with (a) above initiate the design, fabrication, and certification of an R-F power source to take 15-g.
  - c) Eliminate the waveguide transmission and generate the R-F at the accelerator utilizing the R-F source developed in (b) above.

Utilizing a flexible waveguide or joint to maintain a particular orientation of the R-F source relative to the centrifuge may simplify the certification to 15-g.

2. In order to make the required measurements from the thousands of images generated at the facility, means must be developed for digital image processing. The image processing must be capable of image enhancement and operation in near real time to complement the real time imaging system as well as image processing for post-test extraction of clearance measurements from film radiographs and video images. Some general purpose image enhancement software is currently available. The algorithms required for image manipulation for the extraction of clearance measurements must be developed. Preliminary efforts along these lines have been initiated and have demonstrated feasibility.
3. A film transport system, video fluoroscope, and solid state detectors must be developed for the TELS due to the remote operation requirement. No current systems that provide remote capabilities are suitable for 15-g operation.
4. Appropriate interface devices must be designed and constructed to accommodate the required interaction between the engine, detectors, positioner, and X-ray source. These include:
  - a) Electronic interface to allow strobing of the X-ray pulses with the engine rotation to provide optimum geometry for unshrouded blade tip clearance measurements and isolation of particular areas of shafts and rotors.
  - b) Electronic interface that allows initiation of radiographic exposures at specific engine RPM or times after initiation of transients.

- c) Electronic interface that provide automatic advance of cameras and control of the X-ray source output.
- 5. Of importance during engine testing on TELS is the measurement of temperatures, pressures, etc., as well as internal clearances by alternate techniques. An evaluation of the special instrumentation requirements for this high-g testing should be performed. Items that would have to be qualified to 15-g's could include slip rings, proximity probes, optical pyrometers and thermocouples, pressure transducers, etc. Development of specific instrumentation to meet the TELS 15-g requirements should follow this initial study.

## RADIOGRAPHIC REQUIREMENTS

### GENERAL

The radiographic measurements of turbine engine internal clearances can be accomplished by the utilization of various types of electromagnetic radiation. As radiation passes through matter, it is modulated by both thickness and absorption coefficient variation. This modulation is detected, recorded, and subsequently used to make a clearance measurement.

X-ray and neutron sources are of special interest in this respect because both have been employed for radiography in the past. X-ray sources are currently employed for turbine engine internal clearance measurements. Neutron sources have been utilized in air frame inspection but its utilization in turbine engine internal clearance measurements has not been implemented to the best of our knowledge. However, X-ray sources of sufficient photon energy can generate a thermal neutron flux that might be usefully employed in engine radiography as an independent radiation source or in conjunction with X-radiation.

In general, neutron radiography offers little or no advantage as replacement for successful X-radiography. In particular, neutron radiography would offer no advantage over X-radiography as applied to the measurement of internal turbine clearances. The primary reason for this is the relatively long exposures required for the neutron flux available from reasonable sized sources. Figure 1 shows typical exposure curves for several materials. For a neutron intensity of  $10^7$  neutrons/cm<sup>2</sup>-sec., the exposure time for a film density of 1.5 through 7.62 cm of iron is about 8 hours. A six minute exposure is required for 2.54 cm of iron. These long exposures are not compatible with the TELS radiographic requirements. Those devices and techniques utilized to reduce the exposure time generally result in poor resolution.

Of the various radio-isotope sources available, Cobalt-60 with its 1.17 and 1.33 MeV gamma-photons is the most suitable for engine radiography. The density of Cobalt is about 8.9 gm/cm<sup>3</sup>. Its activity is roughly 120 curies/gm and the number of roentgens per hour per curies at one meter from the source is 1.35. Several calculations of the source size required to provide the radiation output for engine radiography, resulted in sources abnormally large when compared to any commercially available. For a 10 mm diameter source a length of 50.8 cm would be required to produce a radiograph in one minute. This implies a source of approximately 44,000 curie which is a tremendous quantity of radioactive material. The calculation did not account for self absorption of the Cobalt source or the higher absorption coefficient at 1.33 MeV. These items would further increase the required source size. A factor of 6 increase in output would be required to obtain an effective source diameter of 1 mm.

A reasonably sized source of about 3000 curie would require exposure times of 30 minutes or greater for typical engine radiography. The abnormal size and/or the relative long exposure times make application of radio-isotope sources for TELS unacceptable.



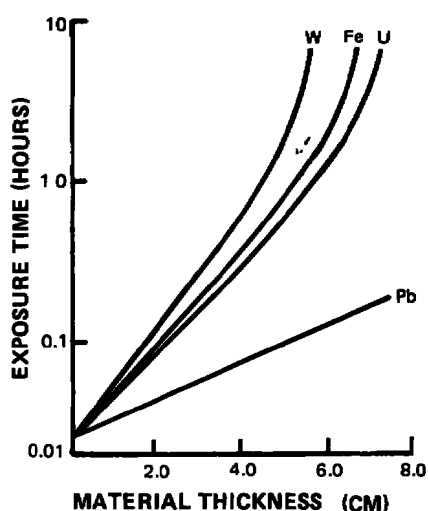


*Figure 1 Typical Exposure Curves for Tungsten (W), Cold Rolled Steel (Fe), Natural Uranium (U), and Lead (Pb), Neutron Intensity  $10^7$  N/cm<sup>2</sup>-sec, and Pysprosium Transfer Method With Kodak Type AA X-ray Film (Ref. 1)*

The only suitable source of radiation for the TELS application is a source generated by the collision of high energy electrons with a suitable target material. This type of source is addressed in the following sections where the basic criteria is established by which to choose a source for the particular task of engine X-radiography.

The selection of X-radiation source for engine internal clearance measurements depends upon a wide range of parameters. Among these are:

1. Engine material thickness
2. Types of engine material
3. Engine operating parameters (time resolution)
4. Size of the clearances to be measured (spatial resolution)
5. Engine geometry.

The above parameters define in a general way the source requirements.

The task is to find the optimum X-ray source required to produce accurate measurements of internal clearances of gas turbine engines. The engine size, material thickness, material type, size of the clearances to be measured, engine operating parameters, radiation detectors and the relative distances between the X-ray source, engine and detector determine the X-radiation spectrum/intensity distribution, target size, X-radiation pulse length and X-radiation flux. These parameters in turn specify the electron beam energy, electron beam current, the charge delivered to the target and the target characteristics. The flow chart in Figure 2 illustrates the approach used to specify the X-ray source for the TELS application.

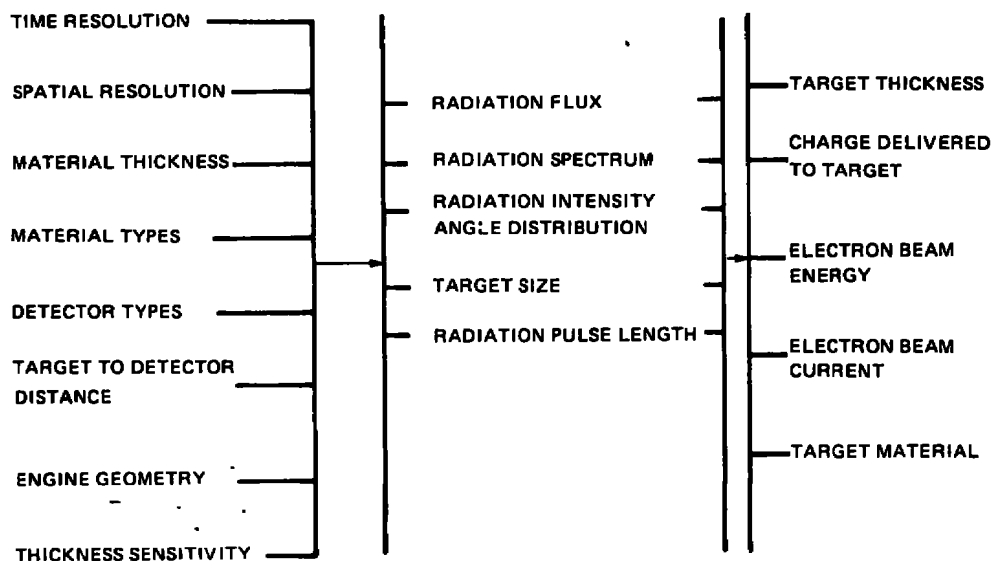


Figure 2 X-Ray Source Selection Procedure

## MATERIAL TYPES AND THICKNESS

In investigating the types of materials that might be encountered during radiographic testing, future structural materials should be considered as well as currently used materials. Some of the materials currently employed and likely to be employed in future engine structures and which may be involved in radiographic measurements are given in Table I.

TABLE I — X-RAY ABSORPTION COEFFICIENT,  $\text{cm}^{-1}$ 

Photon Energy, MeV	4	8	12	16	20
<b>Material</b>					
Aluminum	0.048	0.065	0.060	0.058	0.057
Magnesium	0.055	0.042	0.038	0.037	0.036
Alumina	0.121	0.091	0.081	0.077	0.075
Beryllium Oxide	0.088	0.063	0.053	0.032	0.033
Boron Carbide	0.071	0.049	0.041	0.036	0.033
Boron Nitride	0.066	0.046	0.039	0.035	0.033
Magnesia	0.100	0.075	0.067	0.063	0.061
Silicon Carbide	0.100	0.076	0.069	0.066	0.065
Thorium Dioxide	0.404	0.471	0.520	0.562	0.590
Titanium Diboride	0.137	0.112	0.106	0.105	0.106
Silicon	0.075	0.059	0.055	0.054	0.054
Graphite	0.059	0.043	0.039	0.031	0.031
Steel	0.305	0.281	0.289	0.301	0.313
Titanium	0.143	0.125	0.124	0.125	0.129

The total useful flux transmitted through an object is paramount when radiographing an engine. By considering the linear absorption coefficients at various photon energies, the energy at which minimum attenuation occurs and hence maximum transmitted flux can be determined. The linear absorption coefficients of some of the materials currently utilized in turbine engines are given in the data of Table I.

As can be seen, the linear absorption coefficients of these materials vary considerably. Based strictly on absorption coefficients of the various materials likely to be present within the same engine structure, it would be difficult if not impossible to arrive at a single source of radiation capable of imaging all parts of the structure.

For all the data shown, the absorption coefficients continue to decrease past 5 MeV. For many, they begin to increase slightly after reaching 10 MeV. Due to this, energies higher than 10 MeV would offer no obvious advantage based on useful flux transmission. Real gain in engine radiography would be obtained by increasing the electron beam current (i.e., the radiation flux), rather than increasing the electron beam energy. There is a limitation due to target material properties, target geometry, X-ray conversion efficiency and power supply on the amount of flux deliverable at a particular electron energy. The specific energy chosen will depend upon these parameters and the total flux requirement.

X-ray absorption coefficients were calculated for the compounds shown in Table I by utilizing the equation:

$$\left( \frac{\mu(\gamma)}{\rho} \right)_{A_a B_b \dots} = a \left( \frac{\mu(\gamma)}{\rho} \right)_A \frac{Z_A}{M} + b \left( \frac{\mu(\gamma)}{\rho} \right)_B \frac{Z_B}{M} + \dots$$

Where the formula for the compound is  $A_a B_b$ , and

- $Z$  = atomic number  
 $M$  = molecular weight of the compound  
 $\mu(\gamma)$  = X-ray absorption coefficient  
 $\rho$  = Density of material

If the absorption coefficients are too low, there is insufficient modulation of the transmitted radiation and detection is difficult. Materials such as fiberglass/epoxy and silicon rubber with low absorption coefficient are commonly employed in the low temperature sections of the engines as seal lands. Their shape within the engine is generally cylindrical and concentric with the engine shaft. Since radiographic measurements are generally obtained by aligning the X-ray source normal to the shaft of the engine and radially at the inside of a seal land, the seal land presents a rather long path length along the X-ray beam.

A simple relationship can be derived to illustrate the dependence of path length,  $t$ , through a cylindrical section of engine as a function of the radius assuming a relatively large target-to-object distance or a relatively thin wall thickness. This relationship is:

$$t = \begin{cases} 2(R_1^2 - r^2)^{1/2}, & R_2 \leq r \leq R_1 \\ 2[(R_1^2 - r^2)^{1/2} - (R_2^2 - r^2)^{1/2}], & r \leq R_2 \end{cases}$$

Where  $R_1$  = Outside Radius of Cylindrical shell  
 $R_2$  = Inside Radius of Cylindrical shell  
 $r$  = Radius at which  $t$  is determined.

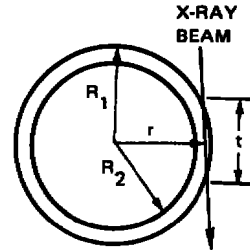


Figure 3 shows a thickness profile calculated for a typical engine geometry case. In this instance, the large thickness compensates for materials with relatively low attenuation coefficient. For engines used for aircraft propulsion that might be tested on TELS, the radius of the engine dictates that the choice of X-ray energy be high for some of the materials used and insures that no significant problems arise due to the variability of material attenuation coefficients.

Problems of imaging the low attenuation materials within an engine occur primarily when clearance measurements are required between blade tips and air seals of unshrouded blades. These free standing unshrouded blades represent the majority of the blades in a gas turbine engine and in some cases present a metal thickness in the direction of the X-ray beam that is below the minimum detectable thickness for the specific radiographic technique available. The parameter that specifies the detectability of these blade tips is termed "thickness sensitivity" and is a function of the material thickness, absorption coefficient, X-ray spectrum, and the detector employed.

The dependence of the thickness sensitivity on the X-ray spectrum is formalized in the following discussion.

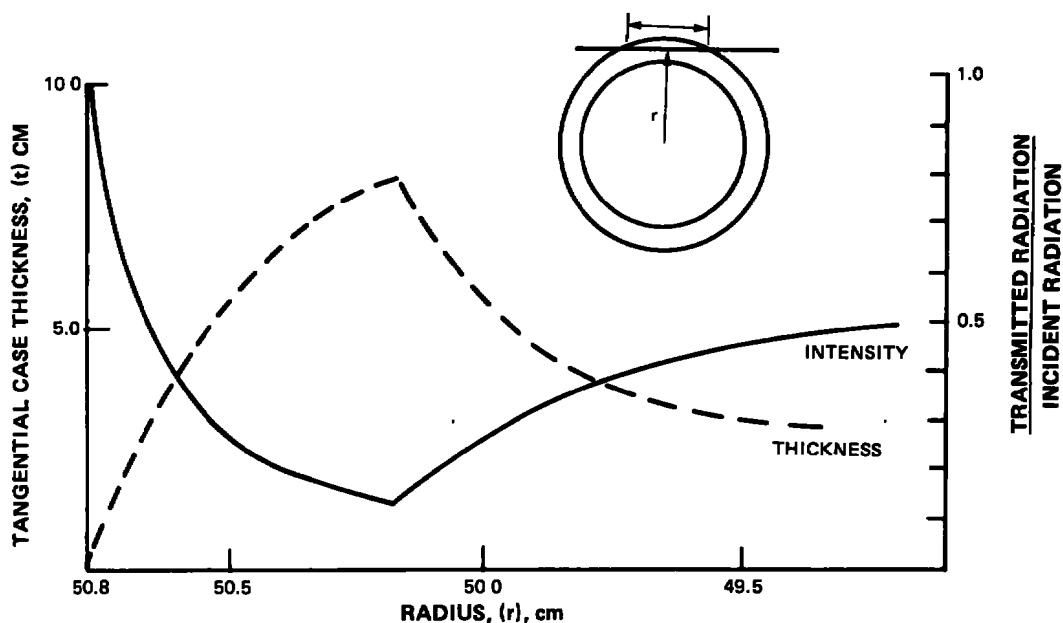
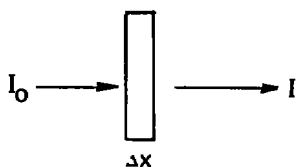


Figure 3 Path Length and Radiation Intensity Through a Cylindrical Section of an Engine

### THICKNESS SENSITIVITY

The general expression for the absorption of radiation as it passes through matter is developed by considering the fraction of the radiation absorbed in passing through a thin layer of matter.



- $I_0$  = incident radiation
- $I$  = transmitted radiation
- $\mu$  = absorption coefficient

The change in the amount of radiation,  $I_0 - I$ , is expressed as:

$$I_0 - I = \Delta I = \mu I_0 \Delta x$$

For monochromatic radiation and an absorber of finite thickness,  $x$ , the above equation can be integrated to give:

$$I_{\gamma} = I_{\gamma 0} \text{EXP} [-\mu (\gamma) x] \quad (1)$$

Where  $\mu (\gamma)$  = linear absorption coefficient at frequency  $\gamma$

$I_{\gamma}$  = the transmitted intensity at frequency  $\gamma$

$I_{\gamma 0}$  = the incident intensity at frequency  $\gamma$

Equation (1) is the exponential absorption law. The monochromatic transmittance is defined as:

$$T_{\gamma} = \frac{I_{\gamma}}{I_{\gamma 0}} = \text{EXP} [-\mu (\gamma) x]$$

If the incident radiation is not monochromatic, then we can define the incident intensity,  $I_0$ , as:

$$I_0 = \int_0^{\gamma_a} \phi (\gamma) d\gamma$$

Where  $\phi (\gamma)$  is the spectral distribution of intensity.

The transmitted intensity can be expressed as:

$$I = \int_0^{\gamma_a} \phi (\gamma) \text{EXP} [-\mu (\gamma) x] d\gamma$$

The transmittance is then given by:

$$T_0 = \frac{\int_0^{\gamma_a} \phi (\gamma) \text{EXP} [-\mu (\gamma) x] d\gamma}{\int_0^{\gamma_a} \phi (\gamma) d\gamma} \quad (2)$$

The average absorption coefficient,  $\bar{\mu}$  for the case of a spectral distribution of radiation can be obtained from Equation 2 by differentiation with respect to  $x$ .

$$\bar{\mu} = -T_0^{-1} \frac{dT_0}{dx}$$

For the continuous spectrum case, the fractional uncertainty in measuring a change in  $x$  can be derived as follows:

Statistical uncertainty resulting from random fluctuation of the incident quanta are the limiting factor to the detection of small thickness provided that detector errors are smaller than the statistical variations of intensity, and if only small numbers of quanta are available for detection.

The probability of a given number of quanta being emitted by an X-ray target in a finite interval of time is governed by Poisson's law. The absolute value of the standard deviation in the numbers of quanta,  $N$ , emitted and incident on an object is:

$$dN = \sqrt{N}$$

It can be seen that the absolute fluctuation increases with  $N$ . The relative fluctuation is given by:

$$\frac{dN}{N} = \frac{1}{\sqrt{N}}$$

and shows that the relative fluctuation decreases with  $N$ .

The exponential absorption law gives the following for monochromatic radiation:

$$N = N_0 \text{EXP} [-\mu (\gamma) x]$$

$$N_0 = \text{incident quanta}$$

Differentiating with respect to  $x$  we obtain:

$$\frac{dN}{dx} = -\mu (\gamma) N_0 \text{EXP} [-\mu (\gamma) x]$$

or

$$dx = \frac{-dN}{N_0 \mu (\gamma)} = -\frac{dN}{N_0 \mu (\gamma)} \text{EXP} [\mu (\gamma) x]$$

but

$$dN = \sqrt{N} = \sqrt{N_0} \text{EXP} [-\mu (\gamma) x/2]$$

and

$$dx = \frac{1}{\sqrt{N_0} \mu (\gamma)} \text{EXP} [\mu (\gamma) x/2]$$

Since

$$T_{\gamma} = \text{EXP} [-\mu (\gamma) x]$$

Then

$$\frac{dx}{x} \sqrt{N_0} = \frac{1}{\mu (\gamma) x \sqrt{T}} \quad (3)$$

For a spectral distribution of intensity we substitute  $\bar{\mu}$  for  $\mu (\gamma)$  in Equation (3) and the appropriate form of the transmission to obtain:

$$\frac{dx}{x} \sqrt{N_0} = \frac{1}{\bar{\mu} x \sqrt{T}} \quad (4)$$

If we differentiate Equation (4) with respect to  $\bar{\mu}x$  (number of mean free paths) we obtain:

$$\frac{d}{d(\bar{\mu}x)} \left[ \frac{dx}{x} \sqrt{N_0} \right] = \left[ \frac{\bar{\mu}x-2}{2(\bar{\mu}x)^2} \right] \text{EXP} [\mu x/2]$$

We find that the minimum fractional uncertainty in measuring a change in  $x$  occurs for a monoenergetic spectrum at a thickness of two mean free paths.

For the continuous spectrum case indications are that this is still roughly true for 5, 20, and 100 MeV tungsten Bremsstrahlung (Ref. 1). This means that the best thickness sensitivity for a given spectrum occurs at a metal thickness of 2 mean free paths for that spectrum, provided that the statistical uncertainties resulting from the random fluctuations of the incident quanta are the limiting factor of the detection process.

Two mean free paths were calculated for steel, iron, titanium, silicon, graphite, magnesium and aluminum for various photon energies. The results are illustrated in Figure 4. We see that for three of the important materials in current turbine engines, titanium and nickel and iron, the minimum fractional uncertainty for measuring a change in  $x$  is obtained at the greatest material thickness in the 8 to 10 MeV range. The other materials, in the energy range shown, continue to improve with energy. However, all material appears to show this optimization of fractional uncertainty with thickness at a specific energy.

This minimum occurs at lower energies and material thickness as the atomic number increases. The energy at which the mean free path is maximized is that energy at which the fractional uncertainty (thickness sensitivity) is optimized with thickness of material.

If large number of quanta are available and if the detector errors are larger than the statistical variation of intensity, then thickness sensitivity depends upon the detector capabilities. We can develop an expression for the thickness sensitivity when utilizing film as a detector. Let  $I_D$  be defined as that portion of the X-radiation reaching the film that provides information about the object and  $I_S$  be defined as scatter X-radiation intersecting the film.  $I_S$  primarily lowers contrast of the resulting image.



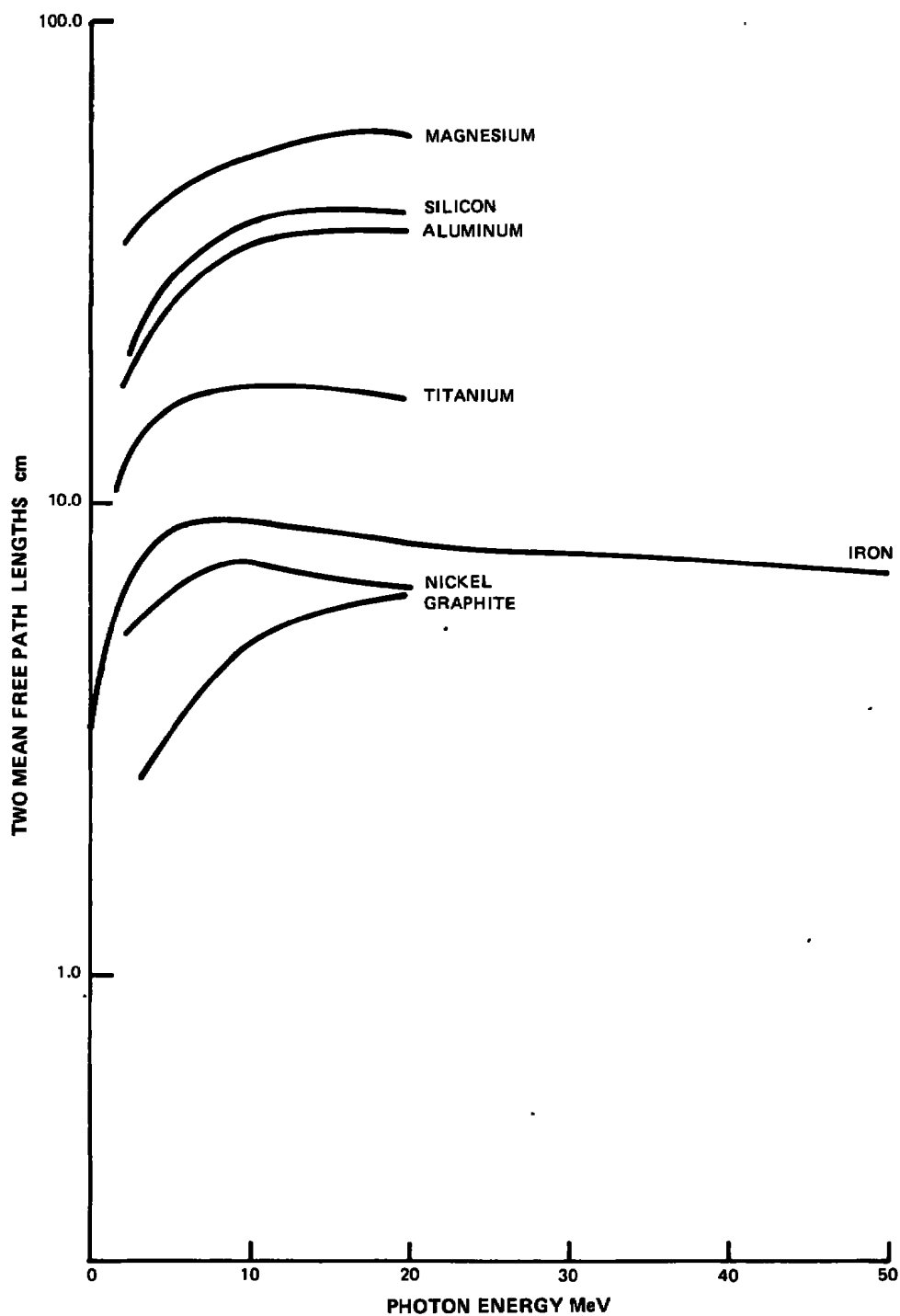


Figure 4 Two Mean Free Path Lengths For Various Materials vs. Photon Energy

Let the smallest observable thickness be  $\Delta x$  in thickness  $x$ . Assume that  $\Delta x$  is small so that the ratio  $I_S/I_D$  is approximately the same for  $x$  and  $(x + \Delta x)$ . The film density changes from  $D$  to  $D + \Delta D$  due to a thickness change of  $\Delta x$ . Over small density changes, the shape of the film sensimetric curve can be assumed constant. The film density,  $D$ , can be expressed by:

$$D = G_D \log E' + h_0 \quad (5)$$

Where  $G_D$  = slope of film sensimetric curve  
 $E'$  = exposure  
 $h_0$  = constant

Differentiating Equation (5) we get:

$$\Delta D = \frac{G_D}{\ln 10} \frac{\Delta E'}{E'} \quad (6)$$

We can write  $E' = I t$ ,  $\Delta E' = \Delta I t$  where  $I$  is the radiation intensity and  $t$  is the exposure time. Substituting into Equation (6) we get:

$$\Delta D = \frac{G_D}{\ln 10} \frac{\Delta I}{I}$$

or

$$\frac{\Delta I}{I} = \frac{\ln 10 \Delta D}{G_D} \quad (7)$$

Now  $\Delta I$  equals  $-\bar{\mu} I \Delta x$ . Substituting into Equation (7) we obtain:

$$\Delta x = \frac{-2.3 \Delta D}{\bar{\mu} G_D} \quad (8)$$

Assuming scatter radiation,  $I_S$ , is distributed uniformly on the film, and the image carrying radiation is  $I_D$ , we have the total radiation on the film,  $I$ , equal to  $I_S + I_D$ . Substituting into Equation (8) we obtain:

$$\frac{\Delta x}{x} = \frac{-2.3 \Delta D}{\bar{\mu} G_D x} \left( 1 + \frac{I_S}{I_D} \right) \quad (9)$$

If  $\Delta x$  is the minimum thickness change which can be detected, then  $\Delta D$  would be the "minimum density difference" discernable (Reference 2).

We can identify various parts of Equation (9) as:

$$\left(1 + \frac{I_S}{I_D}\right) / \bar{\mu} = \text{Radiation component}$$

$$\frac{1}{G_D} = \text{Film Component}$$

$$\Delta D = \text{Optical or viewing component}$$

For a given thickness specimen,  $\bar{\mu}$  and  $1 + \frac{I_S}{I_D}$  change as the X-ray energy is changed. The change in thickness sensitivity depends upon the relative change of  $\bar{\mu}$  and  $1 + \frac{I_S}{I_D}$  and can cause an increase or decrease in thickness sensitivity.

Solving Equation (9) for  $\Delta D$ .

$$\Delta D = \frac{-\mu G_D \Delta x}{2.3} \left( \frac{I_D}{I_S + I_D} \right)$$

If  $I_S = 0$ ,  $\Delta D$  is dependent only on thickness  $\Delta x$  and not on total thickness  $x + \Delta x$ . However,  $I_S \neq 0$ , and the ratio  $I_D/(I_S + I_D)$  is a function of  $x + \Delta x$  and decreases as  $x$  increases causing a reduction in  $\Delta D$  for a specific value of  $\Delta x$ .

We see that for a fixed energy, thickness, and  $\Delta x$ ,  $\Delta D$  increases as  $G_D$  increases. This implies that the larger  $G_D$  the larger  $\Delta D$ . It alternately implies that the thickness sensitivity for a given  $\Delta D$  can be improved if  $G_D$  is increased.

Values of  $(1 + I_S/I_D)$  versus steel thickness are given in Reference 2 and presented in Figure 5. These values were replotted as in Figure 6 to give  $(1 + I_S/I_D)$  as a function of energy. This information was utilized to generate an equation for  $(1 + I_S/I_D)$  for steel as a function of electron energy and thickness. For electron beam energies of 4 MeV to 15 MeV,  $(1 + I_S/I_D)$  is given approximately by:

$$\left(1 + \frac{I_S}{I_D}\right) = 1.4 + (1.06 - 0.0595 E) x \quad (10)$$

Where  $E$  = electron energy in MeV, (to 15 MeV)  
 $x$  = metal thickness in inches

Substituting Equation (10) into Equation (9) we have

$$\frac{\Delta x}{x} = \frac{-2.23 D}{\mu G_D x} [1.4 + (1.06 - 0.0595 E)x] \quad (11)$$

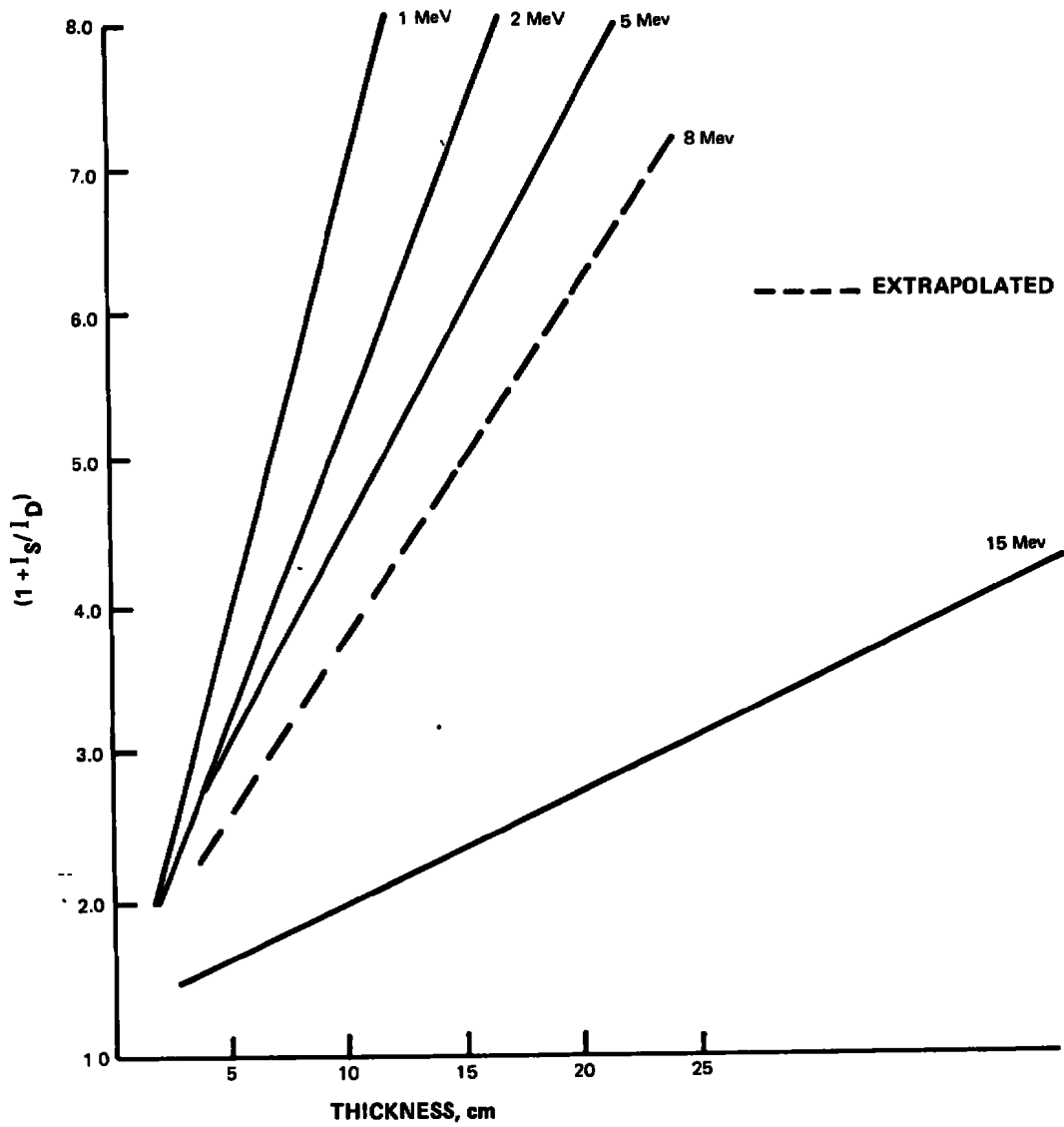


Figure 5  $(1 + \frac{I_S}{I_D})$  For Various Elect. on Energies vs. Steel Thickness

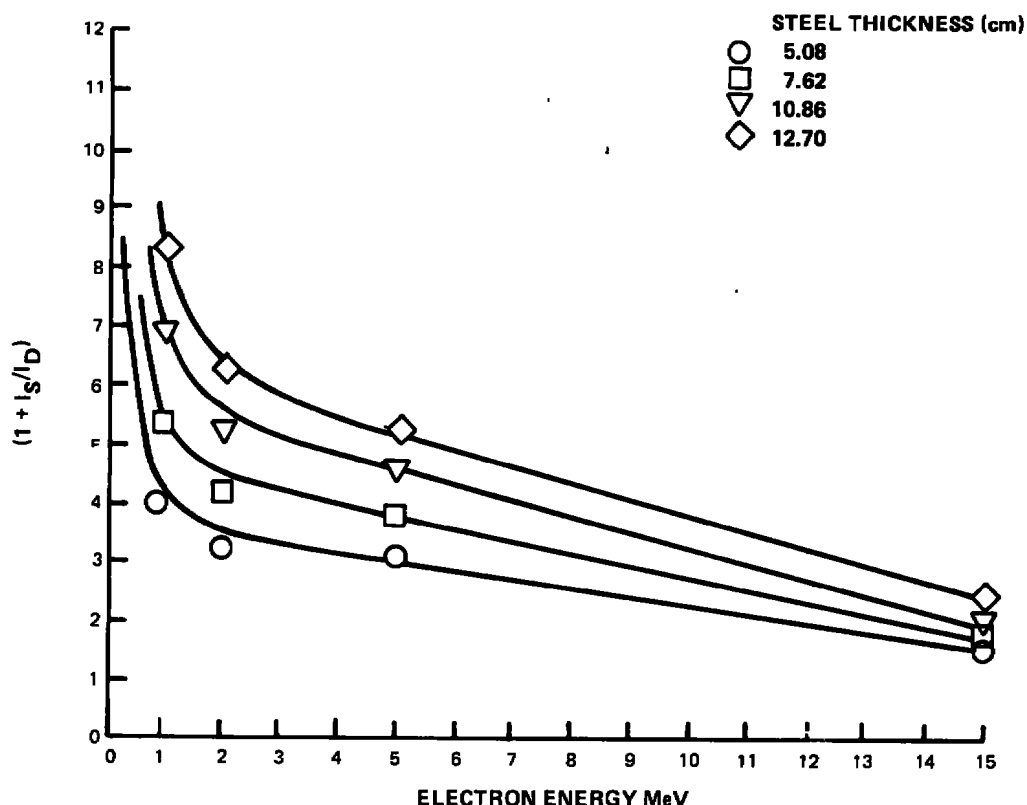


Figure 6  $(1 + \frac{I_S}{I_D})$  vs. Energy for Steel

Using film as a detector we see from Equation (11) that for steel and electron energies to 15 MeV that at a specific energy, the thickness sensitivity gets better as  $x$  gets larger. This is contrary to the results of Equation (3).

If we calculate  $\Delta x$  for 7.62 cm thick steel ( $x = 7.62$  cm) for various values of  $E$  we find that the minimum discernable thickness,  $\Delta x$ , increases to about 5 MeV and then shows a steady decrease to high energies as shown in Figure 7.

It would be suspected that Equation (11) could be extended to other materials by substituting an equivalent thickness of the material for the steel thickness in the equation. If  $x_S$  and  $\mu_S$  are the steel thickness and absorption coefficient respectively and  $x_a$  and  $\mu_a$  are the alternate material thickness and absorption coefficient, we can write the thickness of the alternate material that is equivalent to the steel thickness as:

$$x_a = \frac{\bar{\mu}_S}{\bar{\mu}_a} x_S \quad (12)$$

Substituting into Equation (11) we obtain:

$$\frac{\Delta x}{x} = \frac{-2.3 \Delta D}{\bar{\mu} G_D x} [ 1.4 + (1.06 - 0.0595 E) \frac{\bar{\mu}}{\bar{\mu}_S} x ] \quad (13)$$

Where now we have

$x$  = material thickness

$\bar{\mu}$  = absorption coefficient of material

$\bar{\mu}_S$  = absorption coefficient of steel

Using this equation we calculated values of  $\Delta x$  for several materials and these are shown in Figure 7.

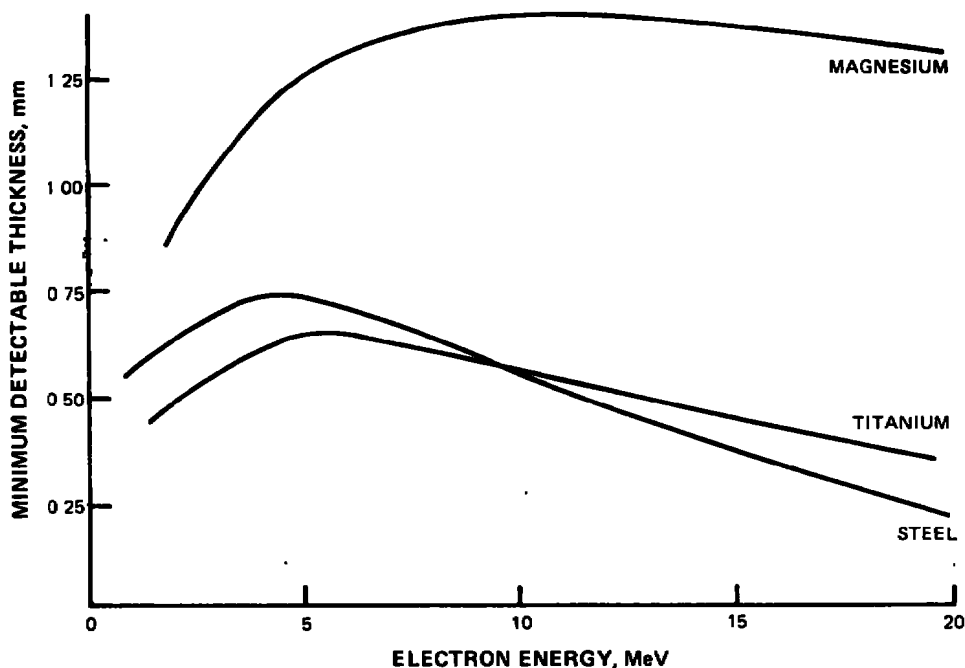


Figure 7 Minimum Detectable Thickness Through 7.62 cm of Specific Materials vs. Photon Energy

This figure illustrates the minimum discernable thickness variations through 7.62 cm of the specific material at various energies. For example, through 7.62 cm of steel at 8 MeV only a 0.635 mm change in thickness (blade tip thickness) could be detected. Likewise, through 7.62 cm of magnesium at 8 MeV a change in thickness of 1.372 mm could just be detected. Figure 7 indicates that for a thickness of 7.62 cm the minimum discernable thickness is maximized at about 4 to 6 MeV for steel and titanium and decreases at higher and lower energies. Lower energies imply lower production efficiencies for X-ray, less penetration and, therefore, extremely long exposure. Therefore we would choose energies higher than 6 MeV for engine radiography involving these materials.

Usually we would have a case of steel, magnesium or titanium with a material of another type for a blade. If we use the above example for 7.62 cm steel at 8 MeV and assume a case fitting these parameters and postulate a titanium blade, we can determine the thickness of the titanium blade tip that is detectable by first calculating the minimum steel thickness and converting to titanium by Equation (12). In steel,  $\Delta x$  ( $x_s$  in this case) was 0.635 mm. The thickness of titanium  $x_a$  is:

$$x_a = \frac{0.596}{0.318} (0.635) = 1.190 \text{ mm}$$

or 1.874 times the thickness of steel would be required for a titanium blade tip to be just detectable through a 7.62 cm steel case.

The problem of detection of unshrouded blade tips is further complicated by the fact that the blade tips are moving relative to the X-ray beam and appear to be oscillating radially. The amount of oscillation in terms of a peak-to-peak measurement is dependent upon the radius of the rotor and the number of blades on the rotor. The magnitude of this apparent radial motion can be on the order of 2.54 mm for the large fan of a high by-pass ratio engine, and in the turbine area it can be on the order of 0.254 mm. This apparent motion causes the blade tip to present a time average apparent thickness to the x-radiation, and a reduction in sensitivity of the radiographic technique. The effect can be characterized by calculating the apparent blade tip thickness presented to the X-ray beam during the detection time.

The problem of insufficient blade tip thickness can be overcome by tabbing blade tips with materials such as tungsten that have high absorption coefficients and by using strobo-radiographic techniques in a continuous or single flash mode. These two techniques should generally be used simultaneously.

From the foregoing it is evident that thickness sensitivity is an important parameter in the measurement of blade tip to outer air seal clearance. The measurement of unshrouded blade tip to outer air seal clearances dictate the strictest radiographic thickness sensitivity requirements. While thickness sensitivity is better at low energy, the requirement for penetration of thick sections encountered in engine radiography dictates higher energies. The data presented in Figure 7 indicates that energies above 6 MeV should be considered for penetration of materials currently utilized for engine cases. X-ray target diameter, X-ray flux and detection time requirements will further determine the X-ray spectrum.

## TIME RESOLUTION OF THE RADIOGRAPHIC SYSTEM

The time resolution required for radiographic measurements is somewhat difficult to define unless specific restrictions are applied to the type of measurements. For example, "flutter" of rotor blades in a compressor is a high frequency phenomena. If time resolved radiographic measurements of events of this type was required, severe requirements on a radiographic system would be imposed. Measurements of this type can likely be obtained by indirect radiographic techniques or by other instrumentation.

Two types of radiographic measurements of internal engine clearances are generally required. These are steady state and transients. Steady state measurements refer to internal clearances measured when the turbine engine is operated at steady-state and is in thermal and mechanical equilibrium. The time resolution of the measurement under these conditions is not generally important except in the sense that longer measurement periods imply longer engine test times.

In order to define the type of transients that might be simulated on TELS, discussions were held with three pilots at Pratt & Whitney Aircraft on the extent of transient throttle excursions during a given flight maneuver. One pilot was of the opinion that high altitude dogfight maneuvers were done at one power setting using the aerodynamics of the plane (ailerons, elevators, etc.) for control during the maneuver. The only time the throttle was changed was to select afterburner in order to maintain a given airspeed during the maneuver. The greatest power lever excursion would be from cruise power to max rotor speed at initiation of the maneuver.

Another type of maneuver discussed was a fighter-bomber ordnance delivery mission with a pull-up at the end to avoid enemy rockets and blast waves. During the glide path into the target the power lever would be retarded as far back as idle. Once the ordnance (bombs or rocket) was released the throttle would most likely be jammed into afterburner as the high g-maneuver begins.

The transients to be dealt with are of two kinds: mechanical and thermal. The mechanical transients are those high frequency changes in clearances due to the rapid acceleration of a turbine engine. These transients can be adequately described with measurements made at rates of one to two per second. Mechanical transients are usually over when the engine acceleration ends. The thermal transients are low frequency changes that lag the mechanical transients and result from the change in heat load to the engine structural members. Measurements at the rate of one measurement every five seconds adequately map the history of the clearance change.

The time resolutions required for the TELS radiographic system are as described above if the radiographic system is mounted on the centrifuge arm as illustrated in the various TELS studies.



However, an alternative approach was investigated that utilized an off-centrifuge system whose output was synchronized with the rotation of the centrifuge. In this approach, the time resolution depended upon the angular rate of the centrifuge. At the maximum rate of 33.4 rpm, a maximum of one measurement every 1.8 seconds was obtained with a single source of radiation. If two sources were utilized, the time resolution would be one measurement every 0.9 seconds assuming the sources are  $180^\circ$  apart, and that each source can produce a measurement in a single pulse. If the radiation is such that a single pulse is not sufficient to make a measurement, the dynamic transients could not be obtained by an off-arm system. For a single source with single pulse measurement capabilities, the ability to make dynamic transient measurements would be marginal.

Time resolution is a secondary source parameter in the sense that a variety of combinations of source and detectors could produce the required time resolution. The question that must be answered is whether a particular choice of source and detection system will give the desired spatial resolution within the time restrictions posed by the engine or radiographic system concept, whichever is most severe.

## **SPATIAL RESOLUTION REQUIREMENTS**

Since a radiographic system would be required to perform a variety of clearance measurements within the engine and the accuracy requirements vary depending on the particular measurement and how it effects the engine's performance, durability, etc., the radiographic system's spatial resolution should be maximized for each measurement made. In the past, spatial resolutions giving measurements to  $0.129 \text{ mm} \pm 0.0127 \text{ mm}$  on particular clearances have been reported. However, a clearance measurement with precision of  $\pm 0.127 \text{ mm}$  are more common, especially when measuring from film by visual techniques. Clearance measurement from 20 cm to 0 cm with accuracy requirements of  $\pm 0.025 \text{ mm}$  are routinely requested of an internal clearance measurement system. Many systems including radiographic systems, can meet these requirements under specialized lab type conditions, but few, if any, can guarantee this under routine engine test conditions. The spatial resolution capabilities of a radiographic system must be weighed against other system parameters when selecting a system for engine radiography. When a trade can be made in favor of system spatial resolution, it should be done. In some instances, e.g., mechanical transients, the short exposure times required might only be obtained for a given source by sacrificing spatial resolution.

Generally, the spatial resolution of a system is established by evaluating it in terms of its spatial frequency response. The frequency response function is called the "modulation transfer function" or MTF. The MTF is the ratio of the Fourier transform of the output and the Fourier transform of the input. As such, it provides a convenient description in frequency space of how a system alters the input. These Fourier transforms and thus the MTF exists if the input and output are smooth and absolutely integrable as is the case in X-radiography. The spatial frequency response of every component of a system can be evaluated individually and the total system modulation transfer function obtained by multiplying the individual MTF's together or the total system MTF can be evaluated as a single entity.

An evaluation of this type does not directly establish the spatial resolution of a system under an arbitrary operational condition, but establishes the optimum that could be obtained under specific ideal conditions. The approach is useful in the sense that if adequate spatial resolution is not obtained under the idealized conditions, it could not be obtained under adverse conditions.

A linear system operating on an input function  $g_1(x, y)$  produces an output function  $g_2(x, y)$ . If the system is spatially invariant, the output can be written in terms of the inputs as:

$$g_2(x_2, y_2) = \iint_{-\infty}^{\infty} g_1(\xi, \eta) h(x_2 - \xi, y_2 - \eta) d\xi d\eta \quad (14)$$

The integral is a two dimensional convolution of the object function with the impulse function:

$$h(x_2 - \xi, y_2 - \eta) \quad (15)$$

In general we can consider clearances as one-dimensional measurements and deal with a one dimensional form of Equation (14).

The above can be written in one dimension as:

$$g_2(x_2) = \int_{-\infty}^{\infty} g_1(\xi) h(x_2 - \xi) d\xi \quad (16)$$

$h(x_2 - \xi)$  is defined as the system impulse function or line spread function. A Fourier transform of the line spread function produces the MTF. The MTF of a system composed of several components consists of the product of the component MTF's.

$$MTF_{sys} = (MTF_{comp.1}) (MTF_{comp.2}) \dots \quad (17)$$

The major components of the radiographic system that cause distortion of the input functions are the source (size and energy distribution) and the detector. These items can be evaluated relative to their effects on resolution and therefore the choice of a radiographic system. Experience to date indicates that the highest spatial resolution is obtained by film detection techniques. Film will be utilized as the detector in evaluating system parameters.

Experimental values of film unsharpness is generally measured as illustrated in Figure 8. The distance  $U_f$  in the figure is defined as the unsharpness. Experimental values of film unsharpness measured in this manner (Ref. 2) were utilized to calculate MTF's for a fine grain film with lead intensifying screens for energies to 30 MeV. In order to calculate the MTF, a Gaussian distribution was assumed for the line spread function. This was Fourier transformed and

made to fit an experimentally determined film MTF for 8 MeV with the film unsharpness as a variable. The equation was of the form:

$$\text{MTF} = \text{EXP} (-k \pi^2 f^2 U_f^2) \quad (18)$$

$f$  = spatial frequency,  $\text{mm}^{-1}$

$U_f$  = Film unsharpness, mm

$k$  = 0.313

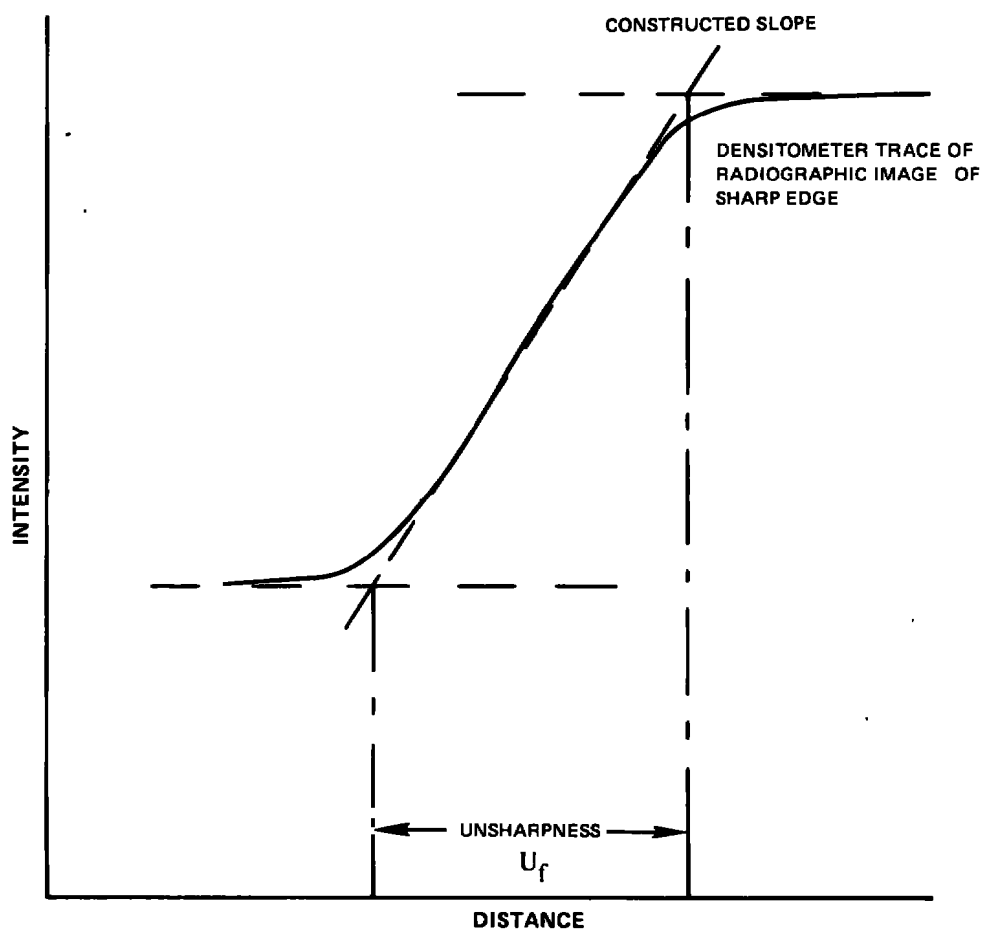


Figure 8 Measurement of Unsharpness

Calculations using this equation produced the data in Figure 9. As can be seen from this data, the higher the energy of the electron beam, the poorer the frequency response of the film. The poorer the frequency response of the film, the less faithful the reproduction of fine detail. Under ideal viewing conditions a density variation of 0.006 to 0.014 can be

detected by the human eye, this translates to an MTF value of 0.1 to 0.2. Using 0.1 as the value of MTF below which a detail could not be seen, the curve established in Figure 10 was generated. The minimum clearance presented is the distance corresponding to one-half cycle of the spatial frequency. Since the image of the engine is magnified, the minimum clearance in object space would be less than the minimum clearance calculated. Assuming a magnification of 1.5, new values of minimum clearance were calculated and are also presented in Figure 10 for comparison. Pratt & Whitney's experience at 8 MeV suggests that these values are reasonable for engine geometrics although in specific instances where very narrow gaps with long paths in the direction of the X-rays existed, high contrast images were obtained at 0.127mm.

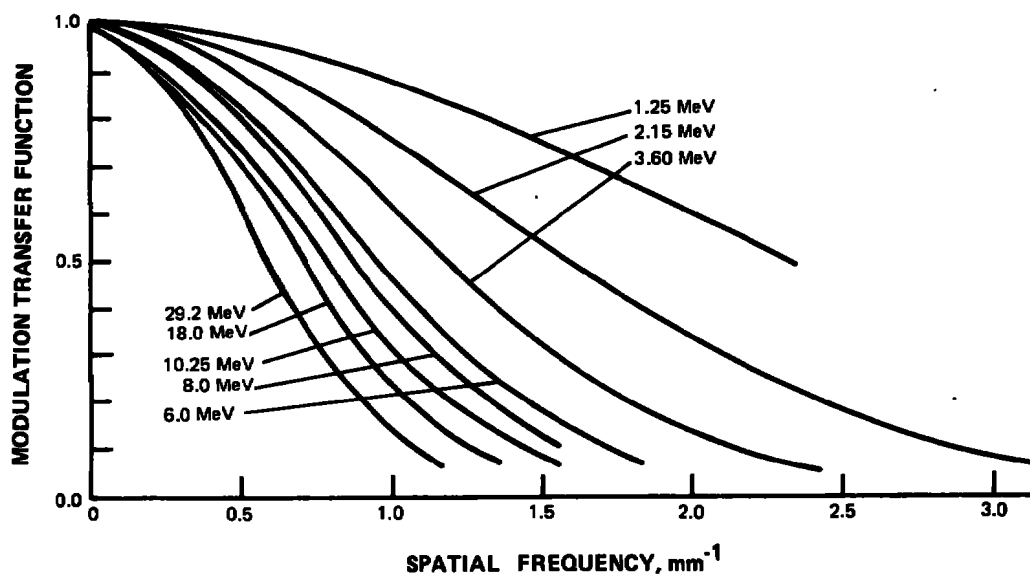


Figure 9 *Modulation Transfer Function For Fine Grain Radiographic Film With Lead Intensifying Screens*

An expression for the MTF of a circular source with uniform emission across its surface can be obtained as follows. Consider a circular source illuminating a sharp edge, and a detector scanning past the edge (Figure 11). For this example source, the intensity at the detector as it is scanned past the edge is proportional to the area of the source seen by the detector. Integration of the function  $G = (a^2 - x^2)^{1/2}$  and substitution of appropriate limits establishes an expression describing the intensity profile measured by the detector. Differentiation of this intensity profile produces the line spread function which is the original function.

$$G = (a^2 - x^2)^{1/2}$$

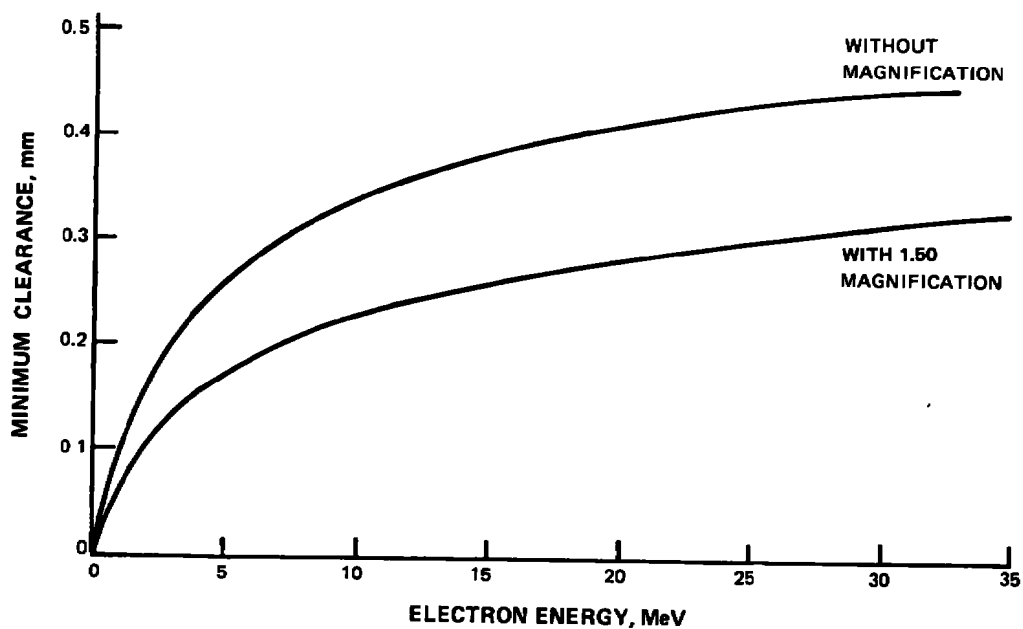


Figure 10 Minimum Visually Observable Clearance Based On Film MTF

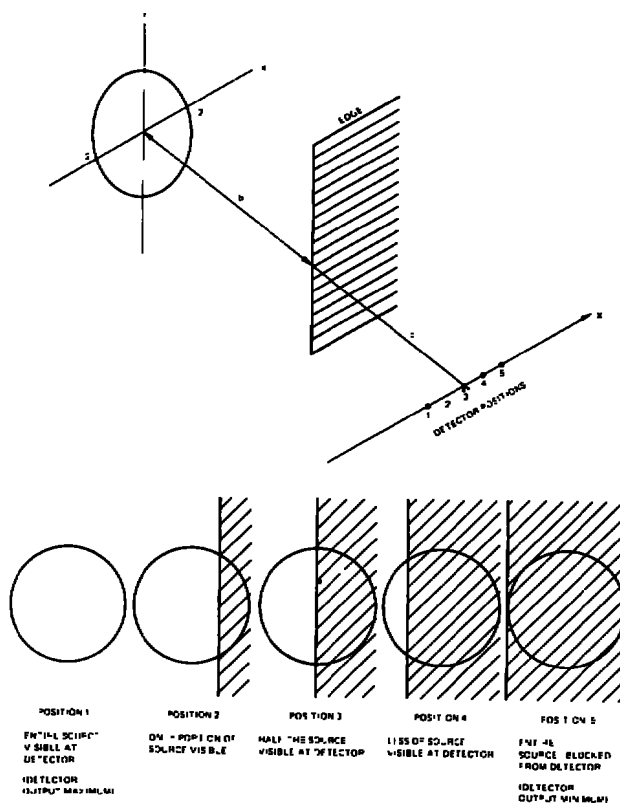


Figure 11 Diagram For Calculation of Uniform Emitting Circular Source MTF

The MTF is obtained by Fourier transformation of this function. This gives the expression:

$$\text{MTF} = \frac{J_1(2 \alpha \pi a f)}{\alpha \pi a f} \quad (19)$$

Where  $a$  = radius of the source  
 $f$  = spatial frequency  
 $\alpha$  =  $\frac{\text{Object to film distance}}{\text{Source to object distance}}$

for the modulation transfer function for a circular source of uniform emission. This equation was utilized to generate MTF's for several conditions of  $a$  and for spatial frequencies in the range of interest and are shown in Figures 12 and 13. From the curves, the effect of varying magnification and source size on the spatial resolution of the system can be seen. In the limiting case where  $\alpha = 0$ , the MTF is strictly due to the detector.

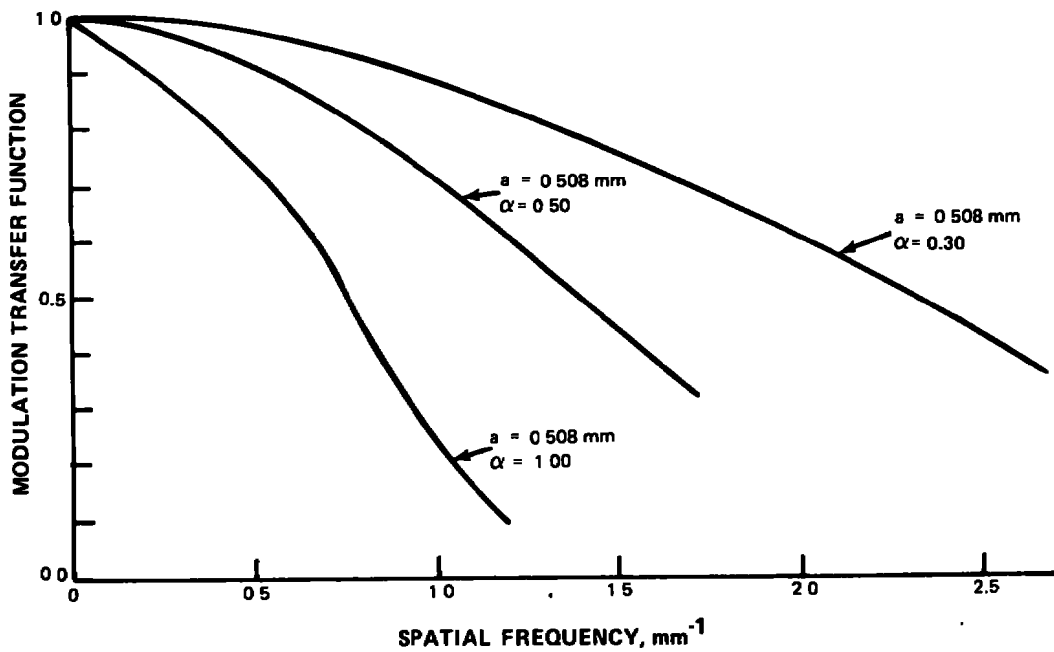


Figure 12 Modulation Transfer Function For Uniformly Emitting Circular Source

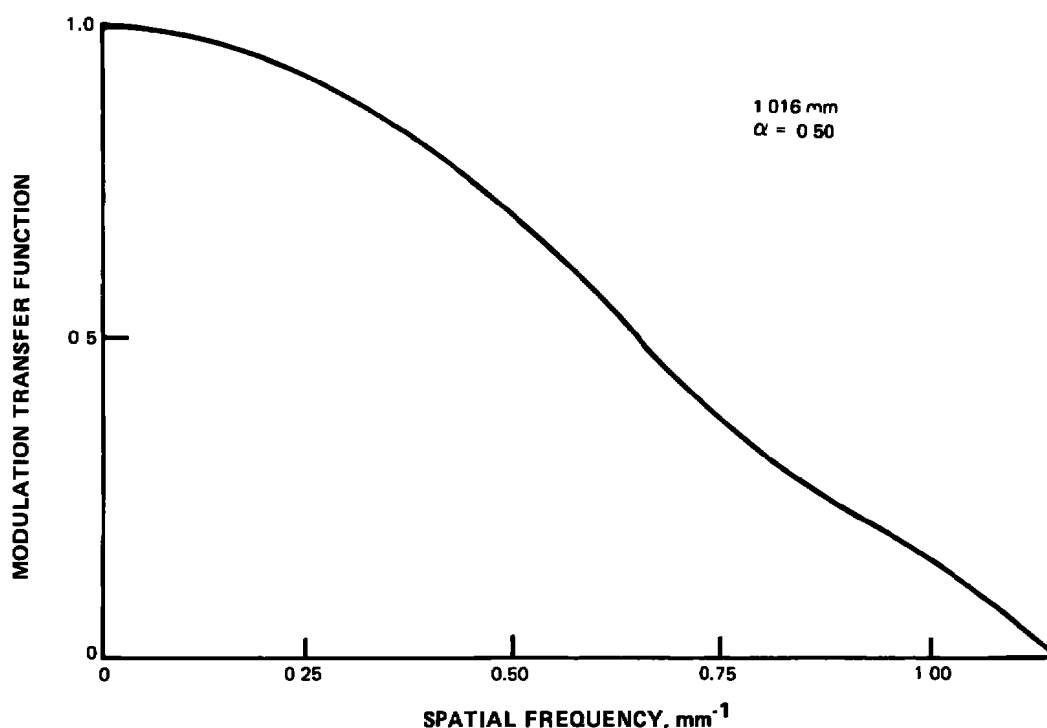


Figure 13 Modulation Transfer Function For Uniformly Emitting Circular Source

The MTF for  $\alpha = 0.3$ ,  $a = 0.508$  mm is multiplied by the calculated MTF for fine grain film for energies up to 30 MeV and is presented in Figure 14. The trends shown in these figures indicates that the minimum discernible clearance would increase with increasing energy. Utilizing 0.1 MTF, a magnification of 1.3, and following the methods used in the evaluation of the minimum discernible clearances for the film, we obtain the minimum discernible clearance as a function of electron energy shown in Figure 15 for the system. The results of the preceding is that the ability to see a specific clearance improves with decreasing energy. In choosing a radiographic system, this must be weighed against parameters such as exposure time requirements and metal thickness sensitivity. However, the direction indicated by spatial resolution considerations is toward the lowest energy consistent with the other system requirements.

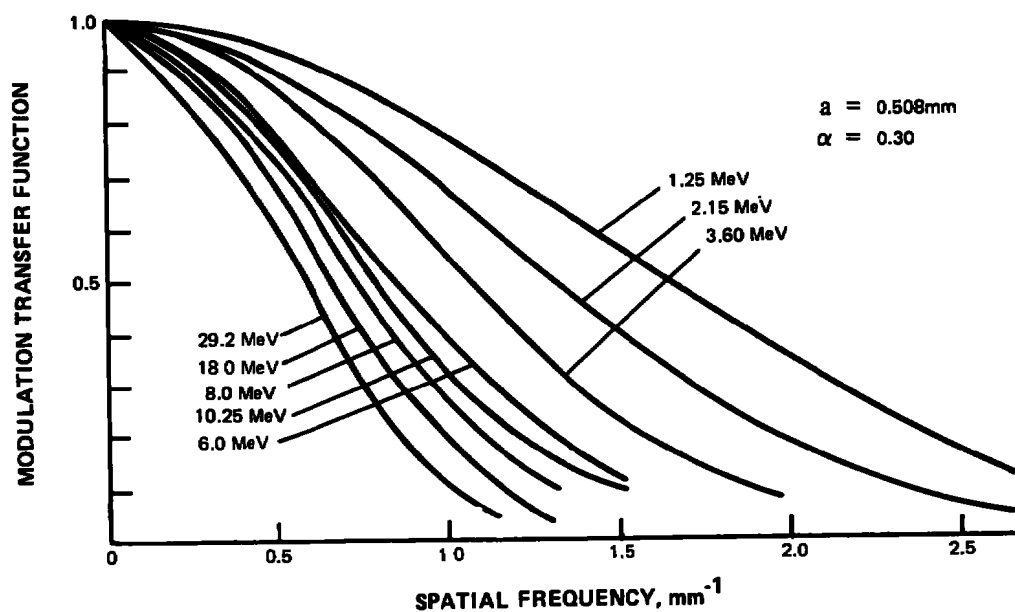


Figure 14 Modulation Transfer Function for Uniformly Emitting Circular Source and Radiographic Film

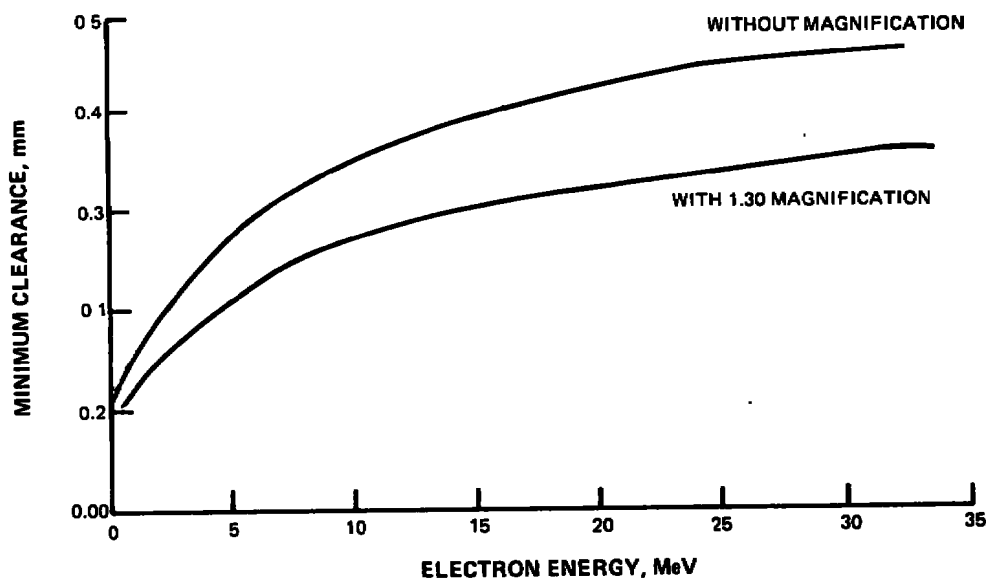


Figure 15 Minimum Visually Observable Clearance Based On Film/Source MTF



## DETECTOR INFLUENCE ON CHOICE OF SOURCE

The detectors that can be used for engine radiography cover the same range as detectors that are used to measure visible light. Detectors can give two dimensional information about the radiation intensity passing through the turbine engine or they can be one dimensional detectors used in a scanning mode to provide two dimensional information. The outputs of the available detectors can be linear or non-linear. The speed of response of the detectors varies greatly. In general, the higher the detection speed the lower the spatial resolution capabilities.

The most common type of detector currently used in engine radiography is radiographic film. Radiographic film is a high dynamic range, non-linear detector. However, to an optical density of about two, it is approximately linear for high energy X-rays and gives a density value roughly proportional to the X-ray intensity incident upon it. It is in this density range that engine radiography is usually done. Higher densities require higher illumination for viewing due to the greater attenuation of the light. This attenuation causes thermal distortion of the film, and the higher temperatures cause discomfort to a reader making measurements from the film. In addition, higher densities mean longer exposure times and generally exposure times as short as possible are desired. Figure 16 illustrates typical radiographic film sensitometric curves utilized in radiography. Curve A is for a high speed film used for engine transient measurements. Curve B is a sensitometric curve of a high resolution fine grain film. The difference in speeds of these two films is about a factor of 15. Figure 17 shows an MTF of a film like that represented by Curve A and Curve B. The loss in spatial frequency response with the fast film is obvious.

Another detection technique is to utilize the fluorescent properties of various materials to convert the incident x-radiation to the visible portion of the spectrum. The visible radiation is then detected by photographic film techniques, low light level television camera or other suitable types of detectors. This technique affords real time, high speed images. However, the conversion of radiation into visible light is accompanied by a rather severe degradation in thickness and detail sensitivity.

The effectiveness of conversion of the X-radiation to visible light depends upon the conversion efficiency of the material used to perform the conversion and the amount of radiation attenuated. The two types of converters commonly used are the single crystal and polycrystalline screen. To maintain high spatial resolution from the polycrystalline screen, the crystal size must be kept small and the thickness of the crystalline layer thin. The previous requirements are contrary to the requirements for attenuation of megavoltage bremsstrahlung. If the polycrystalline screen is made thick to increase the light output, the resolution is degraded. The single crystal converters are in general superior to polycrystalline converters for high energy applications because the total path length traversed by the radiation is converter material, whereas, in the polycrystalline structure some space is occupied by binder. The single crystal suffers a loss of spatial resolution due to the thickness requirements in a fashion similar to the polycrystalline converter.

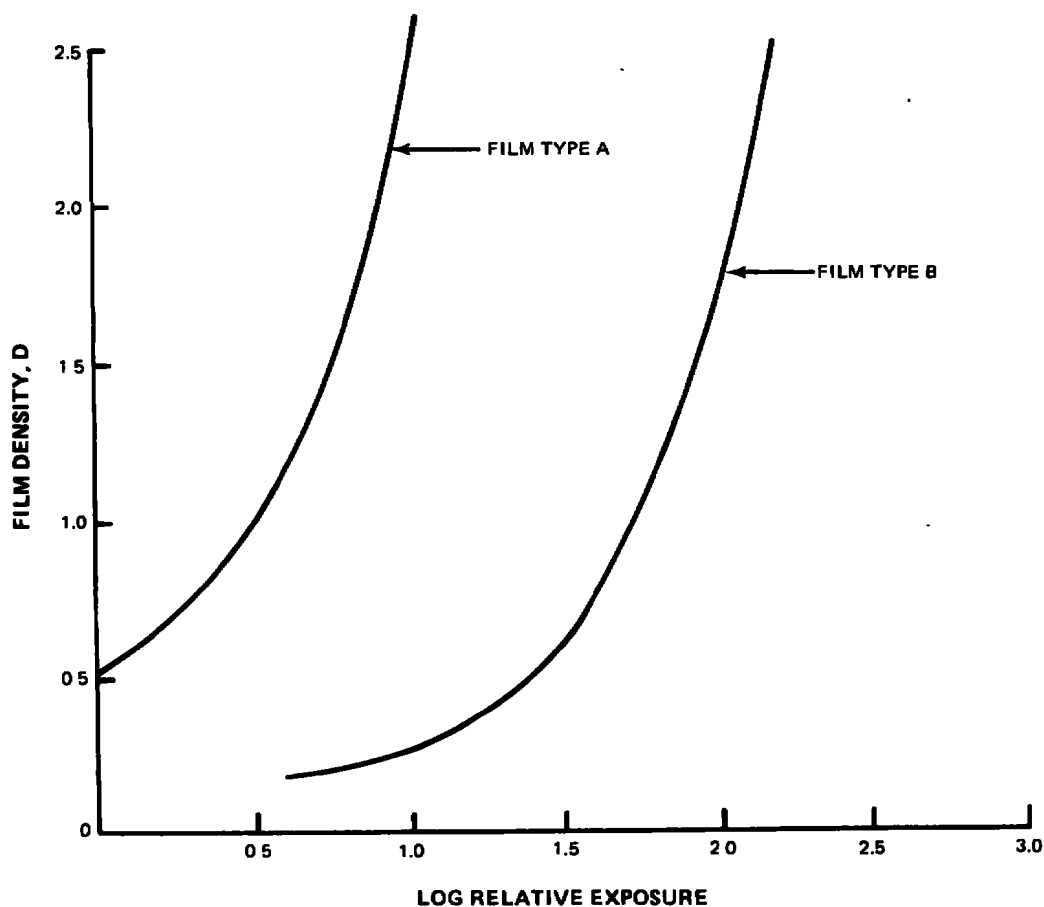


Figure 16 Speeds of Various X-Ray Film

Another form of converter currently being evaluated for turbine engine radiography utilizes the fluorescent material in the form of a coherent fiber optic face plate. In this configuration, the light generated by the incident photon is constrained to move along the direction of the incident photon provided the face plate is properly aligned. This provides the ability to use long path lengths without the degradation of spatial resolution normally encountered with thick converters. In addition, the device reduces the loss of contrast due to scatter radiation. High efficiency crystals grown in a fiber optic array appear to promise high resolution, real time images from high energy radiation sources.

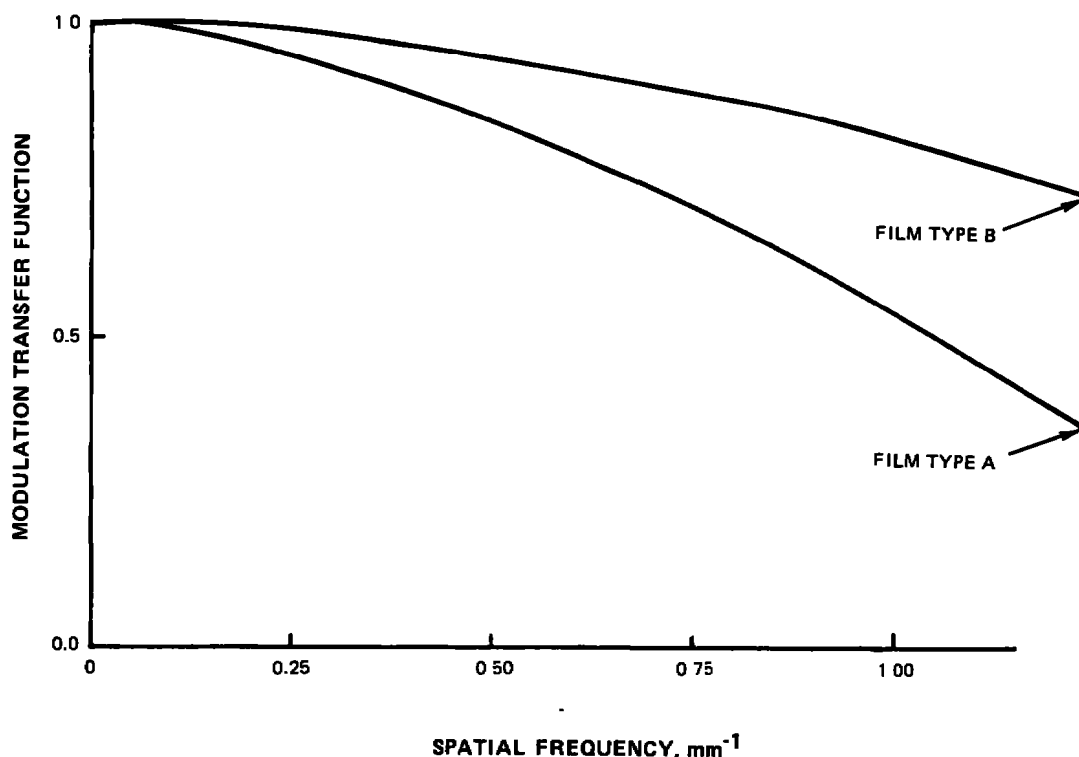


Figure 17 Modulation Transfer Function For Various Speed X-Ray Film

An alternate technique that can be utilized to detect the radiation is the direct conversion of the x-radiation into electrical energy. Two devices that have been utilized in radiographic imagery are the matrix ion chamber and the semi-conductor detector. Both of these devices offer possibilities of high speed detection systems. The semiconductor device also provides the advantages of light weight and durability which should be advantageous in the TELS environment.

The silicon diode semiconductor detector is currently being evaluated as a detector for high energy X-rays. Preliminary results at 8 MeV demonstrate a linear response to the incident energy. Figure 18 shows experimental data demonstrating this relationship. The silicon diode could be utilized in a two dimensional self-scanning array, as a linear array with one dimensional mechanical scanning or as a discrete detector with two dimensional mechanical scanning. In many cases, one dimension arrays or scanning would be adequate for clearance measurements.

The matrix type ion chamber consists of a square array of cathodes and anodes that detects incoming radiation and through electronic scanning and timing circuits gives a two dimensional address and the intensity measured across the array. Devices of this type have been utilized in radiographic imagery. They currently suffer from poor spatial resolution, but provide high detection efficiency and thus operate on small amounts of radiation flux.

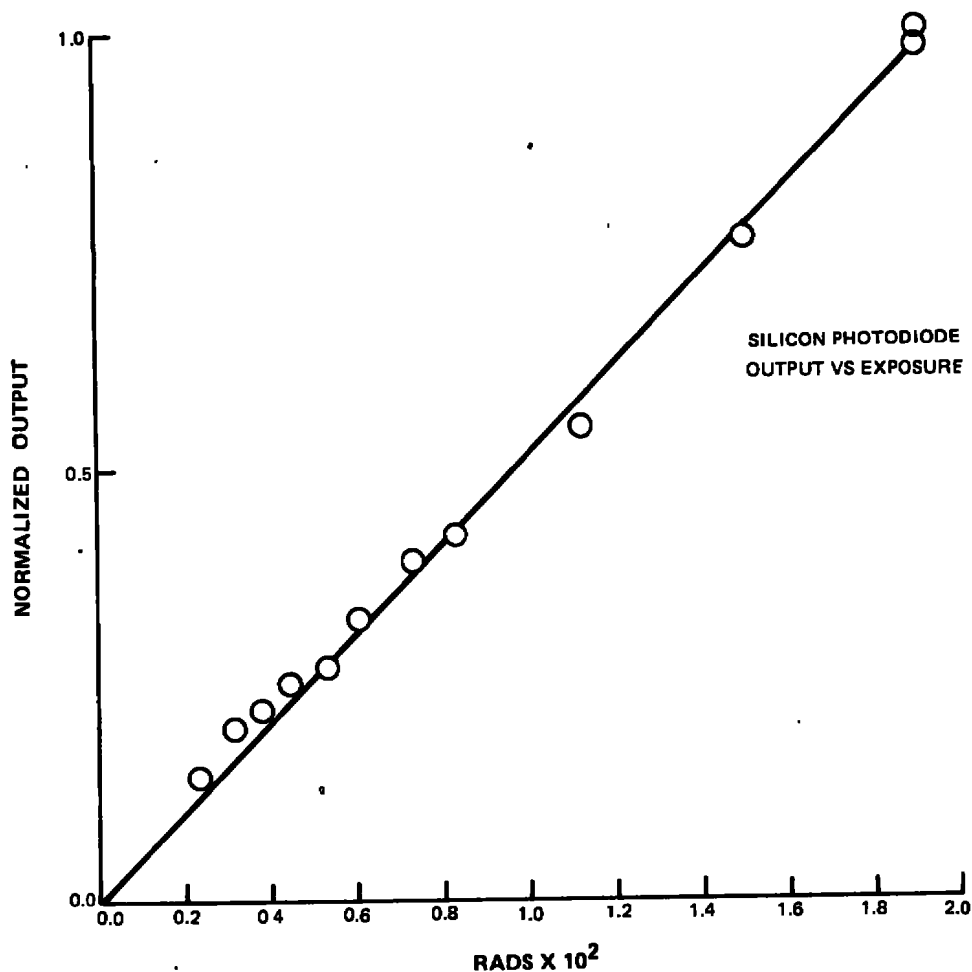


Figure 18 Silicon Photodiode Output vs. Exposure

The parameters of the detectors enumerated that are of interest in X-ray source selection are the spatial resolutions and detection efficiencies, and how they depend upon the X-ray spectrum.

A typical film frequency response is shown in Figure 19. Data beyond that shown has not been found in the literature. We assume that the trend at one MeV is maintained at higher energies. If this is true, selection of an X-ray source would not be based on spectral response of the film to be employed.

Similarly there is a lack of spectral response data for the other detection techniques at high energies, and it is assumed that spectral response of the detector system would not be a primary consideration in source selection.

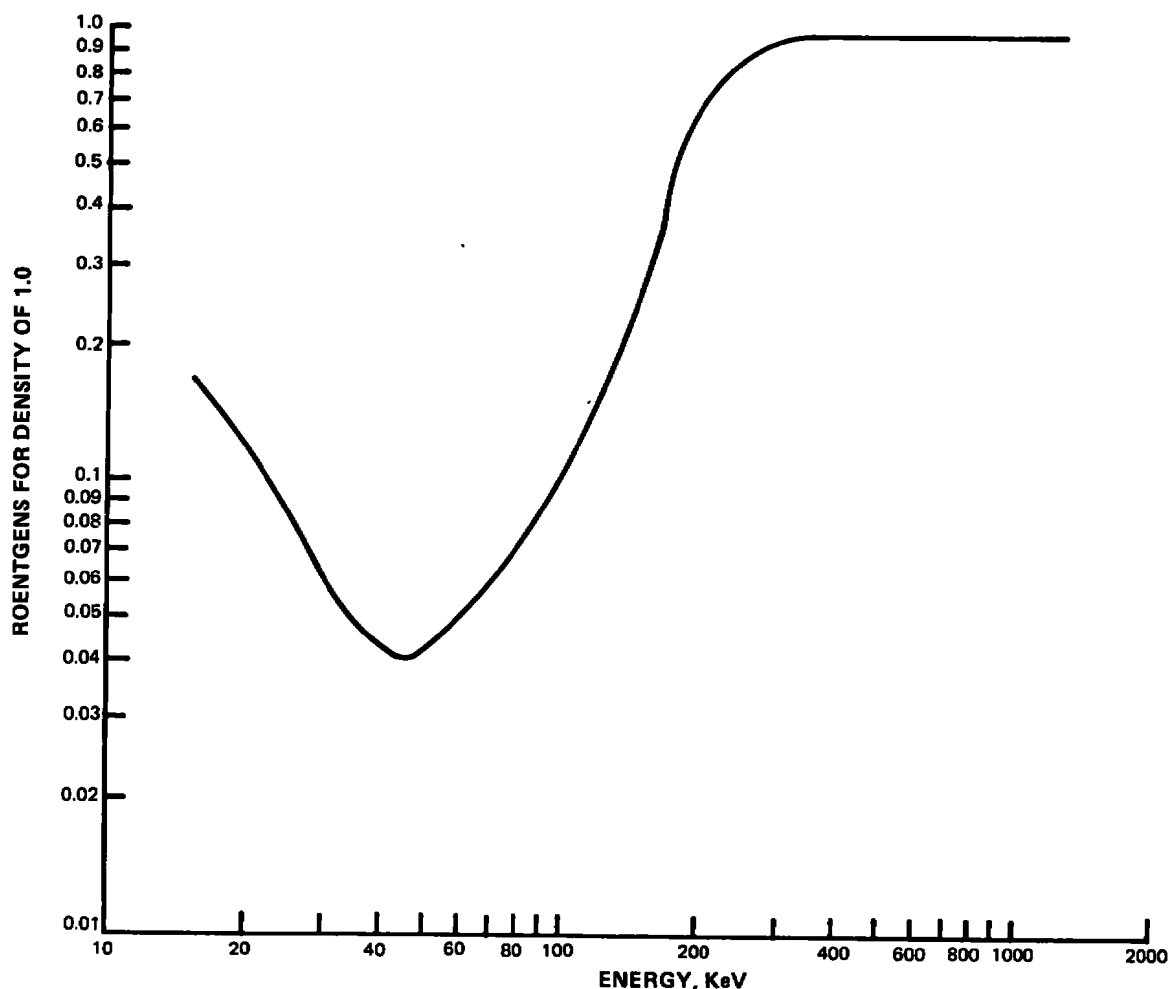


Figure 19 Spectral Sensitivity of X-Ray Film

The effect of energy on film spatial resolution capabilities has already been discussed under the section on spatial resolution. A similar type of degradation is expected in other detector systems. The primary cause of loss of spatial resolution capabilities is due to the generation of secondary electrons in the detectors which actuate adjacent sensing sites. In the case of a two dimensional array of semi-conductor detectors, we would expect a similar degradation of resolution with energy as experienced with film. In a single semiconductor detector and the fiber optic face plate converters, resolution is not expected to be as strongly dependent on energy as with film.

## GEOMETRY

The source size and the spatial relationship of the source, engine, and detector play an important role in determining the spatial resolution and exposure time which in conjunction with other parameters are important in source selection.

In conventional radiography, it is generally desirable to have as small a source of radiation as possible to maintain high spatial resolution. The problem due to finite source size was previously illustrated under the spatial resolution section. In that section, it was noted that the spatial resolution was also dependent upon the ratio of the object to film distance and the target to object distance. As this ratio goes to zero the spatial resolution is only limited by the detector spatial resolution which in turn is a function of the X-ray spectrum.

The image degradation due to geometry can be illustrated by the geometric unsharpness parameter  $U_g$  defined by:

$$U_g = \frac{s}{b} d$$

Where  $s$  = object to film distance  
 $b$  = target to object distance  
 $d$  = source diameter

As can be seen from this equation the geometric unsharpness is directly proportional to the ratio of the distances and to the diameter of the source.

In engine radiography, the ratio  $s/b$  cannot be zero due to the inability to position the detector closer to the object plane than the point where the detector intersects the engine case. This point of intersection depends upon the detector size and the radial position within the engine at which a measurement is to be made. Therefore, for a given source size the only alternative for reducing geometric unsharpness is to increase the target to object distance which also increases the target to film distance, and decreases the intensity reaching the detector. This in turn increases the exposure time. The effect of changing the target to detector distance for a fixed object to detector distance on geometric unsharpness, exposure time, and the intensity reaching the detector is illustrated in Figure 20.

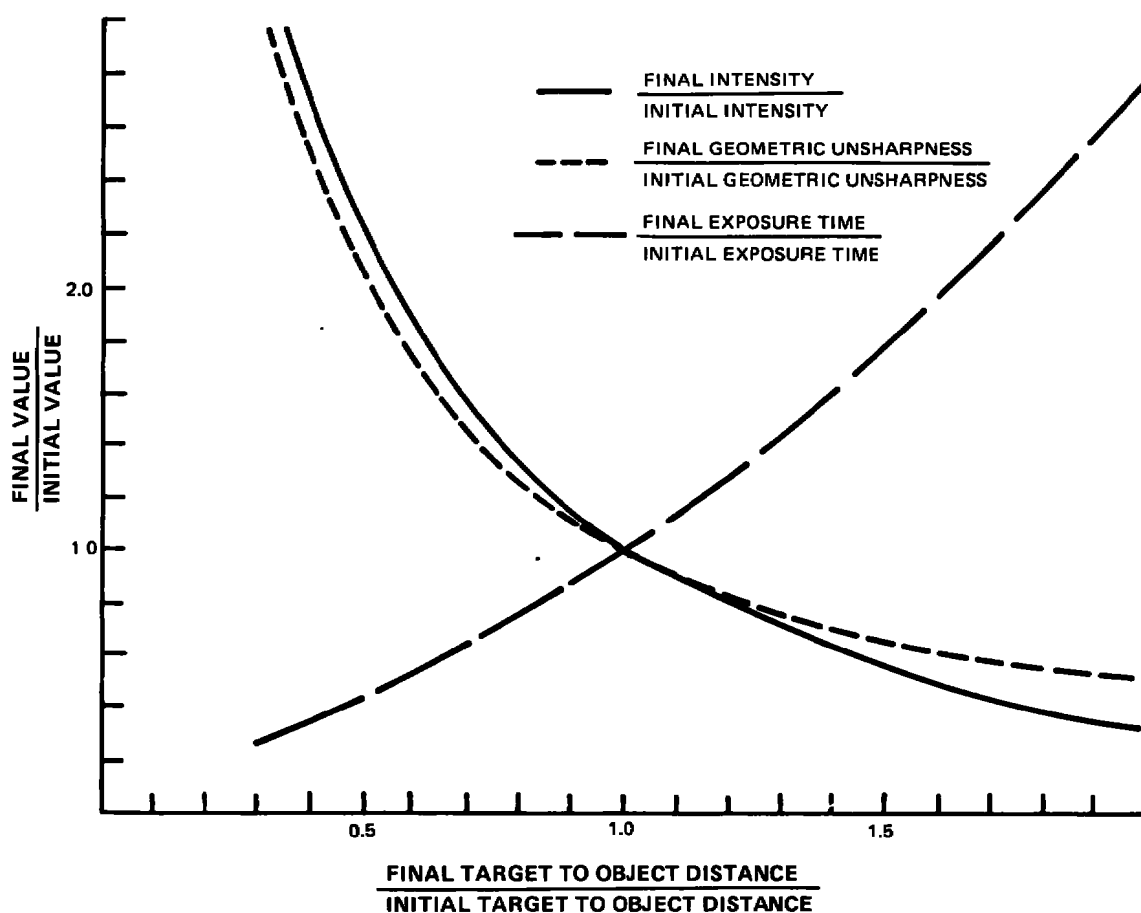


Figure 20 Variation of Geometric Unsharpness, Exposure Time, and Radiation Intensity With Target to Object Distance

At this point, relationships have been established between the engine materials and material thickness, time and spatial resolution, and geometry and the X-ray spectrum. These considerations indicate that what is of interest is utilization of an X-ray energy sufficiently high to give good penetration of the material encountered in turbine engines, good thickness sensitivity, good time and spatial resolution, and small source size. An optimum electron energy appears to be in the range of about 10 MeV. This would provide a spectrum rich in the 6 to 8 MeV photons required for adequate penetration, good X-ray production efficiency that will provide high output from a small target area, a spatial resolution that is acceptable for engine radiography, and sufficient flux for short exposures. The actual value of electron energy will vary depending upon the system concept (on centrifuge or off-centrifuge) due to the difference in radiation flux requirements.

## SOURCE PARAMETERS

### RADIATION SPECTRUM

In order to evaluate the spectral intensity of the radiation emitted from an X-ray source with a thick target we can follow Kramer (Ref. 2), who gives the following expression for the distribution of spectral intensity.

$$I_{\gamma} = \frac{8 \pi h e^2 Z}{3\sqrt{3} c^3 m} (\gamma_0 - \gamma)$$

Where  $I_{\gamma}$  = radiation intensity from the source  
 $h$  = Planck's constant  
 $e$  = electron charge  
 $l$  = constant approximately equal to 6  
 $c$  = speed of light  
 $m$  = electron mass  
 $Z$  = atomic number of target material  
 $\gamma$  = frequency  
 $\gamma_0$  = cut-off frequency and a function of the electron energy.

The solution of this equation at the various values of  $\gamma$  will produce a spectral distribution of intensity for each frequency  $\gamma_0$  determined by the energy of the electron impinging on the target material.

Another approach is described by workers from Los Alamos in Reference 1. The radiation spectrum emerging from a target is calculated in an iterative manner by assuming the target as being composed of a number of thin targets in tandem. The radiation generated in the first target is subsequently attenuated by the remaining target material. By taking into account the absorption coefficient of the target material and the spectrum generated by the first incremental target, the modified spectrum emerging from the target can be approximated. The electron leaving the first incremental target enters the next incremental target and the process is repeated. The spectra for tungsten at various electron energies are presented in Reference 1 and shown in Figure 21.

For a continuous spectrum to include components in a particular energy range, the spectrum must be generated by electrons of energy sufficient to produce a  $\gamma_0$  of frequency greater than or equal to the highest frequency in the energy range of interest.



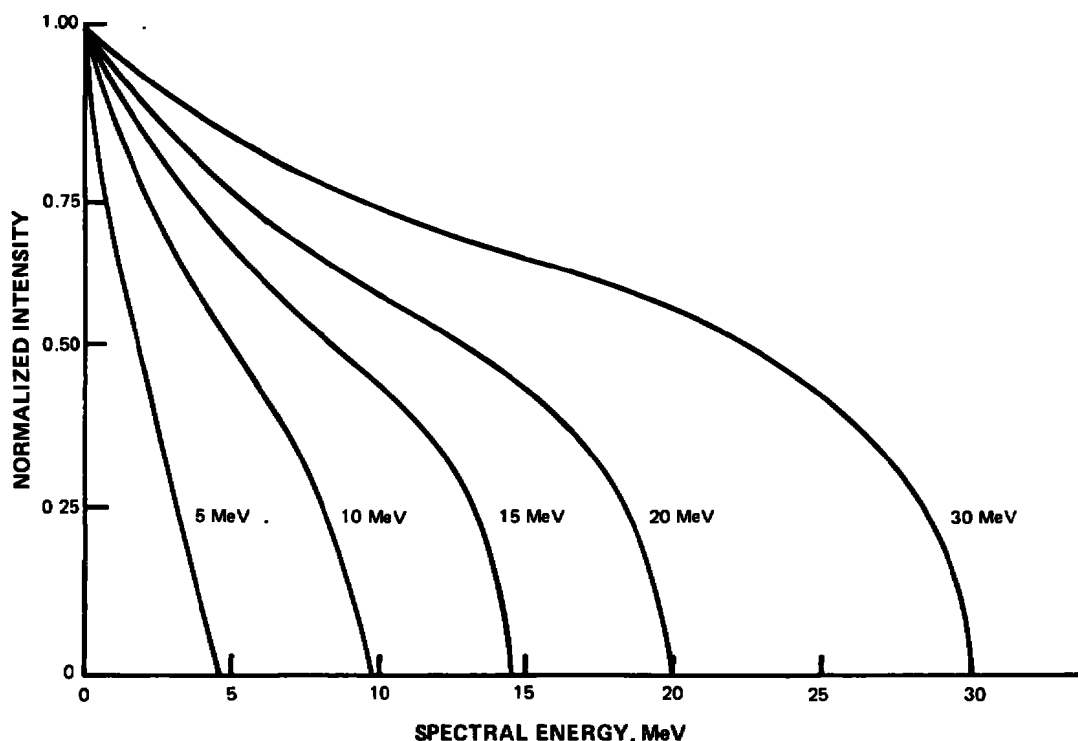


Figure 21 Intensity Spectrum For Tungsten at Various Electron Energies

## RADIATION PULSE LENGTH

The radiation pulse length is dependent upon the engine operation, the centrifuge operation, and whether the X-ray source is mounted on or off the centrifuge.

The requirements for the engine operation during testing under MIL-E-5007D paragraph 4.6.6.7 are essentially steady state. The specification calls for: "Dwell at maximum allowable rotor speed 10 seconds or time sufficient to record data". Therefore it is permissible to exceed 10 seconds for a radiographic exposure and comply with MIL-E-5007D. Although not specified as part of MIL-E-5007D, measurements of very short time duration are likely to be required. An example of this might be the simulation of a landing where the engine operating conditions are being rapidly changed during the time that g-loads are applied and exposure times of a second or less will likely be required. The radiographic system would have to be capable of providing suitable output to accomplish this task.

It is understood that the centrifuge will operate at selected angular rates and will not be capable of simulating large angular accelerations. If this is the case, the centrifuge does not directly affect the radiation pulse length. An indirect influence is experienced for an X-ray source mounted off the centrifuge. In this case, the centrifuge angular rate contributes to the determination of the length of the exposure if multiple pulses of X-radiation are required to make a measurement, and defines the X-ray output per pulse if the exposure times required are shorter than the time required for one rotation of the centrifuge.

For an off-centrifuge radiation source, an exposure can be made by a single pulse of radiation or a number of pulses at one per revolution. Regardless of whether one pulse or multiple pulses are used with an off-centrifuge X-ray source, the X-ray pulse length must be sufficiently short that insignificant motion blur occurs. If motion blur is restricted to 0.051 mm or less, the pulse length would have to be less than 1 microsecond at the maximum centrifuge angular rate (if the engine were moving perpendicular to the X-ray beam). The value of 0.051 mm is utilized because it is of the same order as jet engine vibrations that might be experienced. Longer durations could be tolerated for other engine orientations and the one microsecond pulse length represents a minimum pulse requirement.

In summary, radiation exposures of rather long duration could be tolerated for an off-centrifuge source. For an off-centrifuge system, the pulse lengths must be less than one microsecond to minimize motion blur. For exposures of less than 1.8 seconds, the entire dose must be delivered in a single pulse or multiple sources distributed around the centrifuge could be used. Pulse lengths of the prescribed duration are currently employed in linear accelerators utilized for radiographic purposes.

If the X-ray source is mounted on the centrifuge, the time during which the X-ray dose can be delivered to the engine is determined by the engine operating conditions (transient or steady state). This permits exposure lengths of a second or more. The majority of the high energy, high output X-ray sources operate in a pulsed mode with pulse lengths of microseconds or less and would easily meet these pulse requirements.

## **RADIATION OUTPUT**

The output of large X-ray sources is specified in terms of roentgens per second or roentgens per pulse at one meter from the source. The output required for the TELS facility depends upon the area of the engine to be radiographed, the type detector to be employed, the permissible length of the exposure, whether the source is mounted on the centrifuge or off the centrifuge and the distance from the source to the detector.

Since film is the detector that currently produces the highest quality imagery in high energy radiography and represents a worse case in terms of exposure time, it was utilized to evaluate the source output requirements for a specific geometry and engine metal thickness. Figure 22 shows the outputs required to produce a film density of 1 and 2 above the fog level for several Kodak films at source to film distances up to 14 meters. The radiation output is based on the penetration of 7.62 cms of steel. Kodak M film is used routinely at Pratt & Whitney Aircraft for engine radiography. Kodak AA and R are also utilized for particular applications. Using Figure 22, the source output requirements relative to M film exposed to a film density of 2 through 7.62 cm of steel at a distance of 3.66 meters from the source is 1000 roentgens. If exposures of one second are required, this translates to 1000 roentgens/second at one meter or 1000 roentgens/pulse at one meter (assuming a single pulse) for an on-centrifuge and off-centrifuge source respectively. If a faster film such as Kodak AA is chosen (film density of 2), the output would be 240 roentgens per second or 240 roentgens per pulse.

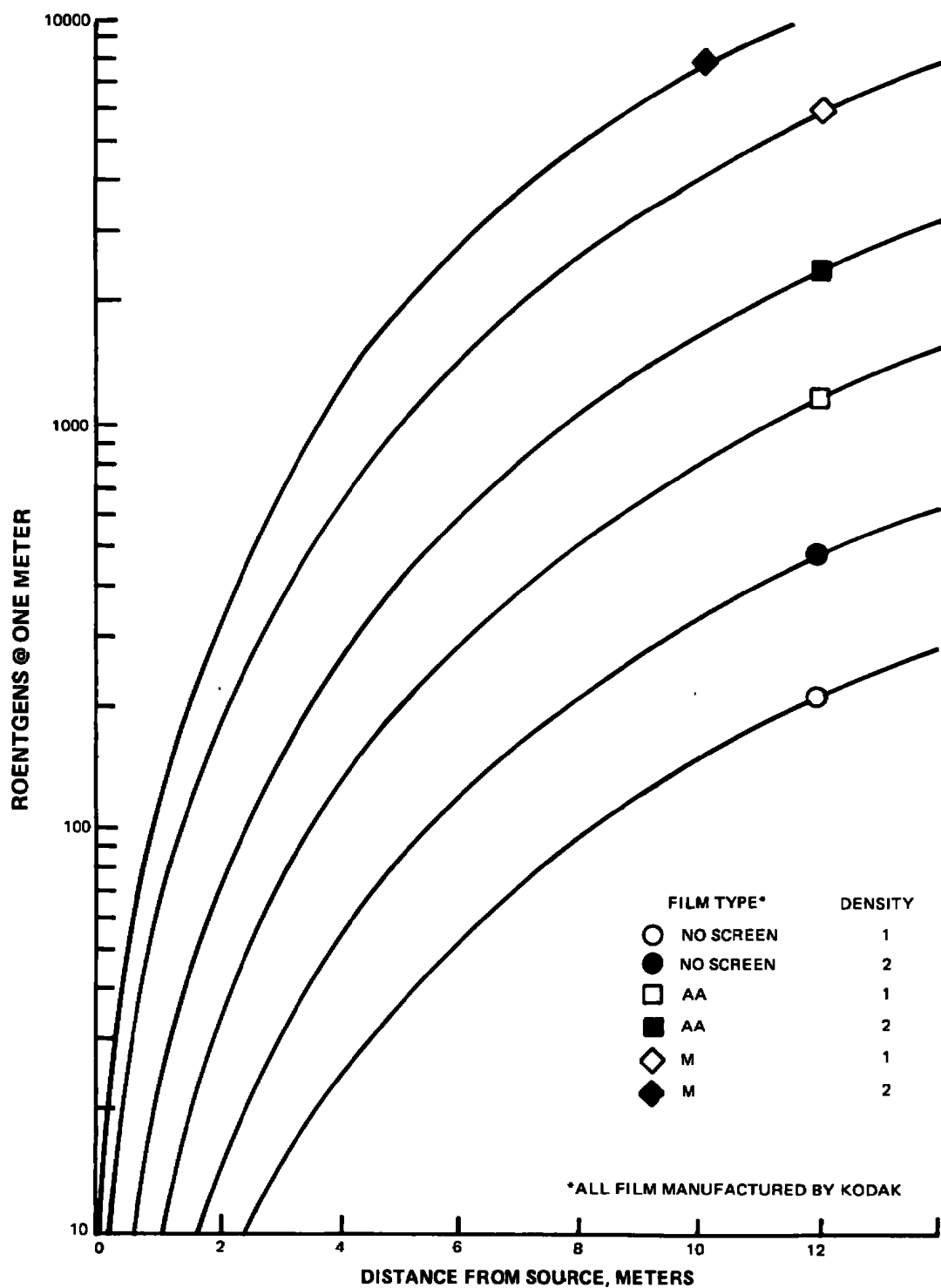


Figure 22 Radiation Required to Expose Kodak Film Through 7.62 cm of Steel

The faster the film the less output is required to expose it to a specified density. But also the ability to make a precise measurement decreases. For film radiography and the nominal conditions set forth here, it is recommended that film no faster than Kodak AA be utilized as a routine recording medium. This is based on Pratt and Whitney Aircraft experience with 8 MeV engine radiography, and the use of this type film in NDT applications of high energy X-rays. If this restraint is imposed, a minimum X-ray source output at one meter from the source of 240 roentgens per second or 240 roentgens per pulse would be required for an on-centrifuge and off-centrifuge source respectively.

The 240 roentgens should be considered as a minimum acceptable output unless exposures longer than one second are permitted. The highest output consistent with technical feasibility and cost constraints should be obtained.

These output levels are currently obtainable from linear accelerators. The significant problem that must be addressed for an on-centrifuge system is whether a linear accelerator can be designed that would sustain the 15g loads applied by the TELS. For the off-centrifuge system, the 240 roentgens per pulse is higher than what is currently available, however, multiple pulses within the permissible 1 microsecond time, several sources, or deletion of the one second exposure requirements could make this a feasible approach. In both concepts, a relative high cost is expected for the X-radiation source due to the high g-load requirements on the one hand and the high output per pulse or multiple source requirement on the other.

The relaxation of the one second exposure requirement and the utilization of fast film and fluorescent intensifying screens significantly reduce the flux requirements with an associated loss of spatial resolution.

### **TIMING ACCURACIES FOR OFF-CENTRIFUGE SYSTEM**

For the off-centrifuge system, the position within the engine to be radiographed is determined by a four dimensional coordinate system. The particular position that is radiographed depends upon the angular rate of the centrifuge and the time at which the source is pulsed. To establish the timing accuracy required we examine a "worst case" condition to be met. This condition occurs when the maximum angular rate is employed and the point of interest is moving perpendicular to the X-ray beam. In this condition the error in timing gives the most significant error in position.

For most measurements with a source capable of producing a radiograph in a single pulse, a timing accuracy of  $\pm 125$  microseconds is sufficient. If multiple pulses are required for an exposure, a timing accuracy of  $\pm 1$  microsecond would be required to restrain the blur to 0.051 mm. An exception to this would be the requirement for measuring a very narrow axial clearance (0.127 mm to 0.508 mm). In this case, slight misalignments would cause severe degradation in the radiograph of the clearance and nanosecond accuracy would be required. However, these measurements are not routinely required and can be obtained by other means.

## TARGET SIZE

The size of the electron target that serves as the X-radiation source is important in radiographic measurements due to its direct effect on spatial resolution. At the source to film distances visualized for TELS (3.66 meters or greater), source sizes of 1.0 mm diameter or less are acceptable for the energies and outputs required for an on-centrifuge system. For an off-centrifuge system, a sacrificial target might be required to satisfy the single pulse output of 240 roentgens and still maintain a 1.0 mm target diameter. If exposures of one second are deemed unnecessary, or if multiple sources are employed, the 1.0 mm source requirement can easily be met. No significant problem with target size is envisioned.

## TARGET MATERIAL SELECTION

As an electron impacts material it loses energy by ionization and by radiation. The rate of electron energy loss per unit path length in various materials is called the energy loss gradient and can be resolved into the portion due to ionization and that part due to radiation. The energy loss gradient in a particular material is a function of the energy of the incident electron. Ideally we would want a material whose energy loss gradient was solely due to radiation. This is not realizable, and for low energy electrons the primary energy loss mechanism is ionization. The electron energy at which the energy loss gradient due to ionization is equal to that caused by radiation is termed the critical energy.

The energy loss due to ionization is a very weak function of electron energy and atomic number above 10 MeV and varies by only a few percent for those materials that would be considered for use as X-ray targets. The lower the critical energy the better the material. Due to this, the critical energy is a good index to use for judging the suitability of a target material. Above the critical energy, any additional energy loss of the electron in the target will be predominantly due to radiation. This is illustrated graphically in Figure 23 (Ref. 1). This figure gives the ratio of the energy loss gradient due to radiation to the total energy loss gradient as a function of energy of the electron to an energy of 30 MeV for Al, Pb, W, and U. From the curve in Figure 24, (Ref. 1), we see that the critical energy decreases as the atomic number increases. This is consistent with the empirical equation of X-radiation production efficiency.

$$\text{Eff} = 1.3 \times 10^{-9} Z E$$

This states that X-ray production efficiency increases with increasing electron energy for a specific target material, and for a specified electron energy increases with the atomic number of the target material. Reference 1 describes a detailed study of possible target materials. The results of this study was that tungsten was "the most favorable target material" from the point of view of production efficiency and material properties.

## TARGET THICKNESS

Having chosen a particular target material, the optimum target thickness must be determined. This optimum thickness is dependent upon the electron penetration of the material, the intensity angle distribution and the self-attenuation of the radiation by the target material. A satisfactory description of this optimum target is one which generates a maximum on-axis radiation intensity for a specific electron energy and flux.

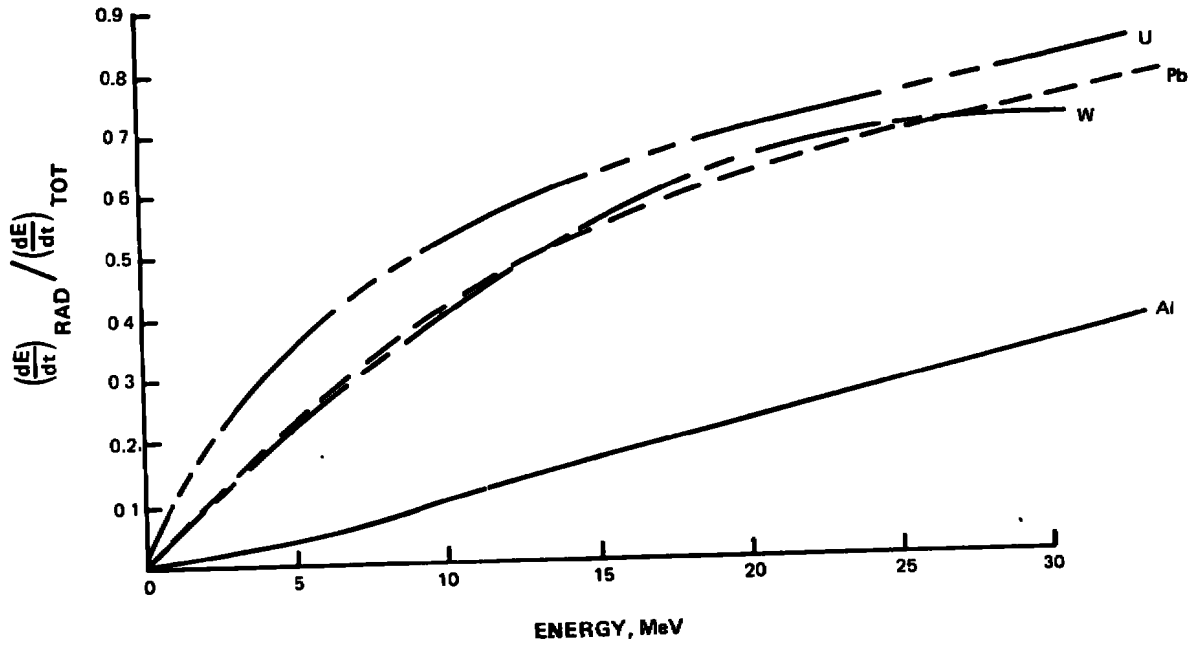


Figure 23 Energy Loss of Electrons in Various Target Materials

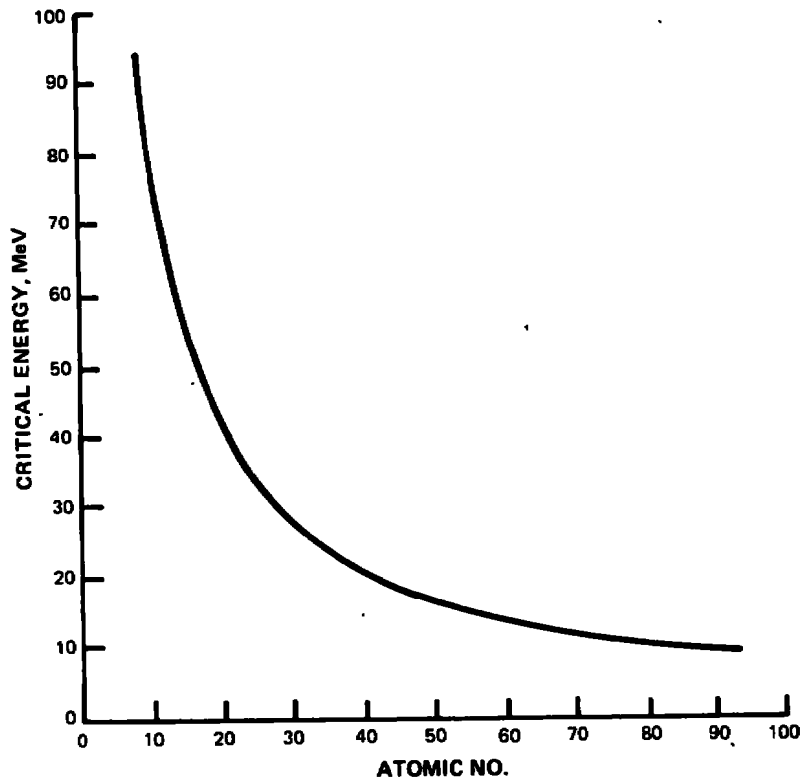


Figure 24 Critical Energy vs. Atomic Number

The electron range is defined as that distance in a material that an energetic electron will travel before expending its kinetic energy and is given by:

$$R = \int_0^{E_0} \frac{dE}{\left(\frac{dE}{dt}\right)_{TOT}}$$

Where  $E_0$  = kinetic energy of the incident electron (MeV)

$\left(\frac{dE}{dt}\right)_{TOT}$  = Total energy loss gradient, MeV/gm/cm<sup>2</sup>

Computations utilizing this equation were carried out in Reference 1 and are given in Figure 25 for tungsten.

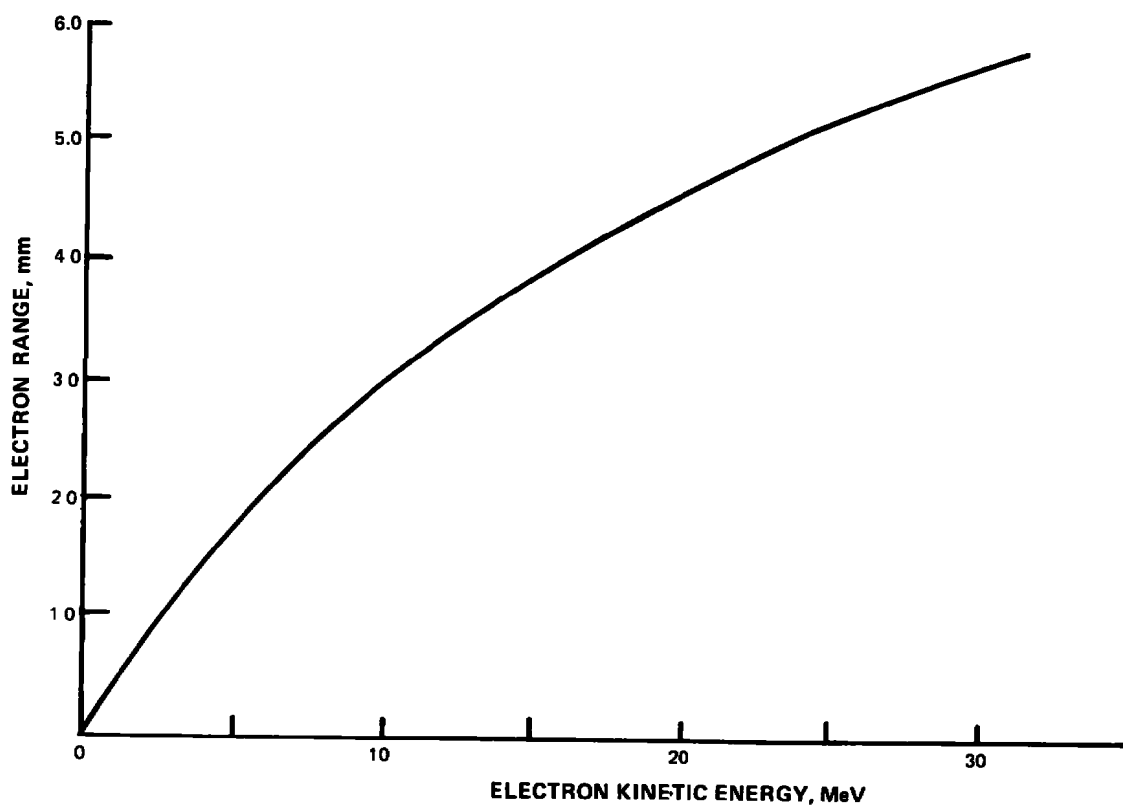


Figure 25 Incident Electron Range Through a Tungsten Target

The relative on-axis intensity as a function of tungsten target thickness for 20 MeV bremsstrahlung was presented in Reference 1 and reproduced in Figure 26. It can be seen that target thickness above about 0.686 mm causes a reduction in the on-axis intensity. Experimentally determined intensity-angle distribution for 20 MeV bremsstrahlung is given in Reference 1 and presented in Figure 27. The target thickness ranges from 1.20 mm to 4.75 mm. No significant change in the distribution is observed. The distribution after traversing 10 cm of uranium is shown in Figure 28. This distribution is approximately the same as for the input distribution shown in Figure 27.

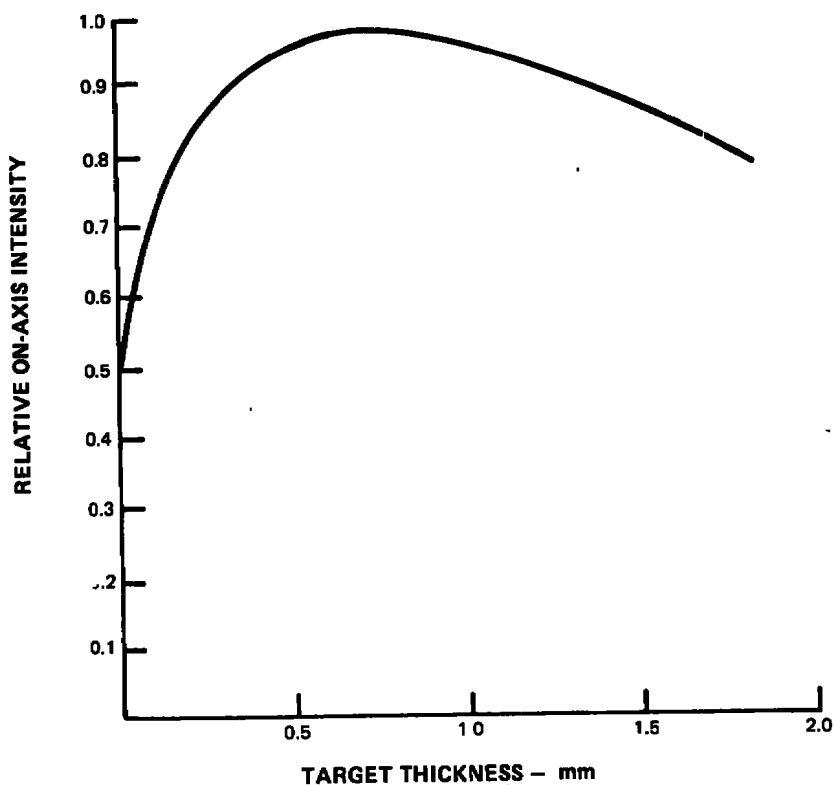


Figure 26      *Relative On-Axis Radiation vs. Target Thickness For 20 MeV Bremsstrahlung*



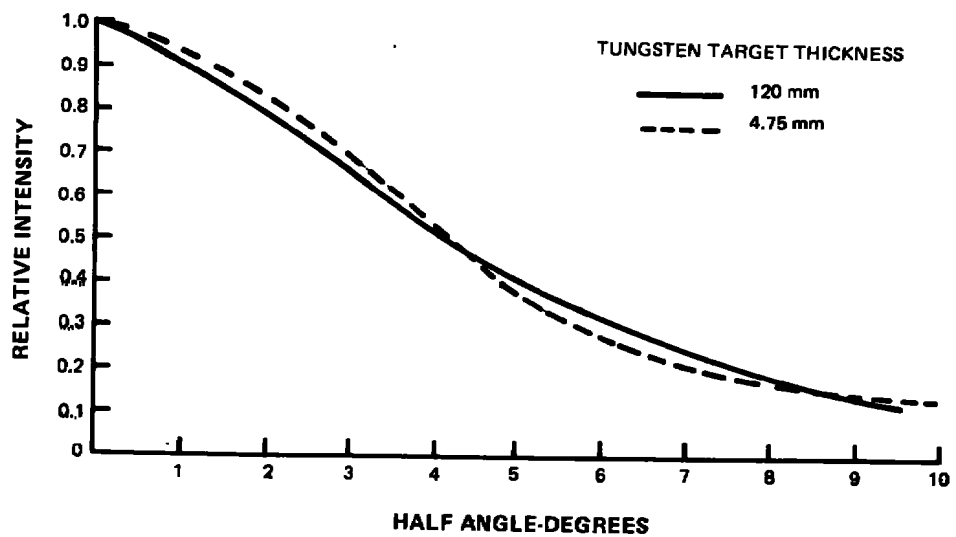


Figure 27 Intensity Angle Distribution For 20 MeV Bremsstrahlung With No Absorber

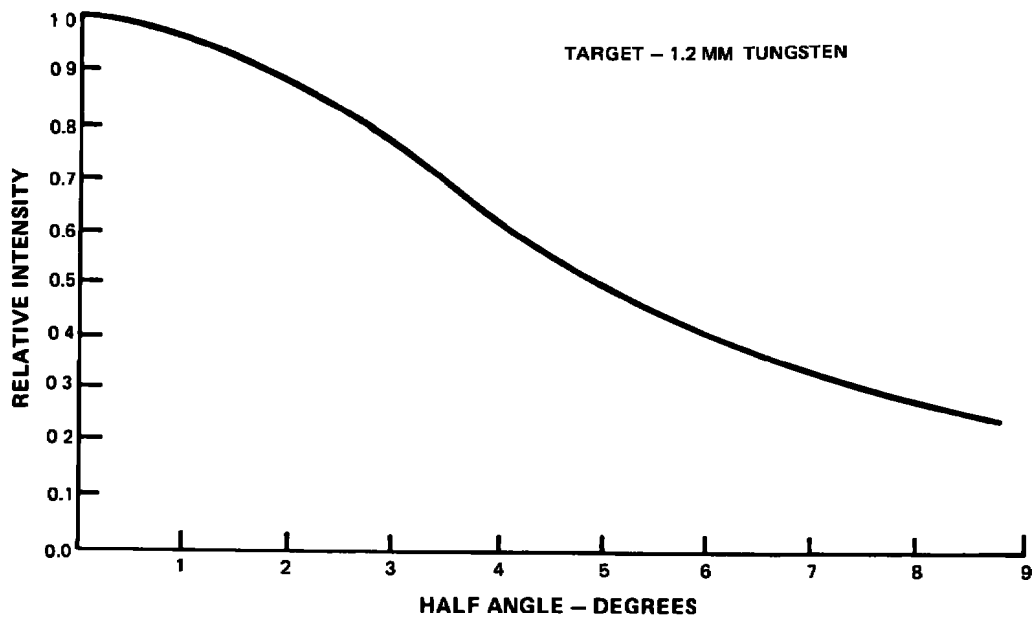


Figure 28 Intensity Angle Distribution @ 20 MeV After Passing Through 10 cm of Uranium

For high energy X-ray sources, the angular distribution is of practical importance due to the fact that it controls the size of the X-ray field from the point of view of uniformity and of maximum useful field size. Figure 29 gives the half-angle to half-intensity for various energies as well as the field diameter at 1 meter from the target (Reference 2). The higher the energy the greater the on-axis intensity for a specific target thickness and the greater the useful energy at the detector for radiography involving large metal thickness.

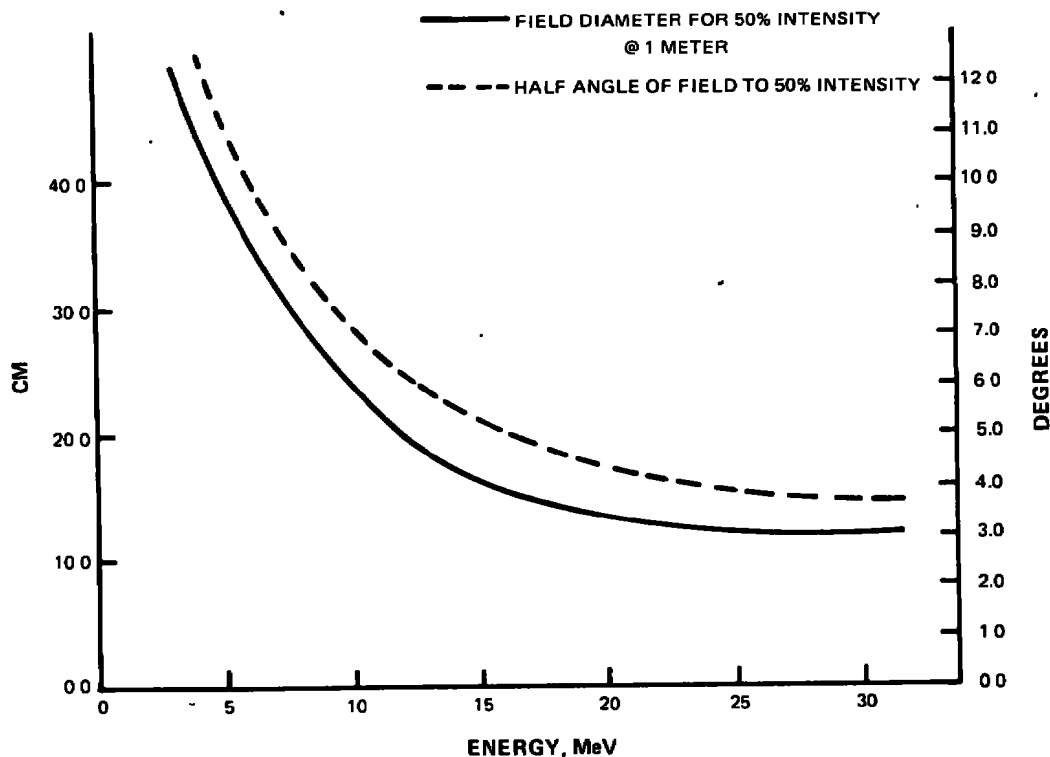


Figure 29 Half Angle to Half Intensity For Various Energies at 1 Meter From Target

For most linear accelerators, the electron beam is focused onto the target after acceleration, and a non-parallel beam of electrons strike the target. The primary purpose of this is to achieve a high X-ray output from a small focal spot, but it has the important secondary effect that the radiation beam angle is increased by the angle of convergence of the electron beam. The beam convergence angle at the target should be less than the bremsstrahlung angle to insure maximum on-axis radiation intensity.

The actual target thickness used at any energy would also depend upon whether a durable or sacrificial (short life) type target would be utilized. It is likely that a durable long life target would be required for a centrifuge mounted radiographic system as well as an off-centrifuge system.

A complete mechanical and thermal design is required to finalize the thickness of the target. The angular intensity distribution and the on-axis intensity must be considered concurrently with the mechanical and thermal design requirements of the target in the final system.

The X-ray flux requirements and the energy spectrum finally chosen depend upon the particular system concept. The specification of these parameters will determine the accelerator and target requirements.

## IMPLEMENTATION OF X-RAY SOURCE

### SELECTION OF CONCEPT

The various approaches to implement the on- and off-centrifuge concepts are given below. A discussion of the advantages and disadvantages of these approaches are presented in Appendix A and tabulated in Table II.

- I. X-ray source mounted on the centrifuge.
  - A. RF power generated at the center of rotation and transmitted to an accelerator at the engine location.
  - B. Electron beam generated at the center of rotation and transmitted to a target at the engine location.
  - C. High voltage generated at the center of rotation and transmitted to RF power supplies and accelerator at the engine location.
  - D. Entire X-ray source at engine position.
- II. X-ray source mounted off the centrifuge.
  - A. Single source capable of producing measurement in a single phase.
  - B. Single source capable of producing measurement in multiple pulses.
    1. Multiple revolutions
    2. Single revolution.
  - C. Multiple sources uniformly distributed around centrifuge each contributing to measurement.

Of the two radiographic concepts proposed for the TELS facility, the on-centrifuge was mutually chosen by AEDC and P&WA. This concept has several possible variations which were investigated. In all cases, the D.C. power supply, coolant system, and any other suitable components were located on the axis of rotation of the centrifuge. The variations that were investigated included:

- A. The complete linear acceleration assembly is mounted at the center of rotation and the electron beam transmitted along the centrifuge to the appropriately positioned target at the engine via evacuated guide, magnetic lens, and turning magnets.
- B. As in 'A' above with the exception that the linear acceleration structure is located at the engine location and the R-F power is transmitted via waveguide structure to the accelerator.
- C. As in 'B' above except that R-F oscillator would be located at the engine location with the accelerator.

TABLE II – CONCEPTS FOR IMPLEMENTATION OF X-RAY SOURCE

CONCEPT	REQUIREMENTS	PROBLEMS/DISADVANTAGES	ADVANTAGES
<b>ON ARM SYSTEMS</b>			
<b><u>IA</u></b> RF power generated at center of rotation and transmitted to accelerator at engine.	Waveguides to transmit RF power to engine and system of bellows to direct X-ray beam.	<ol style="list-style-type: none"> <li>1. Vacuum-ion pump and electron gun redesign.</li> <li>2. Rigid frame at engine to hold assembly in proper alignment.</li> <li>3. Wave guide must be replumbed for each different position to be radiographed.</li> </ol>	<ol style="list-style-type: none"> <li>1. RF power source at center of centrifuge (low g) permits use of available equipment for majority of the system.</li> <li>2. Current technology.</li> </ol>
<b><u>IB</u></b> Electron beam generated at the center of rotation and transmitted to target at engine.	Evacuated tube to transmit electron beam to engine plus turning magnets to direct electron beam.	<ol style="list-style-type: none"> <li>1. Suitable variable angle turning magnets required.</li> <li>2. Secondary sources of radiation from electrons hitting guide tube could affect quality of radiograph.</li> <li>3. Replumbing required for each new engine radius.</li> </ol>	<ol style="list-style-type: none"> <li>1. All critical assemblies placed at center of centrifuge (low g)</li> <li>2. Electron beam is collimated by turning magnets.</li> </ol>
<b><u>IC</u></b> High voltage generated at center of rotation and transmitted to RF power supplies and accelerator at engine.	Complete system located at engine except for power supply.	<ol style="list-style-type: none"> <li>1. Complete X-ray system redesign.</li> <li>2. Substantial structure required to carry weight of entire system ~280 Kg</li> </ol>	Easy alignment and adjustment for different positions and engine radii.
<b><u>ID</u></b> Entire X-ray source at engine.	Complete system including power supply at engine.	Overwhelming.	(Same as IC).

TABLE II – CONCEPTS FOR IMPLEMENTATION OF X-RAY SOURCE (Continued)

CONCEPT	REQUIREMENTS	PROBLEMS/DISADVANTAGES	ADVANTAGES
<b>OFF ARM SYSTEMS</b>			
<b><u>IIA</u></b> Single source capable of producing measurement in single pulse (Los Alamos, Lawrence, Rad Labs, Physics International.	250R in single pulse	<ol style="list-style-type: none"> <li>1. Size: 5.5 m dia. 9 m long or 0.31 m dia. 9 m long 6 m dia. 18 m long</li> <li>2. Sacrificial target.</li> <li>3. Output 50R-100R.</li> <li>4. Weight is 1000's of Kilograms making supporting and positioning equipment massive.</li> </ol>	Instant stop action of transient movement
<b><u>IIB</u></b> Single source capable of producing measurement in either single or multiple revolutions.	<p>Single revolution – multiple pulse per revolution for 1 radiograph.</p> <p>Multiple revolutions – single pulse for each of several revolutions for 1 radiograph.</p>	<ol style="list-style-type: none"> <li>1. (Same as 1, 2, 3 &amp; 4 of IIA.)</li> <li>2. Sophisticated timing system required.</li> <li>3. Centrifuge stability (deflections) critical for multiple revolutions device.</li> </ol>	Output per pulse is lower
<b><u>IIC</u></b> Multiple sources uniformly distributed around centrifuge (conventional commercially available sources).	Multiple revolutions.	<ol style="list-style-type: none"> <li>1. Multiple positioning systems required.</li> <li>2. Critical timing and positioning.</li> <li>3. Pulse length relatively long.</li> <li>4. Centrifuge stability (deflections) is critical.</li> </ol>	Sources commercially available

Variation 'B' and 'C' above are compatible since 'B' could be implemented while appropriate R-F components could be developed for 'C'. The same accelerator and positioning system would be utilized for both 'B' and 'C'.

In variation 'A' involving electron beam transport, some of the questions of importance were:

1. What is the magnitude of the beam deflection due to the earth's magnetic field and what effect does rotation of the beam relative to the earth's magnetic field have on this deflection.
2. What type beam deflection system is required to direct the beam to the appropriate place?
  - a) Electrostatic
  - b) Magnetostatic
3. What quality vacuum must be provided for the beam transport structure?
4. What precautions should be taken against accidental loss of vacuum in the transport structure?
5. What control circuits are required?

In variation 'B' some of the items investigated were:

1. What are the losses associated with long R-F waveguide structures?
2. What type flexibility can be designed into the waveguide structure and the penalty paid in R-F losses.

Problems that were common to the two variations were:

1. How many bending points are required in the transport structure?
2. What are the mechanical effects of the high g loads on the structures located at the engine location?
3. What type positioning system will be required?

Variation 'C' is essentially a problem to be addressed by a designer of R-F components. The basic problem is a mechanical problem, but it must be addressed with an awareness of R-F component design criteria.

## ELECTRON BEAM TRANSPORT (VARIATION A)

### Electrostatic Deflection of Electrons

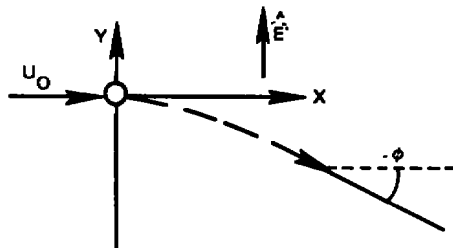
One means of controlling an electron beam is by utilizing an electrostatic field. To determine the feasibility of the technique we derive the equations of motion of an electron in an appropriate electrostatic field. We begin by writing the expression for the electrostatic force on an electron.

The force exerted on an electron of charge  $e$  is:

$$\mathbf{F} = -e\hat{\mathbf{E}} \quad (20)$$

Where  $\hat{\mathbf{E}}$  is the electric field and  $e$  is the electronic charge.

We will assume that the electron is injected into the electric field between two parallel plates at a potential  $V$  and separated by a distance  $d$ . The electron has an initial velocity  $U_0$  along the  $x$  axis.



The  $x$  coordinate is determined by:

$$x = U_0 t \quad (21)$$

Where  $t$  = time

The  $y$  position is determined by integration of Eq. 20. We can rewrite Eq. (20) as:

$$m \frac{d^2 y}{dt^2} = -e\hat{\mathbf{E}} \quad (22)$$

After two successive integrations and utilization of appropriate boundary conditions, we obtain:

$$y = -\frac{1}{2m} e\hat{\mathbf{E}} t^2 \quad (23)$$



For parallel plates,

$$\hat{E} = \frac{V}{d} \quad (24)$$

substituting:

$$y = \frac{-eV}{2md} t^2 \quad (25)$$

Substituting Eq. 21 in Eq. 25 we obtain:

$$y = -\frac{eVx^2}{2md U_0^2} \quad (26)$$

which is the equation of a parabola. Upon leaving the field the electron will proceed in a straight line unless an outside force interacts with it.

To determine the angle  $\phi$  at which the electron travels after leaving the deflector we proceed as follows:

At time  $t = 0$

$$\begin{aligned} U_x &= U_0 \\ U_y &= 0 \end{aligned}$$

$$\text{Vectorially } \vec{U} = U_0 \hat{i}$$

@  $t = \frac{s}{U_0}$ , Where  $s$  is the length of the deflector plates.

$$\begin{aligned} U_x &= U_0, U_y = -\frac{e V s}{md U_0} \\ \text{and } \vec{U} &= U_0 \hat{i} - \frac{e V s \hat{j}}{md U_0^2} \end{aligned} \quad (27)$$

Where  $\hat{i}, \hat{j}$  are unit vectors along the x and y axis respectively.

The magnitude of the velocity is given by:

$$|\vec{U}| = \sqrt{U_0^2 + \left( \frac{-e V s}{md U_0} \right)^2} \quad (28)$$

The vector angle  $\phi$  is defined by:

$$\tan^{-1} \phi = - \frac{e V s}{m d U_0^2} \quad (29)$$

We want  $\phi = \pm 90^\circ$  for a useful deflector system. This is not physically realizeable because the right side of Eq. (29) would have to be infinity.

This can also be demonstrated as follows:

$$U_y = - \frac{e V s}{m d U_0} \quad (30)$$

for a  $\pm 90^\circ$  turn  $U_x = 0$ ,  $U_y = U_0$ , then

$$- \frac{e V s}{m d U_0} = U_0$$

and,

$$\frac{V s}{d} = - \frac{m U_0^2}{e} \quad (31)$$

Where:

- V = voltage across plates
- d = separation of plates
- s = length of plates along X-axis
- m = mass of electron
- e = charge of electron
- $U_0$  = Initial speed of electron

Now, for high energy electrons

$$m = m_0 \left[ 1 - \left( \frac{U_0}{c} \right)^2 \right]^{-1/2} = m_0 \epsilon$$

So that Eq. 31 becomes:

$$\frac{V s}{d} = \frac{m_0 U_0^2}{e} \left[ 1 - \left( \frac{U_0}{c} \right)^2 \right]^{-1/2} = \frac{M_0 U_0^2 \epsilon}{e} \quad (32)$$

Where:

$$\begin{aligned} m_0 &= \text{rest mass of electron} \\ c &= \text{speed of light} \end{aligned}$$

The implication of Eq. (32) is that the parameters  $V$ ,  $s$ , and  $d$  be such that they impart the same energy into the electron as it possessed upon entering the field. This initial energy was of necessity produced by a linear accelerator and cannot be reasonably achieved by a D.C. potential. In addition,  $U_x$  cannot become zero as required but must remain  $U_0$  since no force acts in the  $X$  direction. Therefore, electrostatic deflection cannot be utilized to turn through  $90^\circ$ . A turn through  $90^\circ$  must also be done within the confines of the electric field. The electron would, therefore, collide with the deflection plates. For a reasonably sized deflection circuit only minute changes in direction can be made to the high energy electrons required for engine radiography.

### Magnetostatic Deflection of Electrons

The only practical way to direct a high energy electron beam is through the utilization of magnetic fields.

The equations of motion in a uniform, static, magnetic field are:

$$\frac{d\bar{P}}{dt} = \frac{e}{c} \bar{U} \times \bar{B}, \quad \frac{dE}{dt} = 0 \quad (33)$$

Where:

$$\begin{aligned} \bar{P} &= \text{momentum} \\ \bar{U} &= \text{velocity of particle} \\ \bar{B} &= \text{magnetic induction} \\ E &= \text{energy of particle} \\ e &= \text{total charge} \\ c &= \text{speed of light} \end{aligned}$$

Since the energy  $E$  is constant in time, the magnitude of the velocity is constant and so is  $e$ . Thus Equation (33) can be written:

$$\frac{d\bar{U}}{dt} = \bar{U} \times \bar{\omega}_B \quad (34)$$

Where

$$\bar{\omega}_B = \frac{e\bar{B}}{mc} = \frac{c\bar{B}}{E}; \quad \epsilon = \left[ 1 - \left( \frac{U}{c} \right)^2 \right]^{-1/2}$$

$\bar{\omega}_B$  is the gyration or precession frequency. The motion described is a circular motion perpendicular to  $\bar{B}$  and a uniform translation parallel to  $\bar{B}$ . Solving for the velocity:

$$\bar{U}(t) = U_{11} \hat{k} + \omega_B a' (\hat{i} - i\hat{j}) e^{-i\omega_B t} \quad i = \sqrt{-1} \quad (35)$$

where  $\hat{k}$  is a unit vector parallel to the magnetic field, and  $\hat{i}, \hat{j}$  are the other orthogonal unit vectors,  $U_{11}$  is the velocity component along the field and  $a'$  is the gyration radius.

Integrating again we obtain the displacement as:

$$\bar{X}(t) = \bar{X}_0 + U_{11} t \hat{k} + i a' (\hat{i} - i\hat{j}) e^{-i\omega_B t} \quad (36)$$

Utilizing the expression for velocity in Eq. (35), setting  $U_{11} = 0$ , and considering only the real part we obtain:

$$P_{\perp} = \frac{eBa'}{c}, \text{ where } B = |\bar{B}| \quad (37)$$

$c = \text{speed of light}$

Where  $P_{\perp}$  is the momentum of the particle normal to  $\bar{B}$ .

For particles with charge the same in magnitude as the electron charge the momentum can be written as:

$$P_{\perp} \left( \frac{\text{MeV}}{c} \right) = 3 \times 10^{-4} B a' \text{ (gauss - cm)} \quad (38)$$

Utilizing Eq. (38), the magnitude of the magnetic induction required to turn an electron of specified momentum in a circular path of radius  $a$  can be calculated.

This value in turn can be used to estimate the size of the magnets required for the TELS application.

The control and power supply requirements for the multiple turning magnetics and the magnetic lens (required to maintain electron beam geometry) as well as the mechanical positioning systems, significantly increase the complexity and cost of the radiographic system. At least three turning magnetics would be required each weighing several hundred kilograms, each capable of rotation about the electron beam transport tube, and each requiring a variable magnetic induction vector. The mechanical devices to support and move the magnetics, the separate power supplies and the separate control systems would substantially impact the radiographic system cost and operation. The vacuum requirements ( $10^{-6}$  torr) although easily realizable in a static structure is another potential area of difficulty.

## RF TRANSPORT (VARIATION B)

In comparing the advantages and disadvantages of electron beam and R-F transport schemes, it appears as though the R-F transport would be the easiest to implement. This is primarily due to the various turning and focusing magnets, controls, and power supplies required for electron beam transport, the requirement for a vacuum of  $10^{-6}$  torr or better which implies vacuum pumps, controls, etc. and the problems associated with insuring that a loss of vacuum does not fail the accelerator structure. The R-F transport scheme appears to have similar

plumbing problems as the beam transport and losses associated with the long R-F wave guides but operates above atmospheric pressure and requires no controls along the wave guide structure.

The R-F transport technique implies the need for an accelerator structure at the engine location. Preliminary calculations indicate that an accelerator can quite easily be fabricated that will withstand the high-g loads of the centrifuge. The R-F transport scheme can be used as an interim method until such time as R-F oscillators and water loads can be designed, fabricated, and qualified for the high-g loads. At that time, those components can be attached to the existing accelerator and the R-F transmission guide can be eliminated in lieu of high voltage transmission and control lines to the accelerator.

The things that must be accomplished to implement the R-F transport scheme are:

1. The items of the X-ray source that will be at the center of rotation of the centrifuge must be assembled and packaged in a suitable manner. These include:
  - a) A.C. transformers.
  - b) Focus solenoid power supplies.
  - c) Coolant reservoir and pumps.
  - d) Pulse forming network and high voltage switching.
  - e) High voltage pulse transformer.
2. A source of electrical power must be supplied to the system, and appropriate control lines must be provided to the control room. Both of these items must be transferred to the rotating centrifuge by slip rings or other appropriate means.
3. A linear accelerator must be designed and fabricated to withstand a 15-g load. The portion of this structure that will definitely require design is the electron gun assembly. The ceramic window between the R-F guide and the accelerator may also cause problems. A special vac-ion pump may also have to be manufactured but should present no significant technical problems. Both the ceramic window and electron gun should be attached to the accelerator in a manner that allows ease of replacement. A vacuum roughing pump will be required to rough down the system after repair.

For a machine such as the Varian Linatron that operates at 2.99 gigahertz a standard rectangular wave guide (E1A, WR-284; Jan, RG-48/U) is utilized. From Ref. 3 we obtain the following parameters.

Outer Dimension & Wall Thickness, cm.	7.620 x 3.810 x 0.203
Frequency Range $TE_{10}^*$ Mode, GHz	2.60 - 3.95
Cutoff Wavelength, CM for $TE_{10}$ Mode	14.2
Cutoff Frequency, GHz for $TE_{10}$ Mode	2.08

\*Note:  $TE_{10}$  is defined as the dominant transverse electric mode.

Theoretical Attenuation Lowest to Highest  
Frequency db/30.48 meters 1.102 - 0.752

Theoretical Power Rating in Megawatts for  
Lowest to Highest Frequency 2.2 - 3.2

(Breakdown strength of air taken to be  
15,000 V/cm)

Assuming a maximum length of rigid waveguide of 18 meters, we would realize approximately an 11% loss in R-F power in the WR-284 waveguide.

Flexible waveguide sections are required for fine position adjustments and vibration isolation. Maximum straight run of waveguide would be 12 meters; the expansion that would occur due to a 56°C change in temperature would be about ± 1.27 cm. Therefore, a flexible section should be used to compensate for the thermal expansion.

The losses in the flexible sections are obtained from Reference 3. The data is for a soldered convoluted flexible waveguide that matches WR-284 waveguide.

Outer Dimensions and Effective Wall  
Thickness, cm

7.620 x 3.810 x 0.203

Minimum Bending Radii (cm)  
Standard Molded Assembly

H Plane  
E Plane

35.56  
17.78

Unjacketed or Special Molded Assembly

H Plane  
E Plane

22.86  
11.43

Weight, kg/meter

0.786

Nominal Attenuation db/30.48 meters

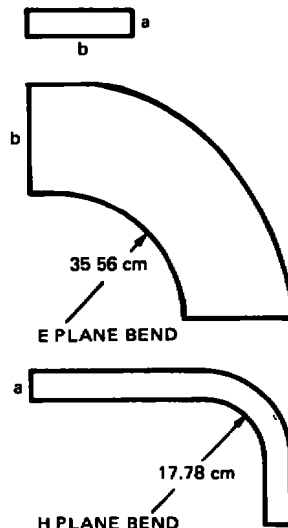
1.50

Nominal Power Rating Megawatts

2.00

Maximum Operating Pressure,  
newtons cm<sup>2</sup>

21



The maximum length of flexible waveguide needed for alignment and thermal expansion will be 6.1 meters. The total RF power loss through the flexible waveguide is about 7%. Total loss through the fix and flexible waveguide is 17%. The total weight of this length of waveguide is about 73 kg.

Losses due to flange leakage are negligible if sensible care is taken in making proper connection. Assuming that the radiation output for a particular system is directly proportional to the total power transmitted, then a 17% loss in power would represent a 17% loss in radiation output. However, in a typical electron accelerator of the standing wave type, the frequency is sometimes stabilized by dissipating a third to a half of the power in a dummy load. It is conceivable that existing equipment can handle the 17% power loss without degradation of performance. If not, an RF oscillator of higher output may be obtained or two oscillators used in synchronization may be used to compensate for the 17% loss.

A circulator is required in the input waveguide. This device passes the R-F going to the accelerator structure. The R-F energy that is reflected from the accelerator to the circulator is diverted by the circulator to high power water load which dissipates the excess power.

By determining the g-load to which the R-F oscillator can be subjected safely, it may be possible to move the oscillator away from the center of rotation and thereby reduce the amount of waveguide required.

The magnetron and the klystron are the two types of R-F oscillators that are in current use as R-F power sources for linear accelerators used for X-radiation production. The magnetron depends basically on crossed electric and magnetic fields for its operation. The basic structure and the electron beam are bent in a circular path so that the path of amplification is a closed loop. The magnetron supplies its own input and thus becomes an oscillator.

A typical electrical circuit structure is illustrated in Figure 30. The cathode is located at the center of the structure and positioned by radial or axial supports that also serve as power leads. The cathode is generally heated by an internal heater and maintained at a negative voltage.

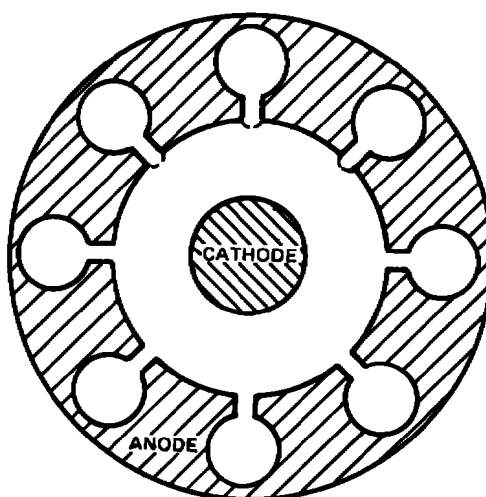


*Figure 30 Typical Electrical Circuit Structure of a Magnetron*

The anode section of the tube surrounds the cathode and is made of oxygen free copper. The anode is basically a rugged component and is generally maintained at ground potential.

The geometry of the magnetron is of primary importance to the operation of the magnetron. The relative positions of the cathode and anode as well as the shape of these items determines

the resonant frequency of the device. Loading along the cathode axis would cause axial and radial deflection of the cathode structure and resulted in a change in output of the device.

A preliminary calculation of the expected deflection of the cathode relative to the anode under a 15-g axial load was done based on the assumption of materials, scaling of dimensions from an actual magnetron, and assuming the cathode was supported on both ends as illustrated in Appendix B. The results of the study indicate that the radial displacement would be approximately 0.127 mm and the corresponding axial displacement of 3.581 mm. The details of the calculations are presented in Appendix B.

The analysis of the effects of a 15-g radial load indicate a radial displacement of the cathode to be  $5 \times 10^{-5}$  mm.

Magnetrons are produced that utilize axial support for the cathode. It is felt that a structure of this type would be dimensionally more stable than the type analyzed. However, sufficient information has not been acquired to determine the availability of this type magnetron in the frequency range and power range required for the specific application.

The klystron tube is shown in Figure 31. The klystron operates on the principle of velocity modulation. Velocity modulation is accomplished by varying the velocity of the electrons in an electron beam of constant density. A small input voltage alternately decreases and increases the velocity of the electrons. The electron beam is converted from a constant density beam into a beam with an a-c component during the transit time of the electron from input to output. This a-c component delivers R-F energy to the output circuit.

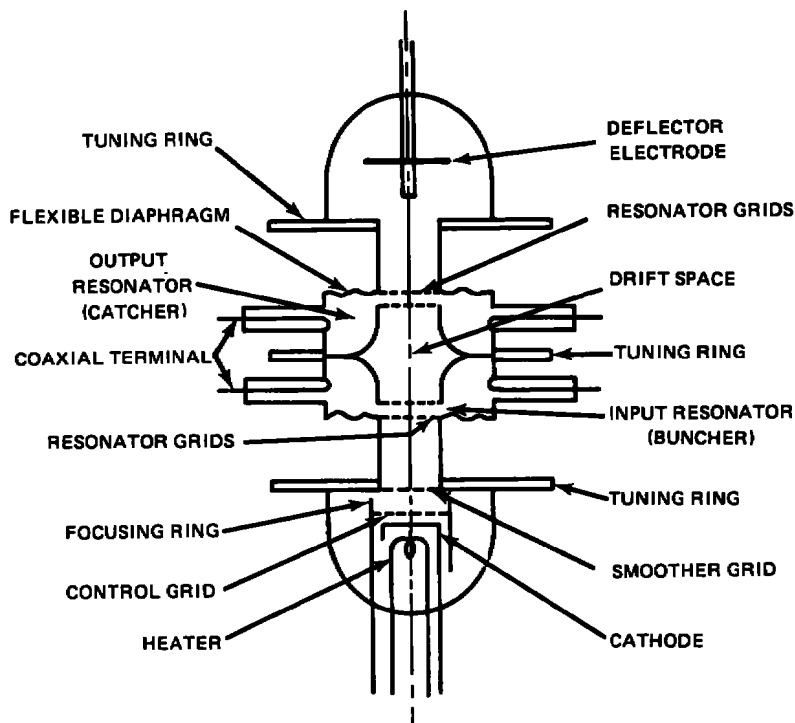


Figure 31 Schematic View of a Klystron Tube



The electron gun is indirectly heated and is usually oxide coated. The placement of the cathode relative to the input resonator affects the transit time. Changes in this position due to deflection of the cathode would cause a change in the output of the device.

The input and output cavities' shape and size determine the output frequency. Dimensional changes of these cavities cause changes in the klystron output. In order for this device to be useful at 15-g acceleration, the various internal parts must be sufficiently designed to maintain their relative positions and their original shapes. Insufficient information could be obtained to warrant a structural analysis.

S-band klystrons capable of providing the same approximate peak power as magnetrons appear to be considerably larger than a magnetron. The klystron tube with focus solenoid could weigh in excess of 136 kilograms and be approximately 1 meter long. A magnetron of equivalent power would be about 54 kilograms and 0.5 meters long.

From size considerations and the structural calculations done for the magnetron, it appears as though the magnetron would be the best candidate for use on the TELS facility. In fact, a detailed analysis of the deflection of the components of the magnetron based on manufacturer supplied dimensions and material properties would likely indicate that at some preferential orientation of the magnetron in the g-field, an existing magnetron would operate satisfactorily. This orientation could be maintained by proper design of the interface between the magnetron and accelerator structure.

#### **ALIGNMENT OF X-RAY SOURCE UTILIZING WAVE GUIDE TRANSMISSION**

The utilization of an X-ray source that is powered by R-F power from the center of rotation of the centrifuge is considerably more difficult than a source with integral magnetron or klystron. Implementation of such a system would proceed as follows:

1. The engine gimbal is positioned radially on the centrifuge and basic plumbing and wiring to the engine completed.
2. After or during the preparation of the engine for test, the R-F waveguide that will run from the center of the centrifuge to the gimbal is lengthened or shortened to terminate near the gimbal at an appropriate position to accommodate connection to the accelerator (properly designed and terminated T-junctions may eliminate this item). When sections of waveguide are removed or otherwise not in use, they should be capped to prevent contamination by water, grease, oil, fuel, etc.
3. Using the coordinates previously determined during the program planning stages, align the X-ray source and detector at a position of interest. The first position selected may be arbitrary, the position that gives the highest priority measurements, or the position providing the greatest number of measurements within the range of the flexible waveguide without replumbing.
4. The appropriate fixed and flexible waveguide sections are assembled between the long radial run of waveguide installed in (2) above and the accelerator structure.

5. The waveguide is then pressurized with an appropriate insulating gas mixture, the air purged, and leaks repaired.
6. The X-ray source is activated and the R-F power supply properly tuned to provide the required R-F fields in the accelerator structure. During this time, personnel must be removed to a safe area and all safety procedures adhered to.
7. The dose rate is measured to determine that adequate radiation is being supplied by the source. This is accomplished remotely by utilizing an ion chamber immediately in front of the X-ray source.
8. A radiographic exposure is made of the area of interest to assure proper alignment and X-ray dose. This can be done by utilizing the video fluoroscope system and another ion chamber that is an integral part of a video fluoroscope system. The ion chamber would provide the dose at the film plane which can be related to film density and the fluoroscope would assure proper positioning.
9. The proper detectors are assembled and readied for test. If film is utilized, the film transport system is loaded with the appropriate film type. If film fluoroscopy is utilized, the same must be done for the fluoroscope.
10. The centrifuge is now activated and brought to the specified simulated flight conditions.
11. The engine is started and the test program is initiated with the radiographic exposures being made as required.
12. After the exposures are completed, the centrifuge is stopped and the film recovered and processed.
13. The processed film is evaluated on-site in approximately 30 minutes after retrieval to determine if satisfactory exposure has been obtained. If not, steps 3 through 13 should be repeated as required to provide the exposures required.
14. After obtaining the required exposures, Steps 1 through 13 would be repeated until the entire test program has been completed.

From the above, it can be seen that utilization of an X-ray source by R-F power at the center of rotation of the centrifuge is much more complex than when the entire accelerator and/or R-F oscillator are located at the engine position.

## **EXPERIMENTAL PROCEDURES FOR ENGINE TESTING**

The following steps outline the procedure for engine radiographic testing:

1. Before testing, identify the areas of the engine to be measured, specify engine operation, and determine suitable image time sequences and image formats.
2. Utilize a full scale print of an engine axial cross section to confirm that the image format is suitable for the required measurement and to provide axial and radial engine coordinates defining the required image position. The coordinates are used to specify the position of the X-ray source and the X-ray detector system. Given detailed engine geometry and X-ray source and detector parameters, the exposures for the areas of interest can be calculated and actual images produced if required using digital techniques.
3. Upon receipt of the engine, make several test exposures and perform a static base line radiographic survey to document the condition and clearance of the various areas to be measured. This static survey verifies and establishes the X-ray source and detector coordinates and the correct exposure.
4. During testing, remote positioning of the X-ray source and detector should be utilized to provide continuous testing. The exact length of test would depend upon the capacity of the film transport, the type of test being run, the total number of images/unit time. etc. (This assumes that sufficient flexibility of source/detector positioning exists).
5. After completion of the test, stop the centrifuge and replace the film in the film transport. Transport the exposed film to the film development laboratory for processing and subsequently to the digital image processing laboratory for analysis. The data provided by the image processing laboratory would consist of tabulations and graphs of clearance versus RPM, time, or other engineering parameters. A quick turn around is required on film processing to insure that adequate radiographs have been obtained from which to make measurements. This information is required before the engine test is to be terminated to allow for repeat tests if required. Therefore, an on-site film processing facility will be required with both manual and automatic processing equipment.

## **POSITIONING SYSTEM – CONCEPTUAL MECHANICAL DESIGN**

The hinge-gimbal positioner proposed in the original TELS study included provision for an X-ray support frame. No details were supplied as to how axial and radial motion of the X-ray

unit and film would be provided. Although external and motorized control of motion of the X-ray source for alignment purposes is not necessary it would be an advantage to incorporate such a feature into the TELS facility. This feature would reduce manpower and time requirements to reposition the source and film during a test program since they would not be attached rigidly with nuts and bolts to the X-ray support. Motorized control of motion of the X-ray source and film would also allow radiography of more than a single position on the engine being tested without having to stop the centrifuge each time in order to reposition the source and film transport system.

The hoop support frame consists of two hexagonal side plates. These two side plates hold the roll bearing with integral gear. In the original TELS assembly the X-ray support is shown rigidly attached to these side plates. In addition the side plates are shown being about 1.52 meters apart. This would allow only a limited axial section of the engine to be radiographed without having to move the engine axially in the hoop. In the case of an engine with after-burner, only the turbine section would be positioned between the hoop support frames. The original design concept does not allow positioning of the source outside this envelope and this means that fan stages as well as most sections of the high compressor will not be in a position to be radiographed. To allow more of the engine to be radiographed the hexagonal side plates should be spaced as far apart as feasible, probably about 3 meters, the width of the centrifuge arm. This should be considered a requirement in the final TELS design phase.

Two possible support concepts were investigated. These are:

1. Modifications necessary to make the originally proposed hinge-gimbal X-ray support system feasible.
2. Design concept allowing motorized orientation of axial, radial and circumferential position of both the X-ray source and film holder.

A detailed study of the source positioning requirements is presented in Appendix C and evaluates the degree of flexibility of a positioning system.

### **Modifications to Existing Design**

The design proposed in the original TELS study consisted of a rigid X-ray support frame attached to the hoop support. The X-ray unit is shown rigidly attached to this support structure. This does not allow for radial and axial motion of the unit relative to the mounted engine at any fixed circumferential position of the frame. The X-ray support should be modified in a manner such as that shown in Figure 32. A frame will have to be constructed around the X-ray unit to allow for support when the unit is repositioned axially or radially. The film holder should be attached to an extension of this same support frame which extends to the opposite side of the engine in such a manner that the film plate will always be perpendicular to the X-ray beam.

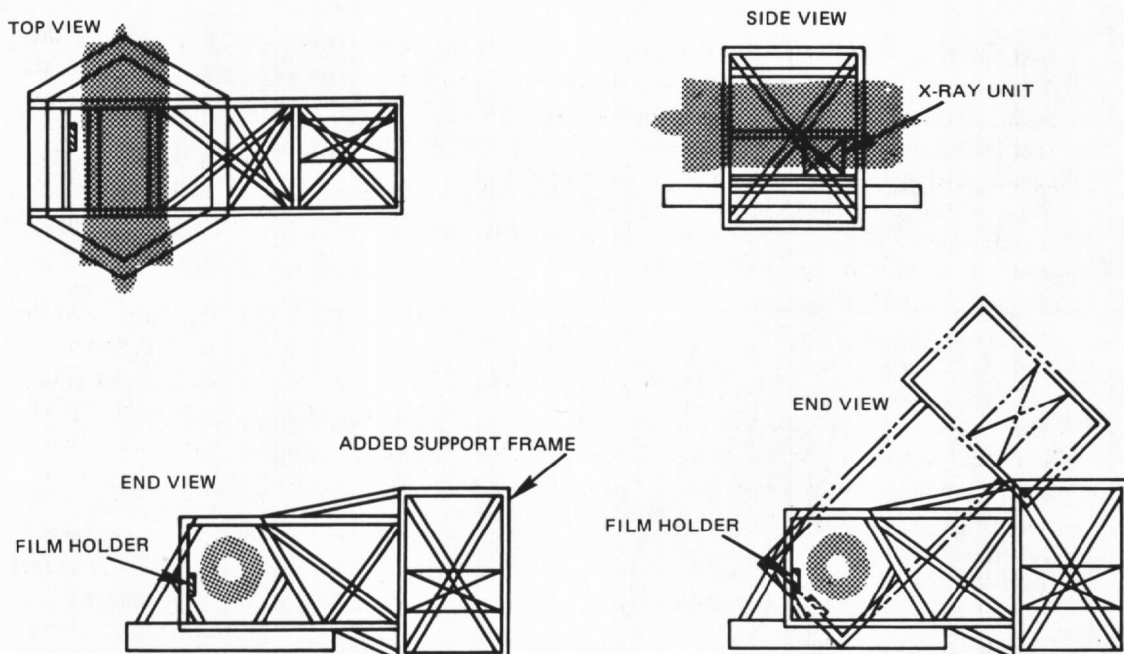


*Figure 32 X-Ray Support To Provide Axial and Radial Repositioning*

The X-ray support frame with the film holder attached to it should rotate as a single unit on rolls bearings attached to either side of the hoop support frame. In doing this the engine mount system will have to be raised approximately 0.6 meters above the turret base so that the side of the X-ray support frame which has the film holder attached to it will not hit the turret base as it rotates around the engine. Incorporation of roll bearings into the X-ray support frame will allow complete freedom in radiographing various circumferential positions on the engine.

Another modification which could be made to the original design would have the X-ray support frame and integral film holder form an "I" structure. This would permit the X-ray unit and film holder to be positioned axially so as to allow radiography of parts of the engine which lie outside the two hoop support frames. A sketch of such a modification is shown in Figure 33. This scheme will add a substantial amount of weight to the hinge-gimbal positioner and its impact on both the roll bearing for the X-ray support and the centrifuge main bearing will have to be determined during the final facility design phase.

#### **Motorized X-Ray Support Frame**

A design concept is proposed that would reduce the size of the actual X-ray unit support structure as well as add versatility to the entire positioning unit. The new frame design allows axial and radial positioning relative to the engine as well as the ability to move circumferentially around the engine. Figure 34 shows a possible design in sketch form.

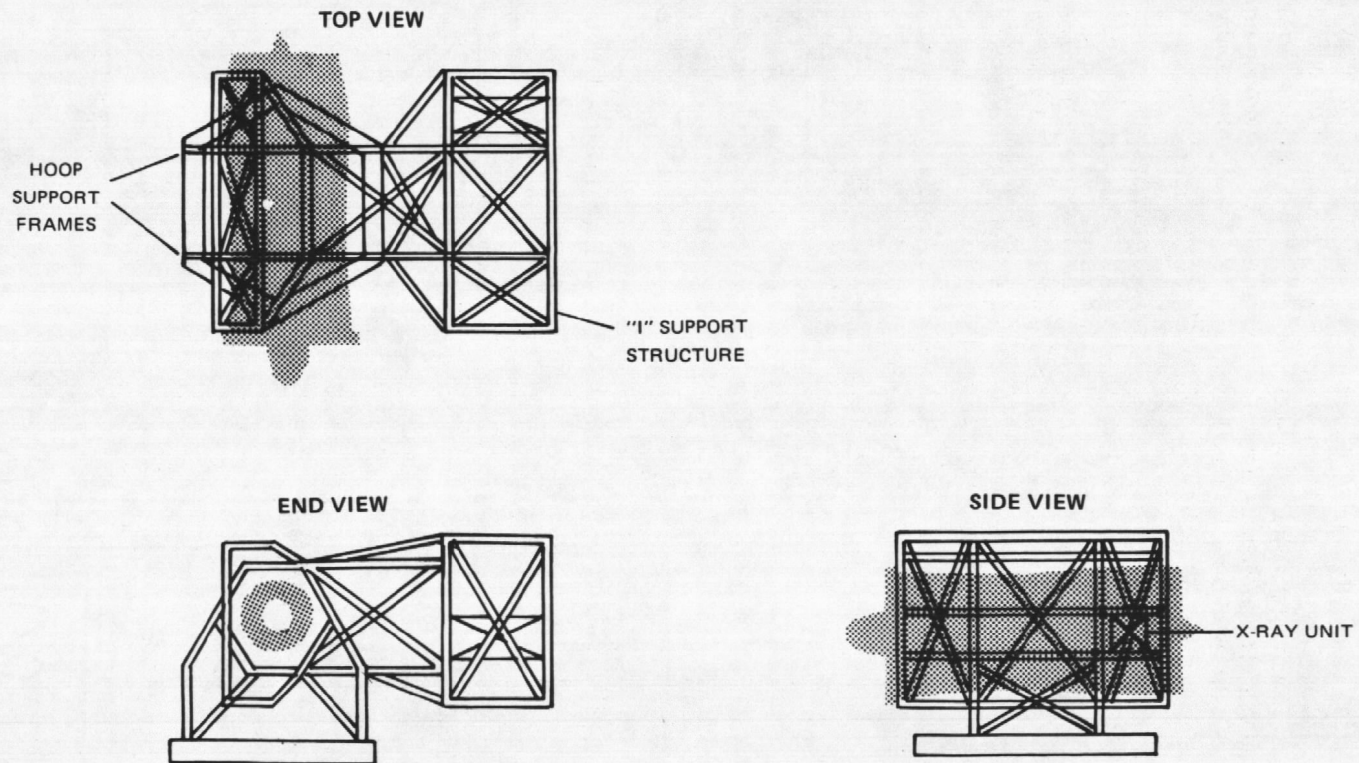


Figure 33 Modification To Original TELS Design Allowing Axial Positioning



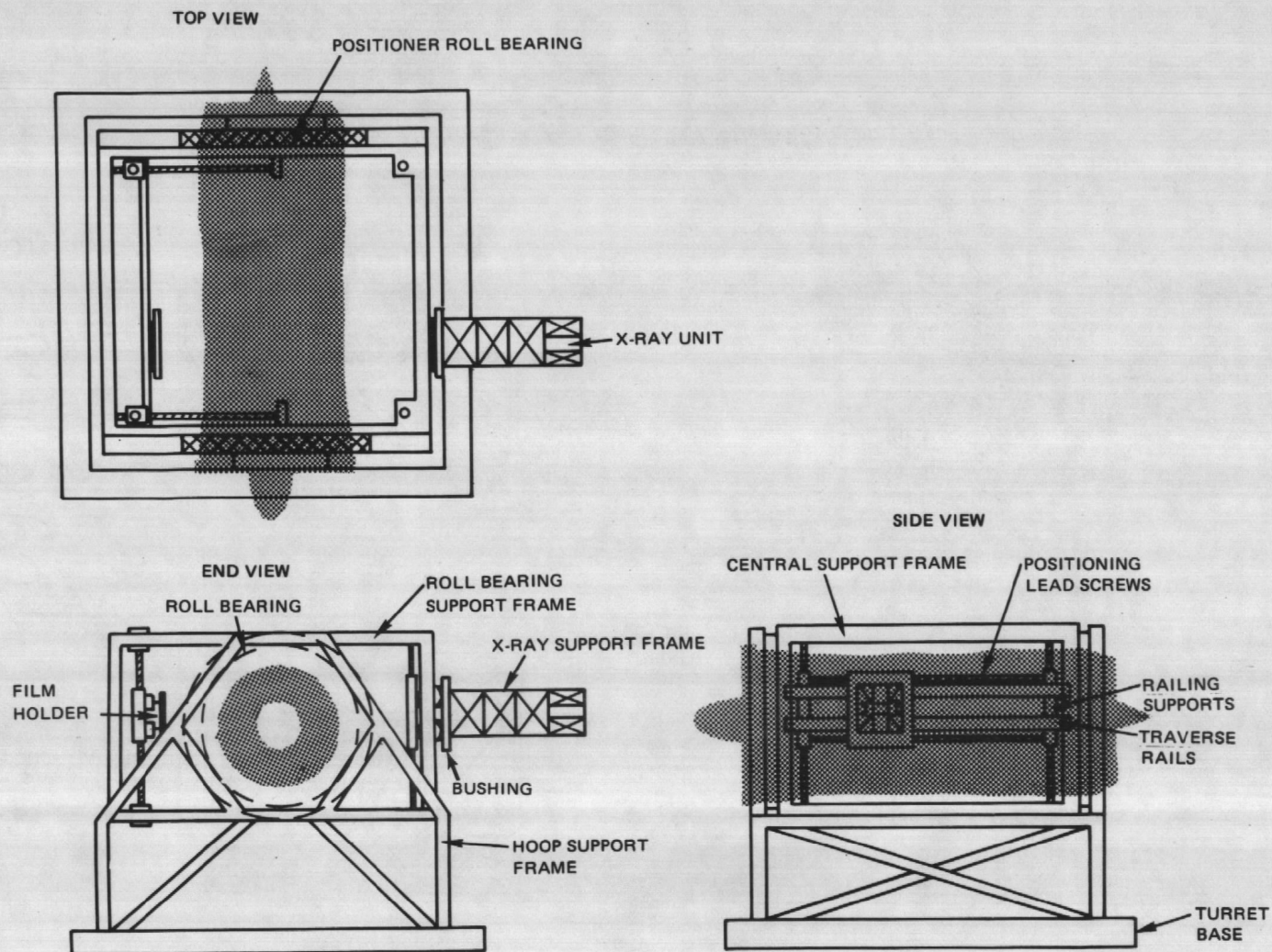


Figure 34 Frame Design For Reducing Size of X-Ray Unit Support Structure



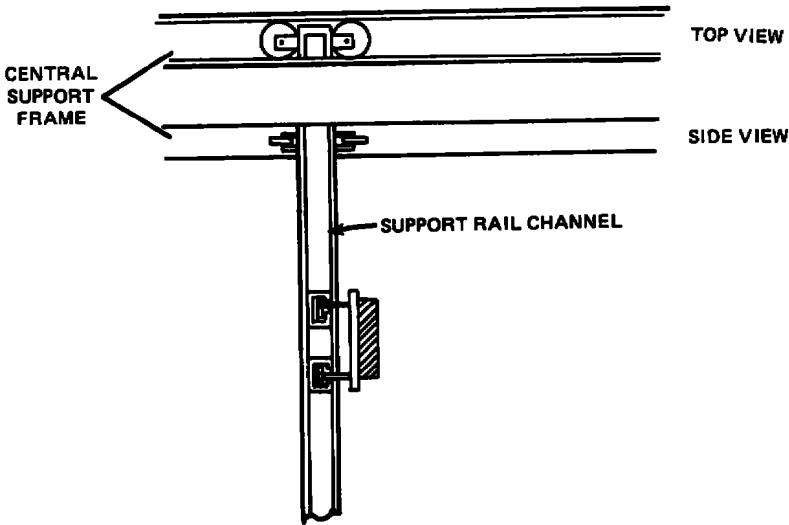
The new support consists of three major components. The first is a central roll bearing support frame which is attached to the hoop support frame via two roll bearings with integral gear. The central frame contains a group of lead screws and support rails, some of which hold the film support while the remaining rails hold the rectangular X-ray support frame to the hinge-gimbal positioner. A small rectangular X-ray support offers advantages both as a weight savings and, due to its reduced cross-sectional area over the originally proposed design, will provide for less drag and thus reduce the load on the main centrifuge motors.

The X-ray support frame is attached to two railings via bushings which allow axial motion. Radial motion is provided by traversing the railing supports along the lead screws. The X-ray film holder is attached to the opposite side of the central support frame in a similar manner. An additional set of four lead screws is provided to allow the film support to move inward towards the engine. In this way the geometric magnification of the object plane on the film can be controlled.

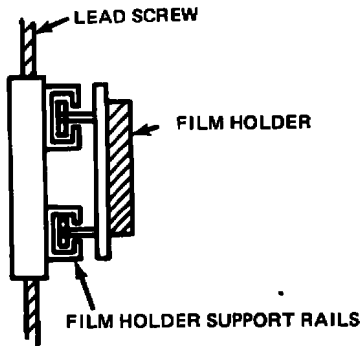
Lead screws were used extensively in this concept. Although they are adequate in carrying tensile loads they are less rigid with regards to lateral loading. In order to provide extra support for the lead screws in resisting side loading, the ends of the support rails should be designed to ride within a channel which is an integral part of the central support frame. In the case of the film support rails, these support channels will have to move laterally along with the film holder when the location of the film plane is adjusted for proper magnification. After the adjustment is made the channel must be locked in place. Figure 35 shows a technique whereby the channel iron which supports the X-ray support rails can be allowed to move. Wheels attached on either end of the channels provide for ease in traversing of the film support rails. In this way, the lead screws which move the film support rails will be restricted from large lateral deflections due to the centrifugal forces.

In order to provide complete motorized control of film holder and X-ray support 12 lead screws will have to be employed. Since two screws can be driven in parallel by a single high torque motor, six such motors will be required. A weight estimate of this positioner is given in Table III. It is felt that a system such as this provides the positioning flexibility required in the TELS radiographic effort.

A set of equations required to locate the position of the X-ray source relative to the pinch points determined in Appendix C are derived in Appendix D.



**FILM HOLDER TRAVERSING SCHEME**



**FILM HOLDER SUPPORT DETAIL**

*Figure 35 Schematic of X-Ray Support Frame Allowing Movement of the Channel Support*

TABLE III – WEIGHT ESTIMATE FOR X-RAY POSITIONER

COMPONENT	COMPONENT WEIGHT BREAKDOWN (Intermediate Engine)*	
	MATERIAL LENGTH (meters)	WEIGHT (kg)
X-Ray Unit		453.6
12 Lead Screws	18.28	751.1
4 Support Rails	9.75	400.5
Film Holder	—	181.4
Central Support Frame	28.04	1151.7
X-Ray Support Frame	12.19	500.8
2 Roll Bearings with Integral Gear	—	1315.4
6 Lead Screw Motors	—	272.2
	Total	5,026.7

- \* For the purpose of estimation we have assumed the positioning system to be constructed of steel ( $\rho \approx 7.833 \text{ gm/cm}^3$ ) with an average circular cross-section 10.16 cm diameter. Therefore, the weight/unit length = 41.073 kg/meter.

## SYSTEM REQUIREMENTS

### GENERAL REQUIREMENTS

The measurement of the internal clearances of gas turbine engines during simulated flight loads by X-radiographic techniques is required. The flight loads will be generated by a centrifuge. The maximum radius and angular speed of the centrifuge are 12.12 meters and 33.4 rpm respectively providing a maximum linear acceleration of 15-g. The X-radiographic system must be capable of producing the required dimensional measurements while randomly oriented relative to the g-vector. To minimize the centrifuge structural requirements the weight and size of the radiographic system should be constrained and as many components as possible restricted near the center of rotation of the centrifuge.

The major components of the X-radiographic system are: 1) The source of X-radiation, 2) the detector system, and 3) the control system.

### X-RADIATION SOURCE REQUIREMENTS

Flexibility in positioning of the X-radiation source is essential to the radiographic measurements of gas turbine internal clearances. Construction of the X-radiation source must be such as to permit positioning and operation at any angle, at elevations up to 6 meters above the centrifuge and any position parallel to the gas turbine shaft for a distance of 6 meters. The most likely choice for an X-radiation source for this application is a linear accelerator. Several concepts for implementing this type apparatus exists. Two that appear most feasible are:

1. The R-F power is generated at the center of rotation of the centrifuge and transmitted via a system of rigid and flexible waveguides and couplings to an accelerator structure mounted at the gas turbine location. A major drawback to this scheme is the lack of flexibility in positioning.
2. The most attractive concept from an operational viewpoint is to have the modulator and pulse transformers located at the center of rotation of the centrifuge and the accelerator structure, R-F oscillator, and other necessary components at the gas turbine location. The high voltage pulses to the electron gun, control grid, and R-F power supply would be supplied with flexible conductors.

A source of X-radiation suitable for these measurements must meet the following requirements:

- Bremsstrahlung Spectrum – Must contain X-ray photons with energies to 10 MeV.
- Bremsstrahlung Flux – A minimum of 50R/sec. @ 1 meter.
- X-Ray Source Shapes – Circular
- X-Ray Source Diameter – Less than or equal to 1.0 mm.
- X-Ray Pulse Width – 2 to 5 microseconds.
- X-Ray Pulse Rate – Adjustable from 50 to 350 pulses per second (1).
- Total X-Ray Field Angle – Adjustable from 8° to 1°.

- (1) The flux rate may vary with the pulse rate.

**Adjustable X-Ray Beam Collimator** – Control of the X-ray beam is essential in high energy radiography. The X-ray field at the detector should be only slightly larger than the detector area. This improves image quality by decreasing scatter and complements the radiation shielding of personnel.

**Electron Beam Control** – Control of the electron beam of the accelerator via an integral control grid provides instant on and off of the X-ray beam. This is required for the rapid acquisition of X-ray images during engine transients. The control grid suppresses the electron beam at the gun of the accelerator and thus stops the production of X-ray. This leaves the cavities of the accelerator in a condition to immediately accept additional electrons for acceleration. When the control voltage is removed from the grid, the electrons are allowed to leave the gun region and be accelerated to produce X-rays. The termination and start-up of the X-ray production occurs in a few milliseconds or less. Without this option, start-up can take 300 to 500 milliseconds.

**Alignment Laser** – A laser that is aligned with the center of the X-ray field is a great aid in alignment of the X-ray source with the engine and detector, and should be a part of the X-ray source.

**Exposure Measurement** – A device for the measurement of radiation dose rate and total dose is required for the TELS X-ray source. Provisions should be made for selecting the total dose required for an exposure and automatic termination of the dose upon completion of the pre-set dose. A monitor for dose rate should also be provided.

The total dose and dose rate measurements should be made at the detector as well as at the target. By calibrating the dosimeter output against total dose or dose rate at the detector, the correct exposure can be determined easily as new areas of the engine are investigated.

## **DETECTOR SYSTEM REQUIREMENTS**

The detector system should permit the detection of the modulated X-radiation with spatial resolution that is limited by test geometric considerations rather than the detector spatial frequency response. The nominal source to object and source to detector distances are 2.54 meters and 3.30 meters respectively. The system should provide means for both film and electronic detection. Both the electronic detection and the film detection systems contained in a single light weight package would be attractive.

The system should provide remote positioning of X-ray film. A capacity for up to 100, 35.56cm x 43.18 cm radiographic images is required. Film translation should occur at a rate of one 35.56 cm x 43.18 cm frame per second.

The detector system should also provide electronic detection at approximately television framing rates. Image areas from 15.24 to 35.56 cm are acceptable as well as alternate electronic schemes for generating the required dimensional measurements. Hard copies of the electronic image are desirable.

## CONTROL SYSTEM REQUIREMENTS

All machine/human interfaces should be designed to facilitate utilization of the system and minimize complexity.

Accurate control of the radiographic exposure is required. This can be accomplished by control of the total dose, dose rate, and time of the exposure. Means should be provided for control of the exposure by direct measurement of the X-radiation being generated, as well as time of exposure. Termination of the exposure should be accomplished by either accumulation of a preset total dose, or a preset time.

The pulse repetition frequency of the source should be controllable from the operator's console. This control must be manually and remotely accomplished. Provisions must be made to accept a tachometer input of variable frequency and amplitude to allow a strobo-radiographic capability. Provisions must also be made to delay the pulse initiation in  $1^\circ$  increments from the receipt of the tachometer pulse. The range of the device should be  $360^\circ$ . This feature allows the investigation of various circumferential positions on a rotating part.

Activation of the X-ray source should be accomplished from an operator's console. Single or multiple exposures at a preset dose should be accommodated. Appropriate interfaces should be provided between the detector and X-ray source to facilitate a selected sequence of exposures with a random time interval between exposures. These exposures will be obtained automatically after manual or external initiation of the sequence.

To accommodate the acquisition of X-radiographs at rates of one per second requires an accelerator with a fast on-off capability. Fast rise to full power is a strong requirement. The utilization of a control grid in the electron gun should be considered.

Sufficient safety interlocks should be provided with the system so that interfacing of the system with an electronic safety system can be accomplished. Separate circuits must be provided for emergency shutdown of the X-ray source from the operator's console or from remotely operated switches. All safety devices or systems required by Federal and local radiation safety standards must be incorporated into the design of the system.

Diagnostic and fault circuits should be incorporated into the design of the system to insure ease of troubleshooting and a low probability of system failure due to improperly operating subsystems.

All control systems will connect to the X-radiographic system through a system of slip rings or other suitable devices. Redundancy in the safety circuits passing through the slip rings should be considered as well as multiplexing of less critical control functions. Other control systems that provide for ease of equipment operation and maintenance or safety should also be considered.

## **FILM TRANSPORT AND VIDEO FLUOROSCOPY**

In order to successfully implement radiographic measurements on the TELS, methods are required for remote handling of radiographic films and other detector systems to eliminate the necessity of physically mounting and removing a film cassette as is the normal practice in X-radiography. By restricting the X-ray beam to the size required to expose the film or excite the particular detector, systems can be developed for remotely translating radiographic film to provide the capability for continuous radiography during the centrifuge operation.

An X-ray film transport system utilizing roll film and capable of operation under 15-g loads could be designed and fabricated that would allow exposures at rates to one per second depending upon the final X-ray source output, image size, film type, and engine component being radiographed. This device coupled with an integral real time fluoroscopic system and the proposed positioning mechanism would allow remote positioning, real time viewing and X-ray film recording of the internal clearances of interest without the necessity of stopping the centrifuge (assuming the 15-g magnetrons, etc. have been qualified and implemented). The real time fluoroscopic system would require a video camera capable of low light level detection and 15-g operation if the camera was to be mounted at the extreme engine location. The 15-g criteria could possibly be met by a diode array solid-state camera utilizing an image intensifier. An alternate approach would be to utilize an image isocon camera located at the center of rotation and coupled to the fluoroscopic screen via an optical system or a coherent fiber optic bundle.

The video fluoroscope/film transport system should have the capabilities of providing critical test information concurrently with the image acquisition so the clearance measurement can be correlated with time, engine rpm, temperature or other engineering parameters. Reliable image identification is a necessity for any system utilized for measurement purposes.

Currently this type of equipment suitable for TELS is not available. Similar equipment for 1-g applications are currently being utilized by P&WA for engine radiography. The design and fabrication of the required remote film handling equipment and video fluoroscopy can be executed utilizing currently available technology.

## **FILM PROCESSING AND DATA ANALYSIS**

For roll radiographic film, an automatic X-ray film processor will be required to provide sufficient control over development speed, chemicals, and temperature. This control is necessary to implement the special film processing techniques developed via the manual processing tanks. Adequate provisions should be made to handle photographic film that would be used in a fluoroscopic system. The provisions consist basically of the appropriate size trays for manual processing and an appropriate automatic processor for photographic film.

### **Processing of Magnetically Stored Images**

The video fluoroscopy used on TELS will produce images on analog and digital magnetic tape and video disk. The usual way to record a video signal is by using a video tape recorder. Alternate ways that are of great use in analyzing the images are digital magnetic tape and

video disk. Recorders and playback units are required for each of these techniques as well as suitable monitors to view the images. Means should be provided to produce hard copies of the images recorded on these devices. This can be accomplished in several ways. The more common are photographic recording directly from the video monitor and electronic hard copy production directly from the video signal. The digital recording is required to implement image processing of the fluoroscopic image.

### **Computer Image Processing**

Acquisition of clearance measurement from X-radiographs has proven to be the most difficult and costly operation involved in a radiographic engine test. During a test, thousands of radiographic images are produced to describe the action of the engine under various operating conditions. Added to the problems associated with the large number of radiographs is the difficulty in analyzing each radiograph to extract the multiple measurements obtainable. Difficulty is encountered primarily because the radiographic blur makes the exact location of edges uncertain. In order to eliminate these problems, increase measurement accuracy, and decrease cost, it is necessary to employ automated computer techniques to obtain the required measurements. A suggested computer image processing system to handle the TELS measurement is shown in the block diagram of Figure 36. The basic components of the system are the image scanner, the computer, the digital storage devices and the interactive console.

The image scanner is a device that automatically scans the image point-by-point and converts the image density and position information into a digital format. This is done under computer control and the information obtained is stored in core memory, on magnetic disk or tape. The computer provides a control function for all the peripherals, data storage, data manipulation and calculation.

The interactive operator's console provides the required interface between the operator and the scanner, computer, recording media, and image processing programs. The operator can control the areas of the image to be scanned via a light pen or cursor. Images stored on magnetic tape or disk can be reconstructed on an interactive CRT display as required.

The magnetic disk storage is required for rapid access to various images for image to image comparison and computation. The magnetic tape provides long-term storage of images and a means to transport images to other locations as needed.



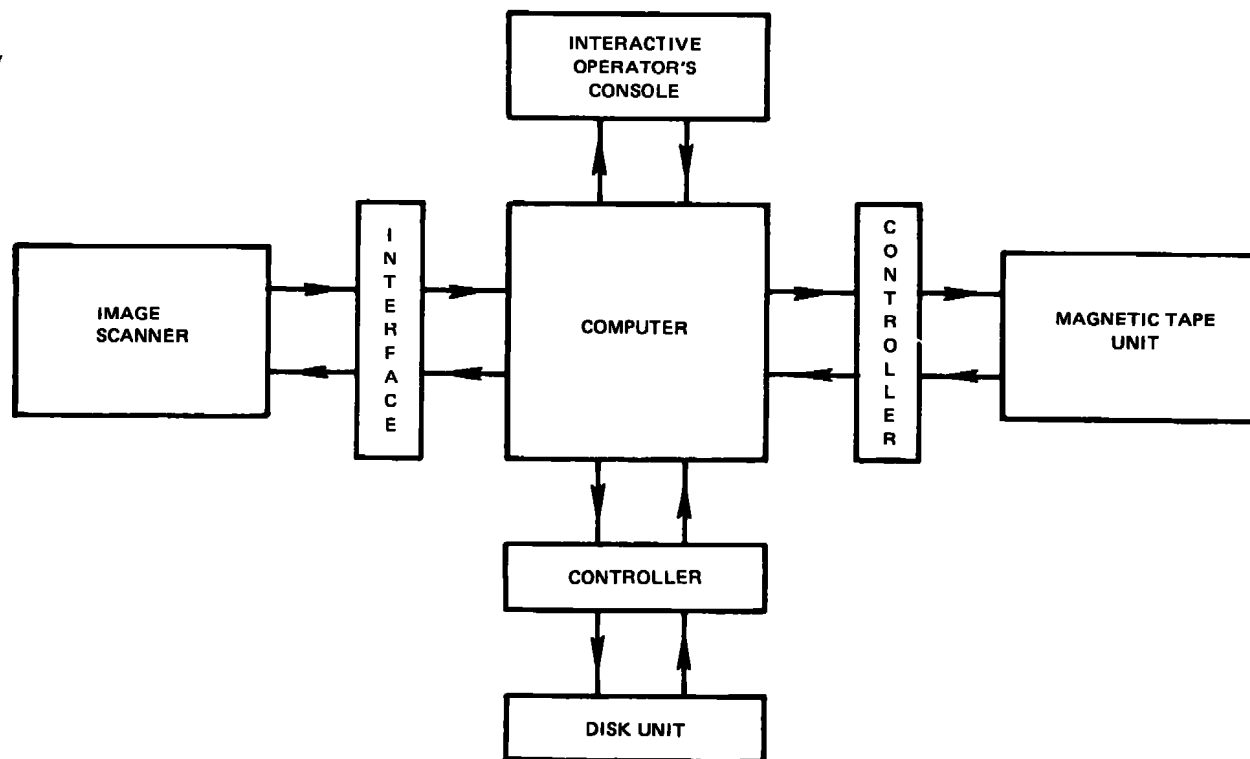


Figure 36 Block Diagram of Computer Image Processing System

Table IV outlines the service requirements for the X-ray system. The exact service requirements depends upon the specific design details of the X-ray source.

**TABLE IV**  
**SERVICE REQUIREMENTS FOR X-RADIATION SOURCE**

**UTILITIES**

<u>X-Ray Source</u>	<u>Positioning System</u>
Electrical	Electrical
45 KVA, 220 VAC $\pm 5\%$ 50 to 60 Hz, 3 phase, 4 wires plus ground	20 KVA, 440 VAC $\pm 5\%$ 50 to 60 Hz, 3 phase, 4 wires plus ground
Coolant	<u>Controls</u>
0.757 Liter/sec @ 20°C, 34 newton/cm <sup>2</sup>	Electrical
<u>Detector Systems</u>	Provisions for
Electrical	20 channels - 20 VDC 8 channels - 100 VDC 8 channels - 110 VDC
10 KVA, 110 VAC $\pm 5\%$ 50 to 60 Hz, 3 phase, 2 wires plus ground	Low current control lines

NOTE: Exact service requirements for TELS depends upon details of radiographic system design.

**TELS SHIELDING REQUIREMENTS**

It is desirable to design the TELS facility so that radiographic measurements of internal clearances of the engine under test can be made without necessity of the proposed earthen revetment and provide the degree of radiation protection for the facility operators as well as the general populace. Elimination of the earthen revetment would reduce the problem of exhaust gas ingestion by the engine during testing and reduce the cost of the installation.

The approach that was investigated to accomplish these objectives consisted of restricting by means of appropriate fences, gates, interlocks, warning lights, audible alarms, local shielding, and operation procedures, access to the area of the facility in which dose rates in excess of the maximum permissible dose could be obtained.

Figures 37 and 38 show the suggested layout of the TELS Facility. The outer fence is placed at a distance,  $b$ , from the centrifuge center to insure that during simultaneous operation of the centrifuge and X-ray source that the maximum permissible dose of X-radiation is not exceeded. This distance was established by calculation, utilizing appropriate values of permissible dose, workload, use factor, occupancy factor, etc., and depends upon the acceptable workload for the facility.

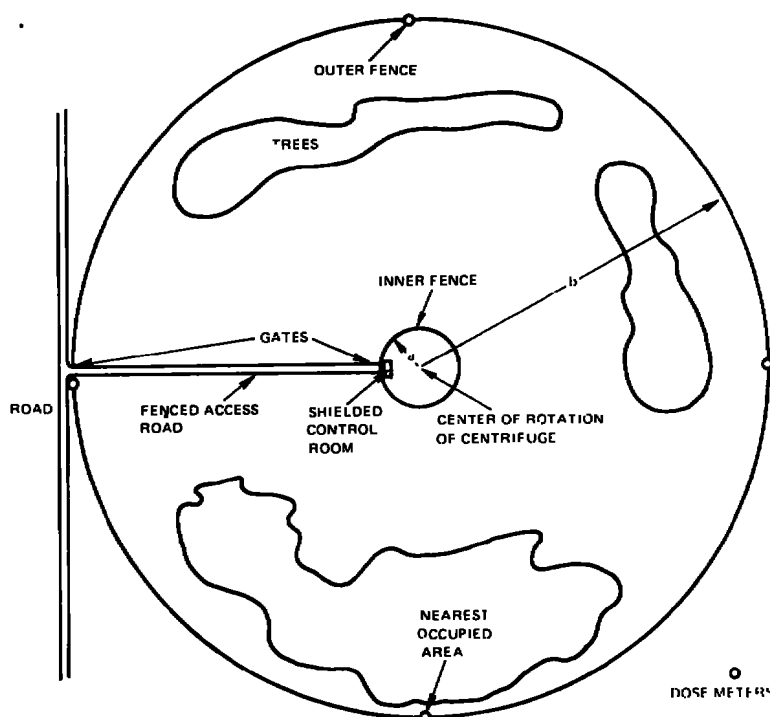


Figure 37 Layout of TELS Facility Without Earthen Revetment

The inner fence and fenced access road serves to constrain the area inside the outer fence to a size easy to control by visual observation and should be kept clear of natural growth. The radius,  $a$ , of the inner fence should be minimized to enhance control of personnel in the area and to reduce cost. Gates at either end of the road must be provided with locks and interlocks so that adequate control of personnel access can be maintained. The locks should be part of the interlock system that controls operation of the X-ray source. The gates must be closed and locked in order for the X-ray source to be activated. Emergency-off switches should be provided along the fenced access road, the inner fence, and other appropriate places.

Additional safety margin could be insured by providing dose rate meters at the outer fence toward the nearest occupied area and at acceptable intervals from that point. These dose meters should record accumulated dose. Readout of the accumulated dose recorded by each meter should be available at the control console so that the permissible dose at the outer fence would not be exceeded. The accumulated dose at the end of each exposure should be recorded. If at the end of any seven consecutive days the exposure at the outer fence ex-

ceeded .01 rad, the X-ray source would not be permitted to operate unless it could be ascertained that no personnel were at the outer fence during the exposures of the past seven days or those persons were restricted from being at the outer fence for the following seven days.

Operation of the X-ray source when the centrifuge is not in operation is required and can be implemented by insuring that it is pointed away from occupied areas and by providing shielding for the primary beam on the service modules that will be required to install and maintain the engine under test.

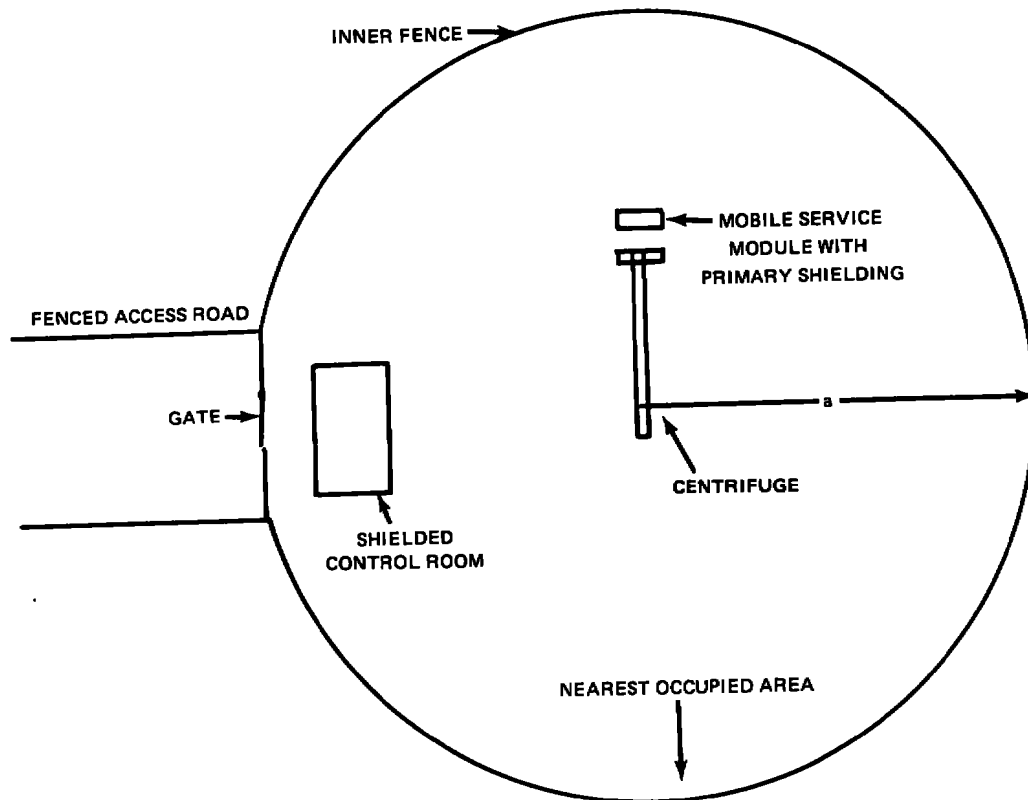


*Figure 38 Adequate Protection Provided by Fencing and Location of Control Room*

Inherent in the calculation of the dose at the outer fence is the "use factor" defined as the fraction of the workload during which the radiation under consideration is directed at a particular barrier. In the case of a rotating source, the use factor is the ratio of the beam angle to a full revolution. When this approach is utilized to calculate dose it is necessary to insure that the centrifuge be rotating when the source is not directed at the primary shielding. Limit switches and angular rate sensors can be utilized as inputs to logic circuits that are part of the safety interlock systems to assure that the proper conditions are met for safe operation.

The calculation of the weekly permissible workload at various distances to the outer fence was based on the following assumptions:

1. The primary beam was aligned directly toward the outer fence with the beam centerline horizontal.
2. The total beam angle was  $8^\circ$ .
3. An "effective" value for the absorption coefficients and build-up factors for the continuous bremsstrahlung spectrum was meaningful.
4. The pulse repetition frequency of the X-ray source was sufficiently high to approximate a continuous source of radiation for the purpose of these calculations.
5. The primary beam was always attenuated by 7.62 cm of steel or equivalent.
6. The use factor, U, for the primary beam calculation could be reasonably represented by the ratio of the total beam angle to one revolution.
7. That the site location is sufficiently remote to assure that the occupancy factor, T, at the outer fence could be assumed 0.25 or less for the primary, leakage, and scatter calculations.
8. The X-ray spectrum was produced by 10 MeV electrons and a tungsten target.

Assumption (1) was chosen as a worst case condition and the workload based on this assumption would be conservative. In routine operation, the source is expected to be oriented toward the ground a great deal of the time. Restricting the beam centerline to angles greater than  $8^\circ$  below horizontal would insure that the beam would strike the ground inside the outer fence for an outer fence radius of 300 meters.

An "effective" value of absorption coefficient has some validity if it is chosen in a manner to produce a reasonable approximation of the absorption of the continuous spectrum.

The pulse repetition frequency of an X-ray source for the TELS application must approach 360 pulses per second. Otherwise, the source is not suitable for turbine engine strobograph purposes. During the majority of the testing, exposures on the order of 10 seconds are likely. This implies approximately 1.8 pulses per degree of rotation for the centrifuge maximum angular rate. This coupled with the  $8^\circ$  total beam angle is believed to be a satisfactory approximation to a continuous, uniformly distributed, (during rotation) X-ray beam.

In order to insure assumption (5) is met, a 7.62 cm steel shield should be built into the detector positioner, and mechanical and electrical interlocks provided to prevent operation of the source without the shield in place. During engine testing, the engine will provide additional attenuation of the primary beam. Therefore, this assumption should provide a conservative estimate of workload during engine testing provided the shield is a required part of the system. A suggested shield configuration is illustrated in Figure 39.

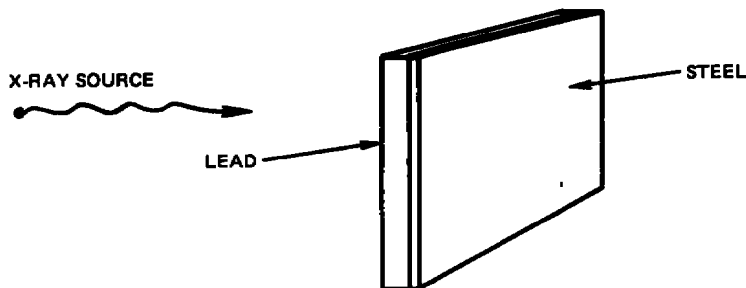


*Figure 39 Shield Construction Composed of Lead and Steel*

The shield construction should be a composite of lead and steel. The lead should face the X-ray source and the ratio of lead to steel thickness should be maximized consistent with design and structural requirements.

The use factor for the primary beam during the centrifuge operation is about 0.022 based on assumption (6). It seems reasonable that this approach be used to calculate the use factor based upon the definition of the use factor.

The site of the facility should be selected such that the occupancy factor at the outer fence is minimized. Otherwise, operation without the benefit of fixed radiation shielding should be reconsidered. An occupancy factor of 0.25 or less should be achievable at the outer fence for the currently proposed site.

The details of these calculations are given in Appendix E. The largest practical radius to the outer fence for the proposed site is approximately 300 meters. The total permissible workload for this distance was estimated to be  $3.002 \times 10^5$  rads/wk. measured at one meter from the X-ray source and based on the stated assumptions. This would give a total beam-on time of 1.66 hours per week for a source with an output of 3000 rads/min. at one meter. This in turn would provide approximately 600 radiographs at 10 seconds per exposure. This quantity is believed to be a conservative estimate, but is considered to be an acceptable number of radiographs based on turbine engine radiographic experience.

A detailed calculation of the workload at 300 meters was performed taking into account the continuous nature of the X-ray spectrum. This produced a maximum permissible workload of  $5.40 \times 10^5$  rads/wk. at one meter from the source for a static source and a workload of  $1.104 \times 10^6$  rads/wk at one meter from the source for a rotating source. This calculation implies a 3.00 hours per week beam-on time for the static source and a 6.13 hour per week beam-on time for the rotating source assuming an output of 3000 rads/min. at one meter from the X-ray source. All of these estimates should be confirmed by a qualified health physicist.

## REFERENCES

1. Venable, Douglas, et al, "Phermex: A Pulsed High Energy Radiographic Machine Emitting X-rays", Los Alamos Scientific Laboratory of the University of California, Los Alamos, New Mexico, May 15, 1967, LA-3241.
2. R. Halmshaw, "Physics of Industrial Radiology", Sliffe Books, Ltd., 1966.
3. "Reference Data for Radio Engineers", 5th Edition, Howard W. Sams & Co., Inc. N. Y. - 1968.
4. Andriulli, John, "Turbine Engine Loads Simulator Study", Planning Research Corporation, Huntsville, Alabama, October, 1974, AEDC-TR-74-73
5. State Regulations for Protection Against Radiation, Division of Industrial and Radiological Health, Tennessee Dept. of Public Health, Nashville, TN, 1972.
6. Non-destructive Inspection Methods, Air Force Technical Manual, T.O. 33B-1-1, TM43-0103, 1 Feb. 1966, Change 13-1, January, 1976.
7. Medical X-ray and Gamma-Ray Protection for Energies up to 10 MeV Structural Shielding Design and Evaluation, National Council on Radiation Protection and Measurements, (NCRP Report No. 34) Washington, D.C., 1970.
8. Industrial Hygiene Standard No. 53, June 27, 1975, ARO, Inc.
9. Stephenson, R., "Introduction to Nuclear Engineering", McGraw-Hill Book Co., Inc., N.Y., 1954.
10. Zirkle, R. E., "Ed. Biological Effects of External X and Gamma Radiation-Part I" McGraw-Hill Book Co., Inc., N. Y., 1954.
11. Jackson, J.D., "Classical Electrodynamics", John Wiley and Sons, N.Y., N.Y, 1967.
12. Jaeger, R. G., Blizard, E. P., et. al., "Engineering Compendium on Radiation Shielding," Vol. I, "Shielding Fundamentals and Methods," Springer-Verlag, New York, Inc., 1968.
13. Reactor Physics Constants, Argonne National Laboratory, United States Atomic Energy Commission, July 1963.

## APPENDIX A

### ON/OFF CENTRIFUGE CONCEPTS

#### X-RAY MOUNTED ON THE CENTRIFUGE

##### **I.A. RF Power Generated at the Center of Rotation and Transmitted to an Accelerator at the Engine Location**

In this approach, the entire electronics package including the RF power source would be located at the center of rotation to minimize the g-loads. This would allow, by judicious placement of parts, the utilization of available components for the majority of the system.

The RF power would be transmitted via waveguides to an accelerator mounted on a positioning system at the engine location. A degree of flexibility can be built into the waveguide structure by the use of bellows type sections and a collection of waveguide sections of various lengths and angles.

The waveguide section would have to be adequately constructed to withstand the g-loads. Aluminum can be utilized for waveguide and could certainly be utilized for those sections that run parallel to the centrifuge arm.

The accelerator structure, vac-ion pump, and electron gun must be designed to withstand the high g-loads encountered at the engine position. It appears that although existing high-g accelerator structures do not exist, they could be designed and fabricated. A design that would likely provide a satisfactory structure would utilize a composite waveguide such as high strength, high modulus steel with the RF cavities copper plated. A similar composite could be utilized for the waveguides. In both cases external reinforcement could be utilized to provide additional stiffness as required.

The vac-ion pump would likely require redesign and the electron gun definitely would have to be specifically designed to withstand the loads, however, no severe complications are envisioned in this area.

The entire assembly located at the engine must be mounted on a frame that has sufficient stiffness and strength to preserve accelerator alignment and the spatial relationships of all components secured to it.

A fairly significant problem associated with this approach is the necessity to do waveguide plumbing each time a new position is radiographed. Long waveguides imply larger losses than short guides but this is not likely to be an important consideration. A variety of alignments are shown in Figures A.1a, 1b, and 1c to illustrate the complexities in routing fixed waveguide sections.



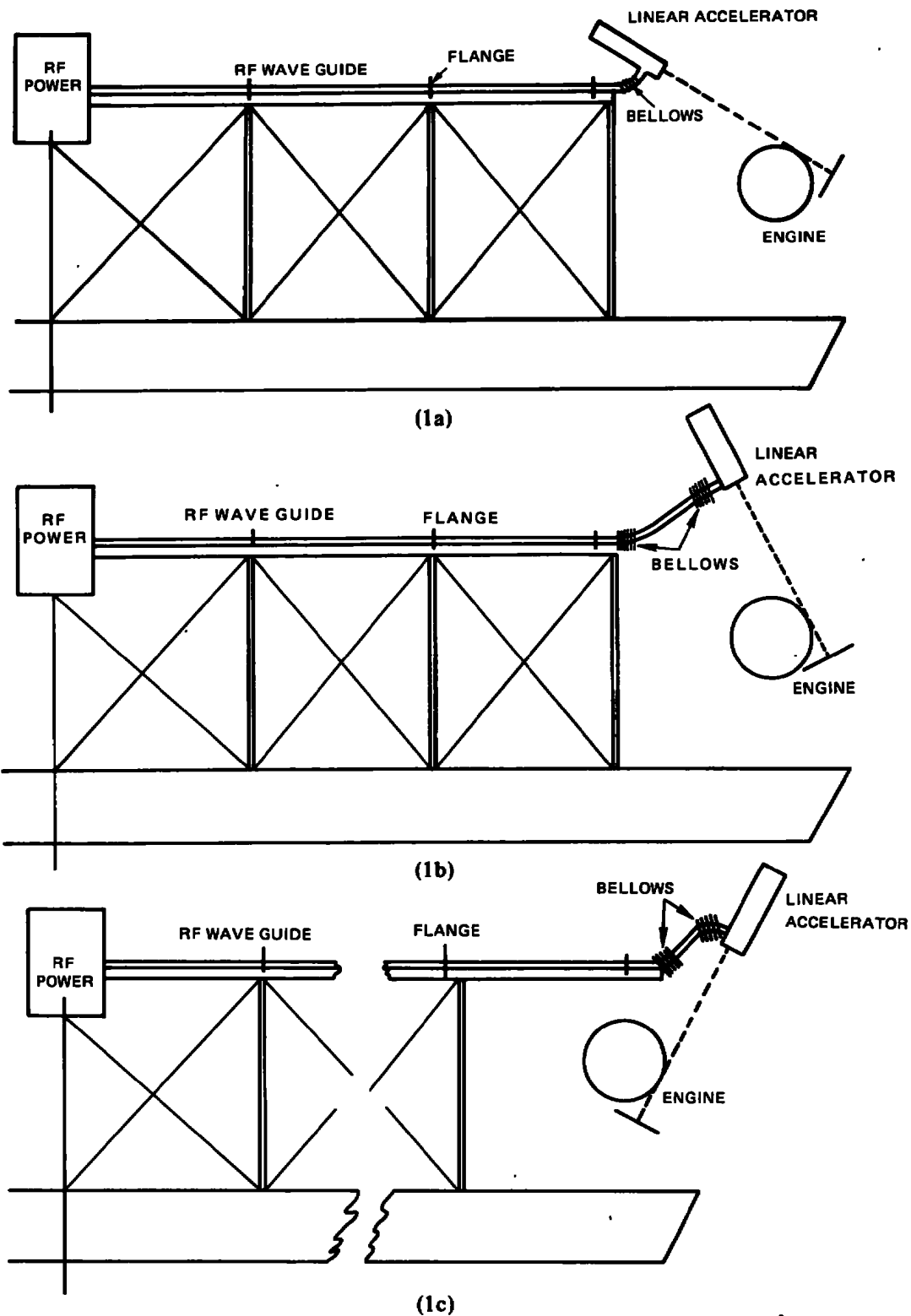


Figure A RF Power Transmission Scheme

### **I.B. Electron Beam Generated at the Center of Rotation and Transmitted to a Target at the Engine Location**

An alternative to I.A. is to actually accommodate the entire accelerator structure at the center of rotation and transmit the high energy electron beam along the centrifuge to the position of the engine. At that point, the beam would collide with an appropriate target and produce the bremsstrahlung radiation required.

The electron beam having been accelerated to an appropriate energy at the center of rotation would be transmitted via evacuated tubular structures to the position of the engine. These tubes would provide sufficient magnetic shielding and focusing magnets to maintain proper electron trajectories. By utilizing flexible joints and turning magnets the electron beam would be directed to the appropriate position relative to the engine and allowed to collide with the target to produce the radiation required. The complexities of this approach is similar to the previous one. The advantage is that critical assemblies such as the accelerator structure, etc. can now be placed in a low-g environment and off-shelf components utilized.

The transmission losses of the electron beam would be primarily due to losses incurred during turning of the beam. The beam bending magnet would be designed to handle monoenergetic electrons. Since the electrons in the beam have varying energy, some will be turned too much and some too little. These will collide with the walls of the guide and represent a net loss of radiation. Several turning magnets (at least two) would be required to accomplish the positioning of the target. Since the turning angles must be variable, the turning magnets must be preprogrammed to provide the correct turning fields for the angle set. This could be done manually but should likely be accomplished using transducers to provide positioning data to a digital computer which would in turn control the applied magnetic fields.

Since the magnetic fields are variable, the losses associated with transmitting the electron beam are also variable. These losses are significant in at least two ways.

The first is that losses imply that a larger input energy is required to provide the required radiation and second, the losses due to collision with the walls of the guide tube produces secondary sources of radiation that would effect the quality of the radiograph.

Turning magnets are currently utilized in industrial and medical radiographic equipment and do not represent a significant design problem except in respect to the high-g loads. However, the magnets are basically solid state devices and should present no difficulties.

### **I.C. High Voltage Generated at the Center of Rotation and Transmitted to RF Power Supplies and Accelerator at the Engine Location**

This approach is similar to I.A. except that the RF generation is moved from the center of the rotation to the engine position. This implies that the RF power source, waveguide, water load, circulator, etc. must be built to accommodate the high g-loads.

Conversations with Varian Associates of Palo Alto, California suggests that a co-axial type magnetron would be a likely choice for a RF power source. This type of structure although relatively rugged has not been tested to the loads to be encountered on TELS and would have to be evaluated and redesigned if necessary.

It was also suggested that in order to decrease the load effects on the accelerator structure and to minimize the structural requirements, that a small light-weight accelerator structure be fabricated. Varian suggested utilization of X or C band for the RF frequency. This implies a relatively small accelerator structure of approximately 6.35cm in diameter by 61 cm long to achieve 8 MeV electrons. Total weight of such an accelerator would be about 57 kilograms. The capabilities of an X band magnetron is about 1.5 megawatts. Two of these devices feeding the accelerator simultaneously would produce between 600 and 900 rads/min. at 1 meter. This is approximately 30% of the output of the device utilized by P&WA for engine radiographs and would require an exposure time 70% longer than currently used. All components of the structure would have to be specifically designed for the TELS application as was discussed in I.A.

Utilization of a S band machine such as the Linatron 2000 implies an accelerator structure of at least one meter and a diameter of about five inches. The weight of the unit would be in the neighborhood of 250 kilograms. Again, the equipment does not currently exist that is compatible with the high g-load requirement.

#### **I.D. Entire X-Ray Source at Engine Position**

All of the problems of I.C. are encountered in this approach. In addition all components of the system would be subjected to the high loads. This does not appear to be a viable approach.

### **X-RAY MOUNTED OFF THE CENTRIFUGE**

#### **IIA. Single Source Capable of Producing Measurements in a Single Pulse**

This technique implies that the entire radiation dose required to produce the measurement is delivered in a single pulse by a device located at a particular circumferential position off of the centrifuge. This pulse length should be kept to one microsecond or shorter. This does not appear to be a significant problem because most single pulse devices used for flash radiography normally operate with pulse lengths in the low nanosecond range. The primary problem associated with this technique is the delivery of the 250R minimum dose (for film measurements) in one pulse.

Phermex is a very large standing wave linear accelerator structure operating at 50 MHz. This requires RF cavities of about 5.5 meters diameter. The three cavities of this system are a total of about 9 meters in length and produce an electron beam energy of about 30 MeV. The resulting dose at 1 meter from the target is about 50R, however, the machine has produced doses of 100R and is currently being modified to produce this output routinely. 100R is not believed to be the upper limit of the device's capabilities. However, there was no estimate of the cost or time involved to develop it beyond the present 100R goal. This 100R output is only 40% of the TELS requirement for a single pulse system utilizing film for detectors.

The tungsten target utilized by Phermex for generation of the bremsstrahlung is destroyed by the electron beam at the point of impingement. A circular target that is remotely indexed is currently utilized. When the target is indexed, a new section of the tungsten is positioned to intercept the electron beam. Multiple pulse operation is not currently obtainable from this equipment. Due to the large size of the structure, positioning would present a problem. The only feasible way to accomplish this would be to utilize turning magnets to direct the high energy electrons to the proper position leaving the more massive structure subject only to gross movements in a horizontal plane above or below the centrifuge system.

The linear accelerator reviewed at Lawrence Livermore Laboratories was an L Band device and of the traveling wave design. The physical size of the accelerator structure was about 0.31m diameter and the five cavity sections had a combined length of 9 meters. The electron beam energy was about 75 MeV and the output per pulse was 50R. This facility was in the process of being upgraded. However, up rating of the output would still produce only marginal quantities of X-radiation for single pulse operation. Multiple pulse operation is not currently obtainable from the equipment.

The accelerators discussed at Physics International for flash radiographic applications were of the field emission variety. A pulse of very high voltage is delivered to a cold diode. Electrons are pulled from the cathode and accelerated toward the anode. Collision of these electrons with the target material produces the bremsstrahlung. The pulse length is in the nanosecond range and a device supplying 400R at one meter is physically about 18 meters long and about 6 meters in diameter. Total weight of the device is  $5.8 \times 10^6$  kilograms. Positioning of such a device would be a monumental feat. Utilization of turning bellows type joints between the Blumlein cylinder and the Marx generator could conceivably provide sufficient flexibility in positioning. Single pulse operation is standard for this type of equipment. To provide capability for multiple pulse would require a good deal of development. Time between pulses can exceed two hours.

## **II.B. Single Source Capable of Producing Measurement in Multiple Pulses**

1. Multiple revolutions.
2. Single revolution.

Utilization of machines of the above mentioned type in multiple pulse configurations could provide sufficient radiation to produce measurements. These multiple pulses could occupy a very short time interval of fractions of a second and produce radiographs at the rate of one per revolution or the pulses could be produced at the rate of one per revolution or less and take many revolutions to accomplish an exposure.

The Phermex source at Los Alamos appears to provide the opportunity of producing multiple pulses in time intervals of a few microseconds. The acceleration of the electron beam does not significantly deplete the stored energy in the accelerator structure. Therefore, provisions could be made to produce more than one radiation pulse, each pulse producing less radiation than the previous one until the stored energy was significantly depleted. At this point, the RF cavities would require filling. Under multipulse conditions, the target becomes

a problem since the area at the impingement point is destroyed. If a one inch radius disk is utilized as a target, approximately 764,000 rpm would be required to provide a new target area on the circumference of the disk if the time between pulse are one microsecond.

In order to track the engine during the multipulse, the electron beam would have to be deflected along the engine trajectory by electrostatic or electromagnetic deflection techniques. If this was not done, the source would appear as a linear series of point sources and would not produce a conventional radiograph.

Multipulse operation could be obtained from the L band device at Lawrence Livermore Laboratories. However, since the energy storage capacity of that device is much lower than the Phermex it is significantly depleted after each pulse and must be recharged. This elapsed time prohibits pulse repetition frequencies of more than about 15 or so per second. Utilization of this type structure would require sufficient revolutions of the centrifuge to accumulate an adequate dose.

Similar problems exist in trying to utilize the field emission type device in a multipulse manner. The system essentially discharges after each pulse and must be recharged. The charge time is sufficiently long that the engine would move significantly before the next pulse could be delivered.

#### **IIC. Multiple sources uniformly distributed Around The Centrifuge Each Contributing to The Measurement**

An approach for the off-arm system that should be considered is the utilization of a series of commercially available sources distributed in some manner about the circumference of the centrifuge and independently positionable. Utilization of this approach foregoes high speed measurement of clearances due to the fact that multiple revolutions of the centrifuge would be required for a reasonable number of sources.

Several problems are associated with this approach. These are indicated below:

1. Multiple positioning systems are required.
2. Positioning and pulse triggering times are critical.
3. Radiation pulse length.
4. Stability of the centrifuge.

The utilization of multiple sources implies the need for multiple position systems. Each of the positioning systems must be capable of placing each of the individual sources in the required spatial position relative to the engine within the tolerance specified. This requirement inflates the system cost. However, the design cost of the positioning system could be distributed among all the positioners.

The remaining items – positioning and radiation pulse triggering accuracy, radiation pulse length, and centrifuge stability – directly effect the quality of the radiographic image because they control the effective size, shape, and intensity distribution of the X-ray source relative to the engine.

Since multiple sources and multiple pulses from these sources are required to form the radiographic image, the effective source is the resultant of the multiple pulsed sources. Instability in the centrifuge or source positioning system, delayed pulses or improper positioning of the sources will result in an effective source that would produce a poor radiographic image.

Assuming that the radiation pulse timing tolerance must be such as to restrict motion blur below that expected from the engine component vibration, the timing tolerance would have to be approximately  $\pm 1$  microsecond as a worst case. The positioning of the sources would have to be accomplished to within approximately  $\pm 0.254$  mm of the true position relative to the engine. This restricts the unsharpness due to geometry below that due to screen and film and assumes a 1.0 mm diameter source. The stability of the centrifuge is more critical than the stability of the source positioning systems. The centrifuge vibration would result in a linear displacement of the image on the detector since the detector is envisioned attached to the engine. By simple geometric construction, this is shown to cause more degradation than source vibration. To maintain the image quality required of engine radiographic measurements, the degradation due to centrifuge motion should not exceed that due to engine vibration. Therefore, the centrifuge vibration would have to be restricted to  $\pm 0.051$  mm in any direction.

Commercially available X-ray sources have pulse durations of 2 to 4 microseconds and would not be suitable as currently designed. In the literature there is mention of modification to reduce pulse length and/or subdividing pulses to obtain flash radiographic capabilities. The modification would directly affect the exposure time due to duty cycle considerations. Exposure times depend upon the source radiation output per pulse, the number of sources and the type of detector. Exposure times of three to fifteen minutes are to be expected according to preliminary estimates.

In this multi-source approach, the source at each location would consist of an accelerator and associated RF components. The pulse repetition frequency of the collection of sources would be such that a common pulse forming network and pulse transformer could possibly be utilized. If high voltage switching proves to be a problem or switching cost is prohibitive, several independent radiographic systems could be utilized.

## APPENDIX B

### DEFLECTION ANALYSIS OF MAGNETRON CATHODE

A simple diagram for a magnetron cross section is shown in Figure B-1. The cathode is supported on either end by a clip, probably made of copper alloy. The cathode is located in the center of a cylindrical copper anode. The distance between the cathode and anode must remain unchanged under various conditions of centrifugal loading when positioned on the linear accelerator.

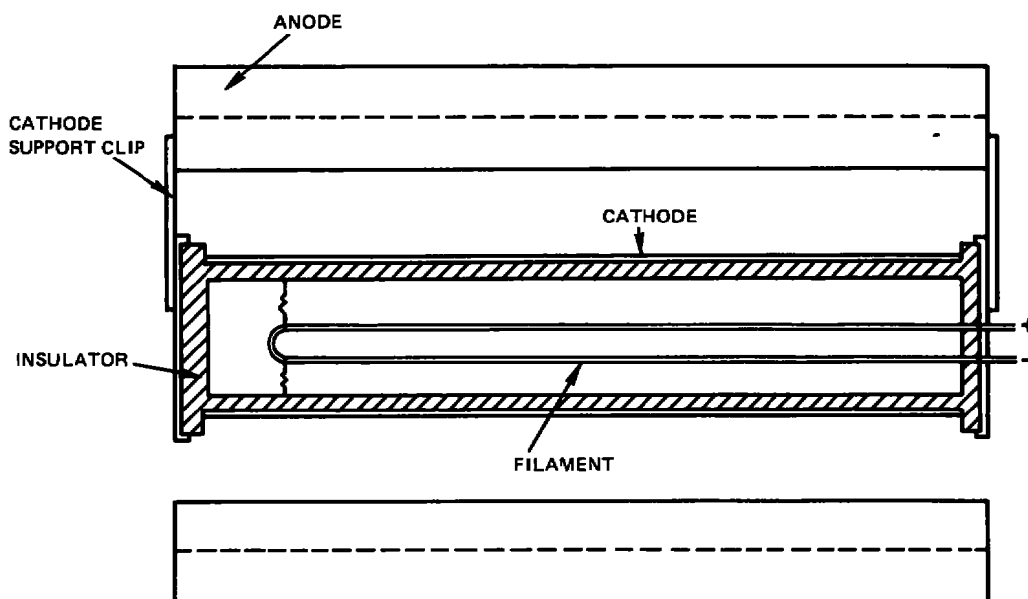


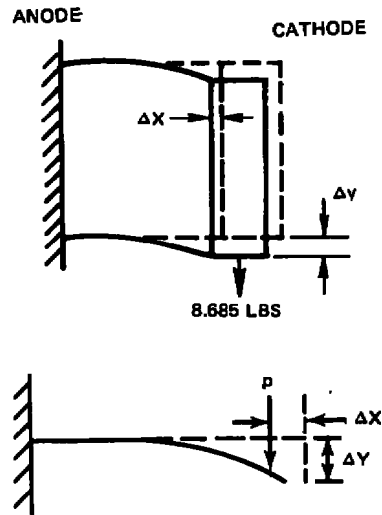
Figure B-1 Magnetron Cathode Cross Section

Material properties and weights for the cathode and its supports are shown below:

#### MAGNETRON COMPONENTS

	MATERIAL	MODULUS OF ELASTICITY		VOLUME (cm <sup>3</sup> )	WEIGHT (kg)
		(newton/cm <sup>2</sup> )			
Cathode	Tungsten	$3.45 \times 10^7$		10.42	0.201
Insulator-Body Side Plates (2)	Mg O	$4.48 \times 10^6$		18.13	0.031
	Mg O			2.20	0.004
Side Plates (2)	Beryllium-Copper	$1.10 \times 10^7$		3.05	0.025
Filament (0.762 mm dia.)	Tungsten	$3.45 \times 10^7$		0.10	0.002
Total					0.263

Under the 15g centrifugal loading the copper alloy clips that hold the cathode in place must support 38.63 newtons without any measurable deflection. In this situation each copper clip must support a side load at its tip equivalent to half the centrifugal loading acting on the cathode. In this case the support clips can be analyzed as a simple cantilevered beam of an equivalent cross-section. The lateral deflection of the end of the cantilever will correspond to motion of the cathode along the centerline of the anode. Axial deflection of the cantilever will result in deflection of the cathode towards the anode. It is this deflection that is most critical.



An equivalent beam analysis problem is shown below:

$$p = 19.32 \text{ newtons}$$

$$L = 2.54 \text{ cm}$$

From elasticity:

$$\Delta x = \frac{px^2y}{2E*J} - \frac{pLyx}{E*J}$$

$$\Delta y = \frac{pLx^2}{2E*J} - \frac{px^3}{6E*J}$$



Where:

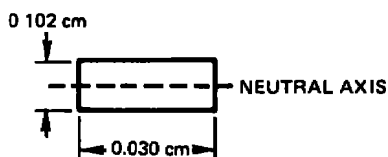
$P$  = lateral load

$L$  = length of beam

$x$  = distance from fixed end

$y$  = distance from neutral axis to beam surface

Assuming the clip has a cross-section equivalent to a rectangle with dimensions shown below:



The moment of inertia  $I = 2.66 \times 10^{-5} \text{ cm}^4$

If the clip is made of Beryllium-Copper alloy then  $E^* = 1.1 \times 10^7 \text{ newtons/cm}^2$  and  $E^* I = (16 \times 10^6) (6.4 \times 10^{-7}) = 293.39 \times \text{newtons} \cdot \text{cm}^2$

For the clip:

$$x = 2.54 \text{ cm}$$

$$y = 0.051 \text{ cm}$$

$$\therefore \Delta x = 0.011 \text{ cm}$$

$$\Delta y = 0.358 \text{ cm}$$

This means the deflection of the cathode parallel to the centrifugal load will be approximately 0.358cm and the deflection of the cathode towards the anode will be 0.011cm.

For the case where the centrifugal load is perpendicular to the axis of the cathode there will be a distributed load acting on the cathode itself due to its own weight. In a case like this we can ignore the weight and rigidity of the insulator and just analyze the deflection of the center of the cylindrical cathode fixed at both ends.

The deflection of the center of the cathode is given by:

$$y_{\max} = \frac{w L^4}{384 E^* J}$$

and

$$w = \rho A \ddot{z}$$

Where

$\rho$  = density of cathode

$A$  = cross-sectional area of cathode

$\ddot{z}$  = 15 g's

$L$  = length of cathode

Let:

$$A = 2\pi (1.143\text{cm})(0.127\text{cm}) = 0.912\text{cm}^2$$

$$\rho = 19.293 \text{ gm/cm}^3 \text{ (Tungsten)}$$

$$L = 11.176\text{cm}$$

$$E^* = 3.45 \times 10^7 \text{ newtons/cm}^2$$

$$J = 0.541\text{cm}^4$$

$$E^* J = 6.5 \times 10^5$$

$$\text{and, } Y_{\max} = 5.612 \times 10^{-6} \text{ cm}$$

This deflection is negligible when compared to the deflection towards the anode when the load is parallel to the cathode.

## APPENDIX C

### LOCATION OF X-RAY SOURCE

#### SOURCE POSITIONING

In addition to identifying the X-ray source to be used in the TELS facility it is necessary to determine where the source shall be positioned with respect to the engine itself. In addition to engine axial motion, internal radial clearances will have to be determined when the engine is subjected to flight maneuver loads on the centrifuge. We would like to be able to align the X-ray source in order to radiograph the smallest and largest gap between the engine rotor and its surrounding casing. The gaps of interest at any axial station along the engine will lie in a plane A running through the engine centerline which contains the rotor displacement vector  $\bar{D}$  (Figure C-1). In order to successfully radiograph the clearances between the rotor and the case the X-ray beam will have to be aligned perpendicular to the Plane A at the engine axial station and engine radial position of interest. The location of the displacement vector  $\bar{D}$  and thus the gap to be radiographed is dependent upon the centrifugal forces and gyroscopic moments acting on the engine during centrifuge operation.

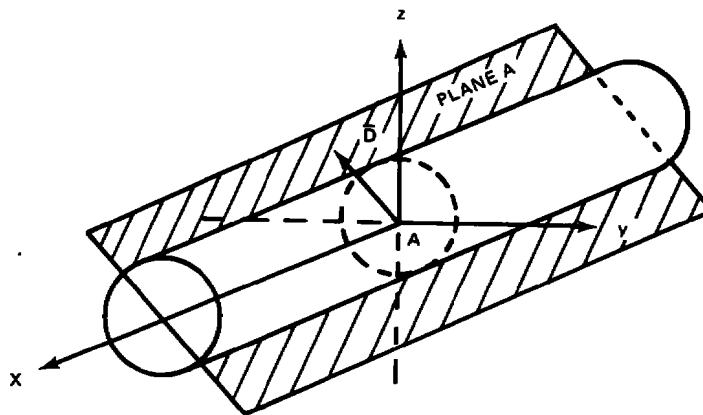


Figure C-1 Alignment of X-Ray Beam At the Engine Axial Station

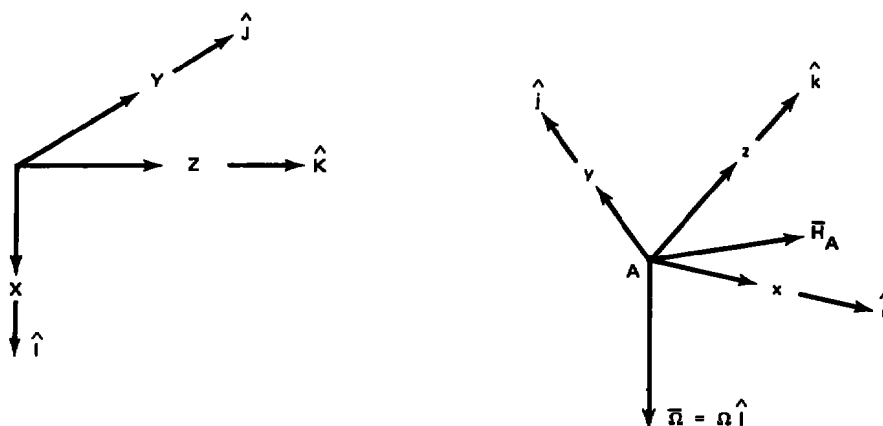
A set of equations defining the gyroscopic moment induced on the rotor by the angular rate of the centrifuge was desired. This analysis was done to identify the important parameters required to correctly simulate the flight maneuvers. In addition, the displacement of the rotor due to the gyroscopic moment must also be considered in locating the rotor-case pinch points. It is these points which we are interested in radiographing. Once the pinch point on the engine circumference is located we are then able to determine where the X-ray beam must be aligned.

The initial analysis of the gyroscopic moments assumed the engine rotor was a right circular cylinder rotating about its axis. The cylinder was then said to have some orientation relative to the angular rate vector of the centrifuge. The interaction between the angular momentum of the cylinder and the angular rate vector of the centrifuge results in the creation of a gyroscopic moment.

### GYROSCOPIC MOMENTS ACTING ON A TURBINE ENGINE ROTOR DURING SIMULATION OF FLIGHT MANEUVERS EMPLOYING A CENTRIFUGE.

The angular rates that simulate flight maneuvers can be applied to a turbine engine by a centrifuge. When the engine rotor rotates about its own axis while the entire engine structure is rotating at a given angular rate, a gyroscopic moment is exerted on the rotor supports by the rotor itself. A constant speed centrifuge will generate an angular rate vector parallel to its axis of rotation. The gyroscopic moments acting on the rotor supports will depend on how the engine is positioned relative to this rotation vector and the angular velocity of the rotor relative to the engine case.

We must now consider the gyroscopic moments created by the rotation of the turbine rotor within the engine case. Consider two coordinate systems. System XYZ is an inertial reference fixed to the base of the centrifuge. System x, y, z is fixed to the engine case and rotates with angular velocity  $\bar{\Omega}$  relative to the system XYZ. The engine rotor itself rotates relative to x, y, z with angular velocity  $\omega_{\text{rotor}} = \omega_{\text{rotor}} \hat{i}$ . The origin of the engine coordinate system x, y, z, corresponds to A, the engine center of mass. The engine rotor is aligned along the x-axis.



The rotor itself has some angular momentum due to the combined rotations of the rotor within the engine case and the engine case about the centrifuge base (XYZ) or:

$$\bar{H}_A = J (\bar{\omega}_{\text{rotor}} + \bar{\Omega}) \quad (C1)$$

Since point A is taken to be the engine center of mass, the total moment of external forces acting about point A (a non-inertial reference point) is represented by:

$$\bar{M}_A = \left( \frac{d\bar{H}_A}{dt} \right)_{XYZ} = \left( \frac{d\bar{H}_A}{dt} \right)_{xyz} + \bar{\Omega} \times \bar{H}_A \quad (C2)$$

Where  $\left( \frac{d\bar{H}_A}{dt} \right)_{XYZ}$  is the time rate of change of the total angular momentum relative to the inertial reference and the moment is taken about the point A. This is true since the momentum of the engine rotor relative to point A as seen from XYZ is actually the momentum of the rotor relative to the coordinate system x, y, z having A as its origin and translated with respect to XYZ.

We shall now apply equation C2 and use vector components in the x, y, z coordinate system ( $\hat{i}, \hat{j}, \hat{k}$  are unit vectors in x, y, z or engine coordinate system). Since we have chosen the x-axis to correspond to the rotor centerline and this axis is an axis of symmetry then the moment of inertia about this axis vanishes ( $\int yz = 0$ ). Also since A was taken to be the engine center of mass  $\int xy = \int xz = 0$ . This implies the x, y, z axes are principal axes of the rotor and, therefore, we may write the angular momentum of the rotor in the x, y, z coordinate system using equation C1 as:

$$\begin{aligned} \bar{H}_A &= (H_A)_x \hat{i} + (H_A)_y \hat{j} + (H_A)_z \hat{k} \\ &= \int_{xx} \omega_x \hat{i} + \int_{yy} \omega_y \hat{j} + \int_{zz} \omega_z \hat{k} \end{aligned}$$

Since

$$\begin{aligned} \bar{\Omega} &= \Omega_x \hat{i} + \Omega_y \hat{j} + \Omega_z \hat{k} \\ &= (\cos \psi \cos \theta) \Omega \hat{i} + (-\sin \psi \cos \phi + \cos \psi \sin \theta \sin \phi) \Omega \hat{j} \\ &\quad + (\sin \psi \sin \phi + \cos \psi \sin \theta \cos \phi) \Omega \hat{k} \end{aligned}$$

then

$$\begin{aligned} \bar{\omega} &= \bar{\Omega} + \bar{\omega}_{\text{rotor}} \\ &= (\cos \psi \cos \theta) \Omega \hat{i} + (-\sin \psi \cos \phi + \cos \psi \sin \theta \sin \phi) \Omega \hat{j} \\ &\quad + (\sin \psi \sin \phi + \cos \psi \sin \theta \cos \phi) \Omega \hat{k} + \omega_{\text{rotor}} \hat{i} \end{aligned}$$

or

$$\omega_x = \omega_{\text{rotor}} + (\cos \psi \cos \theta) \Omega$$

$$\omega_y = (-\sin \psi \cos \phi + \cos \psi \sin \theta \sin \phi) \Omega$$

$$\omega_z = (\sin \psi \sin \phi + \cos \psi \sin \theta \cos \phi) \Omega$$

Equation C2 can be expanded to:

$$\begin{aligned} \bar{M}_A = & (\dot{H}_A)_x \hat{i} + (\dot{H}_A)_y \hat{j} + (\dot{H}_A)_z \hat{k} + (H_A)_x \left( \frac{d\hat{i}}{dt} \right)_{xyz} + (H_A)_y \left( \frac{d\hat{j}}{dt} \right)_{xyz} \\ & + (H_A)_z \left( \frac{d\hat{k}}{dt} \right)_{xyz} + \bar{\Omega} \times [(H_A)_x \hat{i} + (H_A)_y \hat{j} + (H_A)_z \hat{k}] \end{aligned}$$

Noting that  $\hat{i}, \hat{j}, \hat{k}$  are unit vectors fixed in the x, y, z coordinate system and, therefore, independent of time:

$$\left( \frac{d\hat{i}}{dt} \right)_{xyz} = \left( \frac{d\hat{j}}{dt} \right)_{xyz} = \left( \frac{d\hat{k}}{dt} \right)_{xyz} = 0$$

Equation C2 now reduces to:

$$\bar{M}_A = (\dot{H}_A)_x \hat{i} + (\dot{H}_A)_y \hat{j} + (\dot{H}_A)_z \hat{k} + \bar{\Omega} \times [(H_A)_x \hat{i} + (H_A)_y \hat{j} + (H_A)_z \hat{k}]$$

Where

$$\begin{aligned} \bar{\Omega} \times \bar{H}_A &= \begin{vmatrix} \hat{i} & \hat{j} & \hat{k} \\ \Omega_x & \Omega_y & \Omega_z \\ (H_A)_x & (H_A)_y & (H_A)_z \end{vmatrix} \\ &= [\Omega_y(H_A)_z - \Omega_z(H_A)_y] \hat{i} - [\Omega_x(H_A)_z - \Omega_z(H_A)_x] \hat{j} \\ &\quad + [\Omega_x(H_A)_y - \Omega_y(H_A)_x] \hat{k} \end{aligned}$$

$$(\dot{H}_A)_x = \mathcal{I}_{xx} \dot{\omega}_x = \mathcal{I}_{xx} \frac{d}{dt} [\mathcal{I}_{\text{rotor}} + \cos \psi \cos \theta \Omega]$$

$$(\dot{H}_A)_y = \mathcal{I}_{yy} \dot{\omega}_y = \mathcal{I}_{yy} \frac{d}{dt} [(-\sin \psi \cos \phi + \cos \psi \sin \theta \sin \phi) \Omega]$$

$$(\dot{H}_A)_z = \mathcal{I}_{zz} \dot{\omega}_z = \mathcal{I}_{zz} \frac{d}{dt} [(\sin \psi \sin \phi + \cos \psi \sin \theta \cos \phi) \Omega]$$

The engine positioning with respect to the gimbal does not change in time so that  $\psi = \theta = \phi = 0$

$$\begin{aligned}\dot{(H_A)}_x &= J_{xx} [\dot{\omega}_{\text{rotor}} + (\cos \psi \cos \theta) \Omega] \\ \dot{(H_A)}_y &= J_{yy} [(-\sin \psi \cos \phi + \cos \psi \sin \theta \sin \phi) \Omega] \\ \dot{(H_A)}_z &= J_{zz} [(\sin \psi \sin \phi + \cos \psi \sin \theta \cos \phi) \Omega]\end{aligned}$$

If the engine rotor and centrifuge are running at steady state conditions (zero angular accelerations) then  $\dot{\omega}_{\text{rotor}} = \Omega = 0$

$$\therefore \dot{(H_A)}_x = \dot{(H_A)}_y = \dot{(H_A)}_z = 0$$

With this equation C2 becomes:

$$\begin{aligned}\bar{M}_A = \bar{\Omega} \times \bar{H}_A &= [\Omega_y (H_A)_z - \Omega_z (H_A)_y] \hat{i} + [\Omega_z (H_A)_x - \Omega_x (H_A)_z] \hat{j} \\ &\quad + [\Omega_x (H_A)_y - \Omega_y (H_A)_x] \hat{k}\end{aligned}$$

The three components of the gyroscopic moment acting at the engine center of mass now simply become:

$$\begin{aligned}M_x &= \Omega_y (H_A)_z - \Omega_z (H_A)_y \\ M_y &= \Omega_z (H_A)_x - \Omega_x (H_A)_z \\ M_z &= \Omega_x (H_A)_y - \Omega_y (H_A)_x\end{aligned}\tag{C3}$$

Where the components of the centrifuge angular rate vector are:

$$\begin{aligned}\Omega_x &= (\cos \psi \cos \theta) \Omega \\ \Omega_y &= (-\sin \psi \cos \phi + \cos \psi \sin \theta \sin \phi) \Omega \\ \Omega_z &= (\sin \psi \sin \phi + \cos \psi \sin \theta \cos \phi) \Omega\end{aligned}$$

$\psi$ ,  $\phi$  and  $\theta$  being the angles defining the engine orientation with respect to the centrifuge arm. The components of the rotor angular momentum vector are:

$$\begin{aligned}(H_A)_x &= J_{xx} \omega_x = J_{xx} [\omega_{\text{rotor}} + (\cos \psi \cos \theta) \Omega] \\ (H_A)_y &= J_{yy} \omega_y = J_{yy} [(-\sin \psi \cos \phi + \cos \psi \sin \theta \sin \phi) \Omega] \\ (H_A)_z &= J_{zz} \omega_z = J_{zz} [(\sin \psi \sin \phi + \cos \psi \sin \theta \cos \phi) \Omega]\end{aligned}$$

Since the x, y and z axes of the rotor are principal axes and x-axis is an axis of symmetry then:

$$J_{xx} = J_{yy} + J_{zz}$$

$$J_{yy} = J_{zz} = J'$$

or

$$J' = \frac{1}{2} J_{xx}$$

The components of the rotor angular momentum become:

$$(H_A)_x = J_{xx} [\omega_{\text{rotor}} + (\cos \psi \cos \theta) \Omega]$$

$$(H_A)_y = \frac{1}{2} J_{xx} [(-\sin \psi \cos \phi + \cos \psi \sin \theta \sin \phi) \Omega]$$

$$(H_A)_z = \frac{1}{2} J_{xx} [(\sin \psi \sin \phi + \cos \psi \sin \theta \cos \phi) \Omega]$$

Where  $J_{xx}$  is now a gyroscopic moment of inertia about the rotor axis.

The expressions for the gyroscopic moment components can be further simplified by noting that  $\omega_{\text{rotor}}$  for an engine at power is at least 2 orders of magnitude greater than the centrifuge angular rate  $\Omega$ . With this in mind:

$$(H_A)_x \cong J_{xx} \omega_{\text{rotor}}$$

and  $(H_A)_y$  and  $(H_A)_z$  are small relative to  $(H_A)_x$

With these assumptions, equations C3, the gyroscopic moment components exerted by the rotor on its supports becomes:

$$M_x \rightarrow \text{some small value}$$

$$M_y \cong \Omega_z (H_A)_x = \Omega_z J_{\text{polar}} \omega_{\text{rotor}}$$

$$M_z \cong -\Omega_y (H_A)_x = -\Omega_y J_{\text{polar}} \omega_{\text{rotor}}$$

The moment components acting on the rotor have the opposite sign.

In reality a gas turbine engine rotor is not a single cylindrical rotor. It can be a dual or triple rotor system, with a variable gyroscopic moment of inertia as you traverse the engine axially. At Pratt & Whitney once the moment distribution in the rotors is determined a beam deflection program with variable spring rates is used to determine the relative rotor – case deflections. These in turn are dependent on the number of bearings and whether the shaft is overhung or not. Tables C-I and C-II list the rotor-case deflections due to unit g-loadings and rotation rates about the horizontal and vertical engine axes as determined by this program. We add the components of these displacements vectorially and determine the location of the net displacement and where it lies relative to the engine circumference.



**TABLE C-1**  
**HIGH BY-PASS RATIO TURBOFAN STATIC DEFLECTIONS WITH**  
**NACELLE INSTALLED**

$N_1 = 3780 \text{ rpm}$   
 $N_2 = 8096 \text{ rpm}$

	DEFLECTION FOR 1 RAD/ SEC. HORIZONTAL ROTATION	DEFLECTION FOR 1G HORIZONTAL LOAD	DEFLECTION FOR 1 RAD/ SEC. VERTICAL ROTATION	DEFLECTION FOR 1G VERTICAL LOAD
	$K_{1H} \text{ (cm)}$	$K_{2H} \text{ (cm)}$	$K_{1V} \text{ (cm)}$	$K_{2V} \text{ (cm)}$
Fan	0.8412	0.0041	0.8412	0.0041
LPC-1-1/2	0.2304	0.0086	0.2304	0.0086
LPC-2	0.1537	0.0086	0.1537	0.0086
LPC-3	0.0998	0.0086	0.0998	0.0086
LPC-4	-0.0353	0.0089	-0.0353	0.0089
HPC-5	0.0244	0.0005	0.0244	0.0005
HPC-6	0.0203	0.0020	0.0203	0.0020
HPC-7	0.0165	0.0028	0.0165	0.0028
HPC-8	0.0160	0.0030	0.0160	0.0030
HPC-9	0.0152	0.0036	0.0152	0.0036
HPC-10	0.0124	0.0038	0.0124	0.0038
HPC-11	0.0114	0.0041	0.0114	0.0041
HPC-12	0.0099	0.0043	0.0099	0.0043
HPC-13	0.0058	0.0048	0.0058	0.0048
HPC-14	0.0028	0.0051	0.0028	0.0051
HPC-15	-0.0005	0.0053	-0.0005	0.0053
HPT-1	-0.0851	0.0142	-0.0851	0.0142
HPT-2	-0.1113	0.0165	-0.1113	0.0165
LPT-3	-0.1245	0.0038	-0.1245	0.0038
LPT-4	-0.0998	0.0041	-0.0998	0.0041
LPT-5	-0.0757	0.0041	-0.0757	0.0041
LPT-6	-0.0488	0.0041	-0.0488	0.0041

**TABLE C-II**  
**LIGHTWEIGHT FIGHTER ENGINE STATIC DEFLECTIONS**

$N_1 = 10,500$  rpm

$N_2 = 13,600$  rpm

	DEFLECTION FOR 1 RAD/ SEC. HORIZONTAL ROTATION	DEFLECTION FOR 1G HORIZONTAL LOAD	DEFLECTION FOR 1 RAD/ SEC. VERTICAL ROTATION	DEFLECTION FOR 1G VERTICAL LOAD
	$K_{1H}$ (cm)	$K_{2H}$ (cm)	$K_{1V}$ (cm)	$K_{2V}$ (cm)
1st Fan Stage	0.10325	0.00074	0.10305	0.00084
2nd Fan Stage	0.05725	0.00081	0.05712	0.00086
3rd Fan Stage	0.02101	0.00104	0.02096	0.00107
Comp. Stage 6	0.00975	0.00290	0.01069	0.00277
Comp. Stage 7	0.00775	0.00295	0.00871	0.00282
Comp. Stage 8	0.00475	0.00302	0.00574	0.00287
Comp. Stage 9	0.00297	0.00300	0.00396	0.00287
Comp. Stage 10	0.00147	0.00297	0.00246	0.00282
Comp. Stage 11	-0.00069	0.00305	0.00030	0.00290
Comp. Stage 12	-0.00279	0.00307	-0.00175	0.00292
Comp. Stage 13	-0.00472	0.00310	-0.00366	0.00295
HPT-1	-0.04074	0.00587	-0.03975	0.00582
HPT-2	-0.05578	0.00711	-0.05486	0.00709
LPT-3	-0.10658	0.01473	-0.10605	0.01458
LPT-4	-0.12426	0.01654	-0.12372	0.01638

The rotor deflection vector due to the gyroscopic moments can be represented by:

$$\bar{D}_g = K_{1H} \Omega_y \hat{j} + K_{1V} \Omega_z \hat{k} \quad (C4)$$

Where  $K_{1H}$  is the deflection created by a 1 rad/sec. rotation in the horizontal engine plane and  $K_{1V}$  is a similar deflection due to a loading in the vertical plane.

The linear accelerations in engine components were determined in Appendix B of the original TELS Study (Reference 3). They are as follows:

$$\begin{aligned} \ddot{x} &= \sin \theta / \bar{a} / \\ \ddot{y} &= -\cos \theta \sin \phi / \bar{a} / \\ \ddot{z} &= -\cos \theta \cos \phi / \bar{a} / \end{aligned}$$

Where  $\bar{a}/$  is the magnitude of the centripetal acceleration.

The rotor deflections due to the linear accelerations acting on the engine are then:

$$\bar{D}_a = -(K_{2H} \ddot{y} \hat{j} + K_{2V} \ddot{z} \hat{k})$$

Where  $K_{2H}$  is the deflection due to 1 G loading in the horizontal plane and  $K_{2V}$  is a similar deflection due to a 1 G load in the vertical plane.

$$\begin{aligned} \therefore \bar{D}_{total} &= (K_{1H} \Omega_y - K_{2H} \ddot{y}) \hat{j} + (K_{1V} \Omega_z - K_{2V} \ddot{z}) \hat{k} \\ &\quad \Omega_y, \Omega_z \text{ in rad/sec} \\ &\quad \ddot{y}, \ddot{z} \text{ in g's} \end{aligned} \quad (C5)$$

or

$$\begin{aligned} D_y &= K_{1H} \Omega_y - K_{2H} \ddot{y} \\ D_z &= K_{1V} \Omega_z - K_{2V} \ddot{z} \end{aligned}$$

The location of the displacement vector  $\bar{D}$  in the y z plane locates the pinch point we wish to radiograph. The pinch point has been located using this method for a light weight fighter engine and a high by-pass ratio turbofan engine. Sample centrifuge flight points are illustrated in Figures C-2 and C-3. These figures are a two dimensional representation of a three dimensional engine positioner. The circles in the figure represent the engine cross section at various axial positions along the engine as viewed from the rear. The cross hatched line next to each circle represents the position of the turret base relative to a line normal to the axis of the engine passing through the top ( $0^\circ$ ) and bottom ( $180^\circ$ ) of the engine after the pitch

roll, and yaw angles are set on the hinge-gimbal positioner. The location of the rotor-case, pinch points was obtained by considering the vector summation of the relative rotor to case displacements due to the horizontal and vertical applied loads.  $0^\circ$  corresponds to the top of the engine and  $180^\circ$  corresponds to the bottom of the engine when installed in a static test cell and viewed from the rear. Locations of the rotor case pinch points are illustrated in Figures C-4 through C-19.

Table C-III represents the test conditions achieved and contains any corrections made to the information presented in Figure 1 on Page 39 of Report AEDC-TR-75-137 "Turbine Engine Loads Simulator Exhaust Deflection and Thrust Negation Study".

## CONDITIONS ACHIEVED

$$\begin{aligned}\Omega &= 2.88 \text{ RAD/SEC} \\ \theta &= 11.2^\circ \\ \phi &= -8.5^\circ \\ \psi &= 52.0^\circ \\ |\dot{a}| &= 10.3 \text{ g's}\end{aligned}$$

$$\begin{aligned}\ddot{x} &= 2.0 \text{ g's} \\ \ddot{y} &= 1.493 \text{ g's} \\ \ddot{z} &= -9.993 \text{ g's} \\ |\ddot{a}| &= 10.3 \text{ g's}\end{aligned}$$

$$\begin{aligned}w_x &= -1.739 \text{ RAD/SEC} \\ w_y &= 2.295 \text{ RAD/SEC} \\ w_z &= -0.005 \text{ RAD/SEC}\end{aligned}$$

ENGINE VIEWED FROM REAR

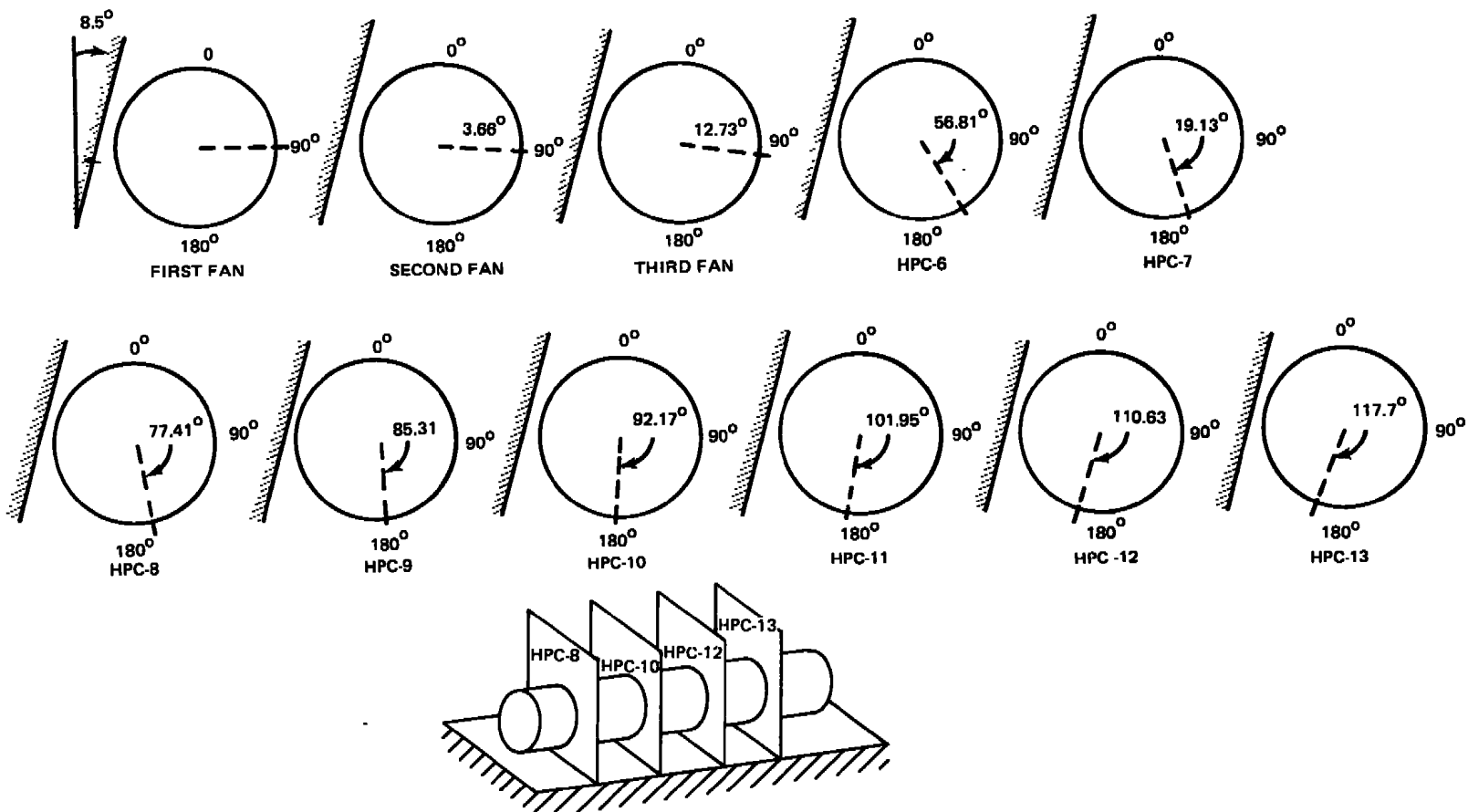


Figure C-2 Lightweight Fighter Turbofan Engine Rotor-Case Pinch Point Locations, Case F1

## STEADY STATE TRANSPORT DESIGN (FAR)

TEST CASE NO F7

CONDITION ACHIEVED

$\Omega$  = 1.75 RAD/SEC  
 $\theta$  = 0°  
 $\phi$  = 0°  
 $\psi$  = 8.2°  
 $|\dot{\theta}|$  = 3.8 g's

$x$  = 0.0  
 $y$  = 0.0  
 $z$  = -3.8 g's  
 $|\dot{\theta}|$  = 3.8 g's

$w_x$  = -1.732 RAD/SEC  
 $w_y$  = 0.2496 RAD/SEC  
 $w_z$  = 0.0

ENGINE VIEWED FROM REAR

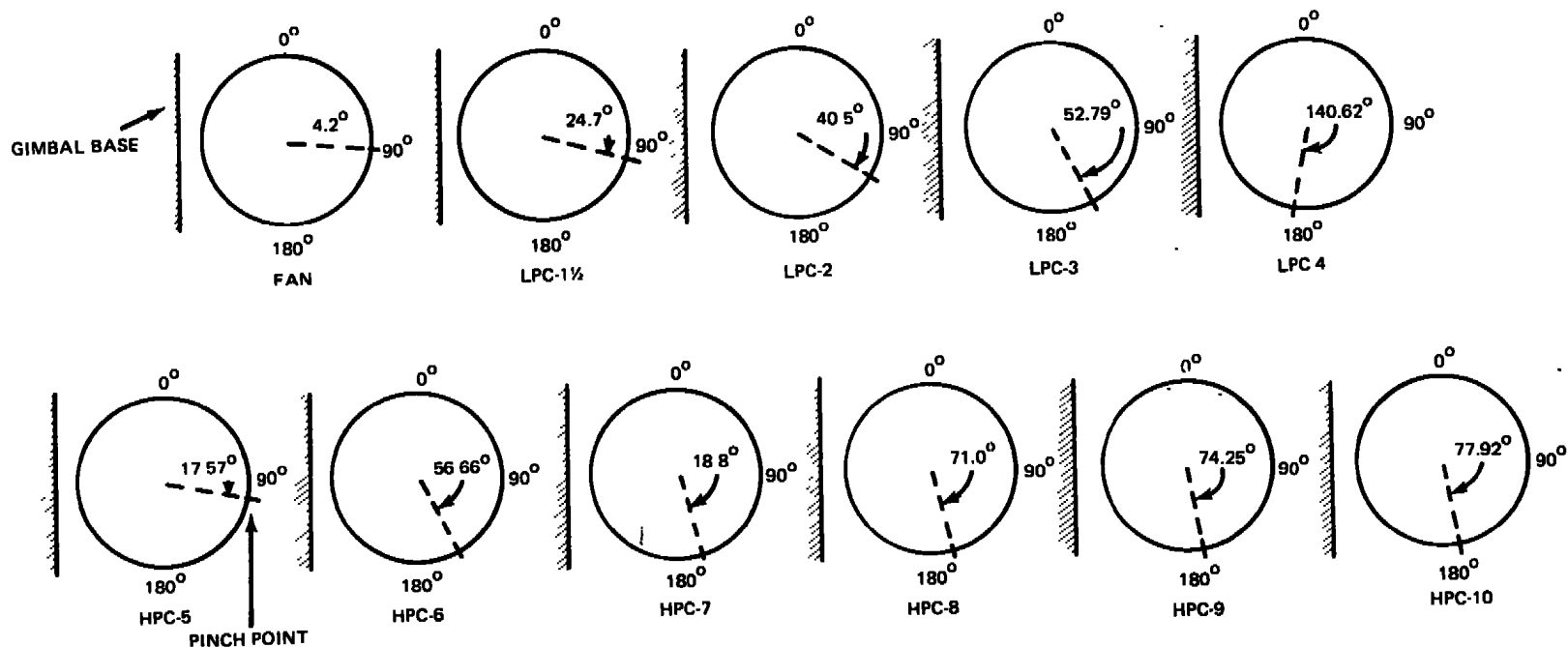


Figure C-3 High Bypass Ratio Turbofan Engine Rotor-Case Pinch Point Locations, Case F7

**TABLE C-III  
TEST REQUIREMENTS**

TEST CASE #	DESCRIPTION	LINEAR ACCELERATION G'S				ANGULAR RATE RAD/SEC			
		$\ddot{x}$	$\ddot{y}$	$\ddot{z}$	$/\ddot{a}/$	$w_x$	$\bar{w}_y$	$\bar{w}_z$	$/\bar{w}/$
F1	Flight Design (Pull up)	+ 2	$\pm 1.5$	-10	10.3	N. S.	+2.3	(2)	N. S.
F2	Flight Design (Nose-down)	+ 3	$\pm 4$	+ 7	8.6	N. S.	-2.3	(2)	N. S.
F3	Steady State Flight	0	0	- 6	6.0	N. S.	+0.6	(6)	N. S.
F4	High Pitch Rate	0	0	- 6	6.0	N. S.	+3.5	(3)	N. S.
F5	High Stall Departure	0	0	0	0.0	N. S.	3	-3.5	N. S.
F6	Future Steady State Flight	0	0	-10	10.0	N. S.	1.0	(4)	N. S.
F7	Transport Design (FAR)	0	0	- 3.8	3.8	N. S.	0.25	(5)	N. S.
F8	Transient Future Flight	0	0	-15	15.0	N. S.	1.0	(4)	N. S.
F9	High Stall Departure	0	-4	0	4.0	N. S.	(7)	-2.0	N. S.
L1	Arrested Landing Runout	- 10	$\pm 2$	+ 3	10.6	N. S.	(3)	(3)	N. S.
L2	Arrested Landing Impact	$\pm 2$	$\pm 2$	-10	10.4	N. S.	(3)	(3)	N. S.
C1	Transient Catapult	+ 9	$\pm 2$	- 5.5	10.7	N. S.	(3)	(3)	N. S.

- (2)  $/\bar{w}_y + \bar{w}_z/ \leq 2.7$  rad/sec.  
 (3)  $/\bar{w}_y + \bar{w}_z/ \leq 3.5$  rad/sec.  
 (4)  $/\bar{w}_y + \bar{w}_z/ \leq 1.2$  rad/sec.  
 (5)  $/\bar{w}_y + \bar{w}_z/ \leq 0.3$  rad/sec.  
 (6)  $/\bar{w}_y + \bar{w}_z/ \leq 0.7$  rad/sec.  
 (7)  $/\bar{w}_y + \bar{w}_z/ \leq 2.2$  rad/sec.

TABLE C-III (Cont'd)  
TELS OPERATING PARAMETERS

TEST CASE #	CENTRIFUGE SPEED	PITCH ANGLE	ROLL ANGLE	YAW ANGLE	LINEAR ACCELERATION G'S				ANGULAR RATE RAD/SEC.		
	$\Omega(\text{rad/sec})$	$\theta^\circ$	$\phi$	$\psi^\circ$	$\ddot{x}$	$\ddot{y}$	$\ddot{z}$	$ \ddot{a} $	$w_x$	$w_y$	$w_z$
F1	-2.88	11.2	$\mp 8.5$	52.0	+2.0	$\pm 1.493$	- 9.993	10.3	-1.739	+2.295 +2.194	-0.005 -0.676
F2	+ 2.63	159.6	$\mp 29.75$	59.0	+2.998	$\mp 4.0$	+ 6.998	8.6	-1.27	-2.192 -1.723	-0.709 + 1.529
F3	-2.2	0.0	0.0	15.8	0.0	0.0	- 6.0	6.0	-2.117	+ 0.599	0.0
F4	-3.5	0.0	0.0	90.0	0.0	0.0	- 6.0	6.0	0.0	+3.5	0.0
F5	-3.5	0.0	90.0	90.0	0.0	0.0	0.0	0.0	0.0	0.0	-3.5
F6	-2.84	0.0	0.0	20.6	0.0	0.0	-10.0	10.0	-2.658	0.999	0.0
F7	-1.75	0.0	0.0	8.2	0.0	0.0	- 3.8	3.8	-1.732	0.249	0.0
F8	-3.47	0.0	0.0	16.7	0.0	0.0	-15.0	15.0	-3.324	0.997	0.0
F9	-2.07	0.0	90.0	75.0	0.0	-4.0	0.0	4.0	-0.536	0.0	-1.999
L1	+ 3.37	-109.4	$\mp 34.6$	90.0	-9.998	$\mp 1.999$	+ 2.898	10.6	0.0	-2.774 $\mp 1.914$	
L2	-3.34	$\pm 11.1$	$\mp 11.3$	90.0	$\pm 2.002$	$\pm 2.0$	-10.008	10.4	0.0	3.275 $\pm 0.654$	
C1	-3.39	57.2	$\mp 20.2$	90.0	+8.994	$\pm 2.001$	5.44	10.7	0.0	3.181 $\pm 1.17$	



Test Case No F1

Flight Design (Pull Up)

Ref MIL E 5007D

$\dot{\omega} = -2.88 \text{ rad/sec}$

$\theta = 11.2^\circ$

$\phi = +8.5^\circ$

$\psi = 52.0^\circ$

$|\ddot{a}| = 10.3 \text{ g's}$

Conditions Achieved:  $\ddot{x} = 2.0 \text{ g's}$

$\ddot{y} = -1.493 \text{ g's}$

$\ddot{z} = -9.913 \text{ g's}$

$|\ddot{a}| = 10.3 \text{ g's}$

$\omega_x = -1.739 \text{ rad/sec}$

$\omega_y = 2.194 \text{ rad/sec}$

$\omega_z = -0.676 \text{ rad/sec}$

$\dot{\omega}$

Engine viewed from rear

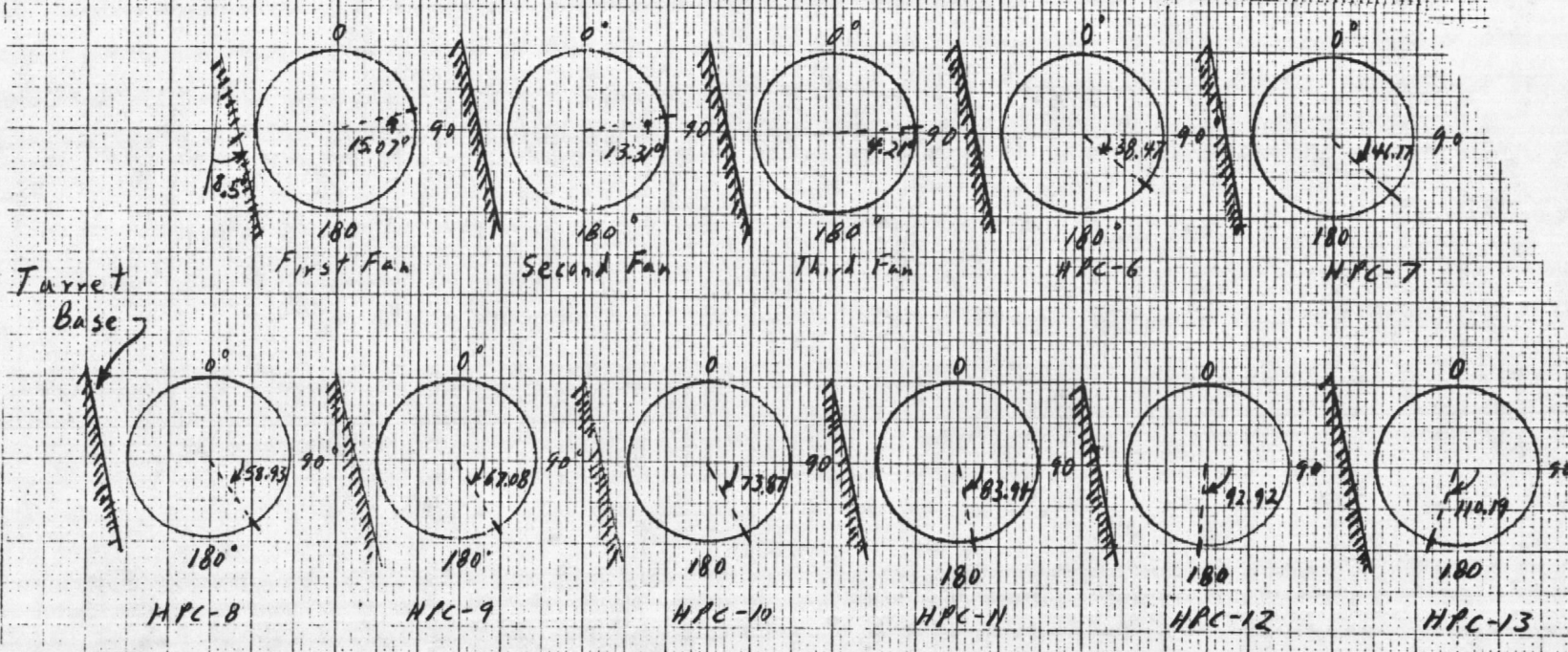


Figure C-4 Lightweight Fighter Turbofan Engine Rotor-Case Pinch Point Locations, Case F1

Test Case No F1 Flight Design (Pull-Up) Ref: MIL E5007D

$$\dot{\alpha} = -2.88 \text{ rad/sec}$$

$$\theta = 11.2^\circ$$

$$\phi = +8.5^\circ$$

$$\psi = 52.0^\circ$$

$$|\dot{\alpha}| = 10.3 \text{ g's}$$

Conditions Achieved:

$$\ddot{x} = 2.0 \text{ g's}$$

$$\ddot{y} = -1.493 \text{ g's}$$

$$\ddot{z} = -9.993 \text{ g's}$$

$$|\ddot{\alpha}| = 10.3 \text{ g's}$$

$$\omega_x = -1.739 \text{ rad/sec}$$

$$\omega_y = 2.194 \text{ rad/sec}$$

$$\omega_z = -0.676 \text{ rad/sec}$$

Engine viewed from rear

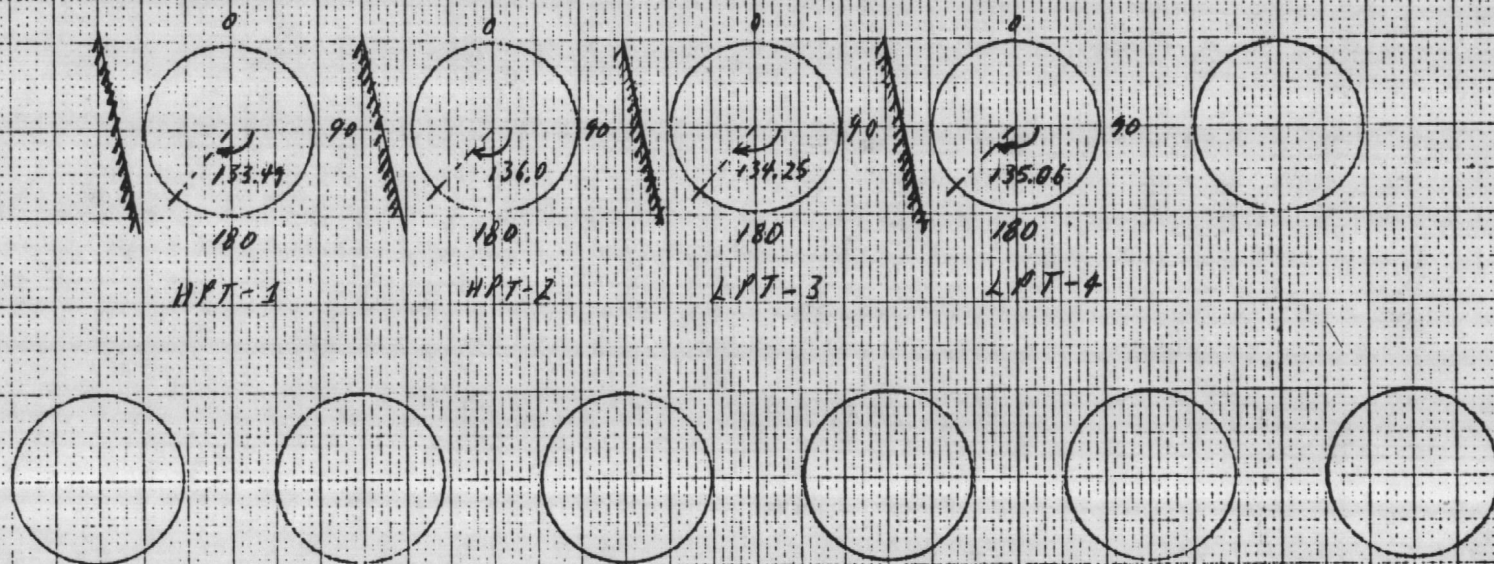


Figure C-4 (Cont'd) Lightweight Fighter Turbofan Engine Rotor-Case Pitch Point Locations, Case F1



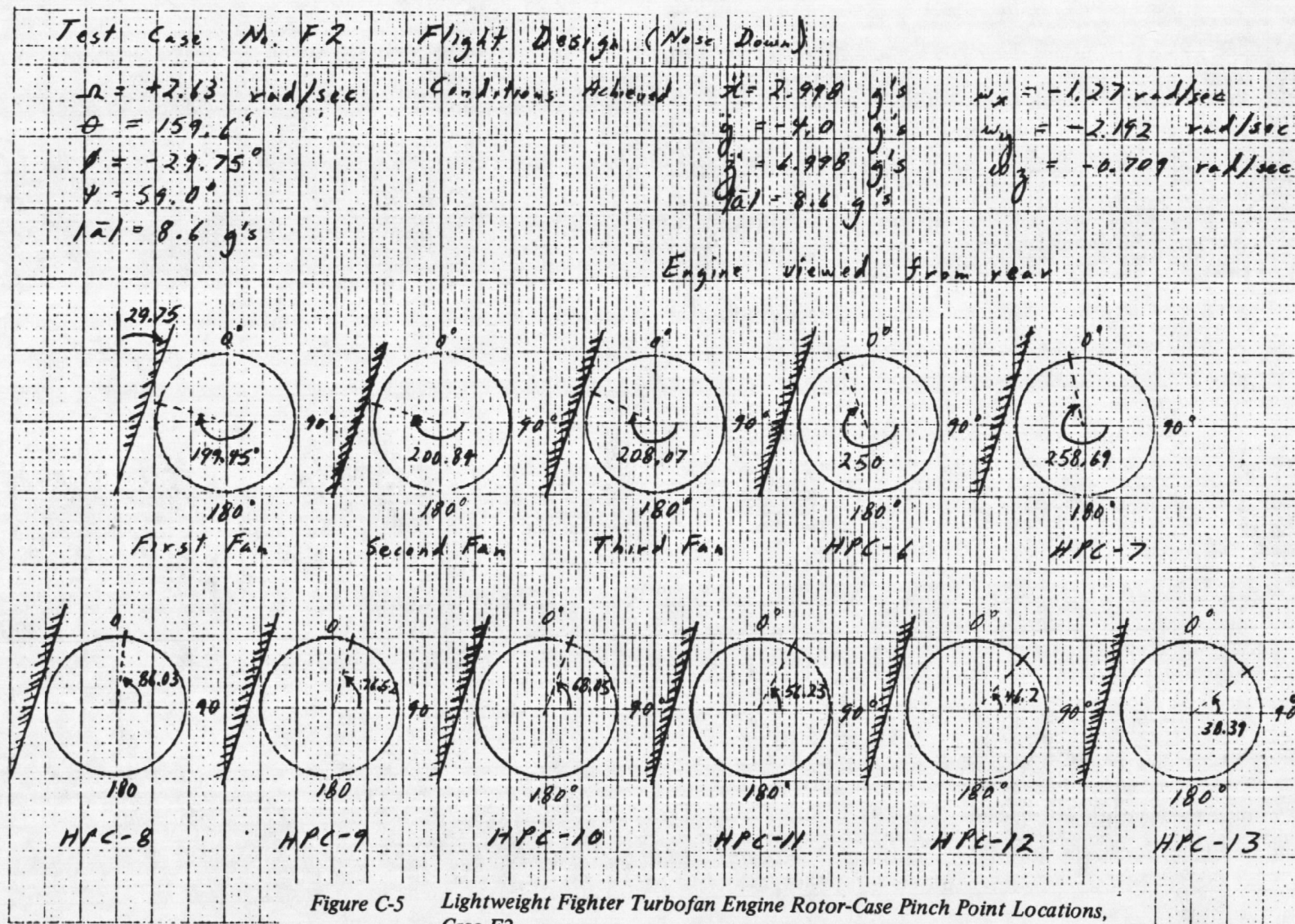


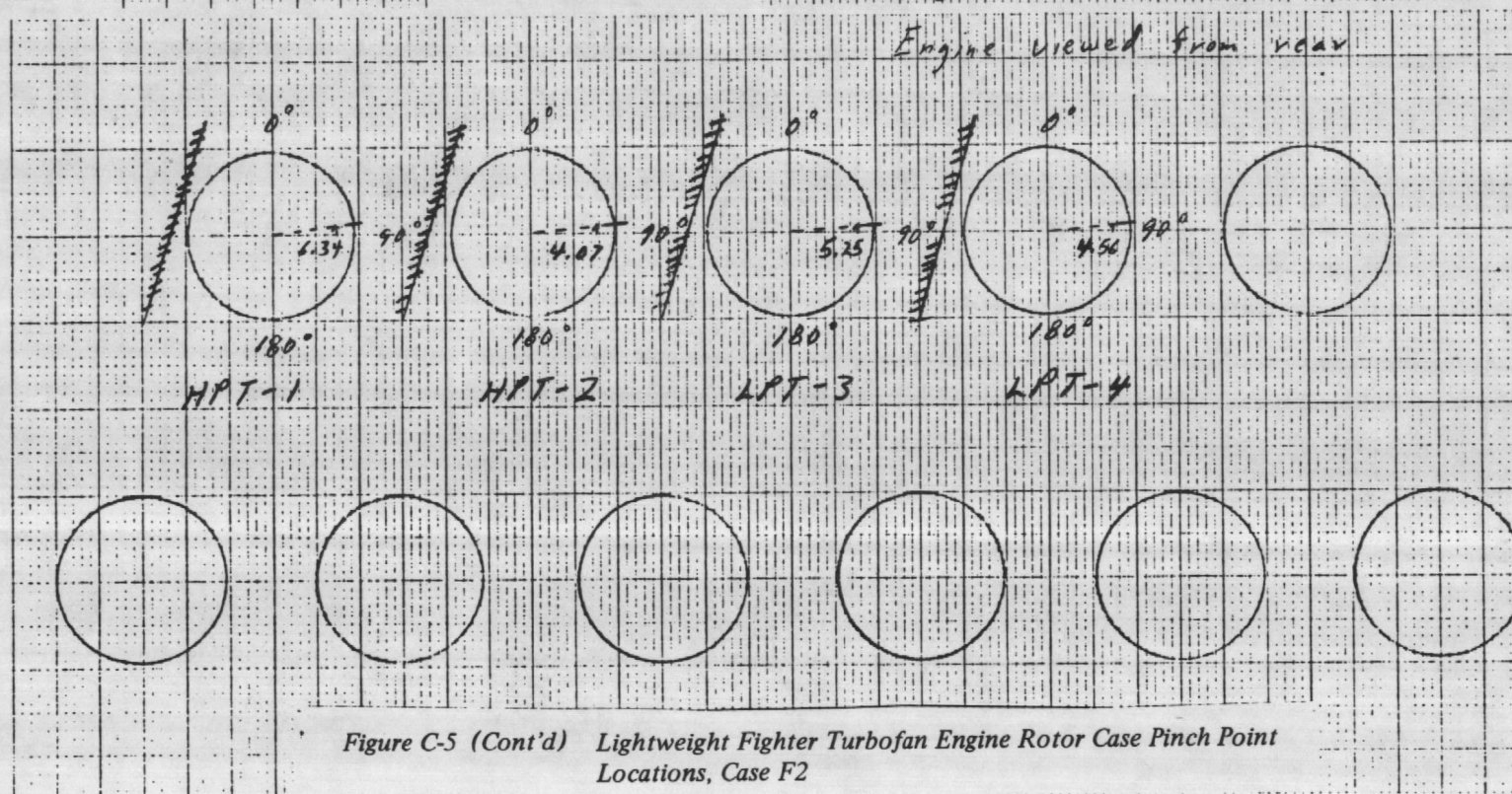
Figure C-5 Lightweight Fighter Turbofan Engine Rotor-Case Pinch Point Locations, Case F2

# Test Case No. F2 Flight Design (Nose Down)

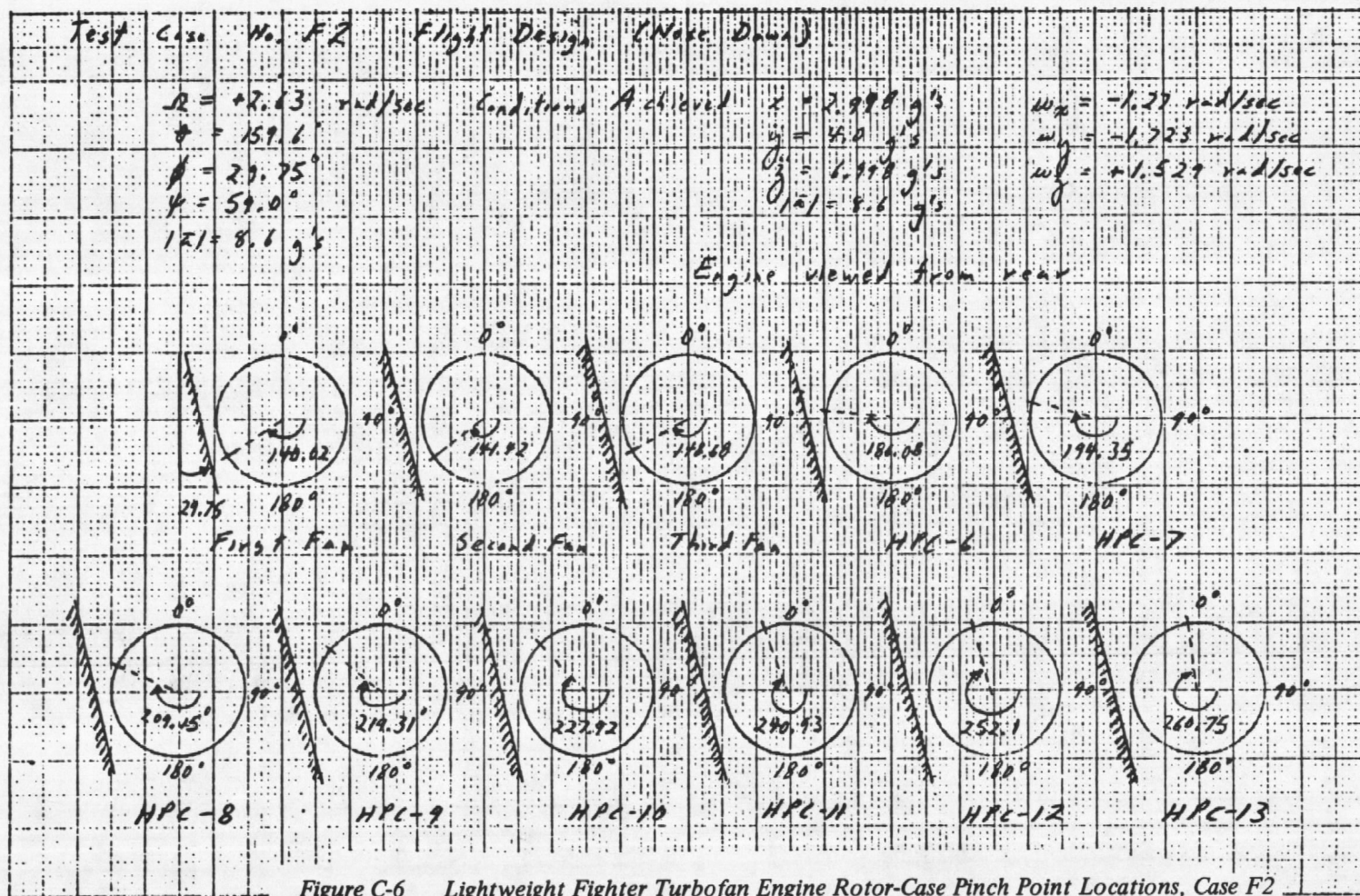
$\Omega = +2.63 \text{ rad/sec}$   
 $\theta = 159.1^\circ$   
 $\phi = -29.75^\circ$   
 $\psi = 59.0^\circ$

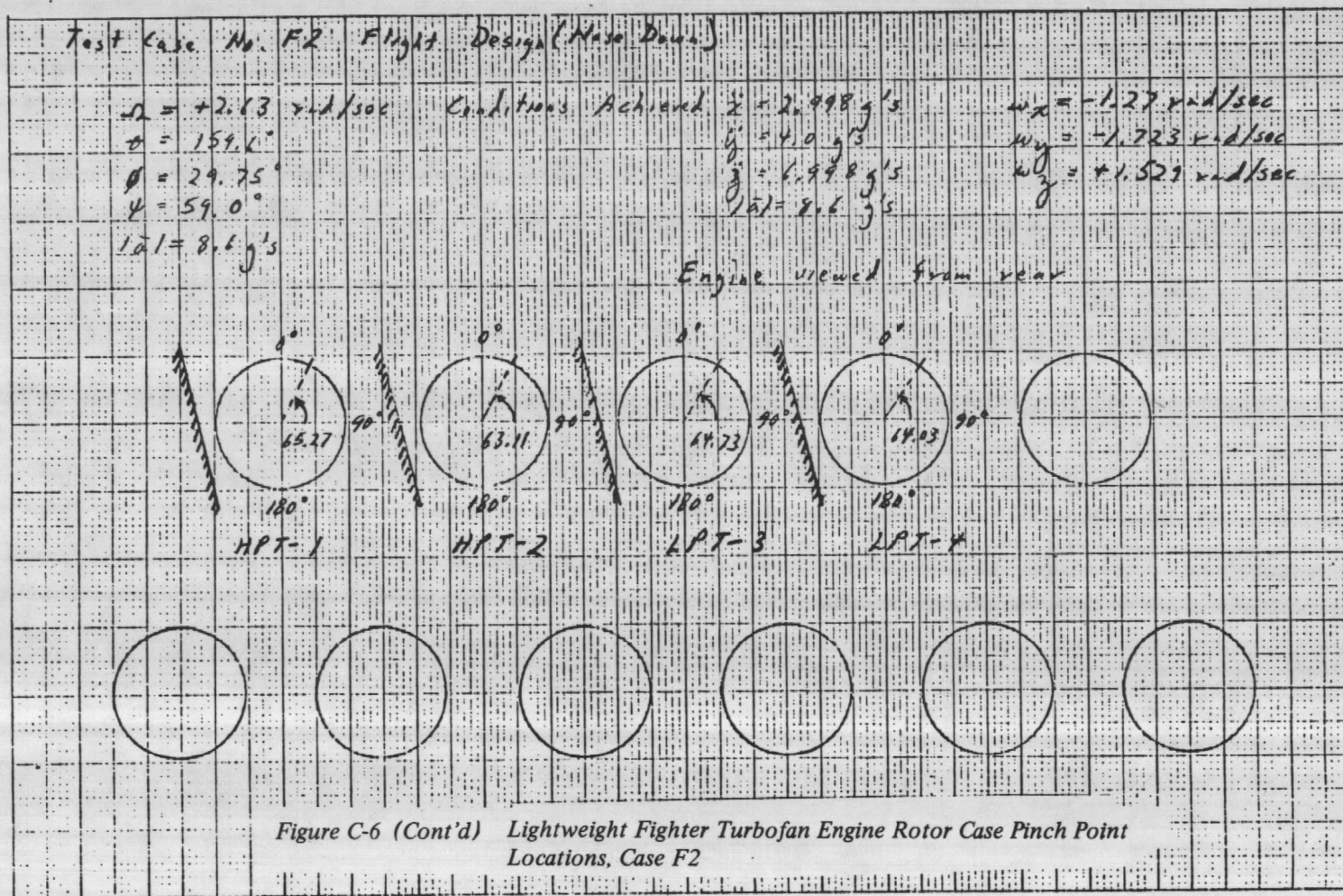
## Conditions Achieved

$\ddot{x} = 2.998 \text{ g's}$   
 $\ddot{y} = -4.0 \text{ g's}$   
 $\ddot{z} = 6.998 \text{ g's}$   
 $\dot{\alpha} = 8.6 \text{ g's}$   
 $\omega_x = -1.27 \text{ rad/sec}$   
 $\omega_y = -2.192 \text{ rad/sec}$   
 $\omega_z = -0.707 \text{ rad/sec}$

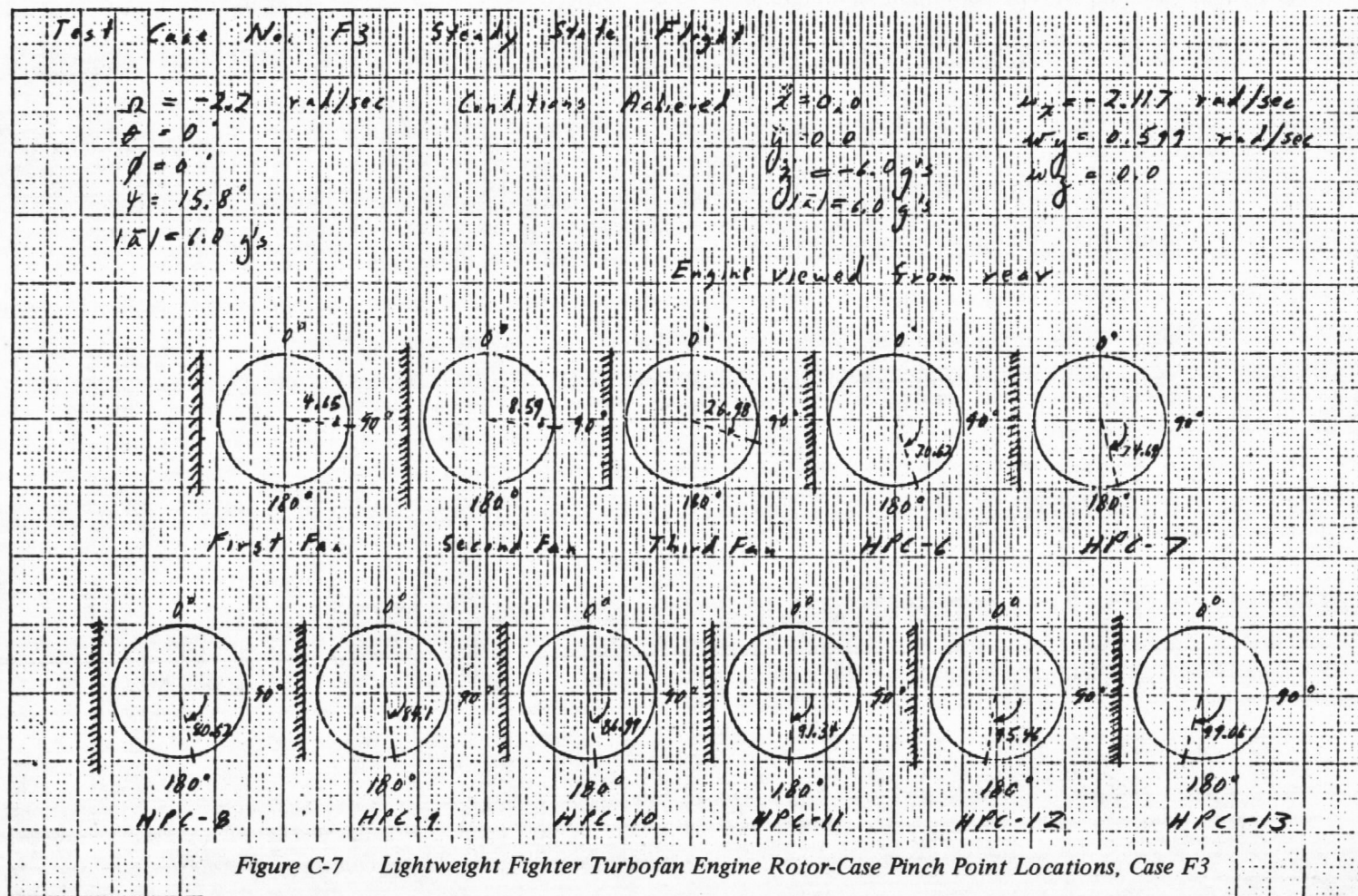


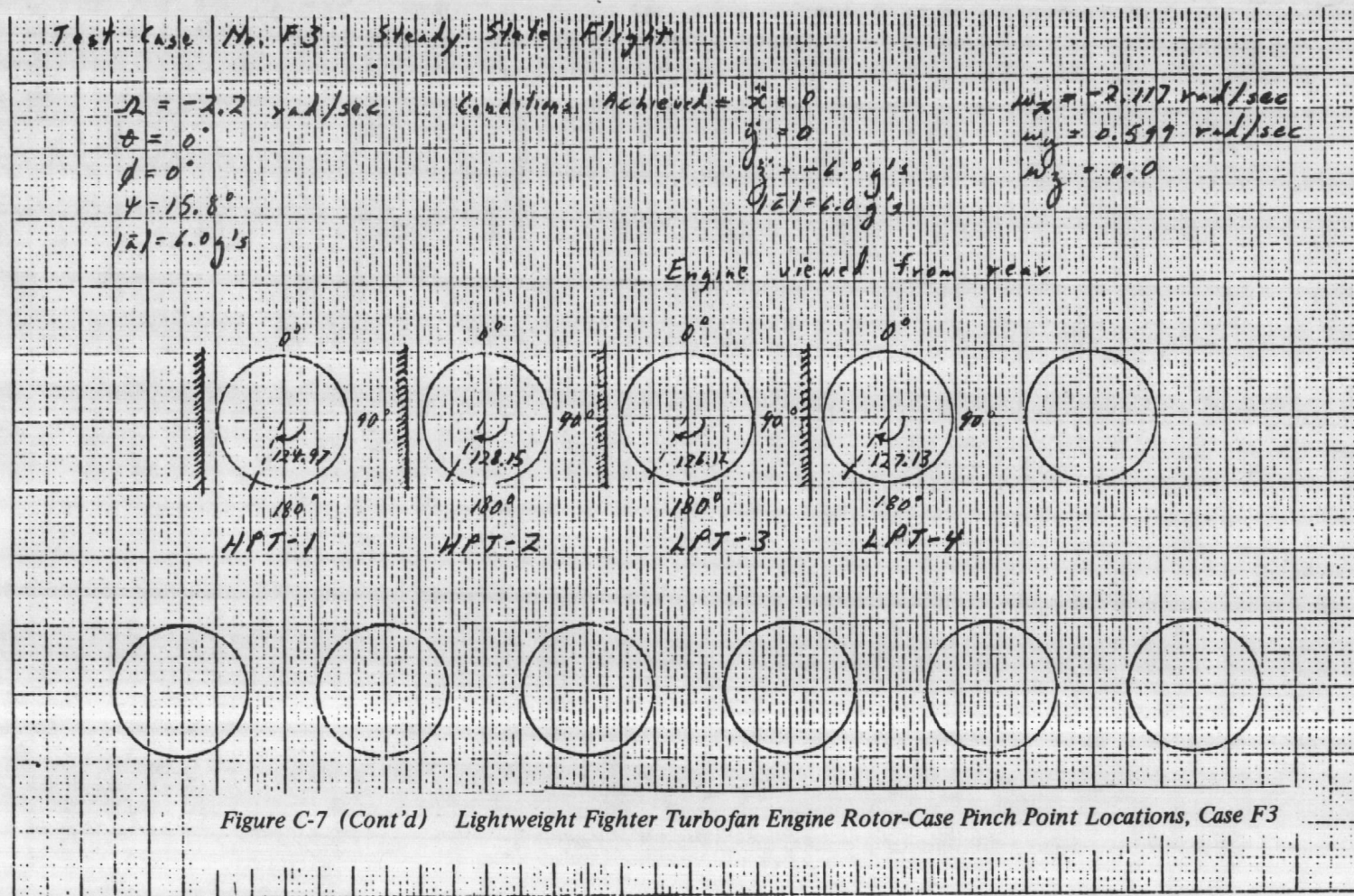














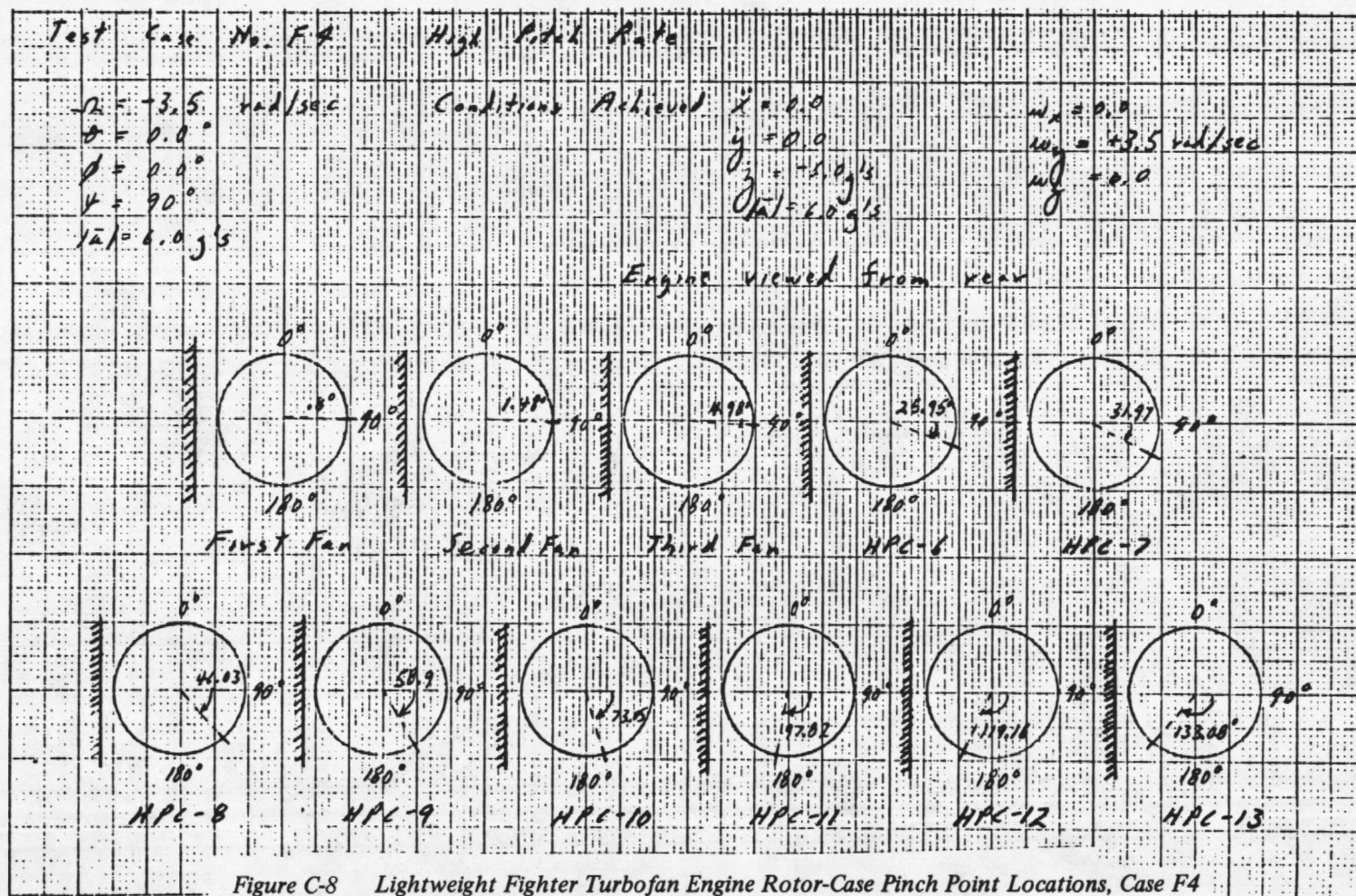
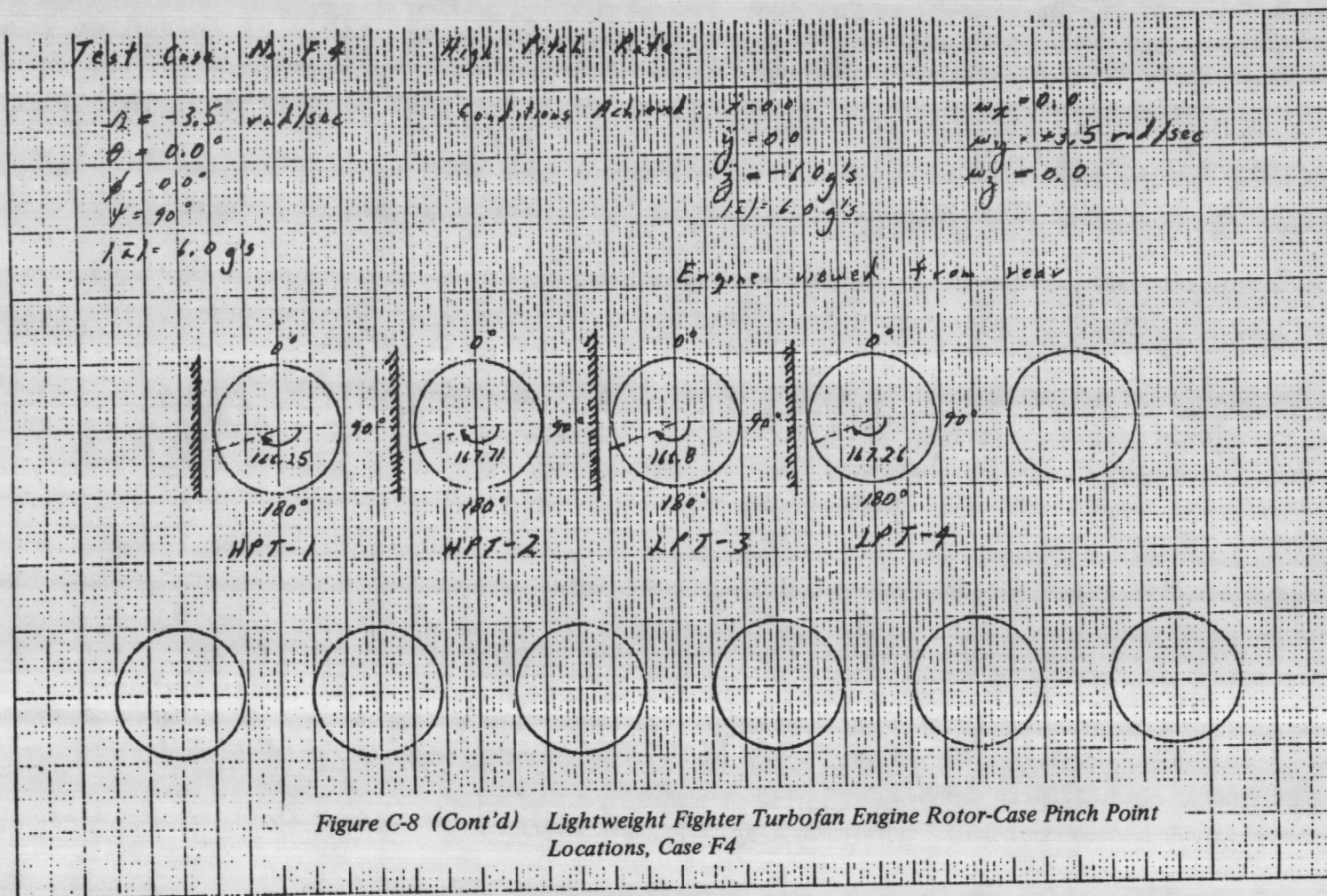


Figure C-8 Lightweight Fighter Turbofan Engine Rotor-Case Pinch Point Locations, Case F4





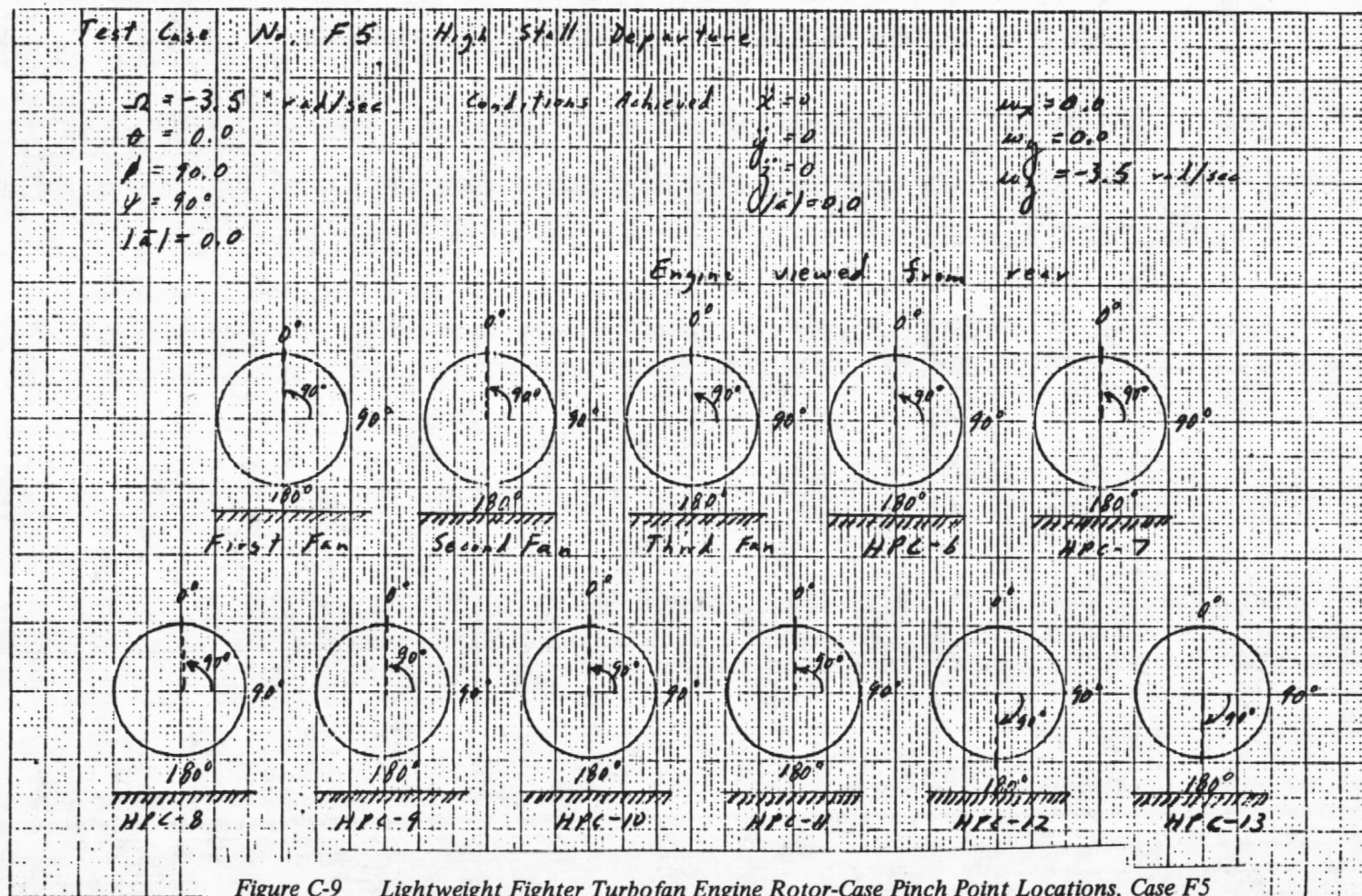
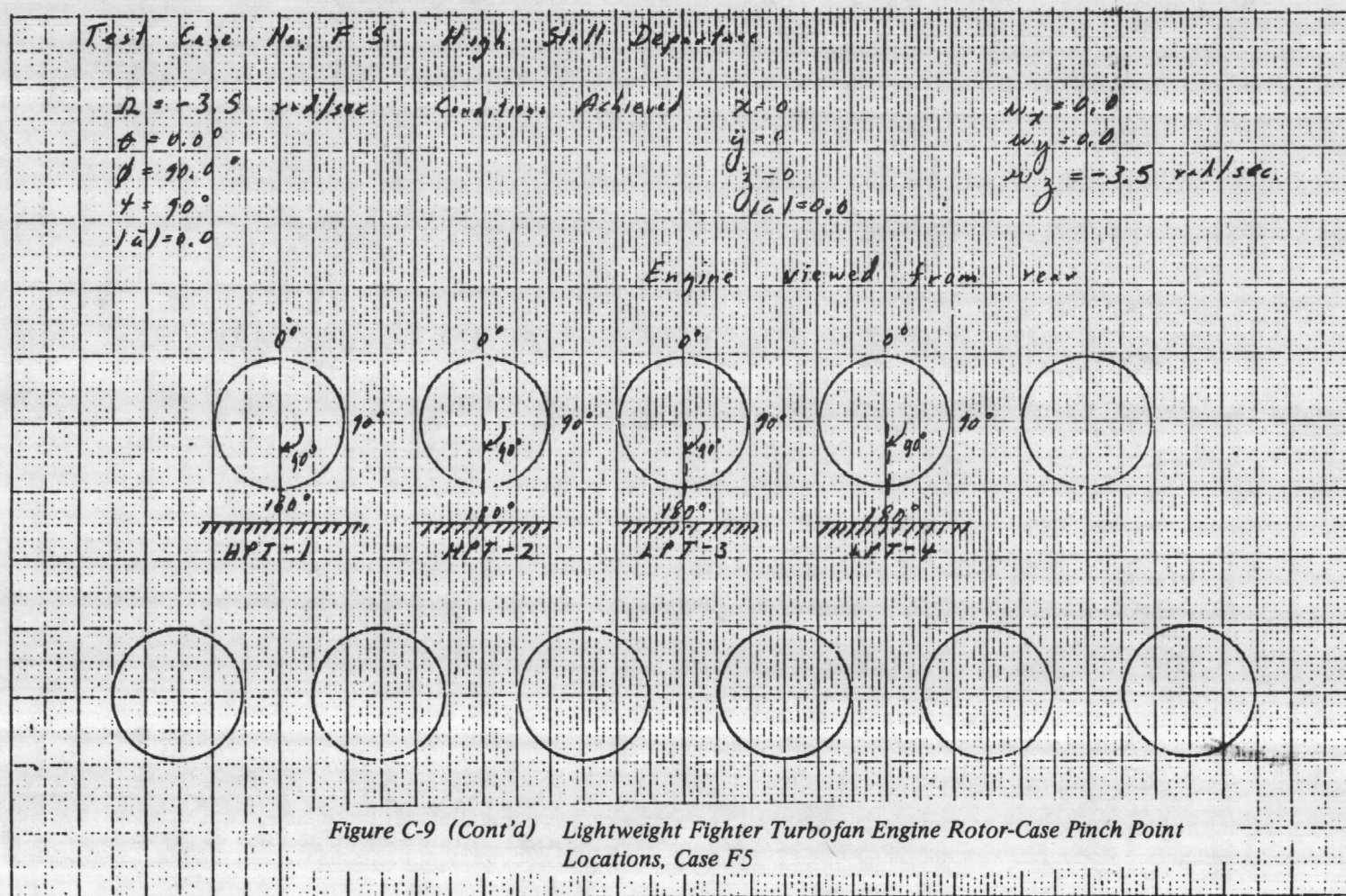


Figure C-9 Lightweight Fighter Turbopan Engine Rotor-Case Pinch Point Locations, Case F5





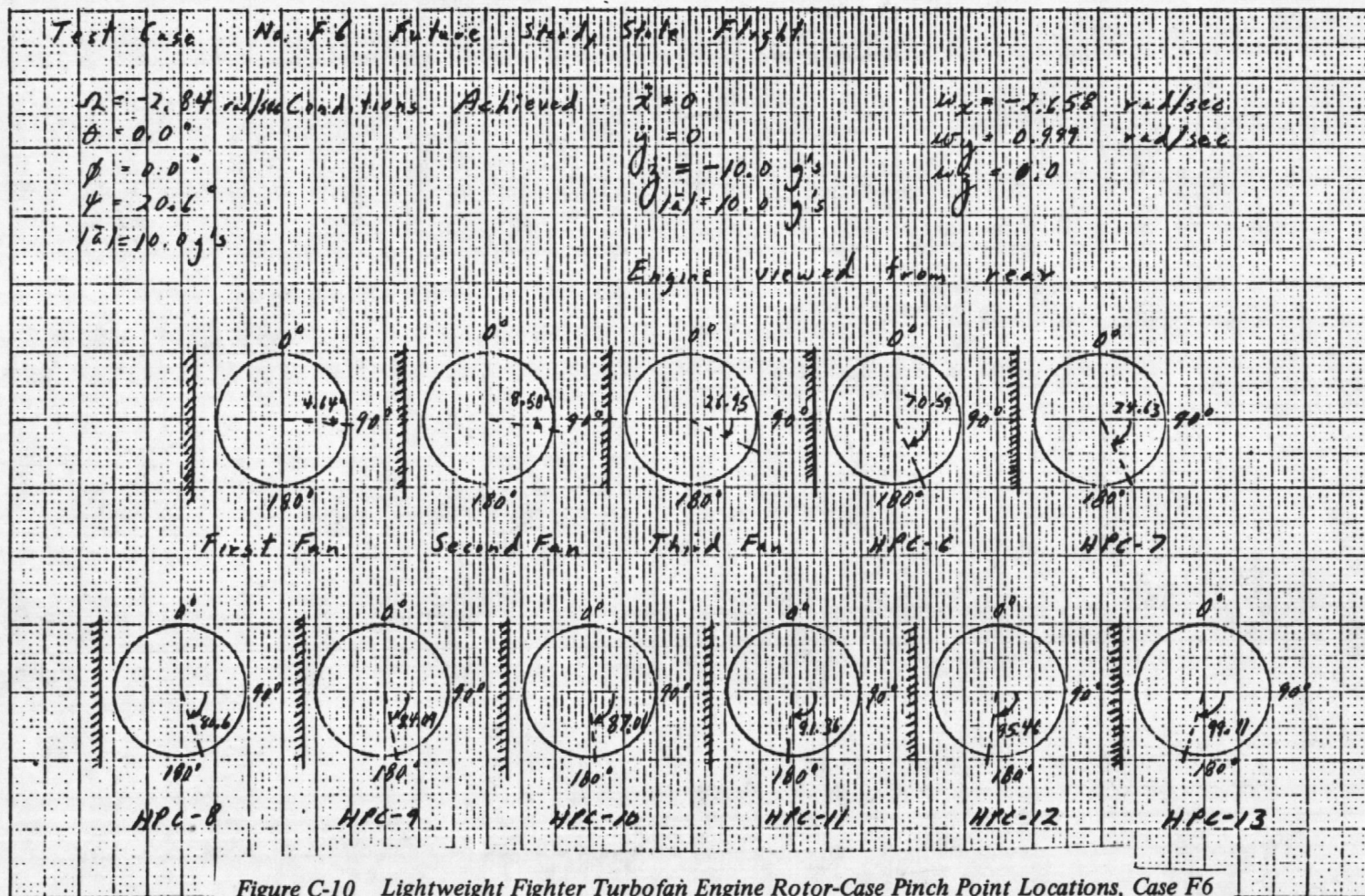
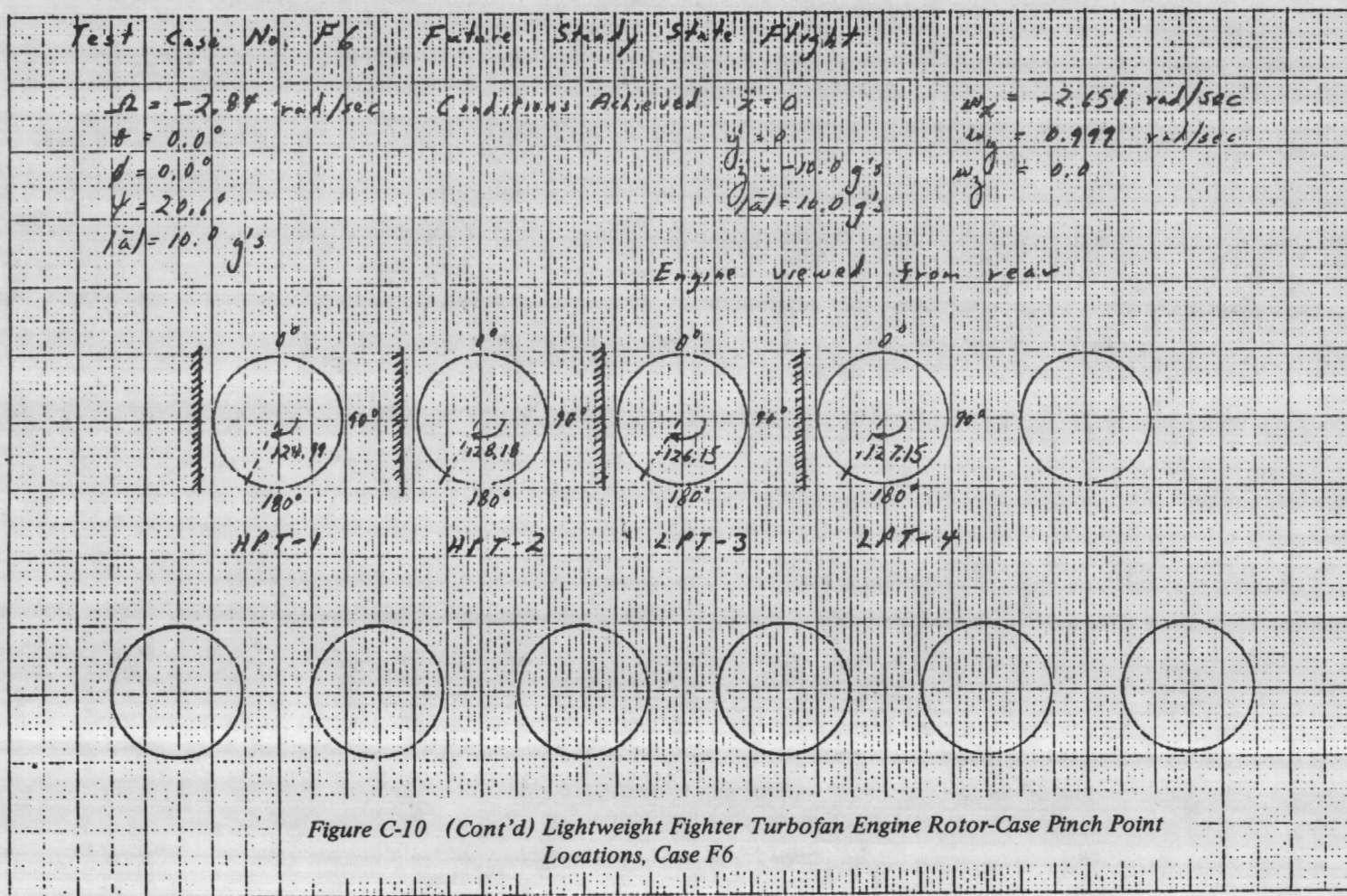
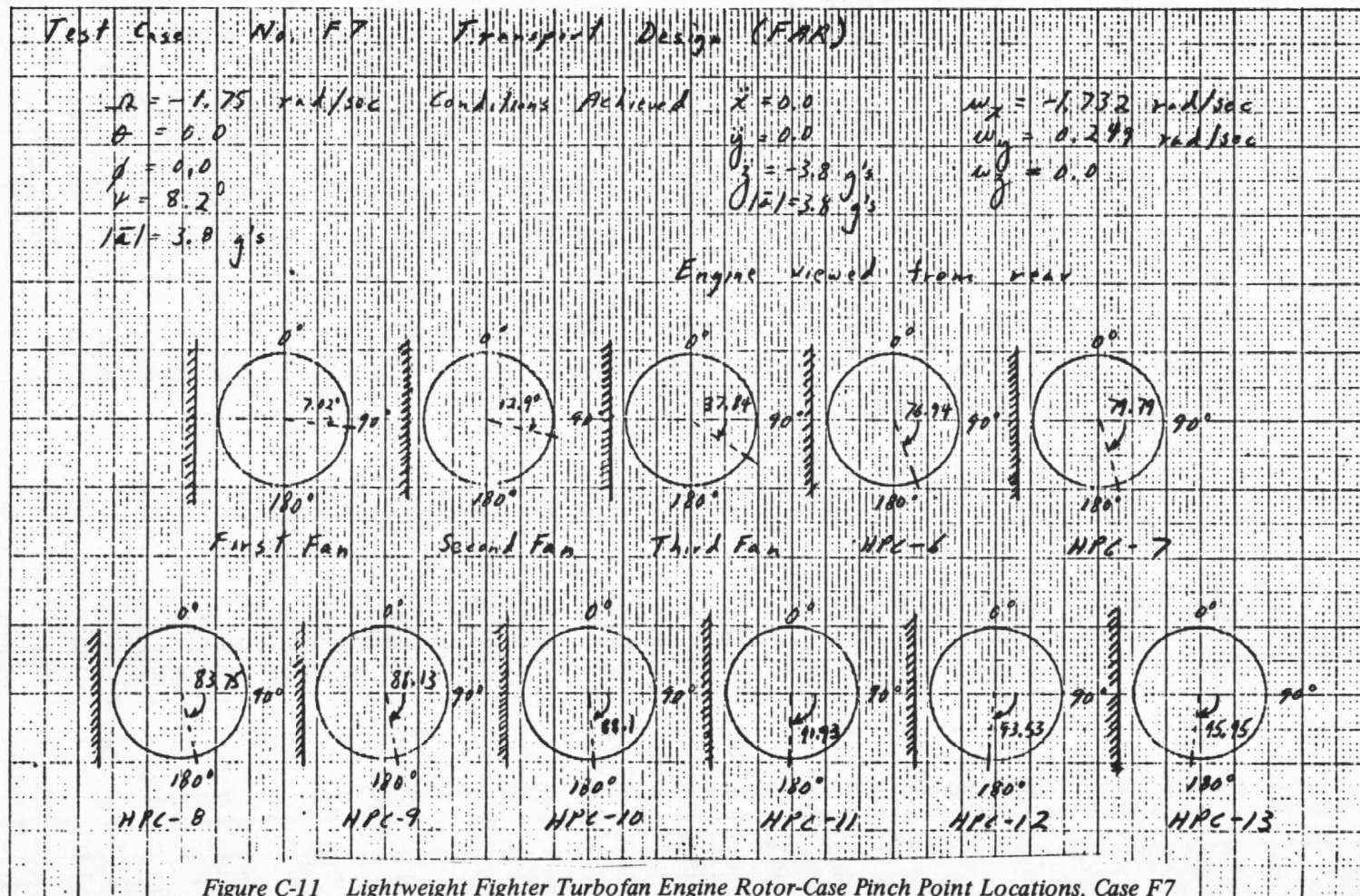
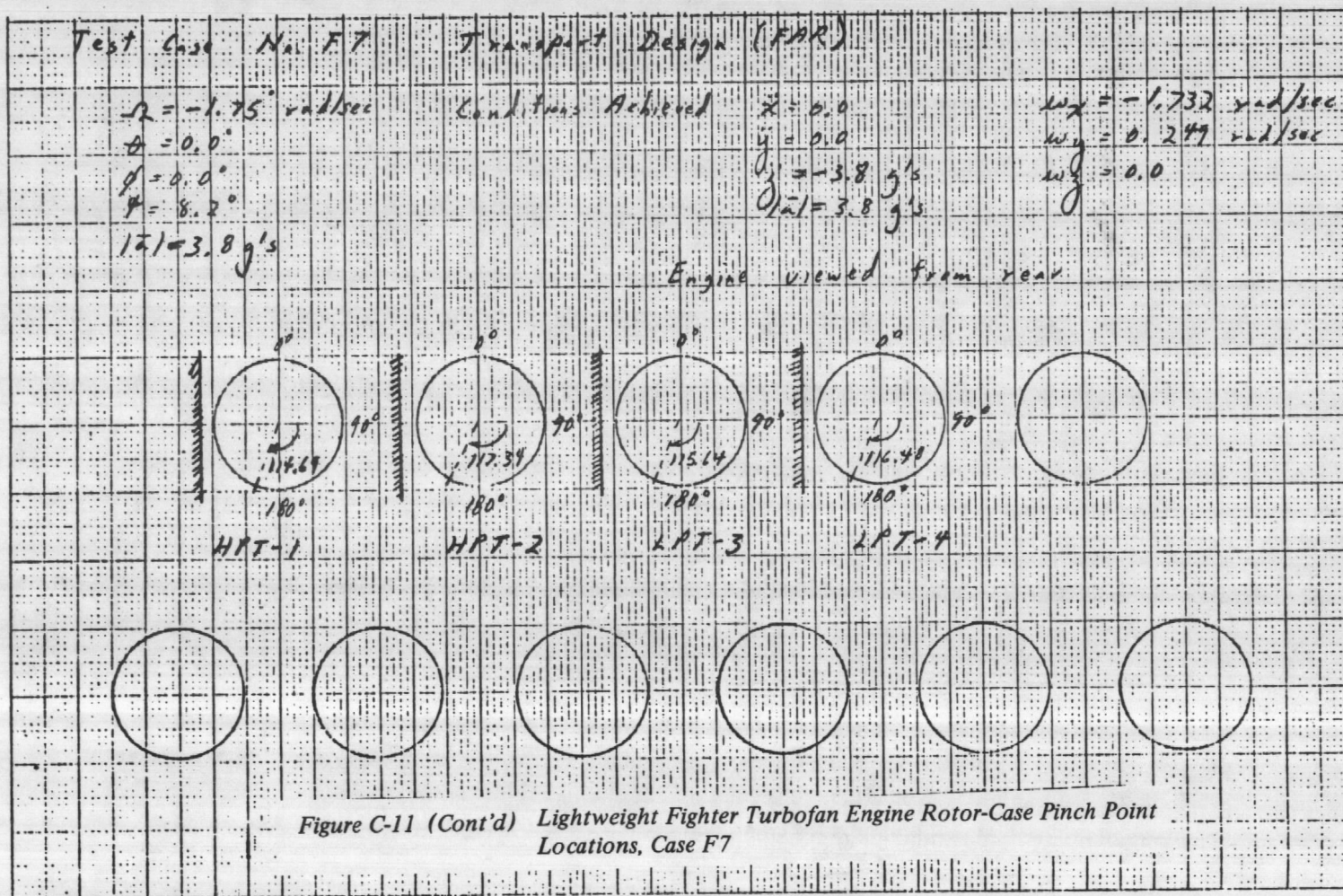


Figure C-10 Lightweight Fighter Turbofan Engine Rotor-Case Pinch Point Locations, Case F6











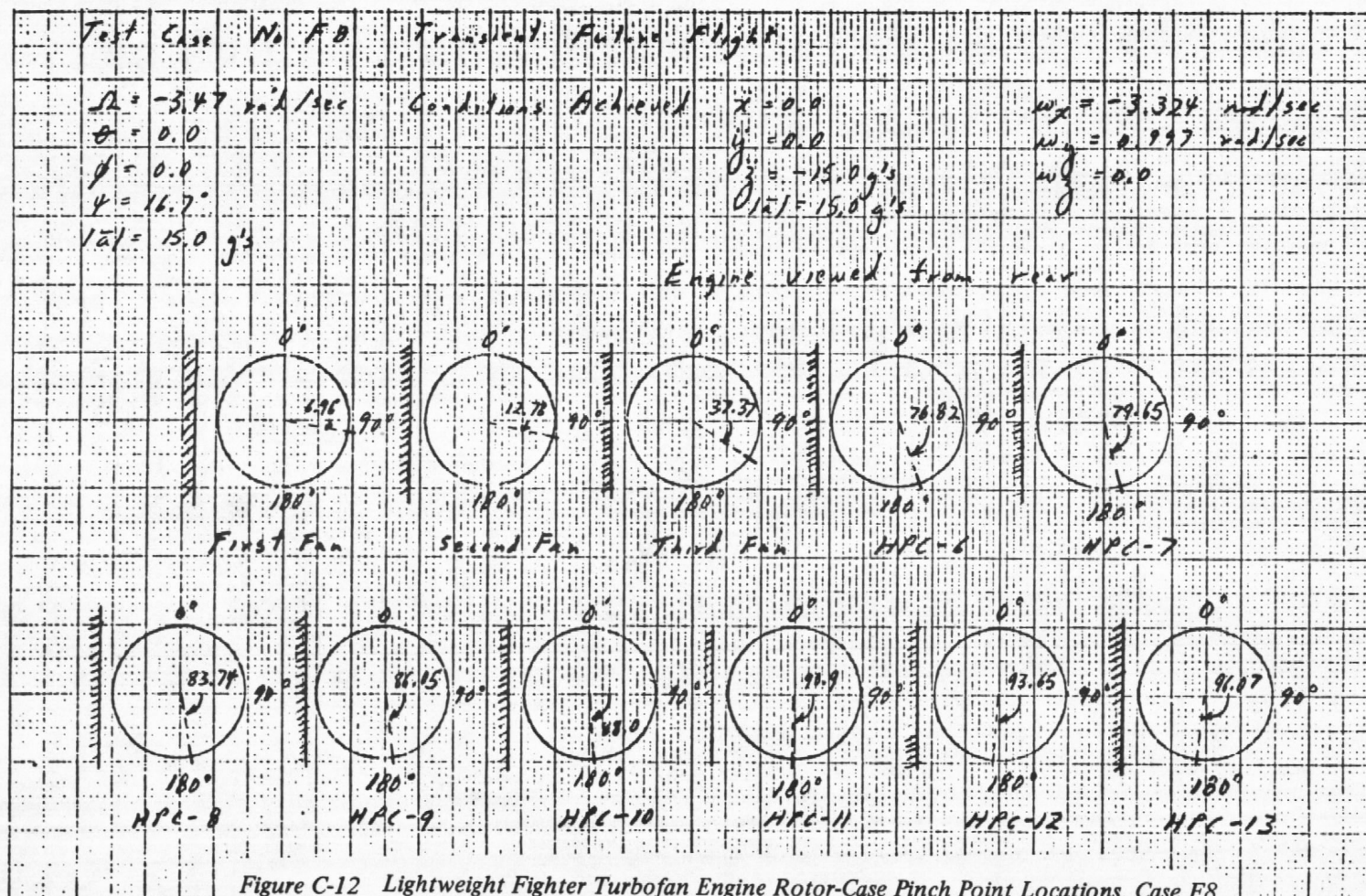
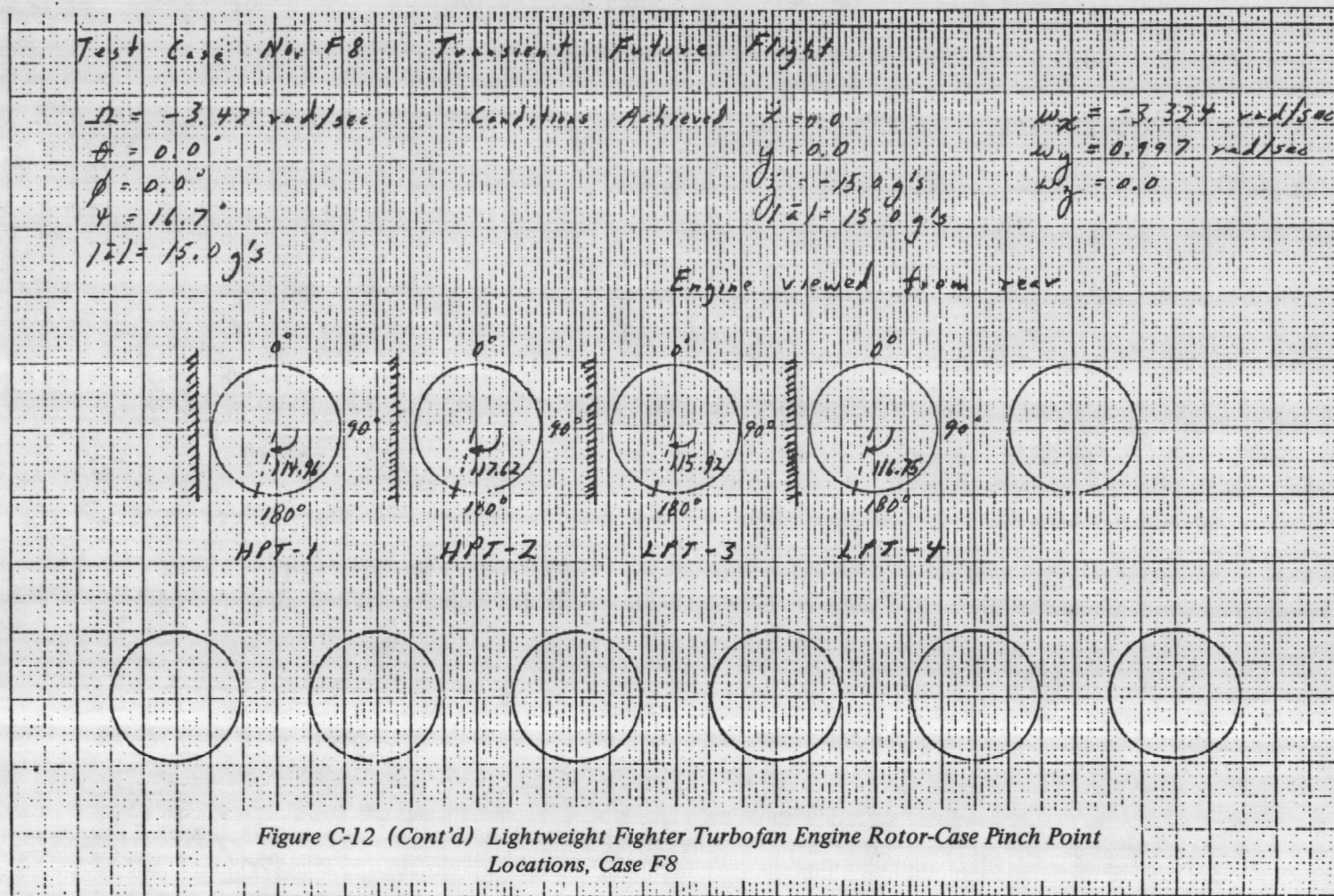
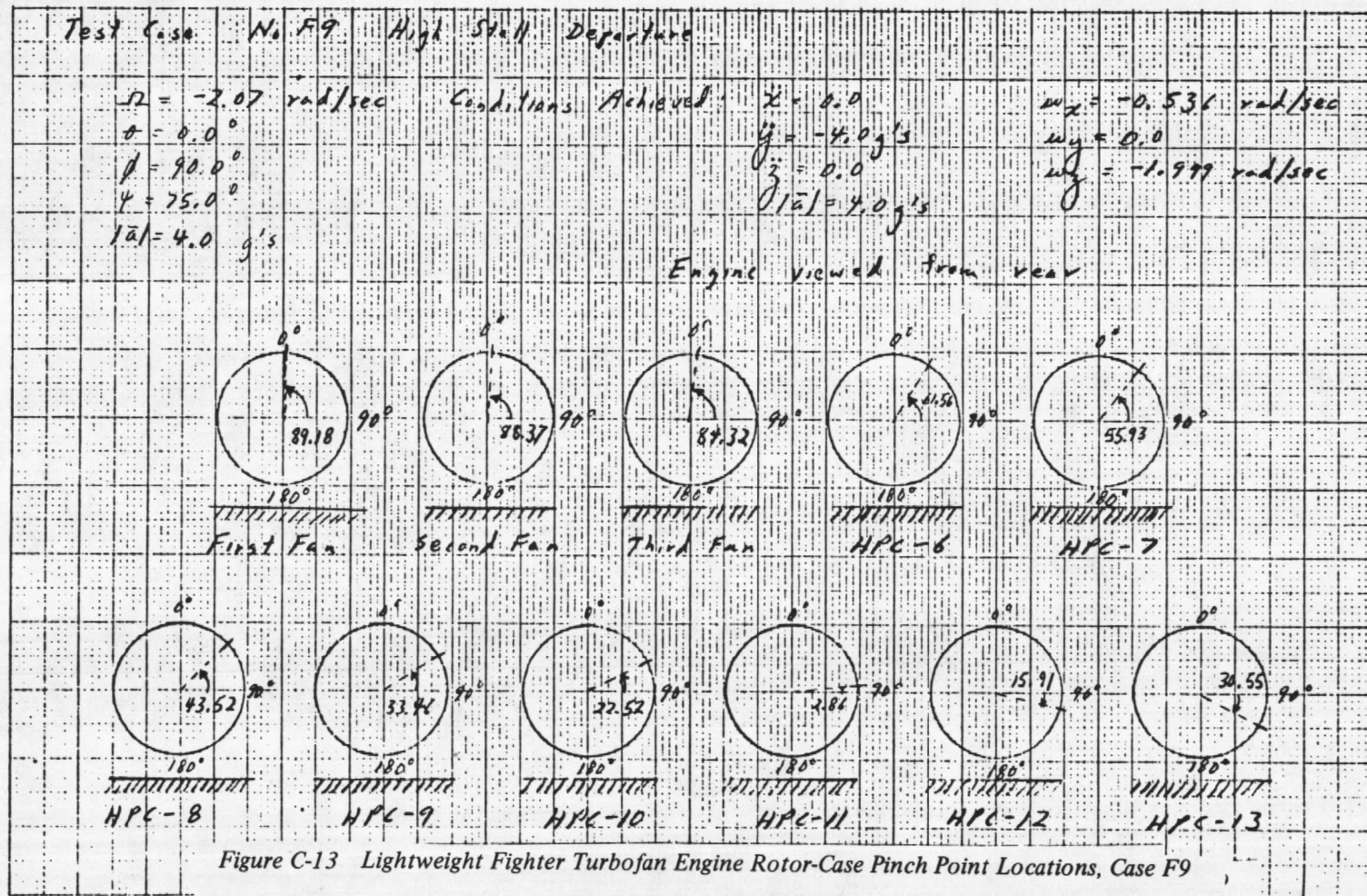
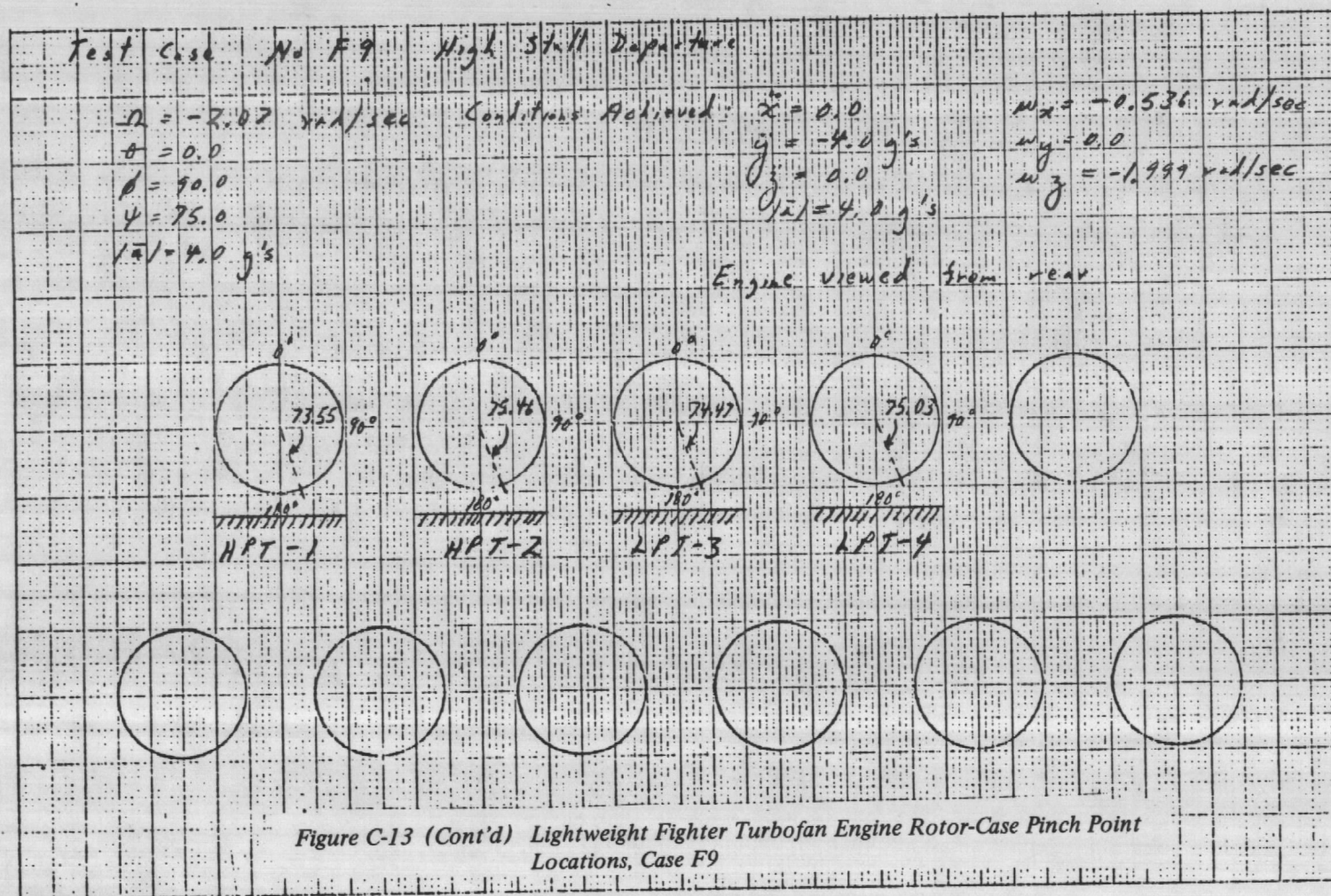


Figure C-12 Lightweight Fighter Turbofan Engine Rotor-Case Pinch Point Locations, Case F8











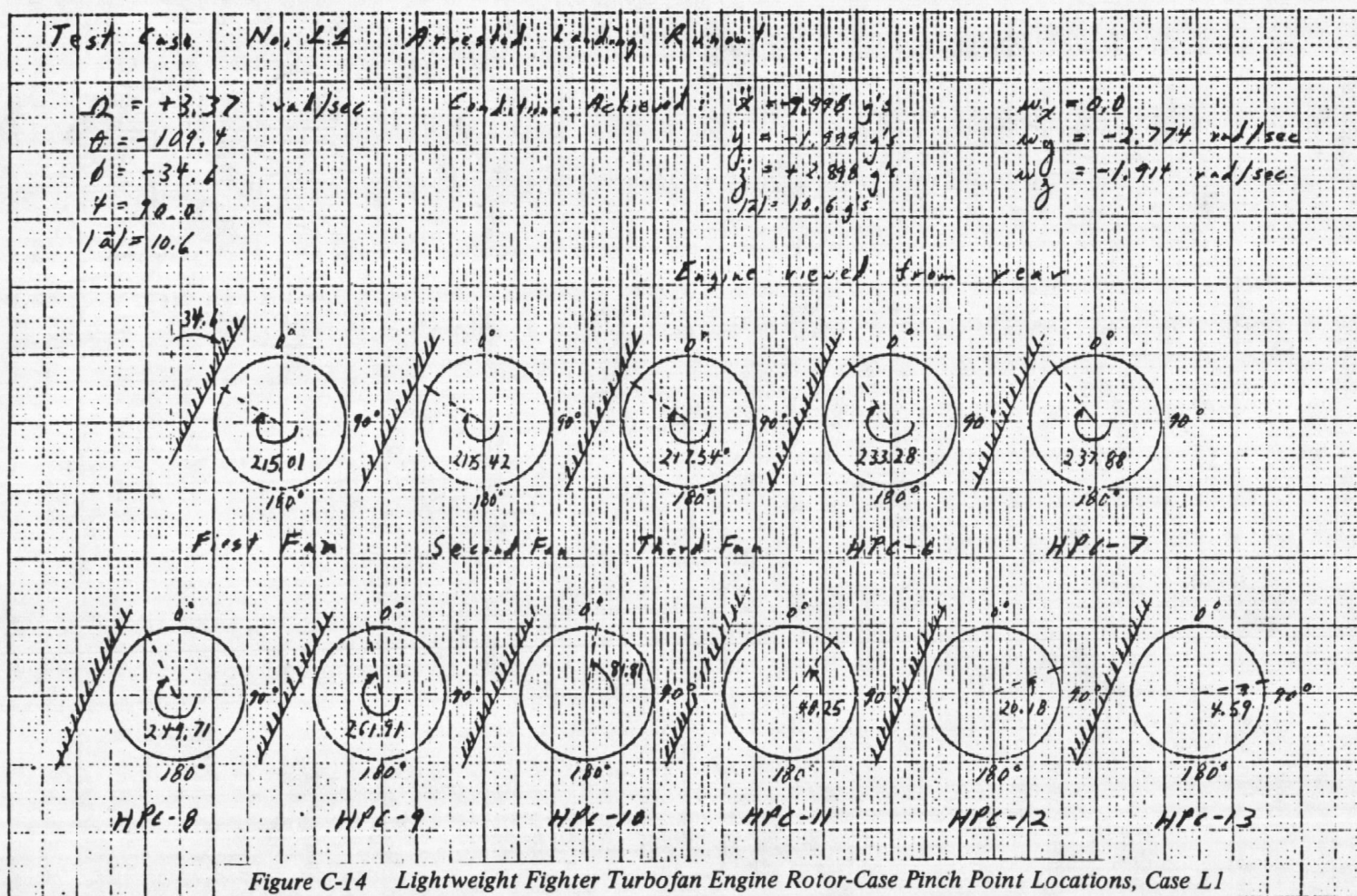
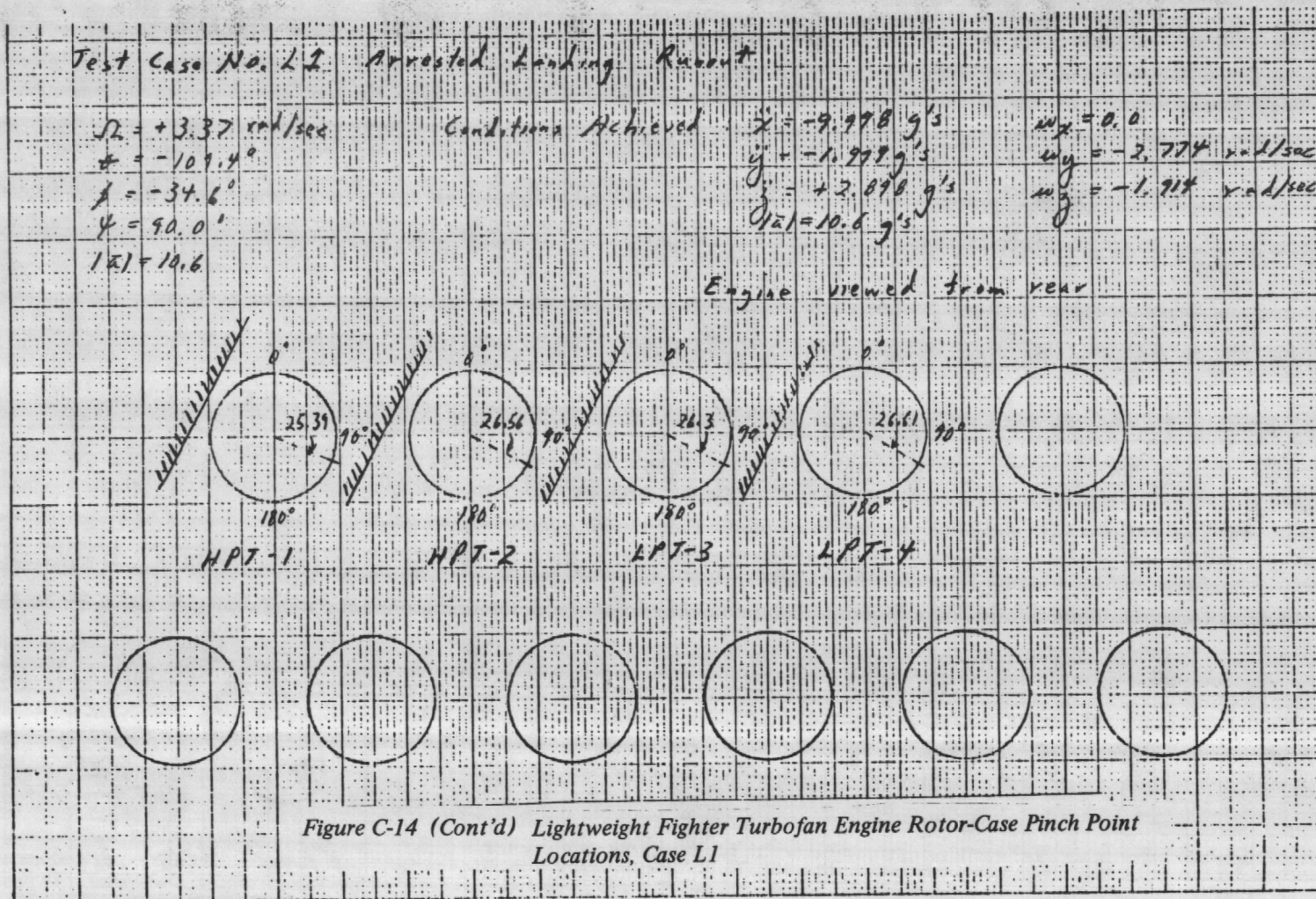


Figure C-14 Lightweight Fighter Turbofan Engine Rotor-Case Pinch Point Locations, Case L1





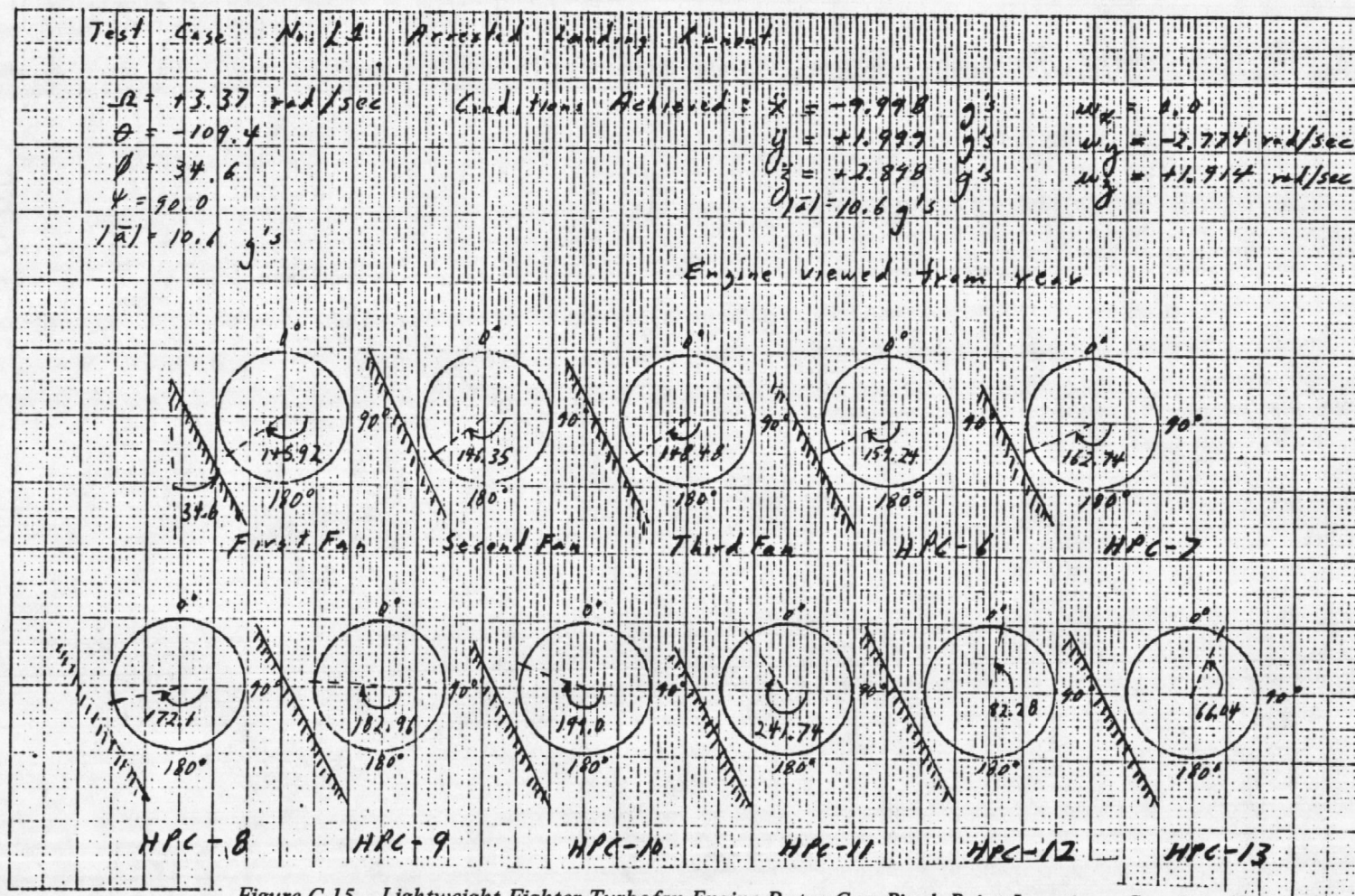
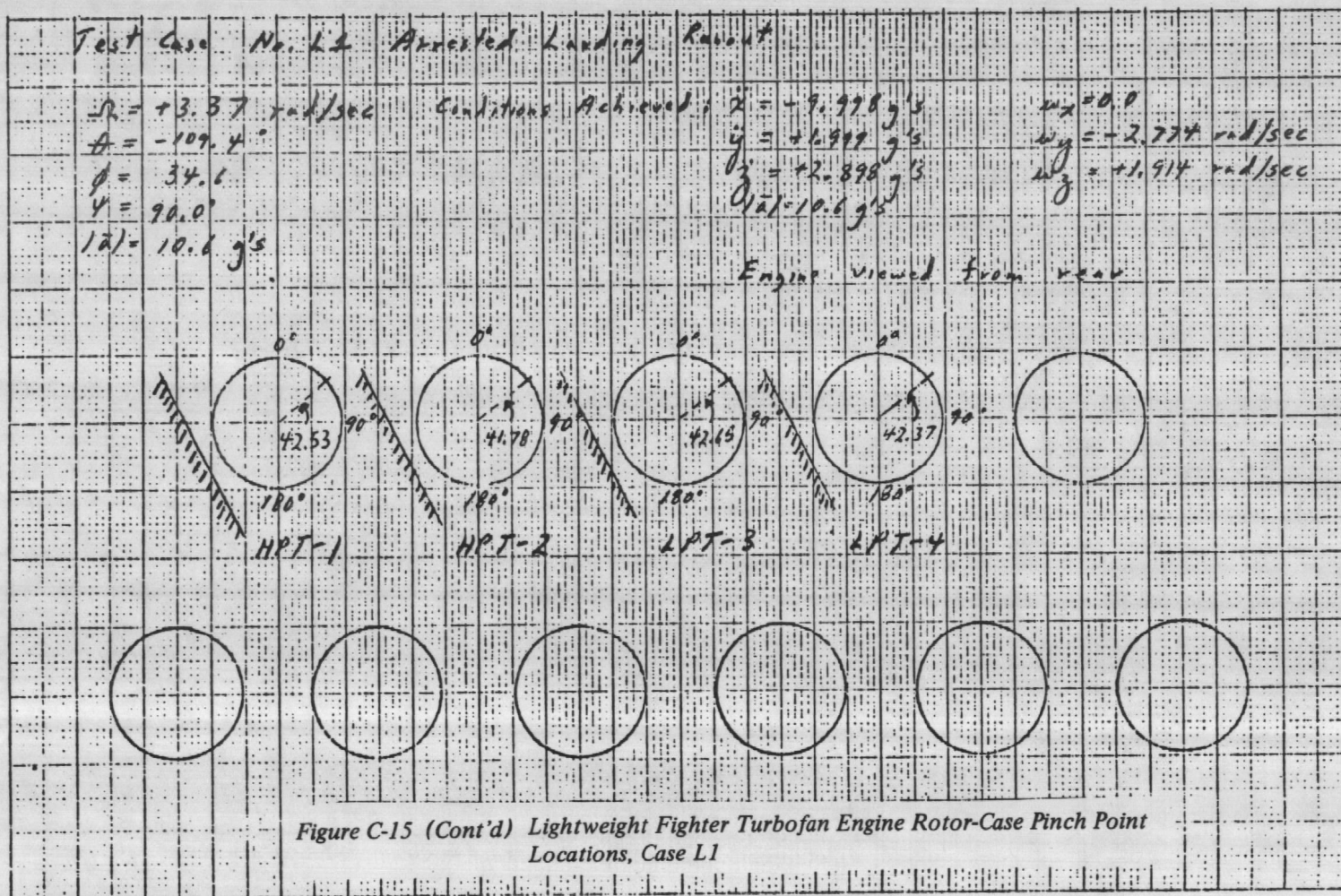
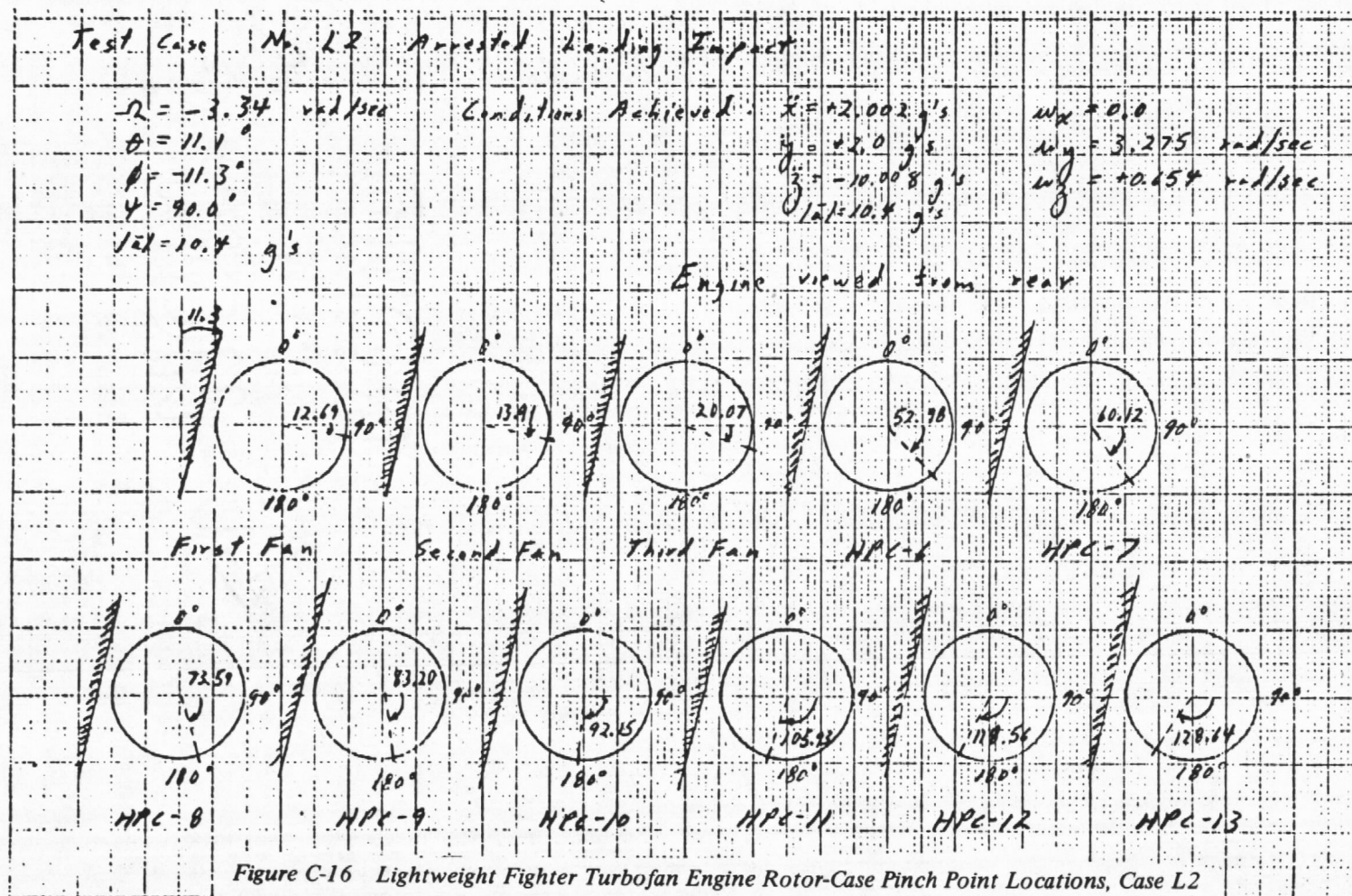
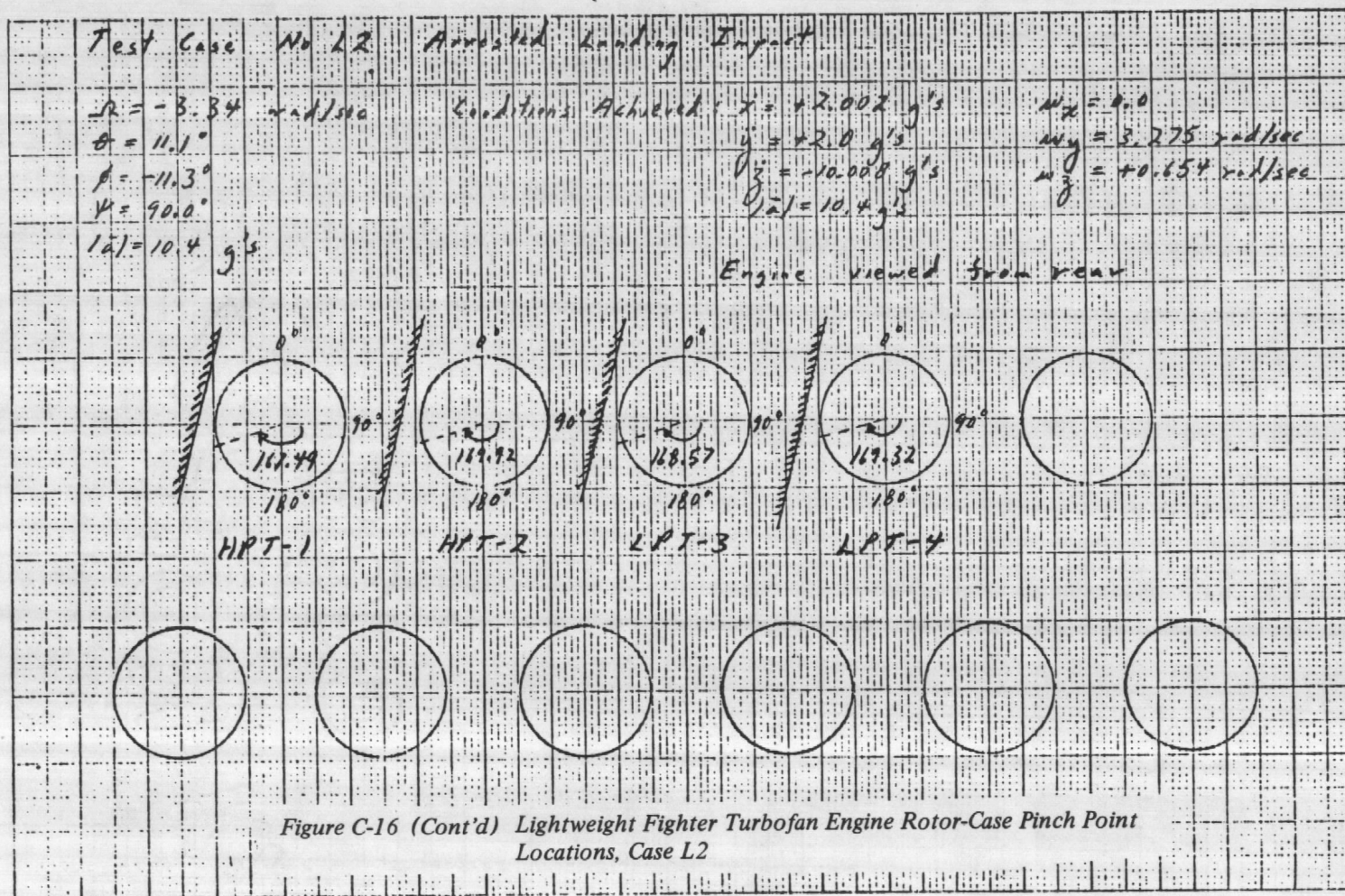


Figure C-15 Lightweight Fighter Turbofan Engine Rotor-Case Pinch Point Locations, Case L1









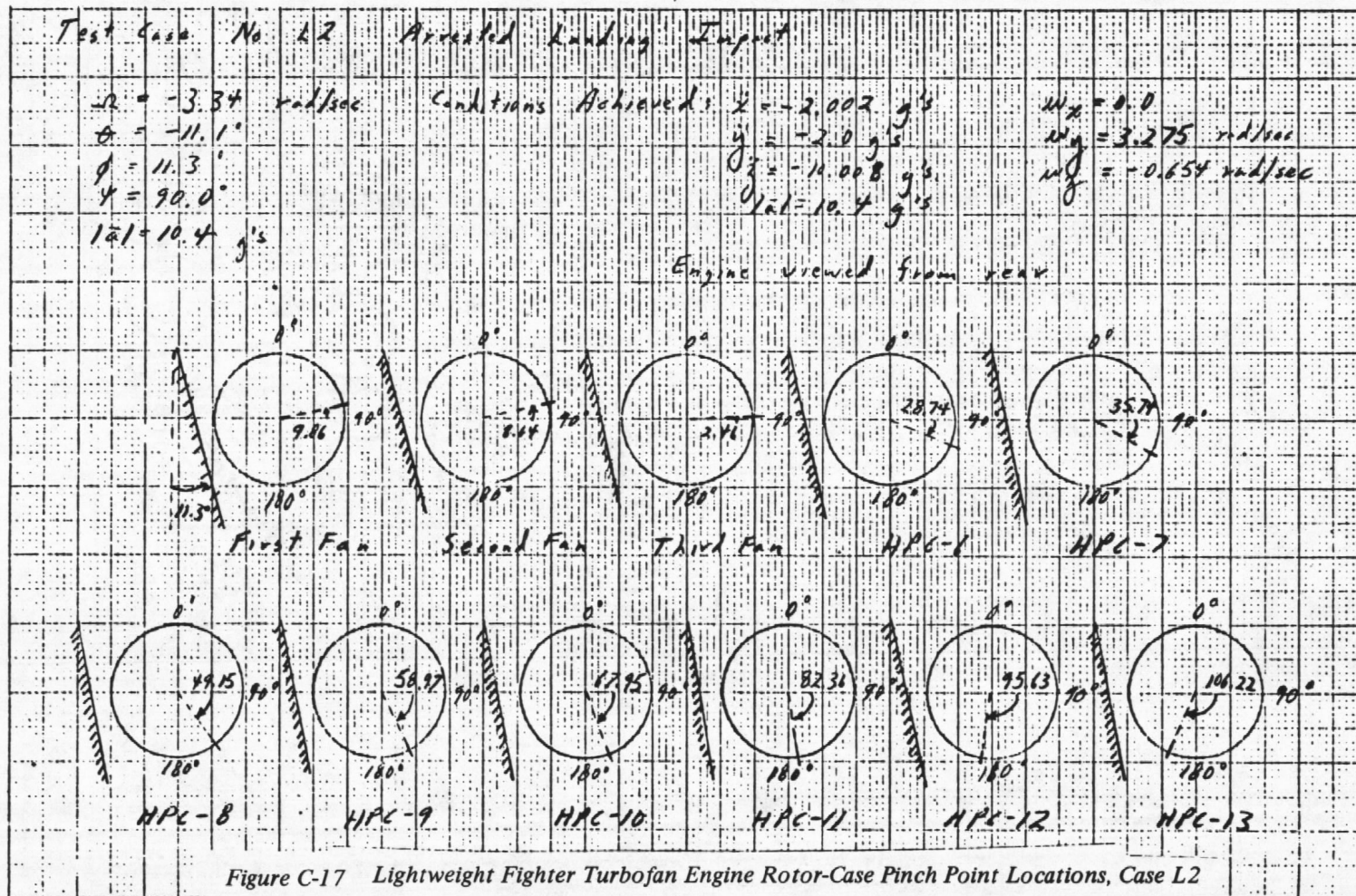
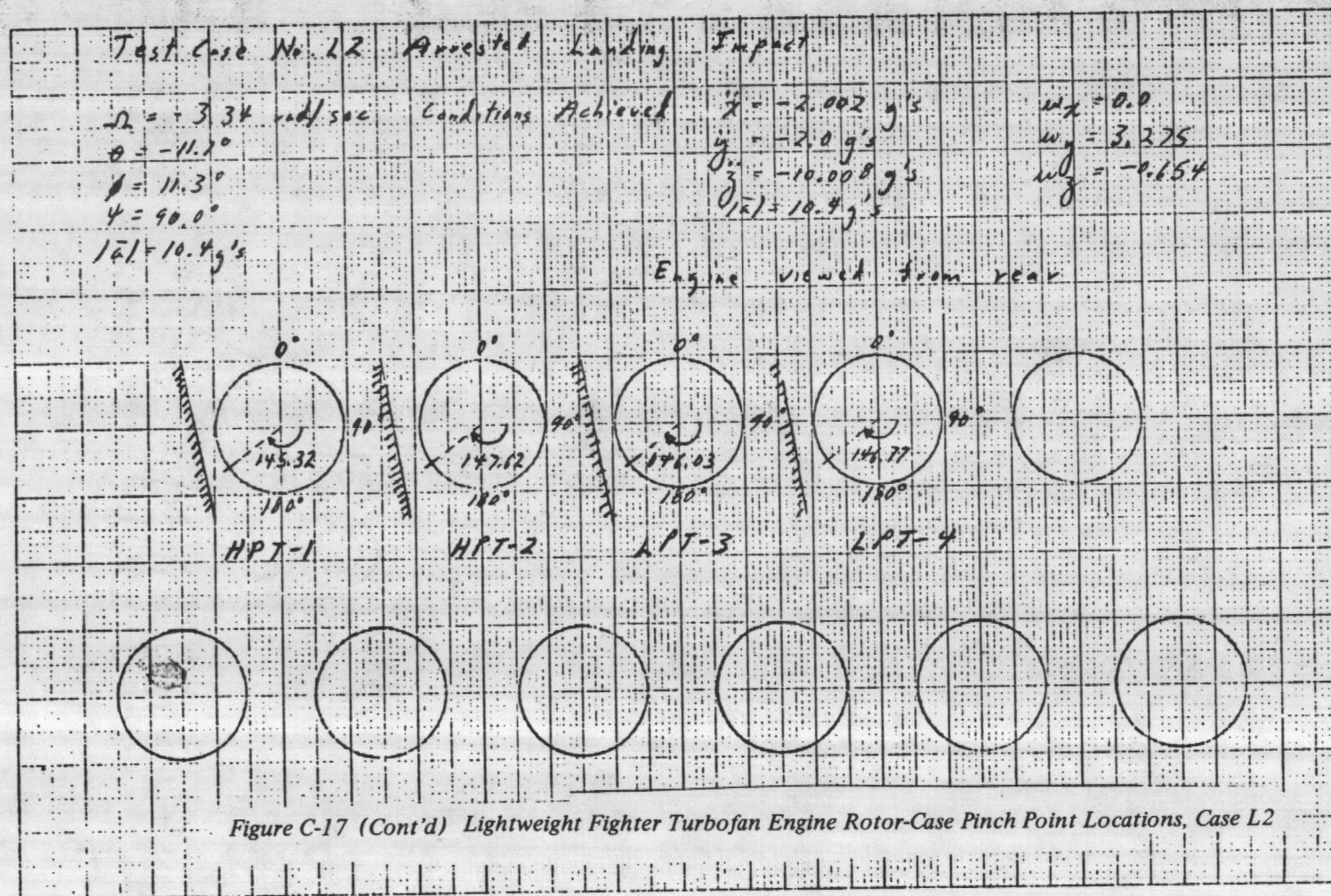
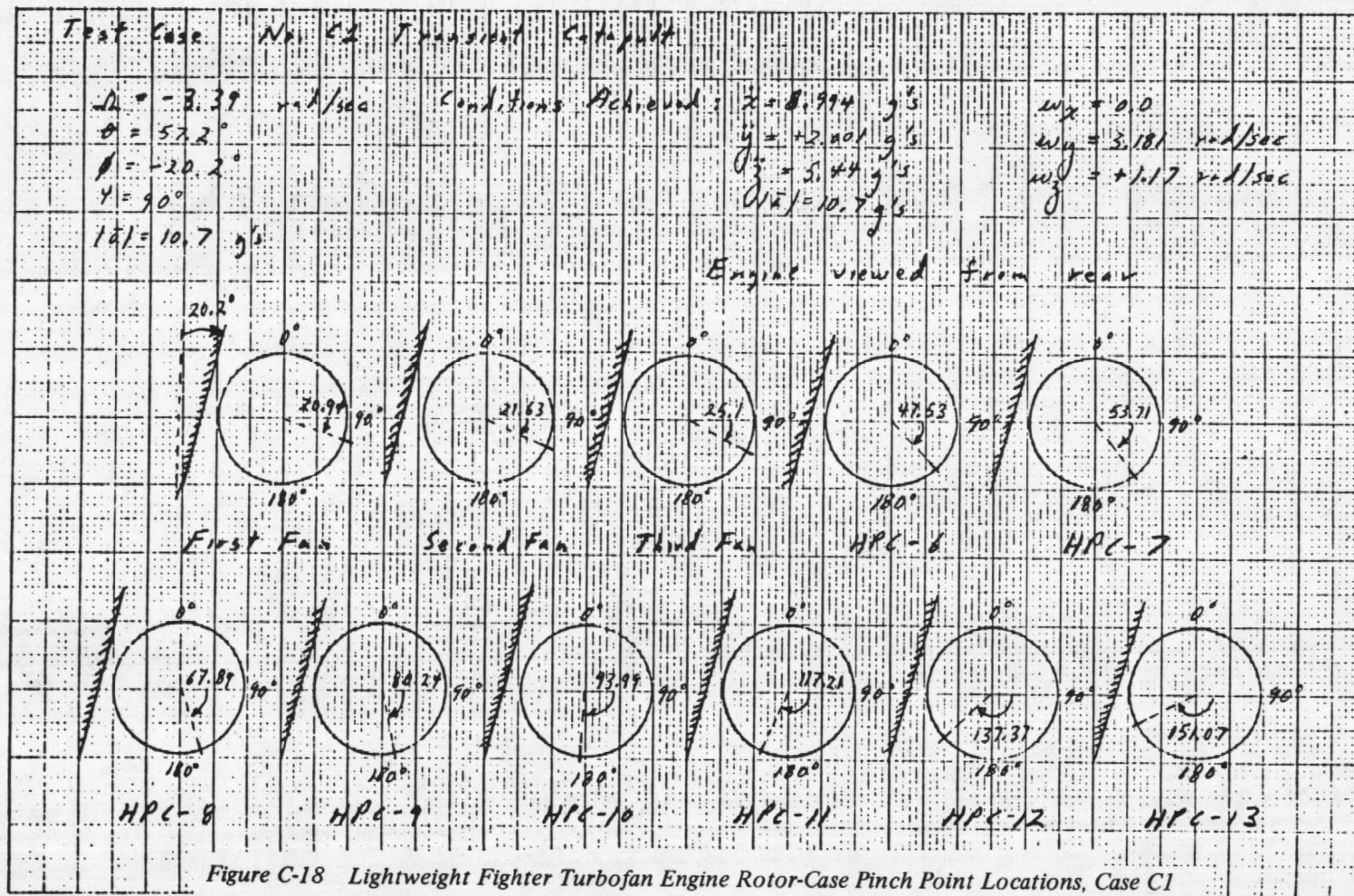


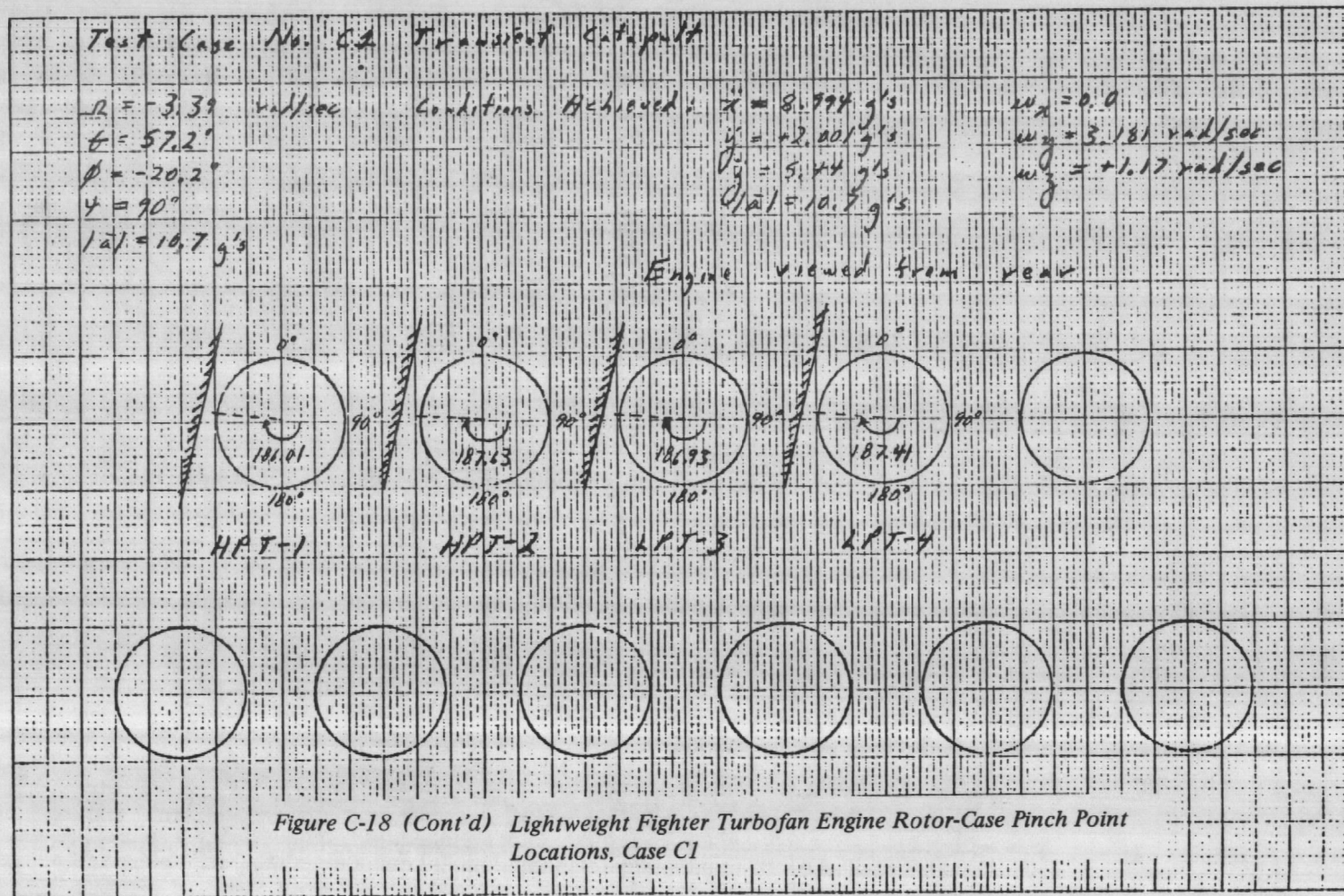
Figure C-17 Lightweight Fighter Turbofan Engine Rotor-Case Pinch Point Locations, Case L2

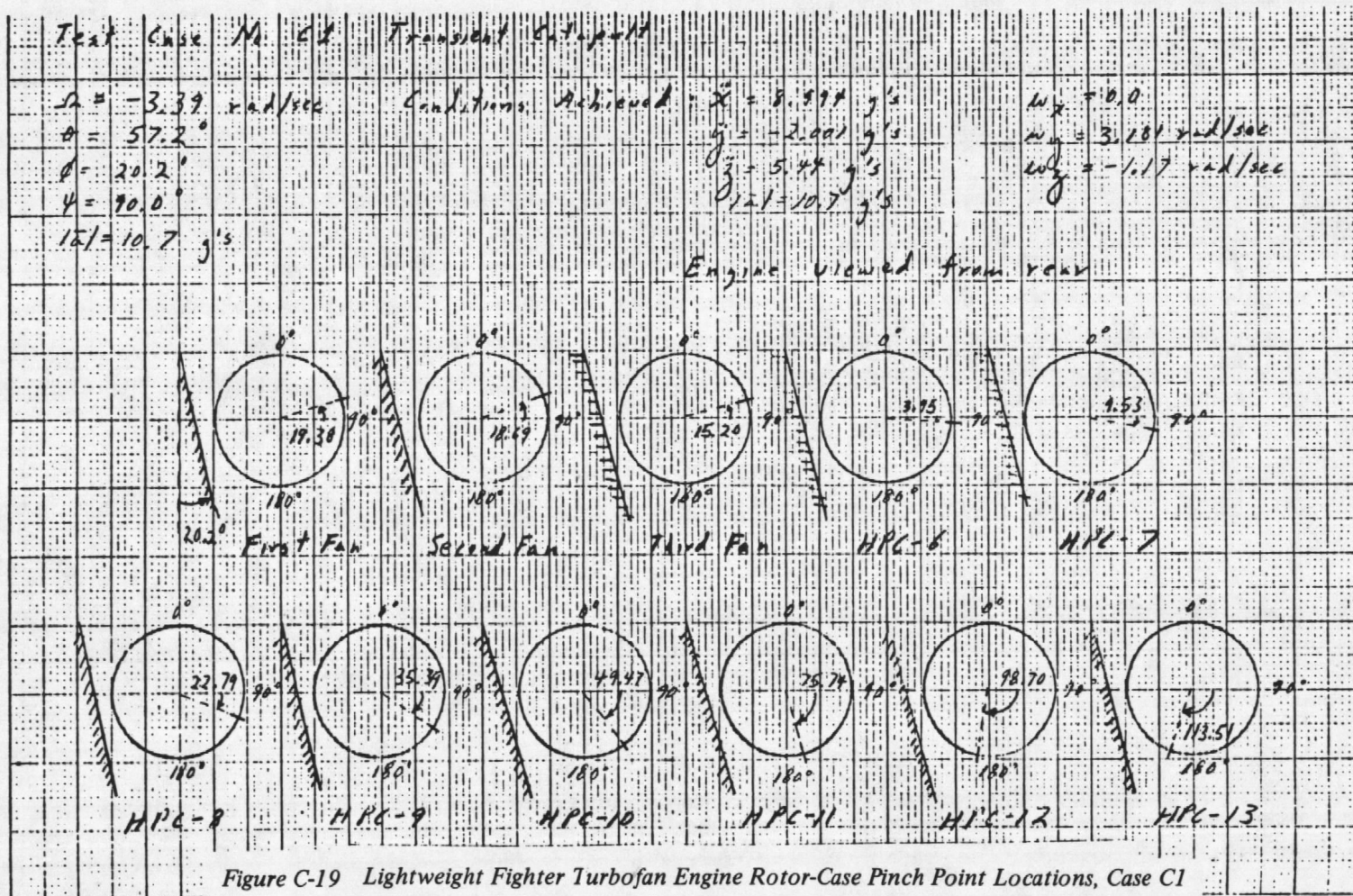














Test Case No. 68 Transient Collapse

$\Omega = -3.39 \text{ rad/sec}$

$\theta = 57.2^\circ$

$\phi = 20.2^\circ$

$\psi = 90.0^\circ$

$|\vec{r}| = 10.7 \text{ g's}$

Conditions Achieved:  $\ddot{x} = 8.994 \text{ g's}$ 

$\ddot{y} = -2.001 \text{ g's}$

$\ddot{z} = 5.44 \text{ g's}$

$|\ddot{r}| = 10.7 \text{ g's}$

$\omega_x = 0.0$

$\omega_y = 3.181 \text{ rad/sec}$

$\omega_z = -1.17 \text{ rad/sec}$

Engine viewed from rear

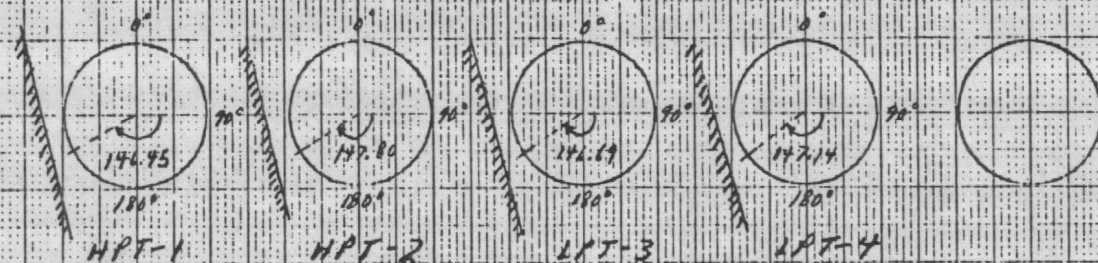


Figure C-19 (Cont'd) Lightweight Fighter Turbofan Engine Rotor-Case Pinch Point Locations, Case C1



## EFFECT OF GRAVITY ON BASELINE KINEMATIC TEST REQUIREMENTS

The question has arisen as to whether it is important to include the acceleration due to the earth's gravitational field with the test required linear accelerations stated in the original TELS study. In normal practice the maneuver g-loads do not include the 1-g load due to the earth's gravity. Although the maneuver load can be considered a constant during a sustained maneuver, the orientation of the engine relative to the earth's gravitational field may be changing. The components of the gravitational field in the engine coordinate system may not be constant. This is especially the case in a maneuver such as a pull up or nose down where the component of the earth's gravity along the engine centerline is changing.

If the major component of the linear acceleration of the maneuver is large relative to a 1 g load in a given direction then the error in ignoring gravity in simulating that component of the linear acceleration in that direction will be small. If the major component of the maneuver load is small relative to 1 g then larger errors are introduced in the loads being simulated.

Certain flight maneuvers being simulated on the centrifuge would not have to be adjusted to take gravity into account. For example test case F4, the high pitch rate maneuver would occur during a 90° banked, high speed turn. In this case the wing would be pointed towards the ground. The centrifuge simulation of this maneuver can be accomplished exactly on the hinged-gimbal support system. Test case F5, the high stall departure, which induces pure gyroscopic moment also provides for proper orientation of the gravity load. For other test cases, however, how close the maneuver linear acceleration is to being perpendicular to the earth's gravitational field will determine how accurately the maneuver is capable of being simulated on the centrifuge.

The equations for the linear accelerations simulated on the centrifuge were presented in Appendix B of the original TELS study. The gimbal angles and test radius were determined by ignoring earth gravity components to be simulated as well as gravity while the engine is mounted on the centrifuge. The equations are more complicated if gravity is taken into account properly. The six equations which represent the linear accelerations and angular rate being simulated are:

$$\dot{w}_x = (\cos \psi \cos \theta) \Omega$$

$$\dot{w}_y = (-\sin \psi \cos \phi + \cos \psi \sin \theta \sin \phi) \Omega$$

$$\dot{w}_z = (\sin \psi \sin \phi + \cos \psi \sin \theta \cos \phi) \Omega$$

$$\ddot{x} + g_x = (\cos \psi \cos \theta) - (\sin \theta) \left( -\frac{r \Omega^2}{32.16} \right)$$

$$\ddot{y} + g_y = (-\sin \psi \cos \phi + \cos \psi \sin \theta \sin \phi) + (\sin \theta \sin \phi) \left( \frac{-r \Omega^2}{32.16} \right)$$

$$\ddot{z} + g_z = (\sin \psi \sin \phi + \cos \psi \sin \theta \cos \phi) + (\cos \theta \cos \phi) \left( \frac{-r \Omega^2}{32.16} \right)$$

Where:

$w_x, w_y, w_z$  are the components of the maneuver angular rate in the engine coordinate system.

$\ddot{x}, \ddot{y}, \ddot{z}$  are the components of the maneuver linear acceleration in the engine coordinate system.

$g_x, g_y, g_z$  are the components of the linear accelerations due to the earth's gravitational field in the engine coordinate system.

Note that:

$$\sqrt{g_x^2 + g_y^2 + g_z^2} = 1 = \text{earth gravity}$$

The Euler angle settings  $\psi, \theta, \phi$  can now be adjusted to take the earth's gravitational field correctly into account. As suggested in the original TELS study, these equations could be solved by an iterative computer program. Since the equations are highly non-linear they would have to be reduced to linear form by expanding each function into a series approximation. Once the equations were in linear form they could be solved by matrix methods.

Including gravity in the simulation of the flight maneuver will also change the location of the rotor case pinch point. The components of the displacement vector now become:

$$D_y = K_{1H} \Omega_y - K_{2H} (\ddot{y} + g_y)$$

$$D_z = K_{1V} \Omega_z - K_{2V} (\ddot{z} + g_z)$$

and

$$\bar{\theta} = \tan^{-1} \frac{D_z}{D_y}$$

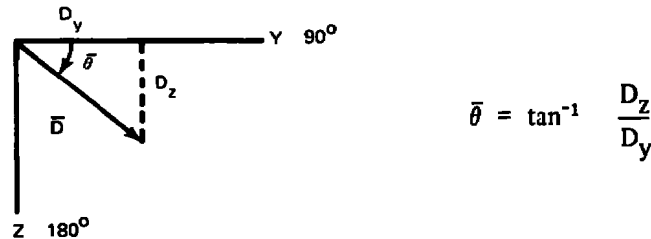
Once again we see that if  $g_y$  and  $g_z$ , the components of the gravitational field, are small compared to  $\ddot{y}$  and  $\ddot{z}$ , the maneuver load, then the location of the pinch point  $\bar{\theta}$  will not change substantially from the angle previously calculated in the radiographic requirements study.

## APPENDIX D

## OFF-CENTRIFUGE SOURCE POSITIONING

This appendix presents the derivation of the equation which define the positioning of an off-centrifuge source relative to the pinch points determined in Appendix C.

The results of Appendix C can be used directly to determine the position of an on-arm X-ray source since the position of the source relative to the base of the gimbal can be seen at a glance. For an off-arm X-ray source the displacement vector can be used to define a unit vector in space which must lie along the X-ray path. We have already defined the rotor displacement vector to be  $\bar{D} = D_x \hat{i} + D_z \hat{k}$  where  $\hat{i}$ ,  $\hat{j}$  and  $\hat{k}$  are unit vectors in a coordinate system (x, y, z) fixed to the engine case. An angle  $\theta$  can be defined to locate the pinch point in the y z plane as follows:



The location of the pinch point at a given engine radius (r) is defined by a point ( $y_p$ ,  $z_p$ ) in the y z plane where:

$$y_p = r \cos \bar{\theta}$$

$$z_p = r \sin \bar{\theta}$$

If we now define the displacement vector as a product of its magnitude and a unit vector

$$\bar{D} = |\bar{D}| \left( \frac{y_p}{r} \hat{j} + \frac{z_p}{r} \hat{k} \right)$$

then the unit vector  $\hat{\eta}$  that lies along the X-ray beam is represented by:

$$\hat{\eta} = \hat{i} \times \left( \frac{y_p}{r} \hat{j} + \frac{z_p}{r} \hat{k} \right) \quad \text{or} \quad -\hat{i} \times \left( \frac{y_p}{r} \hat{j} + \frac{z_p}{r} \hat{k} \right)$$

depending on which side of the engine the X-ray source is to be positioned.

$$\therefore \hat{\eta} = \frac{y_p}{r} \hat{k} - \frac{z_p}{r} \hat{j} \quad \text{or} \quad -\frac{y_p}{r} \hat{k} + \frac{z_p}{r} \hat{j}$$

The unit vectors  $\hat{j}$  and  $\hat{k}$  can be expressed in terms of another set of unit vectors which lie in a coordinate system fixed to the centrifuge arm and moving with it.

$$\hat{j} = (-\sin \psi \cos \phi + \cos \psi (\sin \phi) \hat{I} + (\cos \psi \cos \phi + \sin \psi \sin \theta \sin \phi) \hat{J} + (\cos \theta \sin \phi) \hat{K}$$

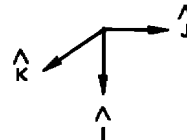
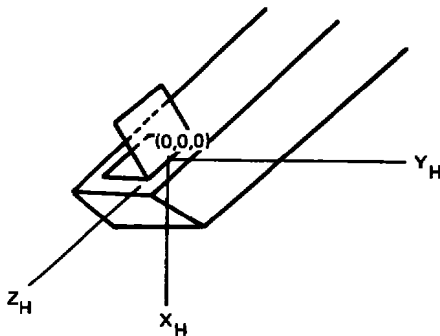
$$\hat{k} = (\sin \psi \sin \phi + \cos \psi \sin \theta \cos \phi) \hat{I} + (-\cos \psi \sin \phi + \sin \psi \sin \theta \cos \phi) \hat{J} + (\cos \theta \cos \phi) \hat{K}$$

Choosing an arbitrary side of the engine to place the X-ray source, the unit vector lying parallel to the X-ray beam become:

$$\begin{aligned} \hat{\eta} = \frac{y_p}{r} [ & (\sin \psi \sin \phi + \cos \psi \sin \theta \cos \phi) \hat{I} + (-\cos \psi \sin \phi + \sin \psi \sin \theta \cos \phi) \hat{J} + (\cos \theta \cos \phi) \hat{K} ] \\ & - \frac{z_p}{r} [ (-\sin \psi \cos \phi + \cos \psi \sin \theta \sin \phi) \hat{I} + (\cos \psi \cos \phi + \sin \psi \sin \theta \sin \phi) \hat{J} + (\cos \theta \sin \phi) \hat{K} ] \end{aligned}$$

Where  $\theta$ ,  $\phi$  and  $\psi$  are the pitch, roll and yaw angles respectively.

At this point we will establish a coordinate system for the off-arm X-ray source. Imagining that at an instant in time, we stop the rotation of the centrifuge. At this instant we will pulse the X-ray beam and make an exposure. Let us now establish the origin for a coordinate system ( $X_H Y_H Z_H$ ) fixed to the centrifuge arm.



The origin of this coordinate system will lie at the center of the line drawn between the hinges which hold the turret base to the centrifuge arm. We can now define the coordinate of the unit vector which lies along the X-ray beam in terms of this new coordinate system.

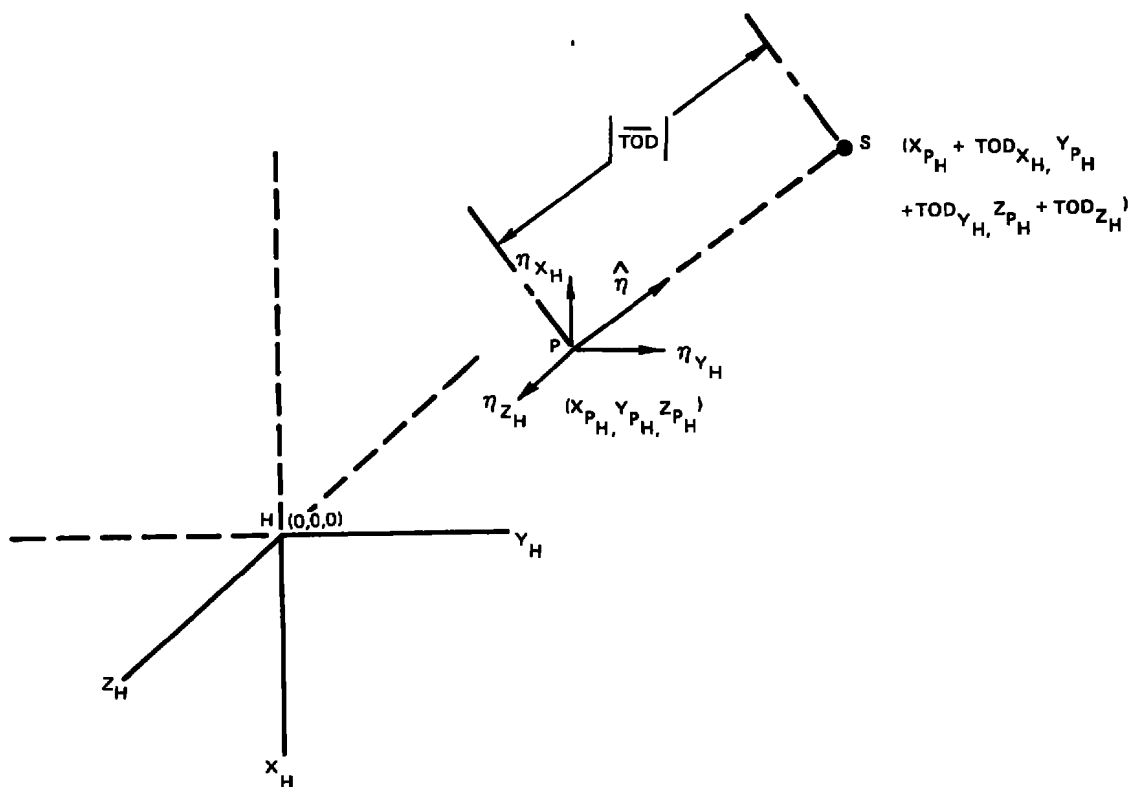
We now have:

$$\eta_{X_H} = \frac{y_P}{r} (\sin \psi \sin \phi + \cos \psi \sin \theta \cos \phi) - \frac{z_P}{r} (-\sin \psi \cos \phi + \cos \psi \sin \theta \sin \phi)$$

$$\eta_{Y_H} = \frac{y_P}{r} (-\cos \psi \sin \phi + \sin \psi \sin \theta \cos \phi) - \frac{z_P}{r} (\cos \psi \cos \phi + \sin \psi \sin \theta \sin \phi)$$

$$\eta_{Z_H} = \frac{y_P}{r} (\cos \theta \cos \phi) - \frac{z_P}{r} (\cos \theta \sin \phi)$$

The pinch point we wish to radiograph as well as the source position can be represented in this new coordinate system. The figure below shows the center of the line between the hinges, Point H, the pinch Point P, and the X-ray target S.



The X-ray target, S, is displaced a distance TOD from the Point P, which is to be radiographed.

When the coordinates of Point P ( $X_{P_H}$ ,  $Y_{P_H}$ ,  $Z_{P_H}$ ) have been defined, the coordinates of the X-ray target (source) can be found by adding the components of the vector,  $\overline{TOD}$ , which we shall call the target to object distance vector, to the coordinate of the Point P. Thus:

$$TOD_{X_H} = |\overline{TOD}| \hat{\eta} \cdot \hat{I} = |\overline{TOD}| \times (\eta_{X_H})$$

$$TOD_{Y_H} = |\overline{TOD}| \hat{\eta} \cdot \hat{J} = |\overline{TOD}| \times (\eta_{Y_H})$$

$$TOD_{Z_H} = |\overline{TOD}| \hat{\eta} \cdot \hat{K} = |\overline{TOD}| \times (\eta_{Z_H})$$

and the coordinate of the X-ray target will be:

$$S_{X_H} = X_{P_H} + TOD_{X_H}$$

$$S_{Y_H} = Y_{P_H} + TOD_{Y_H}$$

$$S_{Z_H} = Z_{P_H} + TOD_{Z_H}$$

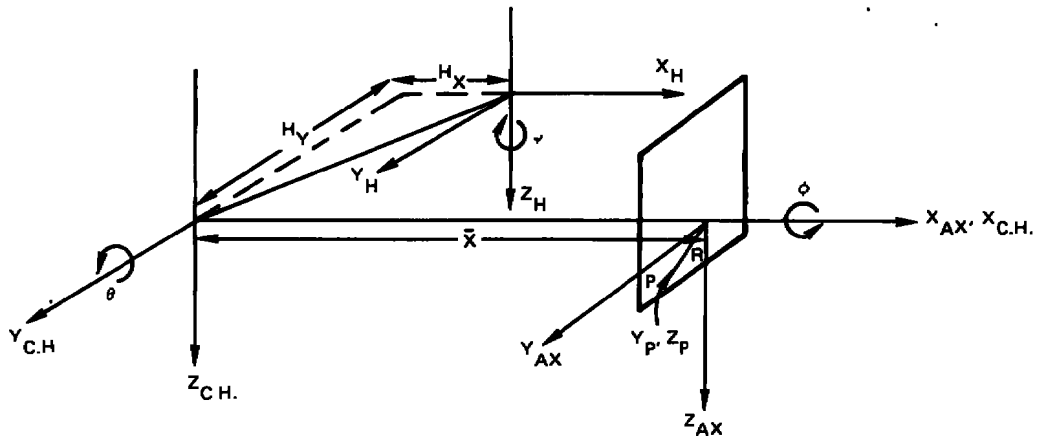
In the original TELS report, a zero position for the engine mounted on the centrifuge is vertical with the inlet towards the ground. If we located the point to be radiographed while the engine is in this zero position, we can transform the coordinates of this point into an off-centrifuge coordinate system through a series of three transformations. The transformations illustrated in the figure below take the point P at any engine cross section through first a roll angle ( $\phi$ ), a pitch angle ( $\theta$ ), and finally a yaw angle ( $\psi$ ) from the original zero position. The values of  $\phi$ ,  $\theta$ , and  $\psi$  would be those required to specify the flight load to be simulated.

The location of the pinch point at a given engine radius (r) and cross-section has already been shown to be ( $y_p$ ,  $z_p$ ) where:

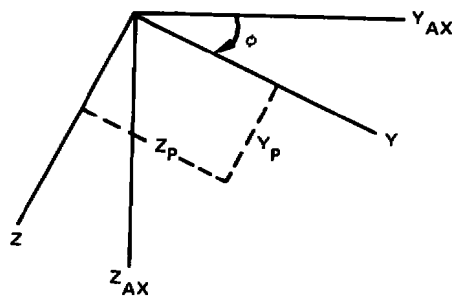
$$y_p = r \cos \bar{\theta}$$

$$z_p = r \sin \bar{\theta}$$

and  $\bar{\theta}$  is measured from the plane containing the engine x, y axes. Clockwise rotation when the engine is viewed from the rear is considered positive.

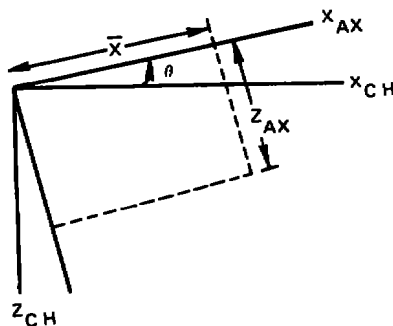


The first transformation is the rotation of the  $y, z$  (an engine cross section) plane about the  $X_{AX}$  axis at the axial location of interest on the engine as shown below:



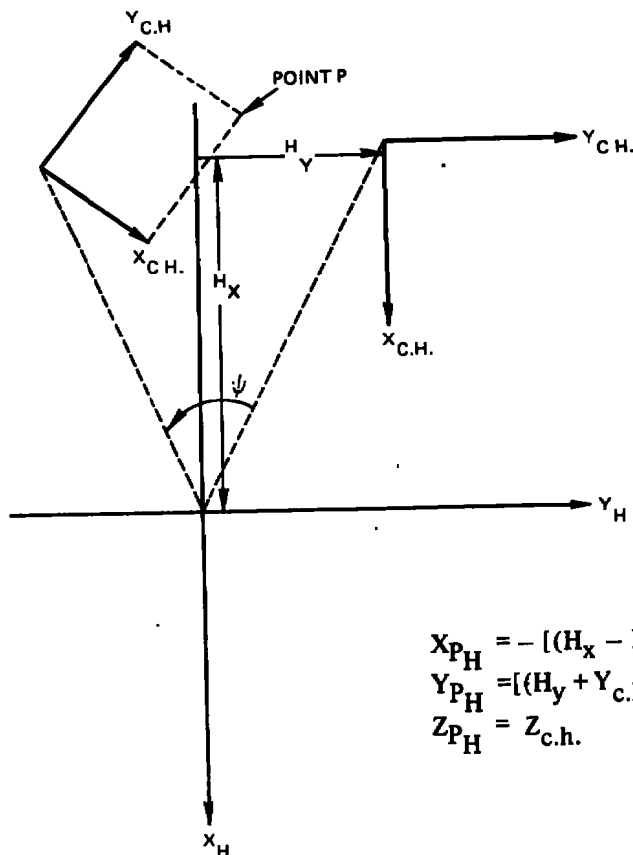
$$\begin{aligned} X_{AX} &= 0 \\ Y_{AX} &= y_p \cos \phi - z_p \sin \phi \\ Z_{AX} &= y_p \sin \phi + z_p \cos \phi \end{aligned}$$

We now locate the origin of an  $X_{C.H.}, Y_{C.H.}, Z_{C.H.}$  coordinate system at the center of roll and pitch rotation on the gimbal unit. We then define  $\bar{x}$  to be the distance from this origin to the engine cross-section of interest. The next transformation then becomes the rotation of the  $X_{AX}, Z_{AX}$  plane about the  $Y_{C.H.}$  axis as shown below:



$$\begin{aligned} X_{C.H.} &= \bar{x} \cos \theta + Z_{AX} \sin \theta \\ Y_{C.H.} &= Y_{AX} \\ Z_{C.H.} &= Z_{AX} \cos \theta - \bar{x} \sin \theta \end{aligned}$$

If we let  $H_x$  and  $H_y$  define the distance between the intersection of the pitch and roll axes and the hinge centerline, the final transformation is the rotation of the  $X_{c.h.}$ ,  $Y_{c.h.}$  plane about the  $Z_H$  axis as shown below:



$$\begin{aligned} X_{P_H} &= -[(H_x - X_{c.h.}) \cos \psi + (H_y + Y_{c.h.}) \sin \psi] \\ Y_{P_H} &= [(H_y + Y_{c.h.}) \cos \psi - (H_x - X_{c.h.}) \sin \psi] \\ Z_{P_H} &= Z_{c.h.} \end{aligned}$$

The pinch point is now defined in a coordinate system with origin at a point directly between the hinges that hold the turret base to the centrifuge arm and the  $Z_H$  axis corresponds to the line joining the two hinges.

We can now locate the X-ray target in an off-centrifuge coordinate system. The position of the target ( $S_{X_H}$ ,  $S_{Y_H}$ ,  $S_{Z_H}$ ) is:

$$\begin{aligned} S_{X_H} &= X_{P_H} + |\overline{TOD}| \times (\eta_{X_H}) \\ S_{Y_H} &= Y_{P_H} + |\overline{TOD}| \times (\eta_{Y_H}) \\ S_{Z_H} &= Z_{P_H} + |\overline{TOD}| \times (\eta_{Z_H}) \end{aligned}$$

Where  $|\overline{TOD}|$  is the magnitude of the vector drawn from the X-ray target to the point on the engine to be radiographed;  $\eta_{X_H}$ ,  $\eta_{Y_H}$ , and  $\eta_{Z_H}$  are the direction cosines of the X-ray beam; and  $(X_{P_H}$ ,  $Y_{P_H}$ ,  $Z_{P_H})$  defines the position of the rotor-case pinch point which is to be radiographed.



## APPENDIX E

### RADIATION SHIELDING CALCULATIONS

In order to determine the permissible dose, levels, and concentrations of radiation and the acceptability of an unshielded accelerator facility at AEDC in Tennessee, the appropriate state, military, and federal regulations (Ref. 5, 6, 7 and 8) are referenced.

Excerpts from Reference 5 that are applicable to the proposed facility.

#### **RHS 2.101. Exposure of Individuals in Restricted Areas**

- A. Except as provided in paragraph B of this section, no licensee or registrant shall possess, use, receive, or transfer sources of radiation in such a manner as to cause any individual in a restricted area to receive in any period of one calendar quarter from all sources of radiation in the licensee's or registrant's possession a dose of radiation in excess of the limits specified in the following table.

	<u>REMS per Quarter</u>
1. Whole body: head and trunk; active blood-forming organs lens of eyes; or	1- $\frac{1}{4}$
2. Hands and forearms; feet and ankles	18- $\frac{3}{4}$
3. Skin of whole body	7- $\frac{1}{2}$

#### **RHS 1.5 Units of Radiation Dose**

- C. . . . . For the purpose of these regulations, any of the following is considered to be equivalent to a dose of one rem.
1. . . . .
  2. A dose of 1 rad due to X-, gamma, or beta radiation;
  3. . . . .
  4. . . . .

### **RHS 2.105 Permissible Levels of Radiation From External Sources in Unrestricted Areas**

- A. Except as authorized by the Department pursuant to paragraph B of this section, no licensee or registrant shall possess, use, receive, or transfer sources of radiation in such a manner as to create in any unrestricted area from such sources of radiation in his possession.
1. Radiation levels which, if an individual were continuously present in the area, could result in his receiving a dose in excess of 2 millirems in any 1 hour, or
  2. Radiation levels which, if an individual were continuously present in the area, could result in his receiving a dose in excess of 100 millirems in any 7 consecutive days.
- B. Any person may apply to the Department for proposed limits upon levels of radiation in unrestricted areas in excess of those specified in paragraph A of this Section resulting from the applicant's possession or use of sources of radiation . . .

The Department will approve the proposed limits if the applicant demonstrates to the satisfaction of the Department that the proposed limits are not likely to cause any individual to receive a dose to the whole body in any period of any calendar year in excess in 0.5 rem.

#### **From Reference 8. Attachment D.**

3. Shielding — Accelerators must be located in shielded places which limit radiation levels at the control panels to less than 2 millirads per hour. Accelerators may be surrounded by fences or revetments which prevent personnel entry into areas where radiation levels exceed 2 millirads per hour, or equivalent protection may be provided by shielding.

#### **From Reference 6, Chapter 5, Section IX, Radiation Protection.**

**TABLE XI**  
**RADIATION PROTECTION STANDARDS**

<u>Occupational Exposure</u>	<u>Condition</u>	<u>Dose (rem)</u>
Whole body, head and trunk, blood-forming organs, gonads, lens of the eye	Accumulated dose	5(N-18): N greater than 18 years
	13 weeks	3
Skin and thyroid	Year	30
	13 weeks	10
Hands and forearms, feet and ankles	Year	75
	13 weeks	25
<b>Population</b>		
Individual	Year	0.5 (whole body)
Average	30 years	5 (gonads)

#### **9.77 Unshielded Installations**

An unshielded installation is one which, due to operational requirements, cannot be provided with the inherent degree of protection specified for either protective or enclosure installations. Such installations include fenced or "roped-off" areas located either in the open or inside buildings such as hangar bays. An installation so classified SHALL conform with all of the following requirements.

- a) The source and all objects exposed thereto are within a conspicuously posted perimeter that limits the area in which the exposure can exceed 2 MR in any one hour or 100 MR in any seven consecutive days. The perimeter SHALL be posted with a sufficient number of AFTO Forms 9, "Caution Radiation Area", so as to be conspicuous from any direction of approach.

- b) If the perimeter is of such a size or is so arranged that the operator cannot readily determine whether the enclosure is unoccupied, a sufficient number of radiographers or radiographic assistants SHALL be strategically located to provide adequate surveillance over the entire area. The personnel SHALL have in their possession an adequate and properly calibrated, operable survey meter. This requirement may not be necessary if the radiographic procedures are to be accomplished in a fenced area access to which is controlled by the operator.
- c) Positive means for preventing access, such as a locked enclosure, SHALL be provided during periods of unattended radiation.
- d) The source and equipment essential to the use of the source shall be inaccessible to unauthorized use, tampering or removal when not in use.
- e) A qualified radiographer is in attendance during all radiographic procedures or the equipment is made inaccessible.
- f) If the installation is in a remote area and if entry into the enclosed area can be absolutely prevented during irradiation, the source and all objects exposed thereto may be within a conspicuously posted perimeter that limits the area in which the exposure can exceed 100 MR in an hour provided.
  - 1. The perimeter is posted with a sufficient number of AFTO Forms 9E, "Caution High Radiation Area", signs so as to be conspicuous from any direction of approach.
  - 2. The requirements of paragraph 9-77b is met when applicable.
  - 3. The requirements of paragraph 9-77e and 9-77g can be met.
- g) No person, either within a controlled area or in the environs of the installations, is exposed to more than appropriate basic radiation protection standard.

#### **9-82 Unshielded Installations**

- A. This class shall be selected only if operational requirements prevent the use of either of the other classes. For radiography, its use SHOULD be limited mainly to mobile and portable equipment when fixed shielding cannot be used. Fluoroscopy shall be done only by remote observations, such as by closed circuit television.
- B. The operational requirements of other types of installations may necessitate use of this class.
- C. The protection of personnel and public depends almost entirely on strict adherence to safe operating procedures. With this adherence, unshielded installations may provide a degree of protection similar to the other classes.

From Reference 7.

	Average Weekly Dose <u>rem</u>	Max. 13-Week <u>dose — rem</u>	Max Accumulated <u>dose — rem</u>
<b>Controlled Areas</b>			
Whole Body, Gonads, Blood Forming Organs, Lens of Eyes	0.1	3	— —
Skin of Whole Body	— —	10	30
Hands and Forearms, Head, Neck, Feet and Ankles	1.5	25	75
<b>Non-Controlled Areas</b>	0.01	— —	0.5

Controlled Area: A defined area in which the exposure of persons to radiation is under the supervision of a Radiation Protection Supervisor.

Non-Controlled Area: Any space not meeting the definition of controlled area:

These regulations indicate that the suggested approach to TELS radiation protection is valid and acceptable provided that the dose levels specified are not exceeded. In addition, many radiographic facilities throughout the United States (e.g., Phormex, Los Alamos; Lawrence Livermore Labs, etc.) utilize fences and distance as primary means of providing radiation protection.

Utilizing these references and Reference 7 in particular, the following calculations were carried out to determine the distance to the outer fence required to provide the necessary radiation protection.

Primary Radiation

The weekly exposure,  $E_u$ , from the useful beam at the point of interest, which is at a distance  $b$  from the source is related to the exposure rate at one meter,  $\dot{E}_w$  by the following equation:

$$E_u = \frac{\dot{E}_w t}{b^2} \quad (E1)$$

Where  $t$  is the number of minutes of beam On-time per week. If  $E_u$  is greater than the permissible weekly exposure,  $P$ , a primary barrier of sufficient thickness, to give a transmission factor of  $B_{ux}$ , must be inserted into the beam between the source and the point of interest. Then,

$$P = B_{ux} E_u = B_{ux} \frac{\dot{E}_u t}{b^2} \quad (E2)$$

or

$$B_{ux} = \frac{Pb^2}{\dot{E}_u t} = \frac{Pb^2}{W} \quad (E3)$$

Where, W is the workload.

However, in order to recognize that the primary barrier might be irradiated for only a fraction, U, of the total beam On-time and that the anticipated occupancy of the point of interest may be a fraction, T, of the total beam On-time of the equipment, the value of W in the denominator of Eq. (E3) must be modified by the product UT. That is

$$B_{ux} = \frac{Pb^2}{WUT} \quad (E4)$$

When B = 1 no shielding is required to provide P for given W, U, T, and b.

Alternately Eq. (E4) can be solved for workload W for B = 1:

$$W = \frac{Pb^2}{UT} \quad (E5)$$

Equation (E5) for workload does not take into account attenuation of the X-ray as it passes through the engine and through the atmosphere.

Attenuation of the primary beam by a series of shields is developed as follows:

Recall Equation (E1) where  $W = \dot{E}_u t$  and U, T have been added. We have:

$$\dot{E}_u = \frac{WUT}{b^2} \quad (E6)$$

Let  $\dot{E}_u$  be attenuated as illustrated in Figure E-1.

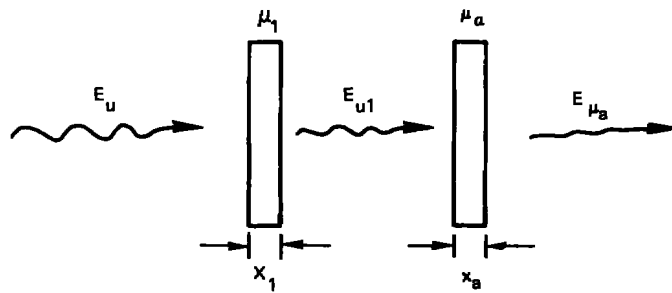


Figure E-1 Attenuation of Primary Beam By a Series of Shields

We have:

$$E_{u1} = E_u K_1 \text{EXP}(-\bar{\mu}_1 x_1) \quad (\text{E7})$$

where  $k$  = build-up factor

$$E_{ua} = E_{u1} K_a \text{EXP}(-\bar{\mu}_a x_a) \quad (\text{E8})$$

Substituting Equation (E7) into Equation (E8):

$$\text{or} \quad E_{ua} = E_u K_1 K_a \text{EXP}(-\bar{\mu}_1 x_1) \text{EXP}(-\bar{\mu}_a x_a)$$

$$E_{ua} = E_u K_1 K_a \text{EXP}[-(\bar{\mu}_1 x_1 + \bar{\mu}_a x_a)] \quad (\text{E9})$$

Substituting Equation (E6) in Equation (E9):

$$E_{ua} = \frac{W UTK_1 K_a}{b^2} \text{EXP}[-(\bar{\mu}_1 x_1 + \bar{\mu}_a x_a)]$$

Let  $E_{ua} = P$  and solve for  $W$ :

$$W = \frac{P b^2}{UTK_1 K_a} \text{EXP}(\bar{\mu}_1 x_1 + \bar{\mu}_a x_a)$$

Let  $\bar{\mu}_a$  be the attenuation of air and  $x_a = b$  the distance through air to the outer fence.

Then:

$$W = \frac{P b^2}{UTK_1 K_a} \text{EXP}(\bar{\mu}_1 x_1 + \bar{\mu}_a b) \quad (\text{E10})$$

Note.  $\bar{\mu}_a = \bar{\mu}_a$  (pressure, humidity, temperature, etc.)

Calculate W for various values of b.

$$\bar{\mu}_a \simeq 3 \times 10^{-5} \text{ cm}^{-1} \quad (\text{Ref. 9})$$

$$\bar{\mu}_1 = 0.29 \text{ cm}^{-1} \text{ (Steel)}$$

$$U = T = 1$$

$$x_1 = 7.62 \text{ cm (steel)}$$

$$K_1 = \text{Build-Up Factor} = 1.8 \text{ (steel)}$$

$$K_a = \text{Build-Up Factor} = 2.5 \text{ (air)}$$

$$P = 0.01 \text{ rad (in any 7 consecutive days)}$$

Table E-1 illustrates the results of calculations based on Equation (E10) and the above values of the U, T,  $\bar{\mu}_a$ ,  $\bar{\mu}_1$ ,  $x_1$  for the various values of b. The workload in minutes and hours was based on a 3000 rad/minute output at one meter from the source.

**TABLE E-1**  
**PRIMARY RADIATION WORKLOAD**

<u>b, Meters</u>	<u>W @ 1m rads/wk.</u>	<u>Minutes @ 3000/min.</u>	<u>Hrs.</u>
100	273.4	0.091	0.002
200	1,476.1	0.492	0.008
300	4,483.3	1.494	0.025
400	10,758.8	3.586	0.060
500	22,692.0	7.564	0.126
600	44,108.7	14.203	0.245
700	81,041.2	27.014	0.450
800	142,882.2	47.627	0.794
900	244,102.1	81.367	1.356
1000	406,794.3	135.598	2.260

#### Radiation Leakage

The protective source housing and therapeutic-type protective tube housing for X-ray therapy equipment operating at 500KV or above, have in their design a limitation on the amount of leakage radiation (0.1 percent of the useful beam dose rate,  $E_u$ , at one meter from the source). Assuming that this requirement is met in the TELS source, the weekly leakage exposure,  $E_L$ , at the point of interest which is at a distance b from the source of radiation, would be:

$$E_L = \frac{0.001 \dot{E}_u t}{b^2} \quad (\text{E11})$$



Where  $t$  is the number of minutes of beam on-time per week. Since  $\dot{E}_u t = WUT$  in R/week at one meter Equation E11 can be written:

$$E_L = \frac{WUT}{b^2} \times 10^{-3} \quad (E12)$$

Let  $E_L = P$  and solve for  $W$

$$W = \frac{Pb^2}{UT} \times 10^3 \quad (E13)$$

The leakage radiation is also attenuated by air, therefore we can write:

$$W = \left[ \frac{Pb^2}{K_a UT} \times 10^3 \right] \text{EXP}(\mu_a b) \quad (E14)$$

Let  $U = T = 1$ ,  $P = 0.01$  rads,  $\mu_a = 3 \times 10^{-5} \text{ cm}^{-1}$ ,  $K_a = 2.5$  and calculate  $W$  for leakage. The results are shown in Table E-2.

**TABLE E-2**  
**LEAKAGE RADIATION WORKLOAD**

<u>b Meters</u>	<u>W @ 1 m, rads/wk</u>
100	$5.399 \times 10^4$
200	$2.915 \times 10^5$
300	$8.854 \times 10^5$
400	$2.125 \times 10^6$
500	$4.482 \times 10^6$
600	$8.711 \times 10^6$
700	$1.600 \times 10^7$
800	$2.822 \times 10^7$
900	$4.821 \times 10^7$
1000	$8.034 \times 10^7$

### Scattered Radiation

Radiation scattered from an irradiated object has a much lower exposure rate,  $\dot{E}_s$ , than that of the incident radiation,  $E_u$ , and usually is of a lower energy. The ratio,  $\psi_o$ , of the scattered to incident exposure is a function of energy and scattering angle. The numerical values of  $\psi_o$  are given in Table B-2, Reference 7, are for a field area,  $F$ , of  $400 \text{ cm}^2$  at the scatterer surface.

Since the exposure rate  $\dot{E}_s$ , of scattered radiation, measured at one meter from the scatter is proportional to  $F$ ;

$$\dot{E}_s = \psi_o \dot{E}_u \frac{F}{400} \quad (E15)$$

The exposure from the scatterer,  $E_s$ , at the point of interest, which is at a distance of  $b$  from the scatter, is related to the scatter exposure rate at one meter,  $\dot{E}_s$ , by the following relation:

$$E_s = \frac{\dot{E}_s t}{b^2} \quad (E16)$$

Substituting for  $\dot{E}_s$ :

$$E_s = \frac{\psi_o \dot{E}_u t}{b^2} \frac{F}{400} \quad (E17)$$

Since  $\dot{E}_u$  is given in terms of the dose rate at one meter from the source, Equation E17 must be multiplied by the term  $(1 \text{ meter}/d_{sca})^2$  in the event the scatterer is located at a distance ( $d_{sca}$ ) from the source. This gives

$$E_s = \frac{\psi_o \dot{E}_u t}{b^2 (d_{sca})^2} \frac{F}{400} \quad (E18)$$

Recalling  $\dot{E}_u t = \text{WUT}$  Equation (56) can be written as:

$$E_s = \frac{\psi_o \text{WUT}}{b^2 (d_{sca})^2} \frac{F}{400} \quad (E19)$$

Solving for  $W$ , and letting  $E_s = P$ .

$$W = \frac{pb^2 (d_{sca})^2 400}{\psi_o U F} \quad (E20)$$

The scatter radiation is also attenuated by passage through air. Therefore W is given by:

$$W = \frac{p_b^2 (dsca)^2 400}{\psi_o UTF K_a} \text{EXP}(\bar{\mu}_a b) \quad (E21)$$

Selecting the maximum value of a from Table B-2, Reference 7,  $\psi_o = 9 \times 10^{-3}$ , let  $U = T = 1$ ,  $\mu_a = 3 \times 10^{-5} \text{ cm}^{-1}$ ,  $K_2 = 2.5$ , and  $P = 0.01 \text{ R}$ ,  $dsca = 3 \text{ meter}$  and  $F = 2580.64 \text{ cm}^2$ , and calculate W as a function of b. The results are given in Table E-3.

TABLE E-3  
SCATTERED RADIATION WORKLOAD

<u>b Meters</u>	<u>W @ 1m rads/wk.</u>
100	$8.369 \times 10^3$
200	$4.519 \times 10^4$
300	$1.372 \times 10^5$
400	$3.294 \times 10^5$
500	$6.947 \times 10^5$
600	$1.350 \times 10^6$
700	$2.481 \times 10^6$
800	$4.374 \times 10^6$
900	$7.473 \times 10^6$
1000	$1.245 \times 10^7$

#### Scatter of Gammas

To confirm that scatter data in Reference 7 was appropriate for TELS calculation, values of the ratio of scatter to incident radiation was calculated using equations from Ref. 9. These calculations are presented in the following.

When a photon of energy  $E_1$  undergoes Compton scattering, the energy  $E_2$  of the scattered photon obeys the relationship.

$$\mathcal{E} = \frac{E_2}{E_1} = \frac{1}{1 + \alpha_o (1 - \cos \theta)} \quad (E22)$$

where  $\alpha_o = E_1/0.51$

With  $E_1$  in MeV, and  $\theta$  is the scattering angle.

For scattering through an angle  $\theta$ , the differential cross section is:

$$\frac{d\sigma}{d\Omega} = \frac{r_0^2}{2} (\mathcal{E} - \mathcal{E}^2 \sin^2 \theta + \mathcal{E}^3) \quad (\text{E23})$$

Where  $d\sigma$  is the differential or partial microscopic cross-section for Klein-Nishina scattering.

$r_0 = e^2/mc^2$  is the classical electron radius.

For a thick absorber ( $\frac{1}{\Sigma} \ll \text{thickness}$ ) the following equation defines the ratio of the scatter to incident radiation, and scatter less than  $90^\circ$  need not be considered.

$$\frac{I}{I_0} = \frac{6.03 \times 10^{23} \rho ZC}{AX_2^2 [\Sigma_1 + \Sigma_2 (\cos \theta_1 / \cos \theta_2)]} \frac{d\sigma}{d\Omega} \quad (\text{E24})$$

$\rho$  = density

$Z$  = Atomic number

$A$  = Atomic weight

$C$  = Area of scatter

$X_2$  = Distance from slab to observer

$\frac{I}{I_0}$  = Ratio of scatter to incident radiation.

$d\sigma/d\Omega$  = Differential cross-section

$\Sigma_1$  = Microscopic cross-section of slab for incidence beam, reciprocal length

$\Sigma_2$  = Microscopic cross section of slab for incidence beam, reciprocal length

For normal incidence,  $\theta_1 = 0^\circ$ , and  
 $\cos \theta_1 = 1$

Then

$$\frac{I}{I_0} = \frac{6.03 \times 10^{23} \rho ZC}{Ax_2^2 [\Sigma_1 + \Sigma_2 / \cos \theta_2]} \frac{d\sigma}{d\Omega} \quad (\text{E25})$$

In order to compare equation E25 with the results in Reference 7, we calculated  $\frac{I}{I_0}$  for titanium and steel.

Titanium, 6 MeV incident photons and  $135^\circ$  scatter:

$$\frac{E_2}{E_1} = .04, \theta_2 = 45^\circ$$

$$E_2 = 0.24 \text{ MeV}$$

$$\rho = 4.54 \text{ gm cm}^{-3}$$

$$Z = 22$$

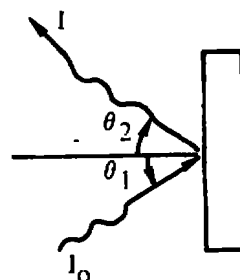
$$A = 47.9$$

$$\Sigma_2 = 0.31 \text{ cm}^{-1}$$

$$\Sigma_1 = 0.129 \text{ cm}^{-1}$$

$$C = 400 \text{ cm}^2$$

$$x_2 = 100 \text{ cm}$$



$$\frac{I}{I_0} = \frac{(6.023 \times 10^{23}) (4.54) (22) (400)}{(100)^2 (47.9) (0.129 + .31/.71)} \times 0.18 \times 10^{-26}$$

$$\frac{I}{I_0} = 0.1599 \times 10^{-3} @ 135^\circ$$

From Reference 7  $\psi_0 = 0.4 \times 10^{-3} @ 135^\circ$

For steel

$$\frac{I}{I_0} = 0.2159 \times 10^{-3}$$

This model assumes no transmission of radiation through scatterer and does not hold for  $\theta_2 \geq 90^\circ$ , and gives a scatter ratio smaller than Reference 7.

For a scatterer whose thickness is small compared to the mean free path of the gamma radiation, absorption of incident or scattered radiation can be neglected. Under these conditions, the scatterer simply becomes a uniformly distributed source of gamma radiation of energy dependent upon the scattering angle and the energy of the primary radiation.

$$\frac{I}{I_0} = \frac{6.03 \times 10^{23} \text{ mZ}}{x_2^2 A} \quad (\text{E26})$$

Where       $m$     =    mass  
                $Z$     =    atomic number  
                $A$     =    atomic weight  
                $d\sigma/d\Omega$  =    differential cross-section  
                $x_2$    =    distance to observer

For steel and  $135^\circ$  scatter.

$$\frac{I}{I_0} = \frac{(28)(6.023 \times 10^{23})(1.75 \times 10^5)(.18 \times 10^{-26})}{(100)^2 (58.71)}$$

$$\frac{I}{I_0} = 9.048 \times 10^{-3}$$

Recall, from Reference 7:

$$\psi_0 = 0.4 \times 10^{-3} \text{ at scatter angle of } 135^\circ$$

This model does not take into account any self-absorption of the scatter and results in a value higher than Reference 7.

It is felt that the scatter values for,  $\psi_0$ , in Reference 7, are appropriate for the TELS calculations.

Since the ratio of the scattered to incident radiation is a function of scatter angle, we should evaluate the workload as a function of scatter angle as well as the distance  $b$ . Using the same parameters as those used to calculate Table E-3 except holding  $b$  fixed at 300 meters and letting the ratio of the incident to scatter radiation vary with angle, we get the results shown in Table E-4.

TABLE E-4  
SCATTERED RADIATION WORKLOAD

Scatter Angle	W @ 1 m rads/wk
$15^\circ$	$1.372 \times 10^5$
$30^\circ$	$1.765 \times 10^5$
$45^\circ$	$6.862 \times 10^5$
$60^\circ$	$1.123 \times 10^6$
$90^\circ$	$2.059 \times 10^6$
$135^\circ$	$3.088 \times 10^6$

We would want the source pointed away from that direction that would likely be occupied to provide maximum W for static radiography. This would reduce the size of the mobile shielding for the primary beam as well as decrease scatter radiation toward the occupied areas.

The scatter workload given in Table E-3 are for a static source, and the highest value of  $\psi_0$ . If the centrifuge was operating then the scatter workload would be given as a weighted average over all angles.

$$W_{\text{rot}} = \frac{\alpha_1}{360^\circ} W\alpha_1 + \frac{\alpha_2}{360^\circ} W\alpha_2 + \dots + \frac{\alpha_i}{360^\circ} W\alpha_i + \dots \quad (\text{E27})$$

Where

$$\begin{aligned} W_{\text{rot}} &= \text{scatter workload for centrifuge rotation.} \\ W\alpha_i &= \text{scatter workload over included angle } \alpha_i. \\ \alpha_i &= \text{included angle over which scatter is calculated.} \end{aligned}$$

For example, we use Table E4 and assume  $W\alpha_1 = W$  calculated for  $30^\circ$  and is good for angles between  $+15^\circ$  and  $+30^\circ$  and  $-15^\circ$  and  $-30^\circ$ .

$$\text{The } \alpha_1 = 30^\circ$$

$$\text{and } \frac{\alpha_1}{360^\circ} = 0.083$$

$$W\alpha_1 = 1.794 \times 10^5$$

Using Table E4 we can write

$$\begin{aligned} W_{\text{rot}} &= 0.083 (1.372 \times 10^5 + 1.765 \times 10^5 + 6.862 \times 10^5 + 11.23 \times 10^5) \\ &\quad + 0.167 (20.59 \times 10^5) \\ &\quad + 0.500 (30.88 \times 10^5) \end{aligned}$$

$$W_{\text{rot}} = 2.064 \times 10^6 \text{ rads/wk @ one meter}$$

We can see that  $W_{\text{rot}}$  at 300 meters is much larger than  $W$  calculated in Table E3 at 300 meters.

@ 300 meters and  $U = T = 1$ , we have,

$$W_{\text{rot}} = 2.064 \times 10^6$$

$$W_{\text{Table E3}} = 1.372 \times 10^5, \psi_0 = 9 \times 10^{-3}$$

When the centrifuge is rotating the contribution of the scatter to the total dose at the outer fence would be smaller than considered in Table E3.

All calculations so far have assumed  $U = T = 1$ . When the centrifuge is in operation, this is not the case for  $U$ . For primary, leakage, and scatter radiation,  $T$ , the occupancy factor at the outer fence should be  $1/4$  or less. When the centrifuge is rotating  $U$  for the primary beam is given by the ratio of the beam angle in degrees to  $360^\circ$ . Assuming a maximum beam angle of  $8^\circ$  (50.4 cm diameter field at 3.6 meters from the source).

$$U = \frac{8^\circ}{360} = 0.022$$

For leakage,  $U = 1$  all the time.

For scatter,  $U = 1$  all the time.

Tables E-1 through E-3 should be revised to take these more realistic values of  $U$  and  $T$  into account. This new data is presented in Table E-5.

TABLE E-5  
PRIMARY, LEAKAGE, SCATTER WORKLOAD

b meters	Rads/week at 1 meter			
	W(Primary)	W(Leakage)	W(Scatter)	Wrot (Scatter)
100	$4.971 \times 10^4$	$2.160 \times 10^5$	$3.348 \times 10^4$	
200	$2.689 \times 10^5$	$1.166 \times 10^6$	$1.808 \times 10^5$	
300	$8.151 \times 10^5$	$3.542 \times 10^6$	$5.490 \times 10^5$	$8.256 \times 10^6$
400	$1.956 \times 10^6$	$8.499 \times 10^6$	$1.317 \times 10^6$	
500	$4.126 \times 10^6$	$1.793 \times 10^7$	$2.779 \times 10^6$	
600	$8.020 \times 10^6$	$3.485 \times 10^7$	$5.401 \times 10^6$	
700	$1.473 \times 10^7$	$6.402 \times 10^7$	$9.924 \times 10^6$	
800	$2.598 \times 10^7$	$1.129 \times 10^8$	$1.750 \times 10^7$	
900	$4.438 \times 10^7$	$1.928 \times 10^8$	$2.989 \times 10^7$	
1000	$7.396 \times 10^7$	$3.214 \times 10^8$	$4.981 \times 10^7$	



The minimum workload is given by the primary beam. We are interested in what the contributions to the total dose the scatter and leakage radiation are for a workload defined by the primary beam calculations. Let  $W_p$ ,  $W_L$ , and  $W_s$  be the workloads calculated for the primary beam, leakage, and scatter radiation respectively. Then for a workload  $W_p$ , the total dose at the outer fence will be given by:

$$\begin{aligned} \text{Total Dose} &= 0.01 + \frac{W_s}{W_L} 0.01 + \frac{W_s}{W_p} 0.01 \\ &= 0.01 \left( 1 + \frac{W_s}{W_L} + \frac{W_s}{W_p} \right) \end{aligned} \quad (\text{E-28})$$

Using Table E-5 we obtain the total dose for workload  $W_p$  at various  $b$ . The results are given in Table E-6.

TABLE E-6  
TOTAL DOSE AT OUTER FENCE

<u>b Meters</u>	<u>Total Dose (rads)</u>	<u>@ 1 m rads/wk. Workload W (primary)</u>
100	0.018	$3.348 \times 10^4$
200	0.018	$1.808 \times 10^5$
300	0.018	$5.490 \times 10^5$
400	0.018	$1.317 \times 10^6$
500	0.018	$2.779 \times 10^6$
600	0.018	$5.401 \times 10^6$
700	0.018	$9.924 \times 10^6$
800	0.018	$1.750 \times 10^7$
900	0.018	$2.989 \times 10^7$
1000	0.018	$4.981 \times 10^7$

The total dose at 300 meters is greater than the 0.01 rads for an uncontrolled area, therefore, the workload must be restricted. Since the contribution from the primary beam is about 20 times that for leakage and 23 times that for scatter a good estimate of workload can be obtained as follows:

$$\begin{aligned}\frac{W_s}{W} &= \frac{0.018}{0.010} \\ W &= \frac{0.010}{0.018} W_s \\ &= \frac{0.010}{0.018} (5.49 \times 10^5) \\ W &= 3.002 \times 10^5 \text{ rads/wk. at 1 meter}\end{aligned}\tag{E-29}$$

Given a source with an output of 3000 rads/minute at 1 meter this would permit a beam on time of 789.6 minutes/wk. or 13.16 hrs/wk with the outer fence at 300 meters. Average beam on time at P&WA's engine radiography facility has been approximately 25 hrs/year.

Equation (29) was applied to the remaining data in Table E-6 and the resulting workloads as a function of distance, b, is given in Table E-7.

**TABLE E-7**  
**WORKLOAD AT VARIOUS DISTANCES**

<u>b Meters</u>	<u>Rads/wk @ 1 m</u>	<u>hrs @ 3000 rads./min</u>
100	$1.860 \times 10^4$	0.103
200	$1.004 \times 10^5$	0.558
300	$3.002 \times 10^5$	1.694
400	$7.317 \times 10^5$	4.065
500	$1.544 \times 10^6$	8.577
600	$3.001 \times 10^6$	16.670
700	$5.513 \times 10^6$	30.630
800	$9.722 \times 10^6$	54.01
900	$1.661 \times 10^7$	92.25
1000	$2.767 \times 10^7$	153.7

The calculation of the workload for various distances to the outer fence presented in Table E-7 are approximations based on values of build-up factors and absorption coefficients that are assumed to adequately describe the attenuation of the X-radiation from the source. In reality, the source spectrum is a continuum. The variation of X-ray intensity with energy for various electron beam energies is shown in Figure 21. To account for this variation, a more extensive calculation of the workload at 300 meters was done taking into consideration the variation of intensity, absorption coefficient, and build-up factor with energy. An electron beam energy of 10 MeV was chosen for the source, and the 10 MeV curve from Figure 21 was used to determine the contribution to the total output at particular energy intervals. Values for the absorption coefficients and build-up factors at various energies were obtained from Reference 12. The procedure used to calculate the workload is as follows:

The 10 MeV energy range was broken into nine energy intervals of 1.1 MeV. The contribution to the total intensity of each interval was determined from the 10 MeV curve in Figure 21. These values are given in Table E-8

**TABLE E-8**  
**SPECTRAL CONTRIBUTION TO INTENSITY**  
**FOR 10 MeV BREMSSTRAHLUNG**

Interval Central Energy, MeV	Percent of Total Intensity
0.55	21.7
1.65	17.6
2.75	15.2
3.85	12.9
4.95	10.7
6.05	9.3
7.15	7.0
8.25	4.3
9.35	0.7

Equation (E-10) was used to calculate the workload in each interval required to produce the maximum permissible dose of 0.01 rad per week for the outer fence at 300 meters. The appropriate values of build-up factor and absorption coefficient of steel and air were used for each interval. The results are presented in Table E-9:

TABLE E-9

**SPECTRAL WORKLOAD REQUIRED TO PRODUCE AN EXPOSURE OF  
0.01 RAD/WEEK FOR 10 MeV ELECTRON BEAM AND OUTER FENCE AT  
300 METERS**

<u>Interval Central Energy, MeV</u>	<u>Workload Rads/Wk. @ 1 Meter</u>
0.55	34,174
1.65	10,570
2.75	7,942
3.85	6,918
4.95	6,483
6.05	6,459
7.15	6,644
8.25	6,578
9.35	6,741

The smallest workload in Table E-9 is for the 6.05 MeV interval. From Table E-8 we know that to achieve this workload at the 6.05 MeV interval, we would have to operate to a significantly larger total workload. That workload is calculated using the following equation:

$$W_T = \frac{6459 \text{ Rad/wk}}{0.093} = 69452 \text{ rad/wk} = \text{one meter}$$

Where 0.093 comes from Table E-8 and 6459 rads/wk comes from Table E-9. Since this value of total workload gives a dose at 300 meters of 0.01 rads for the 6.05 MeV interval, it will be too large when the contributions of the other intervals are added to it. The total dose,  $P_T$ , is given by the following equation.

$$P_T = 0.01 \left[ \frac{L_1 W_T}{W_1} + \frac{L_2 W_T}{W_2} + \dots + \frac{L_i W_T}{W_i} \dots \right]$$

Where

$W_T$  is the total workload

$W_i$  is the workload in the energy interval  $i$

$L_i$  is the fraction of the total intensity contributed by the energy interval  $i$ .

At this point, an iterative technique was employed to determine the workload,  $W_T$ , required to give the total dose,  $P_T$ , equal to the maximum permissible dose. The initial calculated value of  $W_T$  was used as a start point. It was determined that a workload of 9000 rad/wk at one meter produced a calculated  $P_T$  of 0.010 rads. This is about twice as large as the value given for 300 meters in Table E-1. It is felt that this technique of calculation is more accurate than that used for Table E-1 and that the results generated from Table E-1 are very conservative.

The leakage workload was not re-evaluated because the workload based on leakage was 6.45 times the scatter workload and, therefore, a small contribution to the total dose.

The scatter contribution at 300 meters was re-evaluated taking into account the variation in energy with angle and its effect on the absorption coefficient and build-up factor. The results are shown in Table E-10.

**TABLE E-10**  
**X-RAY SCATTER WORKLOAD AS A**  
**FUNCTION OF SCATTER ANGLE**

Scatter Angle Deg.	Workload Rads/Wk @ 1 meter
15	$2.64 \times 10^5$
30	$3.63 \times 10^5$
45	$9.87 \times 10^5$
60	$3.13 \times 10^6$
90	$1.05 \times 10^7$
135	$3.66 \times 10^7$

The values for scatter workload at 300 meters given in Table E-10 are approximately 2 times greater than those given in Table E-4. Again the rougher approximation gave a more conservative value for workload.

The value of the weighted average scatter workload is found in the same manner as before using Equation (E-27). This gives a value:

$$W_{\text{rot}} = 2.045 \times 10^7 \text{ rad/wk. at one meter}$$

This is roughly ten times the value previously calculated for  $W_{\text{rot}}$ .

Using the same technique employed earlier to calculate the workload, we calculated a workload based on this more exact computation of scatter and primary. The values of primary beam workload was adjusted for  $U = 0.022$  and  $T = 0.25$ . Scatter and leakage workloads were adjusted for  $U = 1$  and  $T = 0.25$ . This is given in Table E-11.

**TABLE E-11**  
**PRIMARY, LEAKAGE, SCATTER RADIATION**  
**WORKLOAD FOR 10 MeV AND 300 METERS**  
(rads/wk @ 1 meter)

<u><math>W_p</math></u>	<u>WL</u>	<u><math>W_s</math></u>	<u><math>W_{\text{rot}}</math></u>
$1.636 \times 10^6$	$3.542 \times 10^6$	$1.056 \times 10^6$	$8.180 \times 10^7$

A workload of  $5.40 \times 10^5$  rads/wk at one meter is given based on  $W_s$  in Table E-11. This translates to 3.00 hours per week for a 3000 rad/min at one meter output.

A workload based on  $W_{rot}$  in Table E-11 is  $1.104 \times 10^6$  rads/wk at one meter. This translates to 6.13 hours per week for the same source.

The workload based on  $W_s$  would be utilized for exposures with the centrifuge static and the workload based on  $W_{rot}$  would be appropriate for exposures when the centrifuge is in operation.

In actual practice the X-ray beam will be directed into the ground a great deal of the time. An additional safety margin can be obtained by restricting the center of the X-ray beams to angles  $8^\circ$  below the horizontal.

The total workload calculated for distances,  $b$ , is for operation of the source with the centrifuge in motion and 7.62 cm of steel in the primary beam. With the test engine in place additional attenuation will take place and the total permissible workload will be greater than calculated.

### Static Centrifuge

With the X-ray source static and the arrangement shown in Figure 38, we can calculate the additional shielding required in the primary beam to permit the same workload  $3 \times 10^5$  to be maintained as in the operational case.

Recalling Equation E-10, expanding to include a third shield and letting  $U = 1$ ,  $T = 1/4$ ,  $W = 3 \times 10^5$  rads/wk. at 1 meter, we can calculate the additional thickness of lead required.

$$W = \frac{P_b^2}{UTK_1 K_2 K_a} \text{EXP} (\bar{\mu}_1 x_1 + \bar{\mu}_2 x_2 + \bar{\mu}_a b)$$

solve for  $x_2$

$$\text{EXP} (\bar{\mu}_2 x_2) = \frac{W UTK_1 K_2 K_a}{P_b^2} \text{EXP} [-(\bar{\mu}_1 x_1 + \bar{\mu}_a b)]$$

$$x_2 = \frac{1}{\bar{\mu}_2} \left[ \ln \frac{UTKW}{P_b^2} - (\bar{\mu}_1 x_1 + \bar{\mu}_a b) \right]$$

$$x_2 = \frac{1}{0.502} \left[ \ln \frac{3 \times 10^5 (1.8) (2.5) (1.6)}{4 (0.01) (300)^2} - \{0.29 (7.62) + 3 \times 10^{-5} (3 \times 10^4)\} \right]$$

$$x_2 = 6.55 \text{ cm}$$

Therefore 6.55 cm of lead is required to maintain the  $3 \times 10^5$  rad/wk. workload calculated for a permissible dose of 0.01 rads/wk. at the outer fence located 300 meters from the center of rotation of the centrifuge. The area and therefore the total weight of lead required depends upon the distance of the shield from the source, and the primary beam angle. Assuming a beam angle of  $8^\circ$  and a distance of 762 cm we have a beam radius given by:

$$x = 762 \tan \frac{8}{2}$$

$$= 53.284 \text{ cm}$$

$$\text{Area} = \pi x^2 = 8919.64 \text{ cm}^2$$

$$\text{Volume} = 5.84 \times 10^4 \text{ cubic cm.}$$

$$\begin{aligned} \text{Weight} &= \left( 11.35 \frac{\text{gm}}{\text{cm}^3} \right) \left( 5.84 \times 10^4 \text{ cm}^3 \right) \\ &= 6.631 \times 10^5 \text{ gm} \\ &= 6.631 \times 10^2 \text{ kg} \end{aligned}$$

For a workload of  $3 \times 10^5$  rad/wk at 1 meter and the static centrifuge situation, the dose at the outer fence 300 meters from the center of rotation of the centrifuge will be from Table E-4 and Equation (E-28).

$$\text{Dose} = 0.01 \frac{W_s}{W_{s\theta}} + \frac{W_s}{W_L}$$

Where

$W_{s\theta}$  = Workload at angle  $\theta$  from Table E-4 and corrected for  $T = 0.25$

<u>Scatter Angle</u>	<u>Dose rads</u>
15°	0.006
30°	0.005
45°	0.002
60°	0.002
90°	0.001
135°	0.001

For the specified conditions no problem exists due to scatter or leakage radiation in the static centrifuge condition. The shielding required for personnel within the control room depends upon the distance of the control room from the X-ray source, its geometry and whether it is on the surface or underground. We will assume that the control room is about 37 meters from the center of rotation of the centrifuge and underground. This situation is illustrated in Figure E-2. A worst case would be with the centrifuge static and the beam aligned as shown. In this case  $U = T = 1$ .

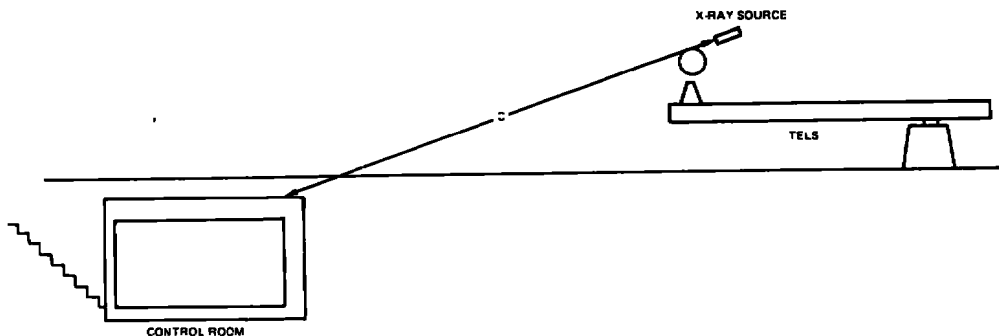


Figure E-2 Relationship of Control Room to X-ray Source

The workload at 1 meter after traversing 7.62 cm of steel becomes:

$$\begin{aligned}
 W_s &= WK \text{ EXP } (-\bar{\mu}_1 \times 1) \\
 &= 3 \times 10^5 (1.8) \text{ EXP } [-(0.29) 7.62] \\
 &= 5.925 \times 10^4 \text{ Rads/wk @ 1 meter}
 \end{aligned}$$

Recalling Equation E-4 we have

$$B_{ux} = Pb^2/WUT$$

Substituting appropriate values gives

$$B_{ux} = \frac{0.01 C^2}{5.925 \times 10^4}$$

Now  $C \approx 27$  meters, and is defined in Figure E-2

$$B_{ux} = 1.23 \times 10^{-4}$$



Referring to Reference 7, we see that for this value of  $B_{ux}$  we require about 152 cm of concrete. The fact that the X-ray intersects the concrete at an angle has not been considered in these calculations. If it were, (the angle of incident considered,  $26^\circ$ ), the ceiling thickness would be approximately 67 cm thick and the wall toward the centrifuge would be approximately 137 cm.

When we take into account the rotation of the centrifuge,  $U = 0.022$ , and  $W_s$  becomes:

$$W_s = 1.304 \times 10^3$$

and

$$B_{ux} = 5.593 \times 10^{-3}$$

This gives a thickness of concrete required for a dose of 0.01 rad/wk of 89 cm.

Taking into account the angle of incident of the primary beam we obtain a ceiling thickness of 39 cm and a front wall thickness of 80 cm. Attenuation of the soil covering the control room would reduce the concrete thickness requirements but the amount would depend upon the depth of the control room and this has not been considered.

A suggested approach to construction is to utilize the values of concrete thickness calculated for  $U = 1$ ,  $T = 1$  and no angle of incident correction. This would give 152 cm of concrete in the ceiling and front wall, use half this thickness in the end walls and whatever is structurally required in the wall away from the X-ray source. The entire structure should be about 2 meters below ground level. These calculation should be confirmed by a qualified Health Physicist prior to construction.

Among the failure modes that might occur that would cause radiation levels higher than those expected under normal operation are: (1) engine detachment from the centrifuge during testing; (2) local shielding at the detector not installed or failure of shielding during testing; (3) local shielding for static radiography not in place; (4) X-ray beam not aligned with the local shielding during static radiography; and (5) failure of safety circuits.

There are two major ways in which engine detachment could occur and cause higher than normal radiation, the engine breaking loose or exploding. In either case the radiation shielding attached to the positioning system would have to be broken or moved or the X-ray source repositioned, so that the primary beam was not directed at the shielding before the dose rate could be exceeded at the fence or in the control room. A combination of micro-switches and pressure transducers could be included in the safety interlock circuits that would sense this type of failure and shut the source down. However, the easiest approach would be to manually shut down the X-ray source in the event it was still operating.

The local shielding at the detector, as previously mentioned, should be made a permanent part of the detector positioning system. When the detector is positioned in the beam, the shielding will be positioned in the beam. Without synchronous operation of the detector and source, the radiographer would have to insure that the two are always properly aligned.

For radiography with the centrifuge static, the primary barrier mounted on the mobile service module should be positioned away from the nearest occupied area and the X-ray source and centrifuge moved so that the primary beam is directed toward the mobile shield. Since all static radiography could be done with the engine in a horizontal position normal to the centrifuge, a set of two limit switches in the safety circuit could be utilized to insure that the beam and shield were properly aligned. One limit switch to sense the correct centrifuge angular position and one to sense the shield position. An angular rate meter previously discussed is required to insure that the source cannot be activated when the centrifuge is not aligned toward the shield unless the centrifuge is rotating.

The failure of the safety circuits can be minimized by redundancy if the cost is not prohibitive. However, no reasonable failsafe system is obvious. Operator surveillance appears the most feasible approach to preventing excessive dose from circuit failure.

With proper design of safety interlocks and emergency off circuits, none of the failure modes considered would be likely to create a hazardous condition at the outer fence 300 meters from the centrifuge for the workload calculated.

### **Impact of Radiation on Wildlife**

There are three easily defined areas associated with the facility as defined by Figure 37: The area near the centrifuge and within the inner fence, the area between the inner fence and outer fence, and the area beyond the outer fence. Regardless of the distance to the outer fence, if the appropriate workload is maintained, the radiation levels are low enough to be of no consequence to personnel or wildlife. The area within the inner fence will normally realize the highest radiation because of the close proximity to the X-ray source. This area should be kept as small as possible and clear of natural cover so that the area can be adequately secured prior to the generation of X-rays. Under these conditions the area will not be conducive to wildlife. Specifically when the centrifuge and/or engine are in operation sufficient noise will be generated to discourage occupation of the area by wildlife.

The area between the inner and outer fences will be the likely habitate of wildlife. The occupancy factor (T) of this area for wildlife would be difficult to determine. Assuming 0.25 as for previous calculations and the workload for an outer fence radius of 300 meters the average dose in any 7 consecutive days would be roughly 0.5 rads.

Reference 10 indicates that in guinea pigs, mice and rabbits exposed to 1.1 and 0.11 rads per 8 hr. day no significant change in mean survival time was found from that of nonirradiated control groups. Total exposure accumulated during the experiments were varied but averaged 1000 rads. The 0.5 rad/wk. nominal dose in the area between the inner and outer fences should cause no significant damage to animals of this type. Total yearly dose in this same area (assuming maximum permitted workload) would be approximately 26 rads. This low level delivered at the rate of 0.5 rads per week to an animal of this type or an animal the size of a deer appears to present no problem. In fact dose levels of this magnitude are commonly encountered in medical applications involving humans.

### **Operating and Safety Procedures**

Detailed written operating and safety procedures are required for a radiographic testing facility. These procedures should include descriptions of the hazards encountered in operating the equipment, procedures to be followed in case of emergencies, safety procedures, safety inspections, etc. Guidelines are established in Reference 5 and 6 for these procedures. Specific procedures depend upon the construction details of the facility, the facility radiation survey and the safety interlock system and should be written after the design of the system is firm.

## APPENDIX F

### TELS LOADS ON THE LINEAR ACCELERATOR

In the design of X-ray equipment for the on-arm concept, as much of the equipment as possible should be placed off the arm or at the center of rotation. This will accomplish two things. It will reduce the forces acting on the power supply and cooling pumps as well as reduce the amount of weight which must be supported by the hinge-gimbal positioner.

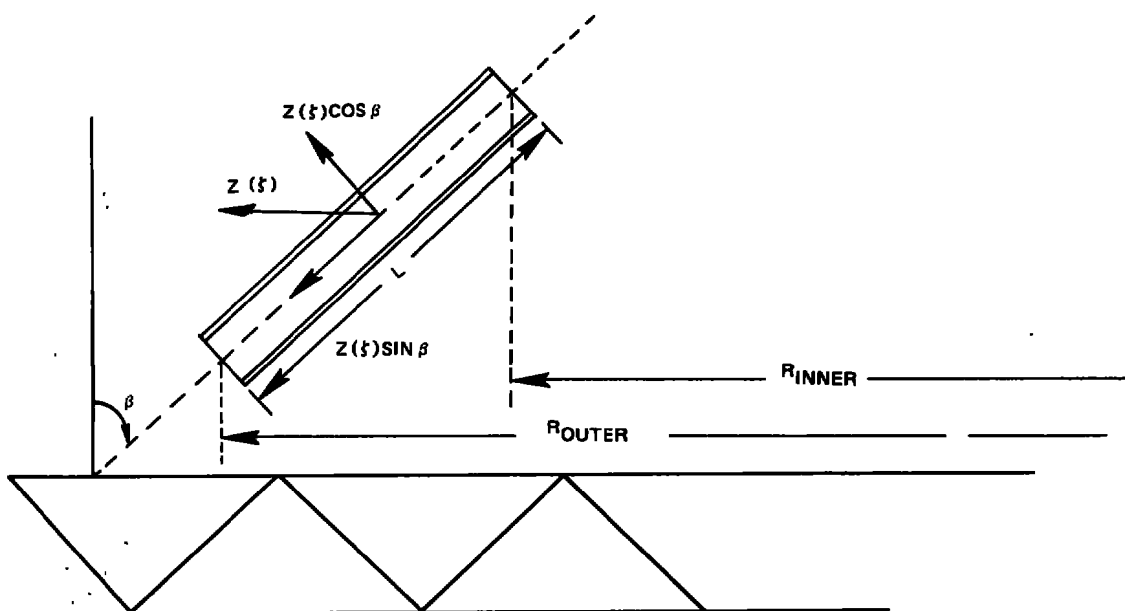
One of the concepts being considered would have the various components of the conventional X-ray unit situated on the hinge-gimbal positioner. This would require that the equipment sustain the same loads being exerted on the engine with no resultant deflection in any system component. The most critical components when positioned in this manner are the waveguide, accelerator, and R-F oscillator. The positioning flexibility required of the radiographic system is developed in Appendix C.

Although no accelerator design has been formulated it is most likely that the accelerator will be approximately 0.7 meters long with a circular cross-section 7.62 cm in diameter. The accelerator cylinder will have to be attached to the X-ray support frame securely in order to prevent deflection during the various hinge-gimbal orientations. The loading on the accelerator will not be uniform because of the linear acceleration gradients present at different centrifuge radii.

There are two components of the centrifugal force induced by the centrifuge that will contribute to the stress distribution of the accelerator structure. Tensile forces acting along the central axis of the accelerator will create axial stresses. The diameter of the accelerator is small, relative to the portion of the centrifuge arm, which the accelerator might span. This means that the linear acceleration gradient across any cross-section of the accelerator unit will be negligible. If there is no variation in the linear acceleration then the axial stress distribution will be uniform and no bending moments will result. On the other hand, the component of the centrifugal force which is perpendicular to the central axis of the accelerator will result in a bending moment when we correctly account for the support reactions.

A complete stress analysis to determine the extent to which the cylindrical accelerator structure will deflect can be quite complicated. Rather than perform a complete analysis, we will determine whether or not major problems in a support system can be expected. In some X-ray source positions a considerable side load will be exerted on the accelerator while in others a combination of side and compressive loads will act on the accelerator. The accelerator will also be evacuated so it will be subjected to an external pressure loading due to the atmosphere. This will effect the cylinder's behavior when considering its resistance to buckling loads created by the axial loading which occurs in some source positions.

We can first consider the side load exerted on the cylinder. Letting  $\beta$  be the angle the accelerator central axis makes with the vertical, the centrifugal force has two components. One component lies perpendicular to the central axis and the other lies along the central axis as shown below:



$\xi$  is the distance variable along the accelerator and  $Z(\xi)$  is the centrifugal acceleration in g's at the given point along the accelerator. The side loads are due to the acceleration component  $Z(\xi) \cos \beta$  and the axial loads are due to  $Z(\xi) \sin \beta$ .

We now define the mass distribution of the accelerator as mass per unit length. The side load is then a body force which is expressed by:

$$w = \frac{W'}{Lg} Z(\xi) \cos \beta$$

Where  $w$  is the side load in lbs. per unit length along the accelerator. The axial loading is similarly defined as:

$$p = \frac{W'}{Lg} Z(\xi) \sin \beta$$

Where  $W' = \text{weight of accelerator}$   
 $L = \text{length of accelerator}$

The centrifugal acceleration exerted by the centrifuge is defined by:

$$Z(\xi) = \Omega^2 R(\xi)$$

Where  $R(\xi)$  is the radius at any point along the accelerator defined by:

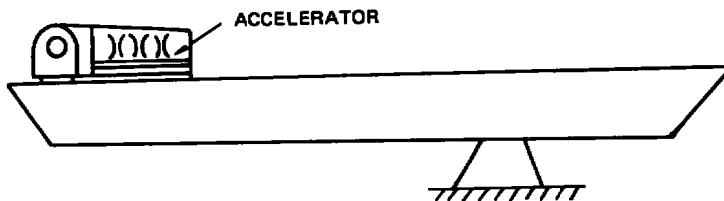
$$R(\xi) = \left( \frac{R_{\text{inner}} - R_{\text{outer}}}{L \sin \beta} \right) \xi + R_{\text{outer}}$$

and, therefore, the centrifugal acceleration per unit length of the accelerator structure becomes:

$$Z(\xi) = \Omega^2 \left[ \left( \frac{R_{\text{inner}} - R_{\text{outer}}}{L \sin \beta} \right) \xi + R_{\text{outer}} \right]$$

Where  $R_{\text{inner}}$  and  $R_{\text{outer}}$  are as shown in the previous diagram.

The worst position for the accelerator with regard to axial loading is when it is parallel to the centrifuge radius arm as shown below:



This corresponds to a value of  $90^\circ$  for the angle  $\beta$ . Due to the acceleration gradient along the centrifuge radius line, the axial loading of the accelerator in this position will be a linear function. We can assume a worst case by equating this distributed axial load to a concentrated compressive load equal to the weight of the accelerator when exposed to the centrifugal force at the maximum radius. Three possible accelerator materials were considered; steel, aluminum, and copper. Their material properties are shown below:

#### MATERIAL PROPERTIES

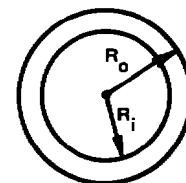
	<u>MODULUS OF ELASTICITY</u> (newtons/cm <sup>2</sup> )	<u>DENSITY</u> (gm/cm <sup>3</sup> )	<u>YIELD STRENGTH</u> (newtons/cm <sup>2</sup> )
Steel	$2.00 \times 10^7$	7.8339	$2.69 \times 10^4$
Aluminum	$7.24 \times 10^6$	2.699	$3.45 \times 10^4$
Copper	$1.10 \times 10^7$	8.968	$2.76 \times 10^4$

The section properties for a cylindrical accelerator structure 7.62 cm in diameter, 76.2 cm long with 0.635 cm sidewalls are shown below:

$$J = \frac{\pi}{4} (R_o^4 - r_i^4) = 85.75 \text{ cm}^4$$

$$\text{Area} = \pi (R_o^2 - r_i^2) = 13.94 \text{ cm}^2$$

$$\text{Volume} = \text{Area} \times L = 1062 \text{ cm}^3$$



The accelerator can be considered a very long monocoque cylinder. The term monocoque cylinder means a thin walled cylinder without longitudinal skin stiffeners or transverse intermediate frames attached to the cylinder skin. If the monocoque cylinder is long, then such cylinders buckle by overall column instability or act as a Euler type column.

We proceed with a buckling analysis of the Euler column shown below:



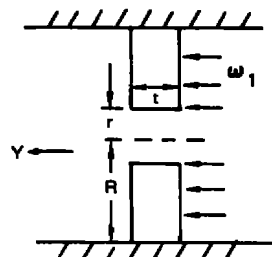
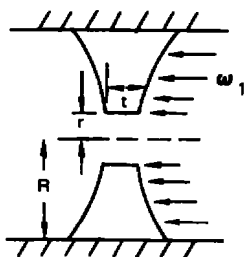
$$P_{crit} = \frac{4\pi^2 E I}{L^2}$$

which approximates the fixed end supports necessary for the accelerator. The results are shown below:

	$P_{crit}$ (kg)	WEIGHT AT 15 G'S
Steel	$1.188 \times 10^6$	124.74
Aluminum	$4.305 \times 10^5$	42.98
Copper	$6.532 \times 10^5$	142.84

These results show that the axial loading exerted by the centrifuge on the accelerator will not be enough to cause any buckling deflections. Comparing the critical loads ( $P_{crit}$ ) to be apparent increased weight of the accelerator we see that loads exerted on the accelerator are far from those necessary for buckling to occur.

The accelerator also contains several bulkheads which separate the unit into several cavities. When the accelerator is parallel to the centrifuge radius then these circular plates will be subject to a uniform distributed load. This load is due to the centrifugal force acting on the plane itself. In reality the plate is a double concave body with a hole in the center. As a worst approximation, we will consider the plate to be of a uniform thickness. The thickness chosen will be the minimum thickness of the concave plate and thus the deflection produced will be the maximum possible. This approximation is shown below:



$$t = 0.635 \text{ cm}$$

$$r = 0.635 \text{ cm} \quad \frac{R}{r} = 5$$

$$R = 3.175 \text{ cm}$$

The equation for the maximum deflection of a fixed edge plate is:

$$y_{\max} = 0.176 \frac{\omega_1 R^4}{E^* t^3}$$

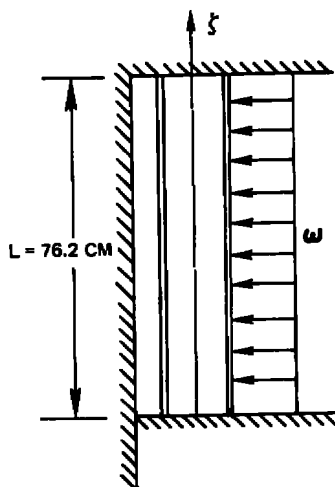
Where  $\omega_1$  is the weight per unit surface area of the plate. If  $\rho$  is the density of the material then  $\omega_1 = \rho t \ddot{z}$  where  $\ddot{z}$  is the linear acceleration imposed on the accelerator by the centrifuge.

We can evaluate the deflection for several proposed materials.

	$\omega_1$ (newton/cm <sup>2</sup> )	$y_{\max}$ (mm)
Steel	0.731	$2.54 \times 10^{-5}$
Aluminum	0.252	$2.428 \times 10^{-5}$
Copper	0.838	$5.304 \times 10^{-5}$

The results show that the deflection of this bulkhead is small enough to be considered negligible.

For small angles of  $\beta$  the accelerator structure will be subject to a side load. This load will be a near constant distributed load. It is felt that in the final design of the on-arm source positioner the accelerator will have to be secured well, especially at either end, in order to minimize the lateral deflections. An estimate of the deflection of the cylinder can be made by assuming a uniform load due to the maximum centrifugal acceleration. A diagram of the worst loading for the accelerator is shown below:



$$J = 85.74 \text{ cm}^4$$

$$y(\xi) = \frac{\omega \xi^3 (L - \xi)}{24 E^* J}$$

$$y_{\max} = \frac{\omega L^4}{384 E^* J}$$



The maximum side load is represented by the following expression:

$$\omega = \rho A \ddot{z}$$

Where:

$\rho$  = density of the accelerator material.

$A$  = Accelerator cross-sectional area.

$\ddot{z}$  = linear acceleration exerted on the accelerator by the centrifuge in g's.

As previously determined  $A = 13.935 \text{ cm}^2$ . The design linear acceleration limit of the centrifuge is 15 g's. Therefore, the side load becomes.

$$\omega = \rho (13.935)(15) = 209.025 \rho$$

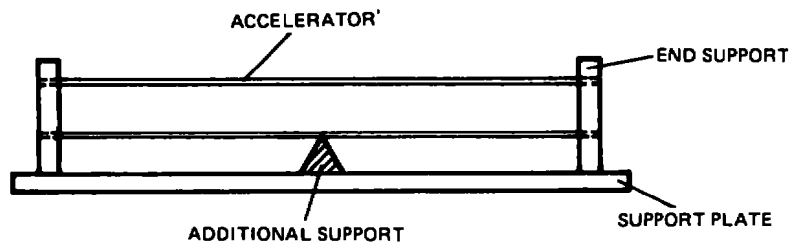
The maximum deflection of the accelerator can now be estimated for three different materials.

	$\omega$ (newton/cm)	$y_{\text{max}}$ (mm)
Steel	16.06	0.0082
Aluminum	5.532	0.0078
Copper	18.384	0.0071

The above analysis indicates that if the ends of accelerator are secured so as to allow the minimum amount of motion then the deflection, due to lateral loading, is less than 0.0254mm.

#### LINEAR ACCELERATOR END SUPPORTS

Additional support would be necessary to minimize lateral deflections of the end supports which would hold the accelerator to the X-ray support frame. Such support could be provided by a flat plate to which the end supports are attached. In addition an extra support could be added to brace the center of the accelerator structure. This is shown below:



The support plate will also be subjected to the same centrifugal forces as the accelerator structure. In sizing this plate a trade-off between the inertial loading due to the plate's thickness and the effect of the thickness on the stiffness of the plate must be considered.

A worst case can be considered for the support plate when all four sides are simply supported and not fixed. Side support could be provided by "I" beams that are affixed to each of the long ends of the plate. The support plate is assumed being 76.2mm long and 12.7mm wide. The objective is to find the smallest thickness which results in light weight and is accompanied by an acceptably small plate deflection for the accelerator end supports.

For a plate simply supported on all edges and under a uniform load  $\omega$  in newtons/cm<sup>2</sup>, the maximum deflection which occurs at the center of the plate is found to be:

$$y_{\max} = \frac{\alpha \omega b^4}{E * t^3}$$

Where:

- $\alpha$  = 0.1421 for a plate with aspect ratio greater than 5.
- $b$  = width of short side of plate.
- $t$  = plate thickness.

The worst inertial load is produced in the 15g field where the distributed load on the plate will be:

$$w = \rho t (15)$$

$$\therefore y_{\max} = 0.1421 \frac{\rho t b^4}{E * t^3} = 0.1421 \frac{\rho (15) b^4}{E * t^2}$$

For Steel:

$$\begin{aligned} E * &= 2.00 \times 10^7 \text{ newton/cm}^2 \\ \rho &= 7.833 \text{ gm/cm}^3 \end{aligned}$$

The maximum deflection will depend upon the plate thickness. For a 0.64cm thick plate the deflection would be 0.005mm.

The deflection for a 0.64cm steel plate is small enough so that it would be adequate. Another support system could be substituted for the plate as long as its structural rigidity is equivalent to 7.62cm x 12.7cm x 0.64cm steel plate. For example, a steel honeycomb structure could be substituted for the steel plate. This would save weight as well as reduce the load on the X-ray positioner.

## UPPER CASE LETTER SYMBOLS

A	atomic weight
$A_a B_b$	chemical formula for a compound (eg. $H_2O$ )
B	$ \vec{B} $
$\vec{B}$	magnetic induction
$B_{ux}$	radiation transmission factor
C	constant
D	photographic density
$\vec{D}$	rotor displacement vector
$D_y$	component of $\vec{D}$ along y-axis
$D_z$	component of $\vec{D}$ along z-axis
$\vec{D}_g$	rotor deflection vector due to gyroscopic moment
$\vec{D}_a$	rotor deflection vector due to linear acceleration
$\left(\frac{dE}{dt}\right)_{tot}$	total electron energy loss gradient
E	electron energy
E Plane	a plane normal to the electric field vector
$E'$	x-ray exposure
$\hat{E}$	electric field
$E^*$	modulus of elasticity
$E_L$	weekly leakage radiation exposure
$E_u$	weekly radiation exposure
$\dot{E}_u$	exposure rate
$E_0$	energy of incident electron

$E_1$	energy of incident photon
$E_2$	energy of scattered photon
$F$	force
$G$	length
$G_D$	Slope of x-ray film sensiometric curve
H Plane	a plane normal to the magnetic intensity vector
$\bar{H}_A$	angular momentum of the turbine engine rotor in the xyz coordinate system
$(H_A)_x$	the component of $\bar{H}_A$ along the x-axis
$(H_A)_y$	the component of $\bar{H}_A$ along the y-axis
$(H_A)_z$	the component of $\bar{H}_A$ along the z-axis
$I$	transmitted x-ray intensity
$\hat{I}$	unit vector along the x-axis
$I_0$	incident x-ray intensity
$I_\gamma$	transmitted x-ray intensity at frequency $\gamma$
$I_{\gamma 0}$	incident x-ray intensity at frequency $\gamma$
$I_D$	image carrying x-ray intensity
$I_S$	scatter x-ray intensity
$\hat{J}$	unit vector along Y-axis
$J_1$	Bessel function of first order
$K$	build-up factor
$\hat{K}$	unit vector along Z-axis
$K_{1H}$	horizontal deflection of the engine rotor due to a one radian/second angular velocity
$K_{1V}$	vertical deflection of the engine rotor due to a one radian/second angular velocity.

$K_{2H}$	horizontal deflection of the engine rotor due to a one g linear acceleration
$K_{2V}$	vertical deflection of the engine rotor due to a one g linear acceleration
$L$	length
$M$	molecular weight of compound
$\overline{M}_A$	the total gyroscopic moment of forces about the turbine engine center of mass
$MTF$	modulation transform function
$MTF_{sys}$	system modulation transfer function
$MTF_{comp i}$	modulation transform function for component i
$M_x$	the component of $\overline{M}_A$ along the x-axis
$M_y$	the component of $\overline{M}_A$ along the y-axis
$M_z$	the component of $\overline{M}_A$ along the z-axis
$N$	number of x-ray quanta transmitted
$N_0$	number of incident x-ray quanta
$P$	permissible weekly exposure
$R$	electron range
$R_1$	outer radius of a cylinder
$R_2$	inner radius of a cylinder
$R_{inner}$	inner radius
$R_{outer}$	outer radius
$R(\xi)$	radius as a function of $\xi$
$T$	the fraction of total x-ray beam on-time that a point of interest is occupied
$TE_{10}$	dominant transverse electric mode

$\overline{TOD}$	x-ray source to engine distance vector
$T_o$	x-ray transmittance
$Z$	atomic number
$T_\gamma$	x-ray transmittance at frequency $\gamma$
$U$	the fraction of total x-ray beam on-time that a radiation shield is irradiated
$\overline{U}$	velocity
$\overline{U}_t$	velocity
$U_x$	component of velocity in x-direction
$U_y$	component of velocity in the y-direction
$U_o$	initial speed
$U_f$	x-ray film unsharpness
$U_g$	geometric unsharpness
$V$	electric potential
$W$	radiation workload
$W'$	weight of accelerator
$W_p$	primary radiation workload
$W_L$	leakage radiation workload
$W_s$	scatter radiation workload
$W_{rot}$	scattered workload during centrifuge rotation
$W_{\alpha_i}$	scatter workload over the included angle $\alpha_i$

# LOWER CASE LETTER SYMBOLS

$a$	radius of x-ray source
$a'$	radius of gyration
$b$	length
$c$	speed of light
$d$	length
$e$	electron charge
$f$	spatial frequency
$g$	acceleration due to gravity
$g_1(x, y)$	a function of $x, y$
$g_2(x, y)$	a function of $x, y$
$h$	Planck's constant
$h_0$	constant
$h(x_2 - \xi, y_2 - \eta)$	two-dimensional impulse function
$h(x_2 - \xi)$	one-dimensional impulse function
$i$	$\sqrt{-1}$
$\hat{i}$	unit vector along the x-axis
$\hat{j}$	unit vector along the y-axis
$k$	constant
$\hat{k}$	unit vector along the z-axis
$l$	constant
$m$	mass
$p$	axial load

$P_{crit}$	the axial load for Euler column buckling
$r$	radius
$r_0$	classical electron radius
$s$	length
$t$	time
$w$	radial load
$x$	thickness
$\Delta x$	thickness
$x_\alpha$	thickness of material $\alpha$
$y$	length
$y_p$	coordinate of a "pinch point" in engine coordinate system
$z_p$	coordinate of a "pinch point" in engine coordinate system



## GREEK SYMBOLS

$\alpha$	ratio of object to film distance and source to object distance
$\alpha_0$	$E_1/0.51$ , $E_1$ in MeV
$\alpha_1$	the included angle over which the radiation workload due to scatter is calculated
$\beta$	angle
$\epsilon$	$[1 - (\frac{U}{c})^2]^{-1/2}$
$\xi$	length
$\eta$	dummy variable
$\hat{\eta}$	a unit vector lying along the x-ray beam centerline
$\omega$	force per unit length
$\theta$	angle
$\mu$	absorption coefficient
$\mu(\gamma)$	absorption coefficient at frequency $\gamma$
$\bar{\mu}$	average absorption coefficient
$\bar{\mu}_s$	absorption coefficient for steel
$\gamma$	frequency
$\gamma_0$	cut-off frequency
$\xi$	dummy variable
$\rho$	density
$\Sigma$	microscopic cross-section
$\phi$	angle
$\phi(\gamma)$	spectral distribution of x-ray intensity
$\psi$	angle
$\psi_0$	ratio of scatter exposure to incident exposure

$\omega$	force per unit length
$\omega_B$	gyration frequency
$\omega_l$	force per unit area
$\bar{\omega}_{\text{rotor}}$	engine rotor angular velocity vector
$\omega_{\text{rotor}}$	$ \bar{\omega}_{\text{rotor}} $
$\bar{\Omega}$	angular velocity vector relative to coordinate system XYZ
$\Omega_x$	component of $\bar{\Omega}$ along the x-axis
$\Omega_y$	component of $\bar{\Omega}$ along the y-axis
$\Omega_z$	component of $\bar{\Omega}$ along the z-axis

$\frac{d\sigma}{d\Omega}$	differential cross section
---------------------------	----------------------------

## SCRIPT

$\mathcal{I}$	moment of inertia
$\mathcal{E}$	ratio of scattered photon energy to incident photon energy
$\mathcal{I}_{xx}$	moment of inertia
$\mathcal{I}_{yy}$	moment of inertia
$\mathcal{I}_{zz}$	moment of inertia
$\mathcal{I}_{xy}$	moment of inertia
$\mathcal{I}_{xz}$	moment of inertia
$\mathcal{I}_{yz}$	moment of inertia

## ABBREVIATED SYMBOLS

cm	centimeters
gm	grams
MeV	million electron volts
mm	millimeters
sec	seconds